JPL D-16333

ARISE

Advanced Radio Interferometry between Space and Earth

Mission and Spacecraft Description

2nd Edition

Edited by:
Artur B. Chmielewski
Muriel Noca
Richard D. Wietfeldt

June 1999

National Aeronautics and Space Administration
Jet Propulsion Laboratory
California Institute of Technology
Pasadena, California

Acknowledgments

This document has become the most comprehensive system description of a space VLBI mission published to-date, due to the relentless dedication of several individuals:

Muriel Noca	Who charmed into submission all members of the ARISE team to produce high quality work, frequently on their own time.
Rick Wietfeldt	Who spent evenings, nights and weekends designing, redesigning and optimizing the ARISE system.
Joel Smith	Without his involvement the second edition would never have become so complete in the aspects of ground segment, uplink and downlink methodology, VLBI system and international collaboration.
Jim Ulvestad	Who never lost patience correcting our misspellings of "blazars".
Firouz Naderi	Who was always quick to get me back on track with sage advice.
David Murphy	Who made sure the mission design will have maximum science return.
Rick Helms	Who combined the structural and thermal codes, allowing us to complete so many configuration iterations.
Bob Freeland	Who is the main reason for the joint NASA/DoD Inflatable Antennas Program, which will save the ARISE project millions of dollars in technology development.
Charles Wang	For creative solutions to our "one PC hard disk per second" telecom problem.
Anna Chavez	Who because of this publication became the only person in the universe who can combine PDF, Postscript, PowerPoint, and Word 6-97-98 into one document!
Corby Waste & Sugi Sorensen	Who created our web site full of animations, graphics, and an entertaining "Black Hole Information Center" hyper-linked by so many other sites.
Professor David Hurst	Who always makes me look up into the sky in amazement.

Thank you all, and the rest of the ARISE team. This would never have been possible without your dedicated help.

ABC.

Document prepared by the ARISE team:

James S. Ulvestad
ARISE
Preproject Scientist
NRAO

Phil Henderson
Deployable Antenna
Harris Corporation

David Murphy
Orbits and Coverage

Art B. Chmielewski
ARISE
Preproject Manager

Rick Helms
Structures

Muriel Noca
Systems

Pradeep Bhandari
Cryocoolers

John J. Kibler
Subreflector
Composite Optics, Inc.

Marco Quadrelli
Antenna Dynamics,
Attitude Control

Dave Cadogen
Inflatable Antenna
ILC Dover, Inc.

Carol Lewis
Power

Yahya Rahmat-Samii
Antenna Design
U.C.L.A.

Robert Chave
Subreflector System

Mike Jones
Mission Operations

Vincent
Randolph
Avionics

Eddy A. Derby
Subreflector
Composite Optics, Inc.

Leo Lichodziejewski
Inflatable Structure
L'Garde

Larry Roe
Inflation System
University of Arkansas

Sal Distefano
Power

Christian Lindensmith
Cryocoolers

Sam Sirlin
Antenna Dynamics,
Attitude Control

Robert Freeland
Inflatable Antenna
Consultant

Roger Linfield
VLBI Science

Joel Smith
VLBI Consultant

Todd Gaier
Science Instruments

Bob Miyake
Thermal Design

James Springett
Telecom/Analog
Downlink
Neocomm Systems,
Inc.

Mark Thomson
Deployable Antenna
TRW

Dan Thunnissen
Propulsion

Jeff Umland
Metrology System

Charles Wang
Telecom

Paul B. Willis
Antenna Materials

Rick Wietfeldt
Systems/VLBI

Also:
Henry Garrett - Space environments
Gene Wester- Power
Robert Hoferer - Antenna Design & RF compensation (UCLA)
Tsun-Yee Yan - Telecom

The **ARISE** team wishes to express thanks to its partners:

- COI, Inc. — Adaptive Subreflector Design
- Harris Corporation — Mechanical Antenna Design
- ILC Dover — Rigidizable Structures
- L'Garde, Inc. — Inflatable Antenna Design
- University of Arkansas — Inflation System
- Univ. of Calif. L.A. — Antenna Design and Performance

ARISE Science Advisory Group

A. Marscher (chair)	Boston U.	R. Linfield	Caltech/IPAC
P. Diamond	NRAL (U.K.)	C. Moore	Kapteyn Astr. Inst.
M. Elitzur	U. of Kentucky	D. Murphy	JPL
D. Gabuzda	JIVE	R. Mutel	U. of Iowa
M. Garrett	JIVE	S. Neff	GSFC
L. Greenhill	Harvard CfA	R. Preston	JPL
L. Gurvits	JIVE	J. Romney	NRAO
J. Hewitt	MIT	R. Taylor	U. of Calgary
H. Hirabayashi	ISAS	E. Valtaoja	Tuorla Obs. (Finland)
A. Konigl	U. of Chicago	A. Wehrle	Caltech/IPAC
J. Krolik	Johns Hopkins	A. Zensus	MPIFR

The research described in this publication was carried out in part by the Jet Propulsion Laboratory, California Institute of Technology, under a contract with the National Aeronautics and Space Administration.

Table of Contents

Executive Summary

Chapter 1: Scientific Impact of ARISE

1.1 Background 7
1.2 ARISE Science Overview 9

Chapter 2: Space VLBI

2.1 Principles of Ground-Space Interferometry 15
2.1.1 Radio Interferometry 15
2.1.2 Very Long Baseline Interferometry (VLBI) 16
2.1.3 Space VLBI 17
2.2 Current and Planned Space VLBI Missions 18
2.2.1 QUASAT 18
2.2.2 The TDRSS Demonstrations 18
2.2.3 The RadioAstron Mission 18
2.2.4 The VSOP Mission 19
2.2.5 The VSOP-2 Mission 19
2.2.6 Other Future Space VLBI Missions 20
2.3 Space VLBI Overview 20
2.3.1 System Overview 20
2.3.2 Mission Operations Overview 22
2.4 ARISE Mission Concept 24

Chapter 3: Observational Capabilities of the ARISE Mission

3.1 Science Requirements 26
3.1.1 Frequency Coverage 26
3.1.2 Sensitivity 27
3.1.3 Digitization 29
3.1.4 IF Channelization 30
3.1.5 Polarization 31
3.1.6 A-priori Calibration Accuracy 31
3.1.7 Sky Coverage and Duty Cycle 31
3.1.8 Orbit 32
3.1.9 Mission Lifetime 33
3.2 ARISE Spacecraft Constraints 33
3.2.1 Sun 33
3.2.2 Moon 33
3.2.3 Earth 33
3.2.4 Eclipses 33
3.3 ARISE Orbit Trade-off Study 33
3.3.1 Orbit Sensitivity 34
3.3.2 Orbit Normal and (u,v)-Coverage 36

3.3.3 Precession of the Orbital Elements 37
3.3.4 ARISE Tracking Coverage 41
3.3.5 Impact of ARISE Eclipses 42
3.3.6 Preliminary Orbit Selection 45
3.3.7 Additional Note on Mission Lifetime Requirements 46

Chapter 4: Science Payload Front-end Description

4.1 Science Payload Requirements 47
4.1.1 Frequency Coverage 47
4.1.2 Sensitivity 47
4.1.3 Polarization 47
4.1.4 Calibration Accuracy 47
4.1.5 System Temperature 47
4.1.6 Sky Coverage and Duty Cycle 48
4.1.7 Antenna Microwave Performance 48
4.2 Front-end Overview 48
4.3 Main Reflector 49
4.3.1 ARISE Antenna System Configuration 49
4.3.2 High Precision Inflatable Reflector 50
4.4 Subreflector (Mechanically Shaped) 59
4.4.1 Subreflector Description 59
4.4.2 Present Tunable Subreflectors Flight Technology Development 62
4.4.3 Antenna System Projected Performances 63
4.4.4 Metrology System 69
4.4.5 Other Current Activities in the Subreflector Correction Area 69
4.5 Adaptive Feed Array (Optional) 70
4.6 Receivers/Amplifiers/IFs 71
4.7 Instrument Thermal Control 72
4.8 Main Reflector: Non-Inflatable Options 75
4.8.1 Harris Concept 75
4.8.2 TRW AstroMesh 77

Chapter 5: ARISE VLBI Data System and Ground Support System

5.1 Spacecraft and Ground System Data Processing Requirements 81
5.2 Channelization and Telecommunication System Assumptions 82
5.3 Spacecraft Science Subsystem: The Digital Telecommunication Link Option 82
5.3.1 Space Radio Telescope (SRT) 82
5.3.2 Receiver, Pol-Select, LNA, RF-IF, IF Switch, IF-BB 83
5.3.3 LPF, ADC 83
5.3.4 Multi-Channel Data Formatter 83
5.3.5 "Data Modulator Mapping" 85
5.4 Science Data Downlink: The Digital Telecommunication Link Option 85
5.4.1 Baseline Multi-Gbps Modulation Scheme 85
5.4.2 Advanced Multi-Gbps Modulation Schemes 87
5.4.3 Multi-channel Data Modulator 88
5.4.4 U/C, Combiner, PA 88
5.4.5 Diplexer 89
5.4.6 Transponder 89
5.4.7 Phase Calibration Generator 90
5.5 Ground Tracking Station (GTS): The Digital Telecommunication Link Option 90
5.5.1 Diplexer, Pol-Sel 90

5.5.2 LNA, D/C 90
5.5.3 Multi-channel Data Demodulator 91
5.5.4 "Data Demodulator De-mapping" 91
5.5.5 Multi-channel Decoder 91
5.5.6 Re-channelization Filter (optional) 91
5.5.7 VLBI Recorder Interface Adapter (VIA) 92
5.5.8 VLBI Recorder 92
5.6 Science Data Downlink: The Analog Telecommunication Link Option 92
5.6.1 Space Radio Telescope (SRT) 92
5.6.2 Ground Tracking Station (GTS) 94
5.6.3 Discussions and Technology Assessment 94
5.6.4 Analog versus Digital Tradeoff Summary 95
5.7 VLBI Processing Center 96
5.7.1 VLBI Correlator 96
5.7.2 Image Analysis Center 96

Chapter 6: Mission Analysis

6.1 Launch Vehicle and Injection Capabilities 97
6.2 Launch and Orbit Transfer 98
6.3 Deployment Sequence 99
6.4 Space Environment 99

Chapter 7: Spacecraft System Description

7.1 Spacecraft Requirements 100
7.1.1 Mission Lifetime 100
7.1.2 Sky Coverage and Duty Cycle 100
7.1.3 Orbit Determination Accuracy 100
7.1.4 Pointing Requirements 100
7.1.5 Launch Vehicle 100
7.2 Spacecraft Configuration 101
7.3 System Functional Description 103
7.4 System Budgets 106
7.4.1 Mass 106
7.4.2 Power 106
7.4.3 Propellant 107
7.4.4 Pointing Budgets 108
7.4.5 Observation Timeline 108
7.4.6 Slew Time and Settling 108
7.5 Command and Data Handling 109
7.5.1 Requirements and Assumptions 109
7.5.2 Design Implementation and New Technology 109
7.6 Telecommunication Subsystem 111
7.6.1 X-band Subsystem 111
7.6.2 Ka-band Subsystem 111
7.7 Thermal Design 113
7.8 Attitude Determination and Control Subsystem (ADCS) 114
7.8.1 ADCS Requirements 114
7.8.2 Components 115
7.8.3 Spacecraft Model 115
7.8.4 Disturbances 116
7.8.5 Momentum Management 118

7.8.6 Dynamic Analysis and Control 119
7.9 Structure and Mechanisms 122
7.10 Power Subsystem 123
7.11 Propulsion subsystem 125

Chapter 8: Flight and Science Mission Operations

8.1 Mission Operations Overview 126
8.2 Principal Investigator - Science Proposal (ME-1) 129
8.3 ARISE Science Review Committee (ASRC) (ME-2) 129
8.4 ARISE Science Operations Group (ASOG) (ME-3) 129
8.4.1 Mission Analysis 131
8.4.2 Calibration and Instrument Analysis 131
8.5 ARISE Space Radio Telescope (SRT) (ME-4) 132
8.6 ARISE Flight Operations (F-OPS) (ME-5) 133
8.6.1 ARISE Flight Operations Group (AFOG) (ME-6) 133
8.6.2 ARISE Ground Command Station (GCS) (ME-7) 134
8.6.3 ARISE Spacecraft (ME-8) 135
8.7 ARISE Ground Operations (G-OPS) (ME-9) 135
8.7.1 ARISE Ground Operations Group (AGOG) (ME-10) 136
8.7.2 JPL Multi-Mission Navigation (MMNAV) (ME-11) 137
8.7.3 DSN Multi-Mission Scheduling (MMSCH) (ME-12) 137
8.7.4 ARISE Ground Tracking Station (GTS) (ME-13) 138
8.8 Ground Radio Telescope (GRT) (ME-14) 139
8.8.1 Ground Radio Telescope (GRT) Regional Servers (ME-15) 139
8.8.2 Ground Radio Telescopes (GRT) (ME-16) 140
8.9 Space VLBI Correlator (ME-17) 140
8.10 Principal Investigator -- Science Product (ME-18) 141

Chapter 9: ARISE Technologies and Roadmaps

9.1 ARISE Technologies Overview 142
9.2 Inflatable Antenna Technology 143
9.3 L'Garde's Inflatable Antenna Technology Program 144
9.3.1 Reflector Manufacturing 144
9.3.2 Design/Analysis 144
9.3.3 Materials/Coatings 146
9.3.4 Correction Technologies 146
9.3.5 Rigidizable Structure 146
9.4 Low Noise Cryogenic Amplifier Technology 147
9.5 Cryocooler Technology 148
9.6 Data Systems Technology 149
9.6.1 Telecommunication Link Issues 149
9.6.2 VLBI Acquisition, Tape Recording and Correlator Systems 149
9.7 ARISE Technologies Summary 150

Appendix A: ARISE Structures and Thermal Analysis Systems viii
Acronyms ix
References xii

List of Figures

Fig. 1: Artist's Rendering of ARISE Mission 1
Fig. 2: Schematic Diagram of ARISE Resolution vs. Other Instruments, for Imaging of Supermassive Black Hole Environments 2
Fig. 3: ARISE New Technology Needs Met By Existing Technology Development Programs. 3
Fig. 4: 14 m Inflatable Antenna Experiment (IAE) Reflector during L'Garde Ground Test 4
Fig. 5: Large Aperture Technology Development Roadmap 5
Fig. 6: 3.3 m Adaptive Reflector Built by Composite Optics Inc. (COI) 6
Fig. 7: Harris Corporation Mechanical Antenna Concept for ARISE 6
Fig. 1.1 VLA/VLBI Radio Images of Virgo A (M87) at Varying Resolutions 8
Fig. 1.2: Spatial and Energy/Frequency Coverage, on a Logarithmic Scale, for a Variety of Existing and Proposed Astronomical Observatories 10
Fig. 1.3: Schematic View of the Central 100 pc (330 light years) of an AGN, including Sketches of the Regions Emitting in Various Wavebands 11
Fig. 1.4: Very Long Baseline Array (VLBA) Imaging of a Disk Orbiting the Massive Black Hole at the Center of the Galaxy NGC 4258 12
Fig. 1.5: EVN 5 GHz Image of the Gravitational Lens System 2016+112 13
Fig. 2.1: Very Large Array (VLA) 16
Fig. 2.2: Very Long Baseline Array (VLBA) Sites 17
Fig. 2.3: Japanese-led VLBI Space Observatory Programme (VSOP) 19
Fig. 2.4: Space VLBI System Simplified Overview 21
Fig. 2.5: ARISE VLBI Mission Operations Simplified Overview 23
Fig. 3.1: Detection Limits for the Four (4) ARISE Observing Bands as a Function of Source Flux Density (*So*) and Maximum Brightness Temperature (*Tb*) 35
Fig. 3.2: Detection Limits for the Four (4) ARISE Observing Bands as a Function of Source Flux Density (*So*) and FWHM Size 36
Fig. 3.3: All-Sky (u,v)-Coverages for a One (1) Orbit Observation with Nominal ARISE Orbit and the VLBA 37
Fig. 3.4: Orbital Period as a Function of Perigee and Apogee Heights 38
Fig. 3.5: Nodal Precession Rate $d\omega/dt$ as a Function of Perigee and Apogee Heights for i=60° 39
Fig. 3.6: Nodal Precession Rate $d\omega/dt$ as a Function of Perigee and Apogee Heights for i=30° 39
Fig. 3.7: Perigee Precession Rate $d\omega/dt$ as a Function of Perigee and Apogee Heights for i=60°. 40
Fig. 3.8: Perigee Precession Rate $d\omega/dt$ as a Function of Perigee and Apogee Heights for i=30°. 40
Fig. 3.9: Eclipse History for $(h_p, h_a, i, \omega_o, \Omega_o)$ = (3000 km, 40000 km, 30°, 0°, 90°) 43
Fig. 3.10: Eclipse History for $(h_p, h_a, i, \omega_o, \Omega_o)$ = (3000 km, 40000 km, 30°, 0°, 270°) 43
Fig. 3.11: ARISE Nominal Orbit: h_p = 3000 km Altitude, h_a = 40000 km Altitude, i = 30° 46
Fig. 4.1: ARISE Spacecraft Radio Antenna System Configuration 48
Fig. 4.2: ARISE Off-axis Radio Antenna System Configurations 49
Fig. 4.3: ARISE Proposed Vertical Cross-section through the Dual Reflector Geometry 50
Fig. 4.4: ARISE Structural Configuration 51
Fig. 4.5: ARISE Reflector Precision Projection 53
Fig. 4.6: ARISE Structural Displacements due to Static Thrust Maneuver Loading 54
Fig. 4.7: Inflatable Antenna Thin Membrane Micrometeoroid Damage 56
Fig. 4.8: Inflatable Antenna Deployment Sequence (by TDM Inc.) 57
Fig. 4.9: ARISE Inflation System 58
Fig. 4.10: Antenna Subreflector with Adjustable Surface Figure 60
Fig. 4.11: Influence of Number of Adjusters on a 3.3 m Reflector 61

Fig. 4.12: Antenna Before/after Surface Adjustment Demonstration..... 62
Fig. 4:13: Antenna Subreflector Optimization Techniques Overview..... 64
Fig. 4:14: ARISE 22 GHz Dual Reflector Far-field Pattern..... 65
Fig. 4:15: (left) ARISE 22 GHz Main Reflector Surface Distortions; (right) Subreflector Surface Shape Difference to Ideal Shape. 65
Fig. 4:16: ARISE Ideal 22 GHz Far-field Pattern..... 66
Fig. 4:17 (left) ARISE 22 GHz Far-field Pattern with 1mm RMS Main Reflector Distortions; (right) ARISE 22 GHz Far-field Pattern with Corrective Subreflector..... 66
Fig. 4.18 (left) ARISE 43 GHz Distorted Far-field Pattern; (right) ARISE 43 GHz Far-field Pattern with Corrective Subreflector..... 67
Fig. 4.19 (left) ARISE 86 GHz Distorted Far-field Pattern; (right) ARISE 86 GHz Far-field Pattern with Corrective Subreflector..... 67
Fig. 4.20: ARISE 86 GHz 19-element Corrective Array Feed..... 70
Fig. 4.21: (left) ARISE 86 GHz Analytic 1 mm RMS Surface Distortions; (right) ARISE 86 GHz Far-field Pattern with 19-element Array Feed Compensation..... 71
Fig. 4.22: a) Mechanical Drawing of the Planck Surveyor Compressor Assembly. b) Photograph of a Single Compressor Bed..... 73
Fig. 4.23: The AIRS 55 K Cryocooler and Electronics [4.5]..... 74
Fig. 4.24: (left) Harris TDRSS Antennas Operate up to 15.5 GHz; (right) Harris 12 m L-Band Commercial Reflectors..... 75
Fig. 4.25: Solid Deployable Graphite Spline Technology for High Frequency Applications..... 76
Fig. 4.26: (left) Harris 25 m Deployed Reflector Concept for ARISE; (right) Harris 25 m Stowed Reflector Concept for ARISE (1.3 m diameter and 2 m High)..... 77
Fig. 4.27: TRW's 12.25 m AstroMesh Reflector..... 78
Fig. 5.1: Space VLBI System Overview..... 80
Fig. 5.2: ARISE VLBI System Data Flow Overview..... 81
Fig. 5.3: ARISE VLBI System Data Flow..... 84
Fig. 5.4: ARISE Analog-downlink VLBI System Data Flow..... 93
Fig. 6.1: Delta 7925 Three Stage Launch Vehicle Capability..... 98
Fig. 6.2: Injected Mass as a Function of Inclination for Delta 7925 2.9 m Fairing..... 98
Fig. 7.1: ARISE Spacecraft in the Stowed Launch Configuration..... 101
Fig. 7.2: ARISE Spacecraft Inside Layout..... 102
Fig. 7.3: ARISE Spacecraft High Level System Functional Block Diagram..... 105
Fig. 7.4: ARISE Command & Data Handling (C&DH) Block Diagram..... 110
Fig. 7.5: ARISE X-band Telecommunication Subsystem Block Diagram..... 111
Fig 7.6: ARISE Ka-band Telecommunication Subsystem Block Diagram..... 112
Fig. 7.7: ARISE Spacecraft and Antenna Finite Element Model..... 116
Fig. 7.8: Solar Torque Magnitude as a Function of Theta and Alpha..... 117
Fig. 7.9: Solar Torque Magnitude as a Function of Theta and Alpha..... 117
Fig. 7.10: X-displacement at Strut/Torus Joint from 2 s Firing of Pair of 0.9 N Thrusters..... 120
Fig. 7.11: Z-displacement at Strut/Torus Joint from 2 s Firing of Pair of 0.9 N Thrusters 121
Fig. 7.12: Y-displacement at the Strut/Torus Joint from 2 s Firing of Pair of 0.9NThrusters..... 121
Fig. 7.13: Deformation at Strut/Torus Attachment Point with Reaction Wheel at 2000 rpm..... 122
Fig. 7.14: ARISE Spacecraft Propulsion System..... 125
Fig. 8.1: ARISE Space VLBI Mission Operations Overview..... 127
Fig. 8.2: ARISE Space VLBI Mission Operations Science Data Flow..... 128
Fig. 9.1: ARISE New Technology Needs Met By Existing Technology Development Programs. 142
Fig. 9.2: 100 GHz MMIC Amplifier..... 148
Fig. 9.3: Noise Temperature vs. Frequency for 6 Amplifiers shown in Figure 9.1..... 148

List of Tables

Table 1.1: Highest Resolution of Astronomical Imaging Techniques 9
Table 1.2: ARISE Science Goals 10
Table 3.1: ARISE Sensitivity vs. Frequency - 8 GHz 28
Table 3.2: ARISE Sensitivity vs. Frequency - 22 GHz 28
Table 3.3: ARISE Sensitivity vs. Frequency - 43 GHz 28
Table 3.4: ARISE Sensitivity vs. Frequency - 86 GHz 29
Table 3.5: ARISE 7-sigma Continuum Sensitivity to VLBA Antenna (25 m) 29
Table 3.6: ARISE 7-sigma Continuum Sensitivity to GBT (100 m) 29
Table 3.7: ARISE 7-sigma Spectral Line Sensitivity to VLBA Antenna (1.3 km/s line) 29
Table 3.8: ARISE 7-sigma Spectral Line Sensitivity to GBT (1.3 km/s line) 29
Table 3.9: ARISE Nominal Orbit Parameters 34
Table 3.10: ARISE Tracking for Orbits with Different Apogee Heights (i=30°) 41
Table 3.11: ARISE Tracking for Orbits with Different Inclinations (h_p=5000 km, h_a=40000 km). 42
Table 3-12: ARISE Average Eclipse Length for Different Orbits with Perigee Height 3000 km Apogee Height 40000 km, and Inclination 30°, over 3 Years (1095 Days) 44
Table 3-13: ARISE Average Eclipse Length for Different Orbits with Perigee Height 3000 km Apogee Height 40000 km, and Inclination 60°, over 3 Years (1095 days) 44
Table 3.14: Summary of ARISE Orbit Investigations 45
Table 3.15: ARISE Selected Nominal Orbit 46
Table 4.1: ARISE Inflatable Antenna Mass Breakdown 51
Table 4.2: ARISE Normal Modes Analysis 54
Table 4.3: ARISE Radiation Performance 67
Table 4.4: ARISE Projected Overall Aperture Efficiency 68
Table 4.5: ARISE RF System Performance at 86 GHz, with 19-element Corrective Feed 71
Table 4.6: ARISE Receiver Performance 72
Table 4.7: ARISE Mechanical Cooler Technology 74
Table 6.1: ARISE Nominal Orbit 97
Table 7.1: ARISE Spacecraft Mass Budget 106
Table 7.2: ARISE Spacecraft Power Budget per Mission Mode 107
Table 7.3: ARISE Spacecraft Propellant Budget 107
Table 7.4: ARISE Mission Functions Resulting in Loss of Science Data Collection 108
Table 7.5: ARISE Link Budget for 8 Gbps Data Downlink 113
Table 7.6: ARISE Spacecraft Stability Requirements 115
Table 7.7: ARISE Spacecraft Power for Reaction Wheels during Observations 118
Table 7.8: ARISE Spacecraft Calculated Solar Array Area and Mass for 2300 W EOL 123
Table 7.9: ARISE Spacecraft Calculated PMAD Mass 124
Table 9.1: ARISE Inflatable Antenna Development Program Schedule 145
Table 9.2: ARISE Mechanical Cooler Technology 148

Executive Summary

The concept of black holes is so outrageous that Einstein, whose theory predicted them, did not believe in their existence. Today, in 1999, we can definitely say that black holes do exist. Supermassive black holes have even moved from the outer reaches of the universe into our immediate neighborhood, since a black hole 3 million times the mass of the Sun now appears to reside in the very center of our own Milky Way galaxy. Black holes are now so widely accepted that they are a permanent fixture of any "Astronomy 101" textbook. Of course, no textbook will ever publish a picture of a black hole, only an artist's conception (or speculation). No electromagnetic waves will ever emerge from within the event horizon. The best we can hope for is to image the wild spectacle surrounding that event horizon. ARISE (Advanced Radio Interferometry between Space and Earth), shown conceptually in Figure 1, is the mission that will provide such images, images of the regions within light days to light months of the event horizon of supermassive black holes.

The gravitational field of a black hole attracts matter that orbits rapidly before disappearing inside the event horizon. This matter includes remnants of stars, dust and gas, which form a spectacular spinning disk, called the "accretion disk." The gas accelerated toward the black hole gets progressively more compressed and heated due to friction, ultimately reaching temperatures of

Fig. 1: Artist's Rendering of ARISE Mission (courtesy of Enrique Garcia).

hundreds of millions of degrees and creating strong X-ray emission. Because scientists predicted these emissions early, almost 50 years ago, the search for black holes as X-ray sources commenced as soon as the first X-ray detector was flown in space in 1962. The first black-hole candidate actually was identified by virtue of its X-ray emission. Known as Cygnus X-1 (the first X-ray source discovered in the constellation of Cygnus), the candidate was identified as the "invisible" member of the binary-star system identified with the optical star called HDE 226868, also a strong source of radio waves. Thus, from the beginning, it was clear that studies of potential black holes in multiple wavelength regimes were crucial to understanding their properties. ARISE will continue this tradition and complement the lower-resolution observations made by Chandra and Constellation X (X-Ray), NGST (Visible and Infrared) and GLAST (Gamma Ray).

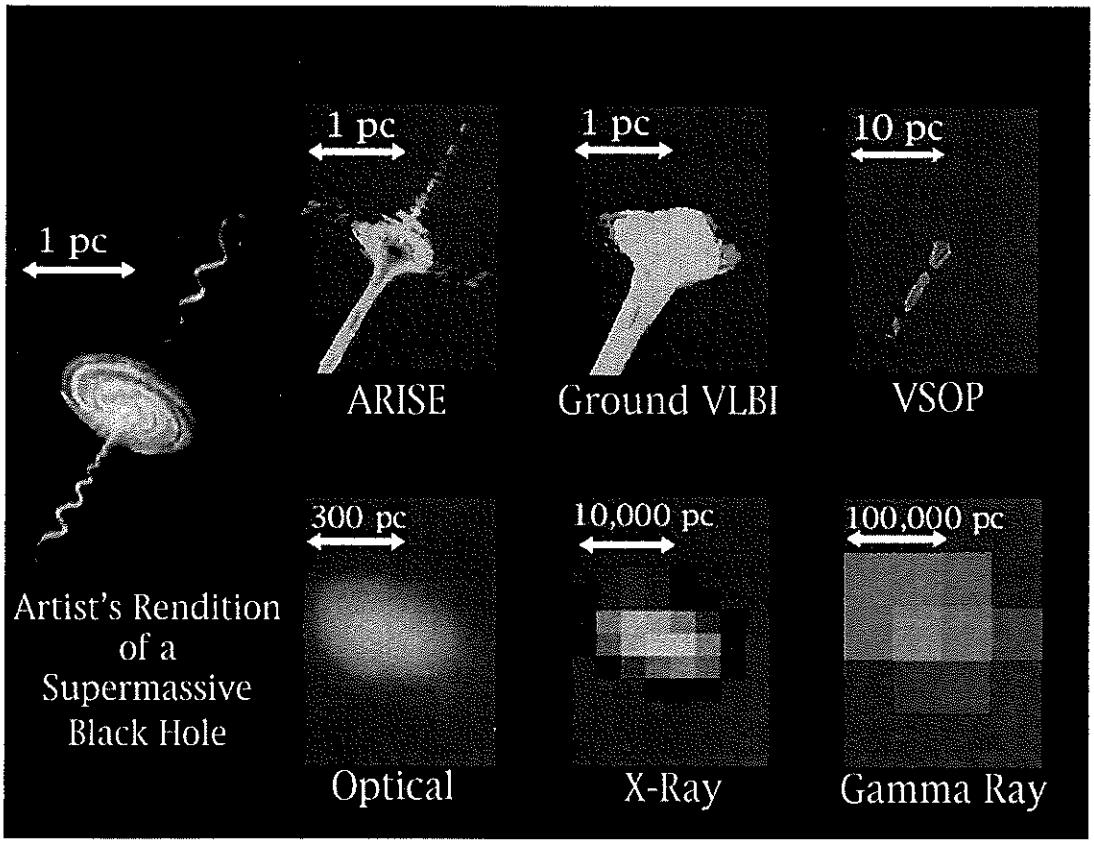

Fig. 2: Schematic Diagram of ARISE Resolution vs. Other Instruments, for Imaging of Supermassive Black Hole Environments. Note the dramatic change in scales for the telescopes operating in different wavelengths.

The value of high-resolution imaging provided by ARISE interferometers can be inferred from Figure 2. Let's assume that we are trying to image the environment of a million solar mass black hole pictured in the leftmost drawing. Let's further suppose that this black hole is located approximately 1 billion light years (300 megaparsecs) away from us. The radiation from the vicinity of the black hole will appear only as an unresolved "blob" across several pixels of an X-ray or Gamma ray telescope, as conceptually shown in the two pictures on the bottom right. In a sense, it is not even fair to compare a radio interferometer with X-ray or Gamma ray telescopes, which are designed to show source strength and variability, and (in the case of X-ray telescopes) perhaps the source spectra, but are incapable of providing well-resolved details. On the other hand, a telescope operating in the visible region, such as the Hubble Space Telescope (HST), suffers from two serious deficiencies when it comes to imaging Active Galactic Nuclei (AGN) hiding black holes. The best resolution of HST is about 0.05 to 0.1 arcseconds, and this resolution is larger than the size of the entire accretion disk. To compound the problem, dust around the AGNs

is opaque to visible radiation and does not permit imaging of the inner regions where the most interesting, extreme physics occurs.

As can be seen on the top rightmost simulated image, the current Japanese Space VLBI mission VSOP has much better resolution than all telescopes listed in the bottom row. The limiting factor for VSOP is its 5 GHz frequency of observation and the apogee height of 21000 km, providing resolution of approximately 0.0003 arcseconds (or 0.3 milliarcseconds). VSOP also has limited sensitivity because of the relatively small 8 m antenna and high receiver noise levels. As a result, VSOP can image the energetic portions of relativistic jets emanating from AGNs only on scales of light years, and is basically blind to the less luminous area of the accretion disk and to the details in the regions where the jets are formed. Indeed, the innermost regions of the jets absorb their own radiation at frequencies lower than about 40 GHz, and cannot be imaged, even in principle, except by observing at higher frequencies. The accretion disk of several nearby AGNs can be detected by the Very Long Baseline Array (VLBA), the worldwide network of ground radio telescopes. However, the resolution of its images, even when fully operational at 86 GHz, will always be limited by the physical size of the Earth; a schematic view of the VLBA ("Ground VLBI") imaging capability is also shown in Figure 2. In contrast, the upper leftmost image illustrates what might be seen with ARISE. At its highest frequency of 86 GHz, ARISE has an imaging resolution of better than 15 microarcseconds, more than 3000 times better than HST! In fact, source structure will be detected on size scales as small as 2 microarcseconds! The sensitivity of ARISE will be high due to its large, 25 m diameter antenna and application of the newest technology in low noise amplifiers cooled to 20 K using recently space-tested sorption coolers. The ARISE data system will also be far superior to any other space or ground asset and will operate at a mind boggling 8 Gbps (equivalent to filling a standard PC hard drive every few seconds!).

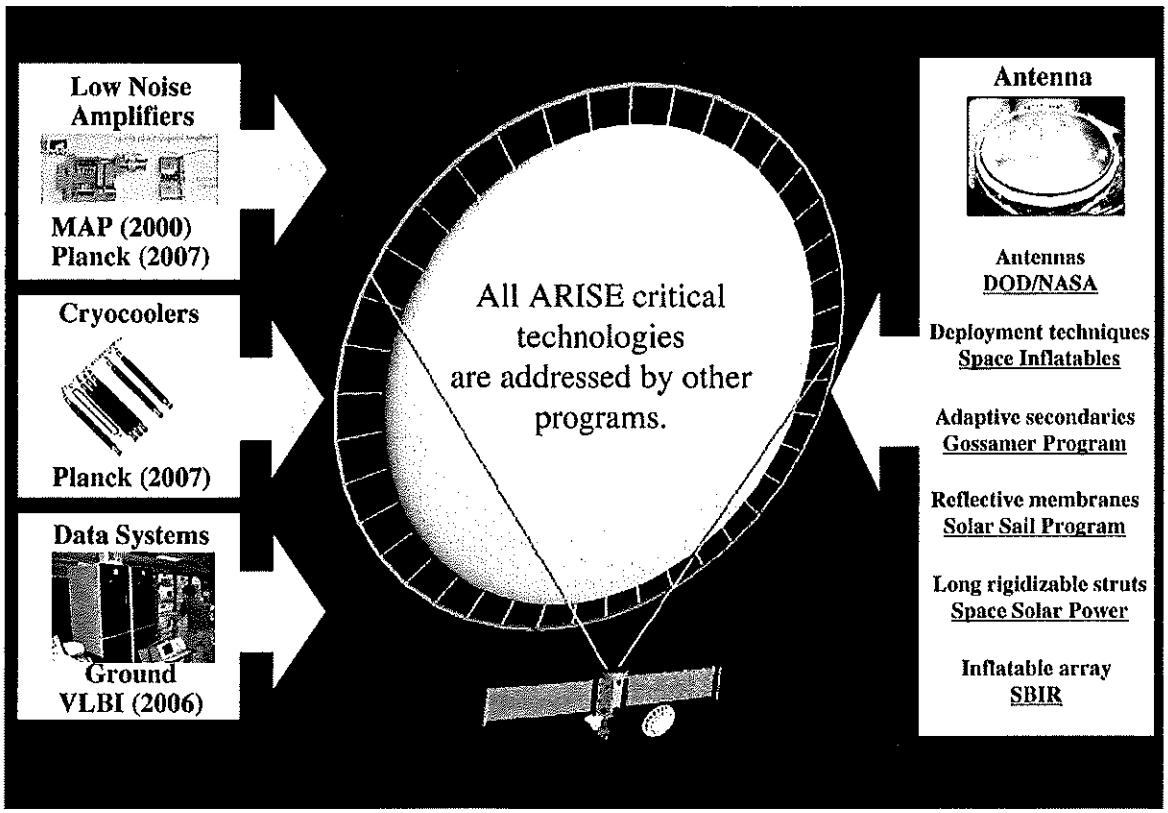

Fig. 3: ARISE New Technology Needs Met By Existing Technology Development Programs and Flight Projects Launched before ARISE.

ARISE could be ready for launch on a Delta II rocket by 2008 for a cost of approximately $340 million. This is about a third of what this sophisticated mission would have cost just a few years ago. The lower cost is due largely to application of new technology developed by other programs. See Figure 3. The critical technology is the 25 m aperture. Inflatable structures technology, under development for a variety of users, is the current baseline choice for the main reflector, although other mechanically deployed reflector alternatives are being explored. On-board low noise amplifiers and cryogenic coolers are being produced for missions such as MAP, Planck, and FIRST. MAP will be launched in 2000, carrying amplifiers in the same frequency range needed for ARISE. Advances in recording and correlation systems, to increase the VLBI data rate to the Gigabit per second (Gbps) regime, are already under development.

The most challenging aspect of the ARISE mission is a large inflatable antenna (e.g., see Figure 4). Inflatable technology is well funded by NASA and DoD. Both agencies have embarked on a joint program to develop inflatable technology. The year 2000 is extremely important from the ARISE inflatable structure point of view, due to the initiation of a multiyear NASA Space Science Gossamer Technology Program. The Gossamer Program will be focused on four areas, each beneficial to the ARISE antenna development: large ultra-light structures, large apertures, large antennas and adaptive techniques.

The large ultra-light structures part of the Gossamer Program will assure that the inflatable rigidizable technology for the ARISE torus and struts is well characterized and flight-tested. The program will also validate the inflation system and controlled deployment techniques. The large aperture and antenna portion of the Gossamer Program will develop technology aimed at improving surface accuracy of large reflectors. The long-term goal of the Program is to create not only a large 20-40 m class aperture operating in the microwave range, but eventually reaching the visible regime. The long-term program shown in Figure 5 will result in a series of large apertures with applications to millimeter, sub-millimeter, infrared and eventually optical telescopes. The ARISE antenna, as difficult as it may seem to develop, is only at the beginning of this chain.

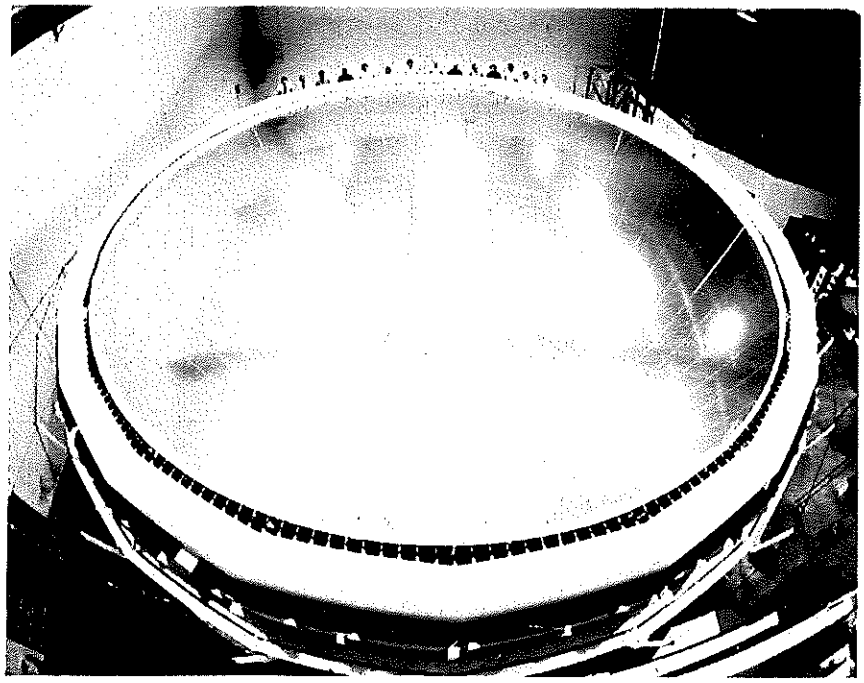

Fig. 4: 14 m Inflatable Antenna Experiment (IAE) Reflector during L'Garde Inc. Ground Test. To visualize the scale of the reflector note the L'Garde personnel standing in the back of the dish. The ARISE reflector will be almost twice this size.

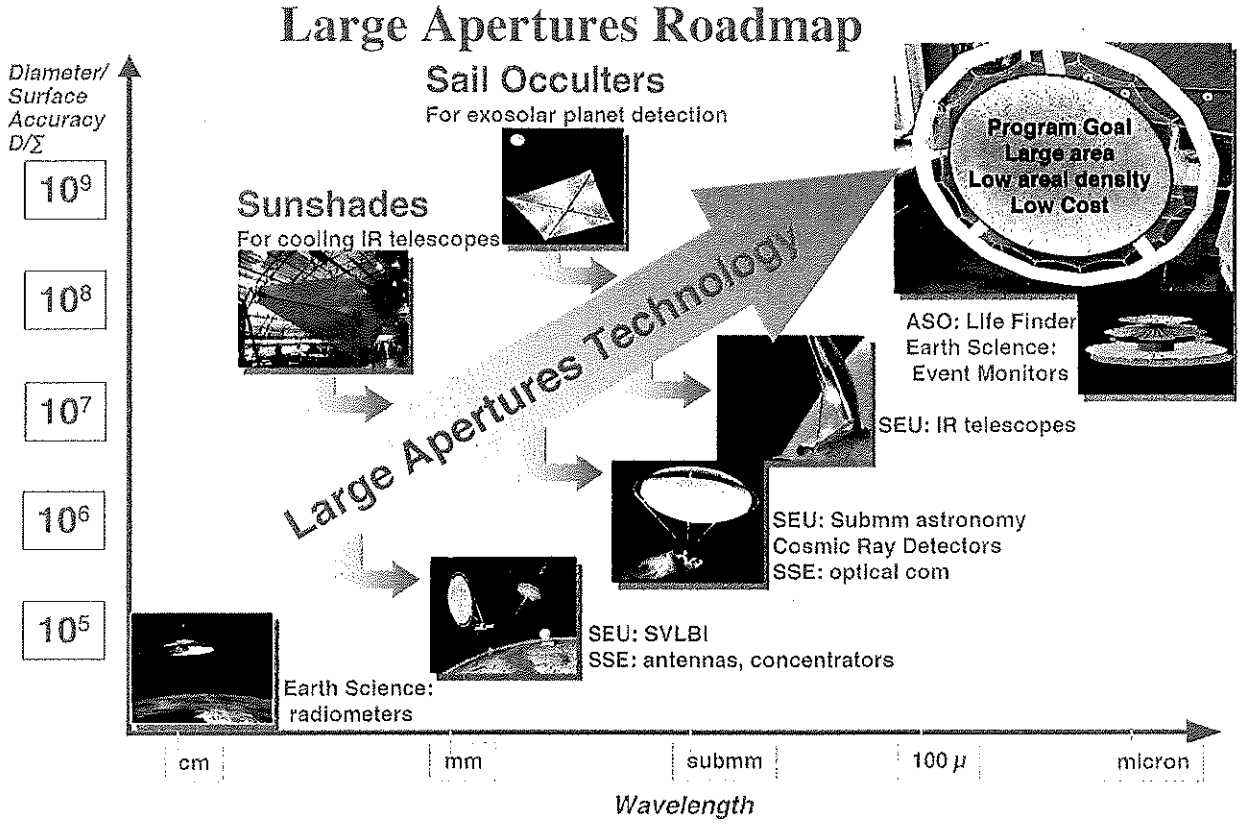

Fig. 5: Large Aperture Technology Development Roadmap.

The final part of the Gossamer Program will address adaptive techniques. There are two aspects of adaptive techniques that are important in construction of the ARISE antenna. The long inflatable struts must be first deployed, then inflated to the appropriate shape and subsequently rigidized. This process may result in small deviations from the desired strut positioning. These deviations will be adjusted using adaptive strut techniques, such as adaptive membranes, shape memory foams, or other techniques. The other aspect of adaptive techniques pertains to the secondary optics shape control. The secondary reflector for ARISE is now envisioned as a 1.6 m semi-major axis ellipsoid. The surface of this ellipsoid will be composed of a thin graphite composite shell. The shell will be attached to a strong-back and its surface adjusted by means of approximately 40-60 actuators. Composite Optics Inc. recently tested a 3.3 m reflector built for the Millimeter Array Program (Figure 6).

The adaptive secondary reflector will be used regardless of the antenna choice. According to calculations conducted by UCLA, the secondary can improve the aperture efficiency at 86 GHz from < 10% to > 40% by correcting large systematic errors common in inflatable antennas. The secondary might also be very beneficial to the mechanical antenna options. It would assure more robustness and lower sensitivity to environmental effects of the Harris antenna. The Harris antenna, illustrated in Figure 7, will use high density mesh spanning 25 m diameter to assure good antenna performance up to 43 GHz. The inner 8 m diameter will utilize precision graphite splines to give high antenna performance at 86 GHz.

ARISE, as a VLBI mission, is an international project by definition. ARISE will take advantage of the worldwide assets in systems and operations that have enabled VLBI to become a routine observing technique. In addition to ground infrastructure, ARISE has initiated cooperation with the

Canadian Space Agency (CSA) and the Joint Institute for VLBI in Europe (JIVE), which may result in a complete development of the recording systems as well as some on-board systems. Discussions are also underway with the Japanese to make ARISE a cooperative mission between NASA and ISAS/NASDA. On the American front, the biggest contributors to the project will be the Department of Defense sponsoring an extensive portion of the antenna development and NSF (NRAO) contributing ground assets and scientific expertise. These close partnerships will make ARISE not only one of the most exciting and innovative missions of the first decade of the new century, but also affordable to NASA.

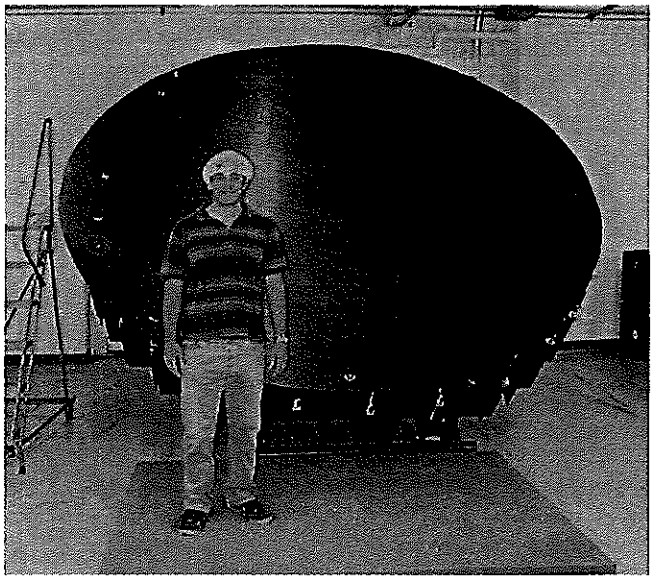

Fig. 6: 3.3 m Adaptive Reflector Built by Composite Optics Inc. (COI).

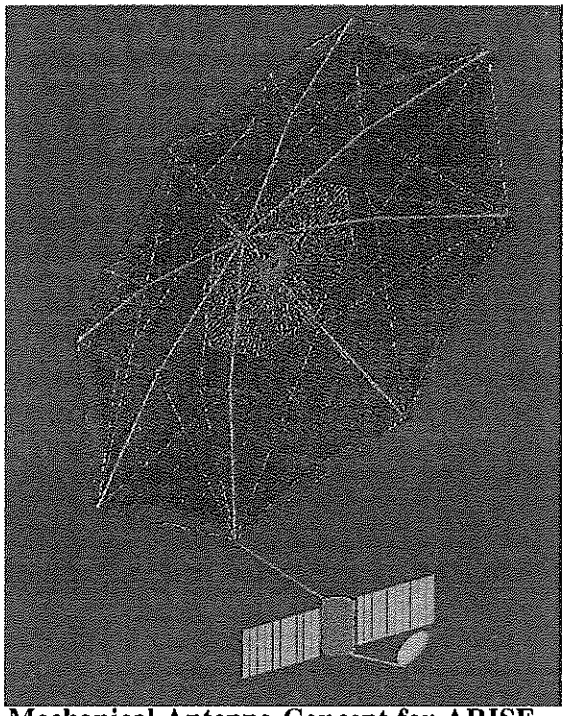

Fig. 7: Harris Corporation Mechanical Antenna Concept for ARISE.

Chapter 1

Scientific Impact of ARISE

(See "ARISE Science Goals" [1.1] for a complete description.)

1.1 Background

Supermassive black holes (SMBH) are thought to be responsible for the astounding amount of energy released from the centers of many galaxies. In fact, there is growing evidence that giant black holes may exist not only at the centers of galaxies containing active galactic nuclei (AGN), but also in many (or even all!) relatively quiescent galaxies, such as our own Milky Way. A supermassive black hole is a spectacular concentration of mass, with as much as several billion times the mass of the Sun contained within the "event horizon," an area no larger than the size of the solar system. This event horizon is the region from which no radiation or information can escape, so that all we may observe about the black hole itself is its mass and angular momentum. These properties dominate the physical behavior of material near the black hole. ARISE is the only astronomical instrument foreseen for the next 20 years that will have the capability of imaging the region dominated by the gravitational potential of the black hole, within light days to light months of the active galactic nucleus.

Radio telescopes such as ARISE provide a view of the Universe that is quite different from that emerging in other wavebands. Nearby stars are the apparently brightest optical objects viewed from the Earth, usually located no more than 300-600 pc (1000-2000 light years) away. In contrast, most of the brightest radio sources seen from Earth are AGNs, typically located far across the observable Universe, often at more than a million times the distance of the brightest stars. The jets emerging from the vicinity of the black holes in AGNs are observed and imaged almost exclusively at radio wavelengths. Figure 1.1 shows a series of radio images at increasing resolution of the dominant elliptical galaxy in the Virgo cluster, M87, at a distance of 15 Mpc (~50 million light years).

For many galaxies, the central black holes produce more power than the entire output of the hundreds of billions of stars that comprise the galaxies. Together with their surrounding accretion disks, the black holes are responsible for producing the observed properties of objects like "quasars," spectacular beacons at the centers of extremely distant galaxies. The black holes power narrow jets of relativistic material that speed away from them at more than 99% of the speed of

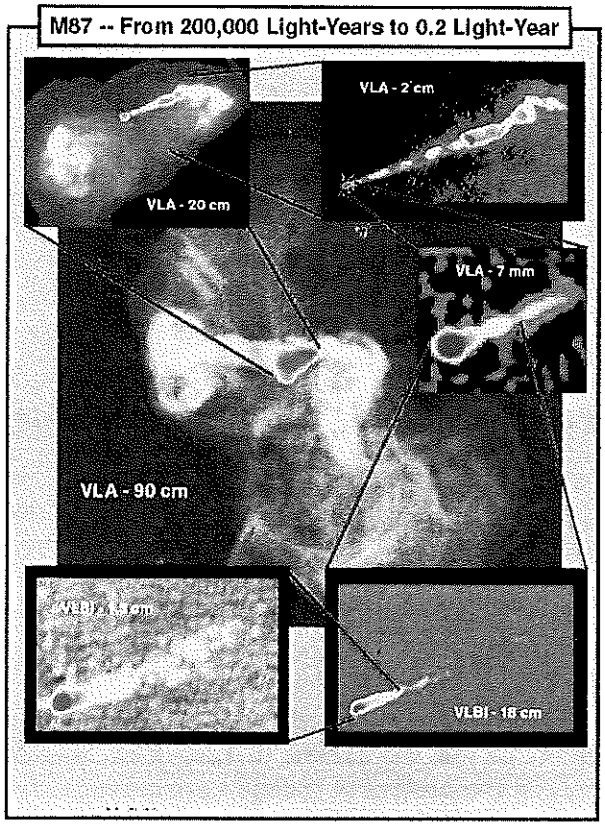

Fig. 1.1: VLA/VLBI Radio Images of Virgo A (M87) at Varying Resolutions. Images of the innermost jet, found within the unresolved active galactic nucleus, and located within light months of the central $10^9 M_o$ black hole.

light ($0.99c$), and that have *apparent* motions as fast as $10c$.[1] Within galaxies, these jets can generate strong shock waves that compress gas and may thus be related to episodes of rapid star formation. They often extend well beyond the visible galaxies, supplying energy to the hot diffuse medium between galaxies. Thus, the black holes may hold the key to the origin and evolution of galaxies; were they "seed nuclei" around which the galaxies condensed? How have they grown as the galaxies evolved, and as galaxies have collided? Perhaps most galaxies went through a quasar phase, possibly related to galaxy mergers, at some point in their evolution.

Supermassive black holes in galaxies and quasars are the most spectacular physics laboratories in the Universe. They can produce energy with efficiencies ~50 times greater (per unit mass) than nuclear fusion, and are the only known way to power quasars and related AGNs. In fact, it is possible that much of the energy produced in the Universe over its lifetime is generated by these enormously powerful black-hole engines at the centers of galaxies. The energy production and related processes are direct consequences of the physics described by general relativity and high-energy particle physics, realms far beyond those we can investigate in any laboratory on Earth. Indeed, in many ways, black-hole physics provides us a glimpse of the physical processes in the very early Universe, when matter was packed much more densely than today, and when energetic particles abounded. Only Very Long Baseline Interferometry (VLBI) has the capability of directly imaging the environments of massive black holes in AGNs, on scales comparable to the sizes of

[1] Apparent *superluminal* motion is actually an optical illusion of special relativity, caused by motion at nearly the speed of light along a direction close to the observer's line of sight.

their accretion disks and (in nearby objects) within factors of 10-100 of the event horizons themselves.

Table 1.1 summarizes the typical resolution of a variety of astronomical imaging instruments; Figure 1.2 shows the same information graphically. The ARISE resolution of better than 15 μas will provide imaging on scales 10 to 10000 times the event horizons of SMBHs in most AGNs, exactly the region where the local physics is dominated by the gravitational pull of the central objects. No other astronomical techniques except VLBI and Space VLBI, including optical interferometry on the ground or in space, can produce images of this region. The unique capability to make images at such high resolution is the basis for the scientific rationale for ARISE.

Technique	Angular Resolution (arcsec)
Gamma-ray telescope	1800
X-ray telescope	1
Ground optical telescope	0.1-1
Space optical/infrared telescope	0.05
Radio VLA at 43 GHz	0.05
Expanded VLA at 43 GHz	0.01
Millimeter Array at 850 GHz	0.01
Optical interferometer, 100-m baseline	10^{-3}
Ground VLBI at 86 GHz	10^{-4}
ARISE at 86 GHz	$\leq 1.5 \times 10^{-5}$

Table 1.1: Highest Resolution of Astronomical Imaging Techniques.

1.2 ARISE Science Overview

ARISE is a versatile, high-sensitivity instrument that will employ the technique of Space VLBI (see Chapter 2) to image a variety of compact objects such as supermassive black holes (SMBH). It will resolve details 5-10 times smaller than can be imaged using ground-based VLBI, and several orders of magnitude smaller than instruments observing in other wavebands. Table 1.2 summarizes the main science goals of ARISE.

The most important goals of ARISE focus on studies of SMBHs and their environments in active galactic nuclei (AGN), the most energetic power plants in the Universe. The popular treatment by Begelman & Rees (1996) discusses observed properties of AGNs over a variety of wavebands that are attributable to SMBHs. A sketch of the currently accepted model for an AGN can be found in Figure 1.3. This model includes, at its center, a SMBH that provides the power for the AGN. Surrounding the black hole is an accretion disk, formed when rotating gas is pulled in by the gravitational field of the black hole. The accretion disk is roughly co-planar (except for disk warps) with a much more extensive "torus" of material that may extend for hundreds of parsecs. As material in the disk drifts toward the central black hole, it loses gravitational potential energy, which, in turn, can power energetic phenomena such as the production of copious quantities of gamma rays and X-rays. A magnetized radio jet of highly relativistic particles is accelerated near the SMBH, and flows outward near the speed of light along the symmetry axis of the accretion disk and torus. Flickering gamma-ray emission reveals the creation of large quantities of high-energy particles in the inner light months of the radio jet. In many cases, this jet can continue far outside the visible galaxy.

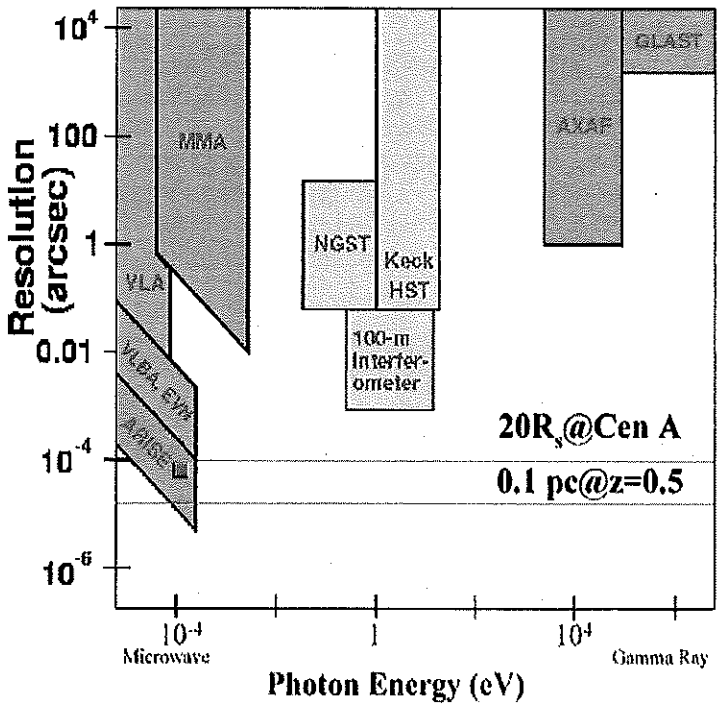

Fig. 1.2: Spatial and Energy/Frequency Coverage, on a Logarithmic Scale, for Existing/Proposed Astronomical Observatories, Ranging from Radio to Gamma-Ray Energies. Lines correspond to 20 Schwarzschild radii for a 10^9 M_o black hole at Cen A, and to 0.1 pc at a redshift z = 0.5. The red square indicates the ARISE resolution for an H_2O megamaser at 22 GHz, corresponding to 0.05 pc at a distance of 50 Mpc. Microwave and high-energy instruments in opposite corners (blue) often investigate different aspects of similar non thermal phenomena. Instruments in the middle of the diagram (yellow) usually observe the thermal emission from objects such as stars/galaxies. Some ground radio-telescope arrays to be used with ARISE are indicated in green in the diagram.

Primary Goals
Supermassive Black Holes and Radio Jets
AGN Fueling
Relativistic Jet Production
Generation of High-Energy Photons
Accretion Disks and H_2O Megamasers
Masses of Supermassive Black Holes
Nature of Megamaser Disks
Accretion Processes
Geometric Distance Measurements
Cosmology
Gravitational Lens Studies
High-Redshift Radio Sources
Additional Goals
Stellar Astrophysics: coronae of active stars
High-energy Astrophysics: hypernovae
Jet Astrophysics: jet physics at light years from SMBHs
Shocks and Turbulence: supernovae and galactic masers

Table 1.2: ARISE Science Goals.

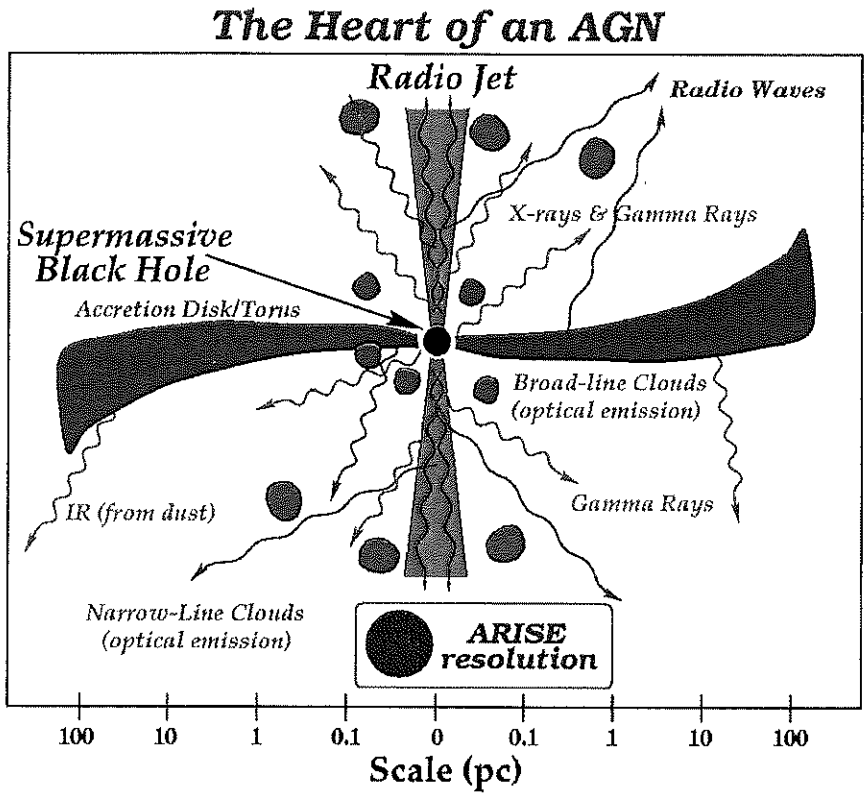

Fig. 1.3: Schematic View of the Central 100 pc (330 light years) of an AGN, including Sketches of the Regions Emitting in Various Wavebands. (Note the logarithmic scale.) The typical linear resolution of ARISE, 0.05-0.1 pc (50-100 light days), is indicated on the bottom. This resolution corresponds to an 86 GHz continuum observation at z = ~0.5 or to a 22 GHz H_2O maser observation at a distance of 50-100 Mpc. For a more nearby AGN, such as Cen A, the resolution can be orders of magnitude smaller, a few light days or better.

In AGNs, VLBI and other radio observations generally detect emission from non thermal processes, both in the radio continuum (e.g., in the form of relativistic radio jets) and in discrete spectral lines (generated in disks that rotate around the central black holes), that are rarely seen in optical and infrared wavelengths. These jets and disks are excellent probes of the central energy source of an AGN and its surrounding environment. In addition, the radiation in other wavebands is often obscured and cannot in any case (due to insufficient angular resolution) be directly imaged on the scale of light weeks to light months. Observations of highly variable radiation, with time scales of months to shorter than one day in all wavebands, imply the presence of substantial energy production on the exact scales imaged by ARISE. For example, the variable gamma-ray emission is thought to come from the inner parts of the relativistic jets; imaging the total and polarized intensity in the jets can help distinguish between competing models for the gamma-ray production.

The gravitational pull of the SMBH results in high velocities in stars and gas clouds near the core of the AGN. In only a few nearby, unobscured systems, these motions can be studied by the Hubble Space Telescope at distances of ~10-100 pc from the AGN. In contrast, VLBI observations reveal the actual velocity structures in the accretion disk within a parsec of the SMBH, even in galaxies whose centers are completely obscured at optical wavelengths.

With ARISE, two critical classes of observations can be made. First, imaging of the inner light months of active galaxies in their continuum radio emission reveals the birthplace of the relativistic

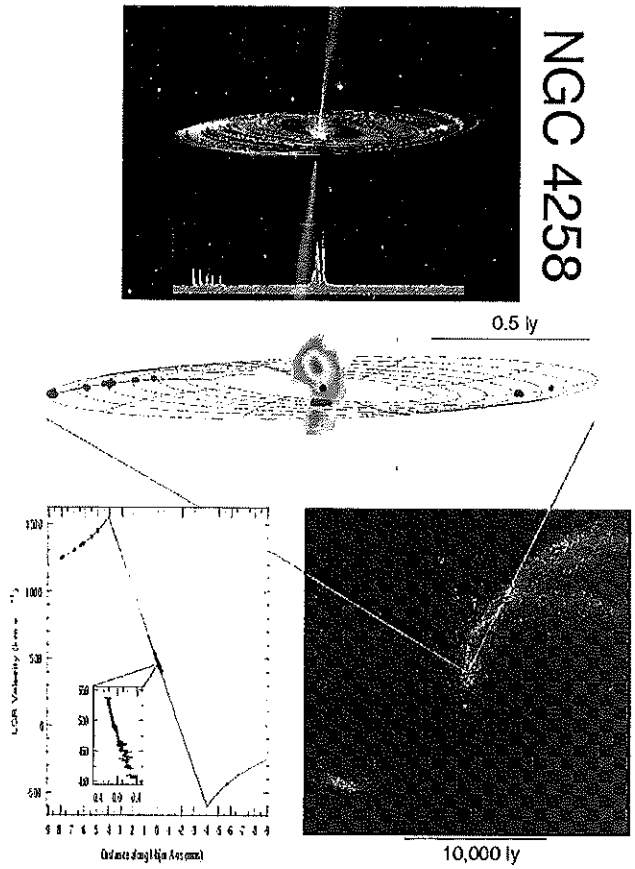

Fig. 1.4: Very Long Baseline Array (VLBA) Imaging of a Disk Orbiting the Massive Black Hole at the Center of the Galaxy NGC 4258, at a Distance of 7.2 Mpc. Top Panel: Artist's conception of the rotating disk, together with the measured radio spectrum showing redshifted and blueshifted H_2O maser emission at a frequency of 22 GHz. Middle Panel: Dots show the actual location of the Doppler-shifted H_2O maser emission imaged by the VLBA, outlining a slightly warped disk about 0.6 pc (2 light years) in extent, while the false color image is the radio jet emerging at a distance of about 4000 Schwarzschild radii from the central black hole. Bottom Panel: *Left*: VLBA measurements of the velocity structure (relative to the Local Standard of Rest) of the H_2O maser spots as a function of distance along the major axis of the disk, showing the Keplerian rotation that is used to determine a black hole mass of 3.9 x 10^7 M_o, with an error of only a few percent. *Right*: Very Large Array (VLA) 20-cm radio image of the inner spiral arms of NGC 4258, on a scale 20000 times larger than the VLBA image.

jets, the generation of shocks near that birthplace, and the key physical parameters in the regions of gamma-ray production. Second, imaging of molecular line (H_2O maser) emission from the inner light months of the accretion disks in AGN directly samples the dynamics of material in the vicinity of the SMBH. Such studies lead to direct measurement of SMBH masses and of the physical characteristics of the accretion process. VLBI in general, and ARISE in particular, provide important information, and actual images, that can be supplied by no other technique in modern astrophysics. As Figures 1.2 and 1.3 show, the improvement in resolution over ground VLBI enables imaging of relativistic jets on the scale of the gamma-ray emission, and also enables superior resolution in the H_2O maser disks in AGNs.

Figure 1.4 shows the VLBI image of the H_2O maser and radio continuum emission from the inner light months of the Seyfert galaxy NGC 4258, at a distance of 7.2 Mpc, where VLBI imaging reveals an almost perfectly Keplerian disk of material orbiting a black hole of mass 3.9 x 10^7 M_o.

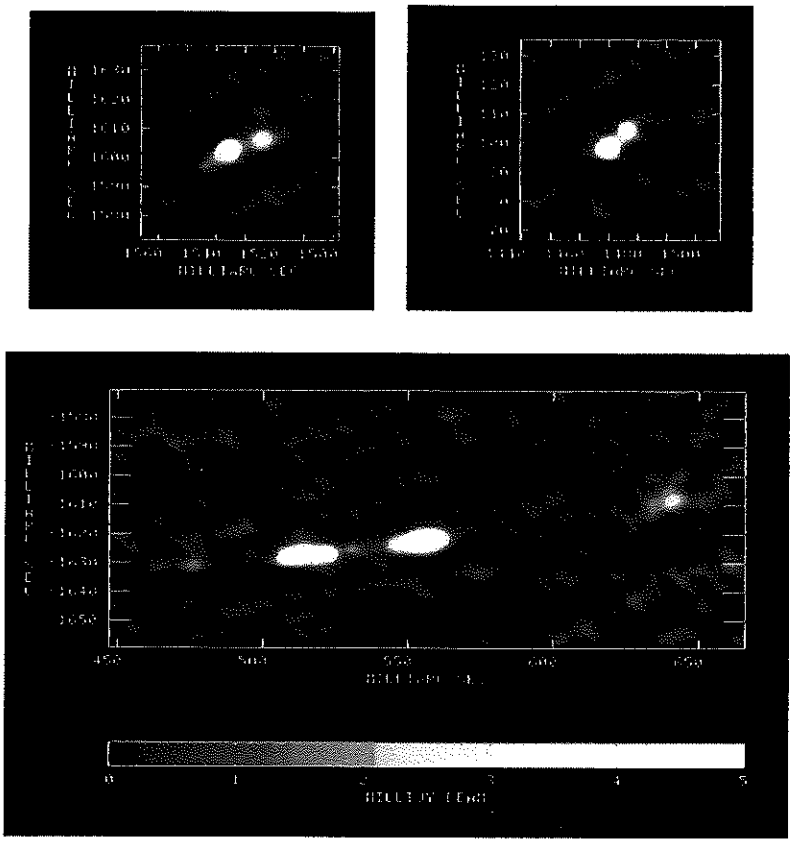

Fig. 1.5: European VLBI Network (EVN) 5 GHz Image of the Gravitational Lens System 2016+112. Core-jet structure is revealed in each of the four images of the background object (one image in each of the upper boxes, and two more near the center of the lower box). The lower box shows two very extended, merging images, suggesting that the distant background radio source (at z = 3.27) straddles a region of high magnification (known as a caustic). Indeed, lens models predict that for these merging images, the magnification of the background source is ~ 40. Without the natural magnification provided by the lens, this source would have appeared unresolved.

Most known H_2O maser disks are in galaxies several times more distant, and weaker H_2O emission in galaxies at distances of 50-100 Mpc is expected to be discovered over the next few years. Only ARISE will have the resolution to measure the gas motions (velocity and centripetal acceleration) in the disks, and resolve the disk thickness, in such objects at distances greater than ~15 Mpc.

Beyond the studies of SMBHs and their environment, ARISE can use AGNs for a variety of important cosmological studies. In particular, ARISE will permit investigation of radio sources with an otherwise unreachable combination of sensitivity and angular resolution, which is crucial for conclusive cosmological tests measuring the dependence of angular size and separation on redshift. Of special interest are the novel investigations that can be made using gravitational lenses. These are systems in which a distant AGN shows multiple images at radio and optical wavelengths due to the gravitational influence of an intervening galaxy or cluster of galaxies. As an example, a ground VLBI map of four images in the gravitational lens system 2016+112, a very distant quasar lensed by intervening galaxies, is shown in Figure 1.5.

In a gravitational lens system, the distant AGN will vary at radio wavelengths; if a model of the intervening mass is available, the time delay between variations seen in the different images enables a direct determination of the distance between the Earth and the lens. Knowledge of the distance can yield an estimate of the Hubble Constant, H_0, which characterizes the overall scale of the Universe. ARISE imaging of lensed AGNs will provide a high resolution probe of the dark matter in the intervening masses, and will improve the modeling of the mass distribution, currently the largest uncertainty in the determination of H_0 by this direct method. A gravitational lens also acts as a "cosmic telescope" in magnifying the background source by a factor of 10 or more, effectively increasing the angular resolution of ARISE to near 1 μas, which will provide resolution of light days even for the most distant AGNs. Finally, the sensitivity of ARISE to structures on the scale of tens to hundreds of microarcseconds will enable detection of compact lenses having masses of 10^3-10^6 $M_\odot$. Such objects are among the candidates for the "missing" baryonic dark matter that may contribute significantly to the density of the Universe.

In addition to the primary goals of studying the environment of supermassive black holes and making unique contributions to cosmology, the versatility of ARISE will enable exploration of a number of additional areas of astrophysics, as summarized in Table 1.2. ARISE will contribute to **(1) stellar astrophysics**, through resolution of the coronae of active stars and their rapid time evolution, on scales smaller than a solar diameter; **(2) high-energy astrophysics**, via observations of the "hypernovae" that may be responsible for at least some gamma-ray bursts; **(3) jet astrophysics**, by studies of the jet structures and interactions at distances of a few light years from the SMBHs (and possibly in a few galactic sources spawned by X-ray binary systems); and **(4) the astrophysics of shocks and turbulence**, which may be constrained through studies of the fine-scale angular structure of supernovae as well as galactic maser sources in star-forming regions and in late-type stellar envelopes. Thus ARISE will be a very versatile user facility that will attract investigators studying a broad range of energetic astrophysical phenomena in addition to its most important goal of imaging and exploring the regions near supermassive black holes.

Chapter 2

Space VLBI

2.1 Principles of Ground-Space Interferometry

2.1.1 Radio Interferometry

A radio interferometer consists of two radio telescopes separated by some distance, both observing the same radio source at the same time, over a common band of frequencies at the same polarization, with a common frequency standard, a common knowledge of the (Universal) time (UTC), accurate knowledge of telescope locations, and a means of combining (correlating) the pair of received signals to produce the mutual coherence function. Practical radio interferometer systems consist of a network of radio telescopes separated by extended distances. Radio interferometry is the technique of imaging radio sources through the use of radio interferometers. Radio interferometers have been operating for nearly 50 years, evolving from the simplest "connected-element" interferometers described above, separated by distances of up to hundreds of kilometers, linked together with data correlation in real-time, to Very Long Baseline Interferometers (VLBI), involving telescopes separated by up to the diameter of the Earth, involving non-real-time correlation, to Space VLBI, involving telescopes in Earth orbit to extend the baselines beyond the diameter of the Earth.

Interferometer resolution is determined by the number of wavelengths in each baseline (i.e., by the distance between pairs of telescopes). Interferometer sensitivity is the geometric mean of the sensitivities of the individual telescopes, and improves with increases in antenna sizes, lower system temperatures, higher observing bandwidths, etc.

The elements of the radio interferometer system are two or more telescopes, a means of receiving the incoming electromagnetic waves, reducing the radio signals down to baseband signals for digitization before correlation, and a means for routing the telescope data streams to a common site for correlation. This process must include a scheme of routing the received signal times of arrival to the common site, a means of determining the telescope locations, a correlator at the common site with provision for adding delay and delay rates to compensate for Earth rotation and the fact that antennas are not co-located, the means of determining the mutual coherence function, and a software system to interpret the correlator output to produce radio images.

The classical example of a connected-element interferometry system is the Very Large Array (VLA), operated by the National Radio Astronomy Observatory (NRAO), near Socorro, New Mexico (see Figure 2.1), which consists of three legs (in a "Y" pattern), each with nine 25 m

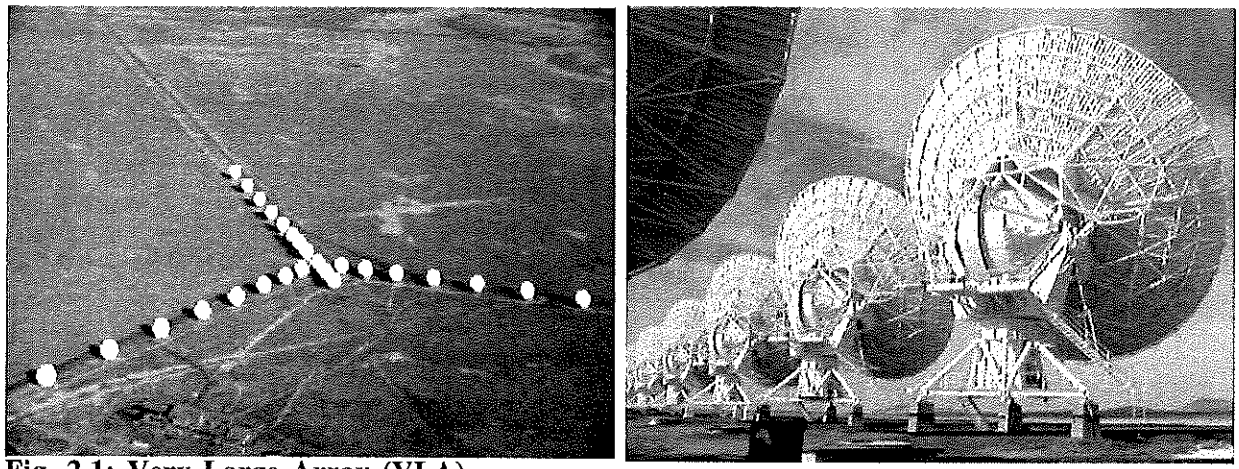

Fig. 2.1: Very Large Array (VLA).

diameter telescopes. The 27 telescopes are mounted along railroad tracks and are capable of being moved to various locations so as to extend or contract the lengths of the legs to define a set of different operating configurations. The telescopes are connected by buried waveguides which provide routing for both timing and data streams to the common site near the apex of the "Y". The telescope locations are determined, here as with most telescopes, off-line, by means of combinations of surveying or GPS, and ultimately for the highest accuracy by astronomical calibration. The correlator processes the data streams in real-time. The VLA observes in standard radio astronomy bands from 1.6 GHz to 43 GHz as well as selected bands near 2.3 GHz and 8.4 GHz.

2.1.2 Very Long Baseline Interferometry (VLBI)

Ground-based Very Long Baseline Interferometry (VLBI) relies on interferometers with telescopes separated by as much as the diameter of the Earth. As a result of the large separation between individual telescopes, it is presently impractical and cost prohibitive (although technically feasible) to electronically link the telescopes in real-time. This results in two distinct characteristics relative to connected-element interferometry described above. First, the use of independent frequency standards generally provided by Hydrogen masers (H-masers), which drive time-keeping systems which are independently synchronized to Universal Time (UTC), generally using GPS receivers at each site. Second, the requirement to record the data on some medium (typically magnetic tape) for subsequent non-real-time processing, generally 1-2 weeks after the observation allowing for tape shipment times from the telescopes to the correlator.

For example, the Very Large Baseline Array (VLBA), operated by the National Radio Astronomy Observatory (NRAO), consists of ten 25 m telescopes located on the continental U.S. including two telescopes in the Virgin Islands and Hawaii (see Figure 2.2). Each telescope operates on its own local Hydrogen-maser (H-maser) atomic frequency standard and time-keeping system. Data are recorded onto magnetic tape with time-tags accurate to better than 100 nanoseconds. The VLBA has established a standard shipping capability for routing the tapes to the correlator within days. The VLBA correlator is located in Socorro, New Mexico. The VLBA telescopes also observe in standard radio astronomy bands from 1.6 GHz to 43 GHz as well as selected bands near 2.3 GHz and 8.4 GHz.

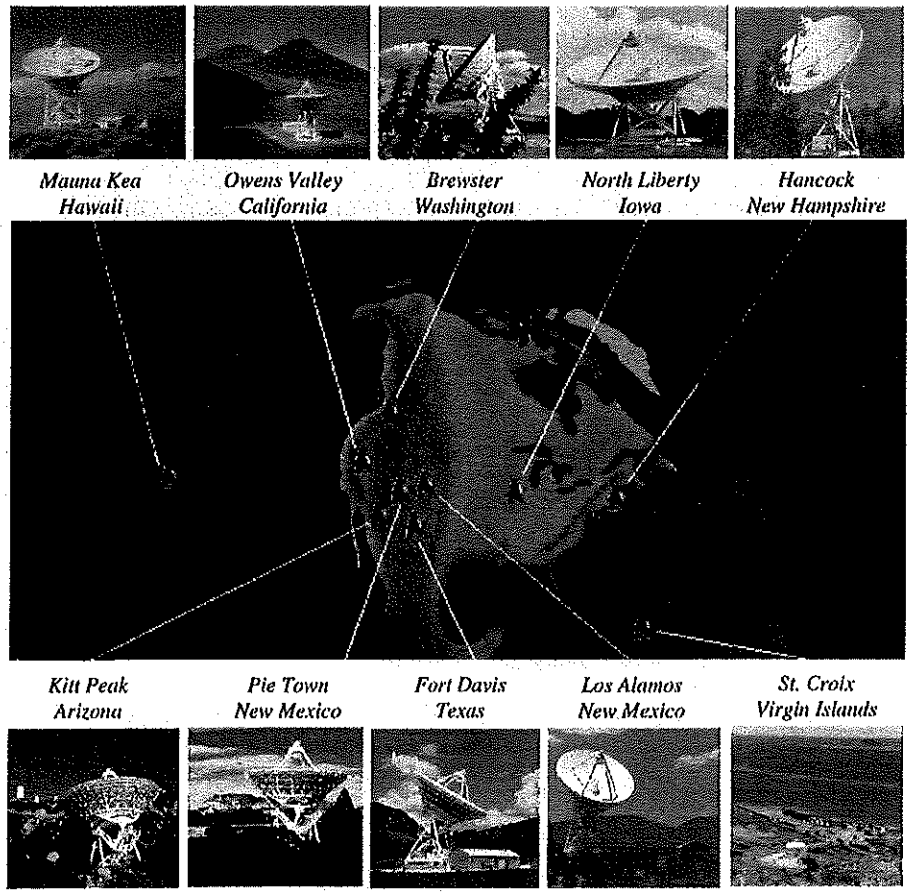

Fig. 2.2: Very Long Baseline Array (VLBA) Sites.

2.1.3 Space VLBI

Space VLBI is VLBI when one or more telescopes are in Space. It is motivated by the desire to achieve baselines exceeding an Earth diameter, hence higher angular resolutions (at a given observing frequency) compared to ground-based VLBI. Space VLBI, like ground-based VLBI, still requires the use of an independent clock on-board the spacecraft as well as the requirement to record its data on magnetic tape for off-line shipment to the correlator. However, in each case, there are differences compared to ground-based VLBI. First, at least for the first generation of Space VLBI spacecraft, in the form of the Japanese VLBI Space Observatory Program (VSOP) and the Russian RadioAstron program, the spacecraft do not carry on-board frequency standards, thus a phase transfer system is employed to uplink the stable frequency reference to the spacecraft from a network of ground tracking stations. Second, it is not feasible to record the signals on-board the spacecraft, hence the wideband data are downlinked for recording in real-time at the network of ground tracking stations. An implied further difference in Space VLBI is the derivation by each tracking station of so-called "time corrections" to compensate for the lack of an accurate clock on board the spacecraft. Time corrections are derived in the tracking station from its two-way phase transfer system to the spacecraft and sent to the Space VLBI correlator to enable correlation.

The first generation of Space VLBI spacecraft operate in standard radio astronomy bands at frequencies of 300 MHz (RadioAstron), to 1.6 GHz, 5 GHz, and 22 GHz (VSOP, RadioAstron). Future missions such as ARISE plan to operate at frequencies up to 86 GHz.

2.2 Current and Planned Space VLBI Missions[1]

2.2.1 QUASAT

The study of how VLBI might be pursued in Space began in the late 1970's, when it was realized that the size of the Earth was a serious limitation to the study of compact radio sources. By going to Space, achieving angular resolution at radio wavelengths that could not be obtained with VLBI systems that were limited by the size of the Earth, important tests could be made of quasar models.

The technology appeared to be within reach, and an early Space VLBI concept, QUASAT, emerged as a joint project, involving both U.S. and European scientists. In 1984, a workshop was held in Gross Enzersdorf, Austria, under joint sponsorship of NASA and the European Space Agency (ESA). The principal conclusion of the workshop was that a VLBI station in Space, telemetering its data to ground tracking stations, working in connection with ground-based radio telescopes, would give the opportunity to achieve angular resolution of a few tens of microarcseconds, and could develop high-quality radio maps of many classes of radio sources. The ground tracking stations would also function as the source of a stable local oscillator for the spacecraft, which needs a highly stable frequency reference.

In the 1987-88 time frame, both NASA and ESA developed their versions of the QUASAT mission. The first proposal to be considered was the U.S. version in response to an Explorer Announcement of Opportunity (AO). The mission failed to obtain approval in large measure because of its expense. The European version was submitted to ESA in October 1988 as a report on the Phase A Study. While ESA also found that the European version of QUASAT was beyond its budgetary allowance, the planning activities of both agencies had allowed all the necessary technical studies to advance to the point where no serious problems were anticipated. The QUASAT Phase-A Study was a clear statement of the scientific goals of VLBI in Space, and a comprehensive study of the technical means by which the goals would be met.

2.2.2 The TDRSS Demonstrations

From 1986 to 1988 a series of Space VLBI test demonstrations were carried out, using one of the two 4.9 m antennas on the TDRSS satellite as a radio telescope, with the other being used as part of a closed-loop phase-measuring system. The first experiment took place at a frequency of 2.3 GHz. Two ground radio telescopes were used for the other ends of the Space-to-Earth interferometer: the DSN antenna at Tidbinbilla, Australia, and the ISAS antenna at Usuda, Japan. With the successful completion of the 2.3 GHz phase of the demonstration, it was decided that a 15 GHz experiment was both possible and desirable. The observations were carried out in 1988, with success . The combination of the 2.3 GHz and 15 GHz experiments demonstrated that Space VLBI was technically feasible, and the fringes that were observed confirmed that the current hypothesis of bulk relativistic motion in radio-loud quasars was correct. Without bulk relativistic motion, synchrotron self-Compton damping should have limited the source brightness temperature to 10^{12} K, in which case only weaker fringes should have been observed.

2.2.3 The RadioAstron Mission

The Soviet Union had also begun planning a mission, with the intent to fly it as soon as they could; the mission was designated RadioAstron. In December 1985 the Soviets formed an international study team for the RadioAstron mission, holding the first meeting in Moscow. By 1987 it was

[1] With extracts from an informal note from Professor Bernard F. Burke, MIT.

clear that U.S. participation in the RadioAstron project was advisable, but not possible because only pre-existing agreements on cooperation in Space were being acted on by the U.S. at that time. The U.S. National Academy of Sciences had signed a cooperation agreement with the Soviet Academy of Sciences, however, so informal science exchanges continued. In 1989, NASA received permission to enter into new collaborations with the Russians, and since then NASA/JPL has been supporting the RadioAstron mission despite continued delays in launch dates due to economic constraints within Russia. RadioAstron will observe at bands at 0.3 GHz, 1.6 GHz, 5 GHz, and 22 GHz, with a 10 m observing antenna from an apogee of 80000 km, although an even higher apogee of 300000 km is under consideration.

2.2.4 The VSOP Mission

The Japanese radio astronomers had been actively engaged in VLBI studies from an early stage. At the 1984 QUASAT Workshop in Gross Enzersdorf, the Japanese gave a brief communication, stating that they had been exploring what they might build and launch as a Japanese mission. They also participated in the first TDRSS Demonstration in 1986 and 1987. In 1987 they submitted their first conceptual proposal. Since 1989 NASA/JPL has been supporting the VSOP mission (see Figure 2.3) which launched in February, 1997. VSOP is currently producing high dynamic range images of unprecedented resolution despite the loss of its highest observing band at 22 GHz during launch. VSOP is observing at bands at 1.6 GHz and 5 GHz, with an 8 m observing antenna from an apogee of 20000 km.

2.2.5 The VSOP-2 Mission

The Japanese are at the time of writing studying a follow-on mission to VSOP, with anticipated launch in 2006, and observations at 5 GHz, 22 GHz, and 43 GHz, with a 10 m observing antenna from an apogee of 30000 km with a data rate of 1 Gbps, which improves both the resolution and sensitivity by a factor of 10 relative to VSOP.

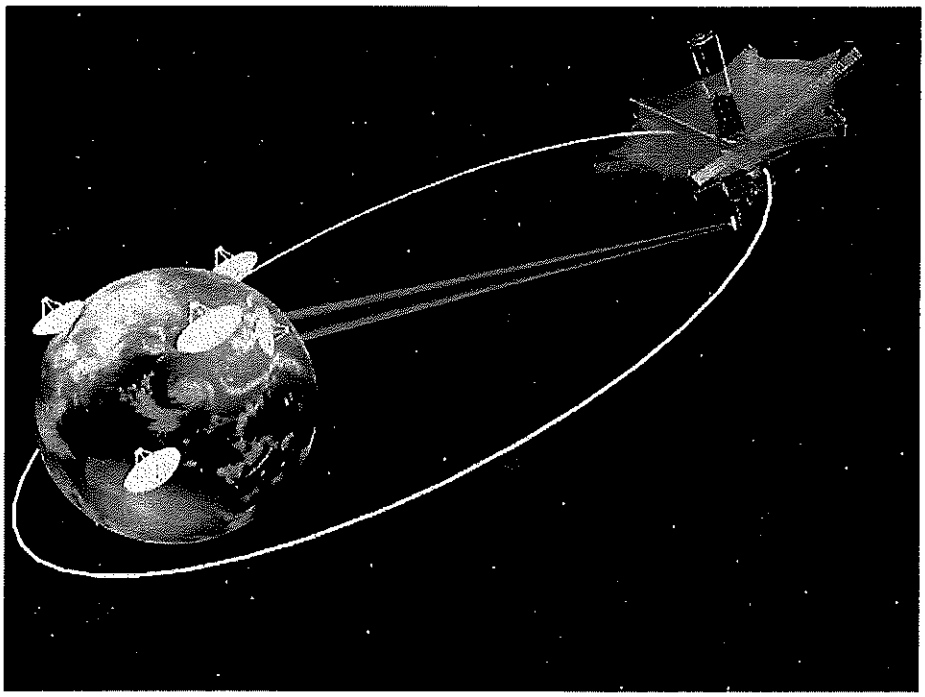

Fig. 2.3: Japanese-led VLBI Space Observatory Programme (VSOP).

2.2.6 Other Future Space VLBI Missions

The Astronomical Low Frequency Array (ALFA) mission has been proposed by JPL to NASA as a Mid-Ex mission for launch in 2002. ALFA would consist of an array of sixteen low-cost satellites operating together as an interferometer array in a cluster in a distant retrograde orbit about the Earth, and would observe below the Earth's ionospheric cutoff (0.3 to 3.0 MHz).

Millemetron is under study within the Lebedev Physical Institute of the Russian Academy of Sciences. Millemetron would provide observations at selected bands from 0.3 mm to 1.5 mm, with a 0.6 m antenna, from the Russian segment of the Space Station. The launch date is indeterminate.

The Europeans at the Netherland Foundation for Reasearch in Astronomy (NFRA) in Dwingeloo, the Netherlands, have proposed the construction of a large precise antenna by astronauts on-board the International Space Station, with subsequent launch into a highly elliptical Earth orbit. No specifics are known at the time of writing.

The Japanese have noted that use of the Japanese H-2 rocket rather than the smaller M-V rocket used for VSOP would allow them to launch two spacecraft simultaneously, each three times the mass of VSOP, into highly elliptical Earth orbits, and allow still higher dynamic range imaging through both Space-ground and Space-Space interferometry links.

2.3 Space VLBI Overview

2.3.1 System Overview

In this section, we provide an overview perspective of the Space VLBI system, consisting fundamentally of the Space-to-ground interferometer. The basic Space-to-ground interferometer, including the Space radio telescope (SRT) in Earth orbit and its counterpart ground radio telescope (GRT) on the Earth surface, is shown schematically in Figure 2.4. A more detailed description of the Space VLBI system is presented in Chapter 5.

In VLBI each interferometer forms a "baseline" consisting of two radio telescopes, which in synthesis imaging theory is shown to provide measurements (in the so-called (u,v)-plane) that ultimately contribute to the estimation of the two-dimensional brightness distribution of the target radio source. The two distinctive characteristics of VLBI systems compared to connected-element interferometry systems are the requirements for independent frequency standards at each telescope, and the requirement for the recording of the wideband astronomical data to tape, for subsequent correlation and analysis in non-real time, generally some number of weeks after the observation. In Space VLBI the two distinctive characteristics of the SRT compared to its GRT counterpart are that the SRT does not have an on-board H-maser frequency (and timing) standard, nor an on-board wideband recorder. Instead, the SRT must therefore receive an uplinked coherent reference from its serving ground tracking station (GTS), and it must downlink its wideband VLBI data to the GTS for wideband data recording in the GTS. From the perspective of the correlator, wideband data from the SRT (via its GTS) and the GRT must correspond to the same band of observing frequencies in the same polarizations, and should be digitized in a uniform manner. Figure 2.4 presents the SRT and GRT radio telescopes, where the SRT as a complete functional system, referred to elsewhere in this document as the "effective SRT," includes the SRT proper (in Space), its serving GTS (on the ground), and the infrastructure required for control and monitor (not shown). In particular, we note the two-way phase transfer to the spacecraft for provision of the SRT on-board frequency standard, and the derivation of "time corrections" of the SRT wideband VLBI data based on phase difference (phase residual) measurements recorded by the GTS in real-

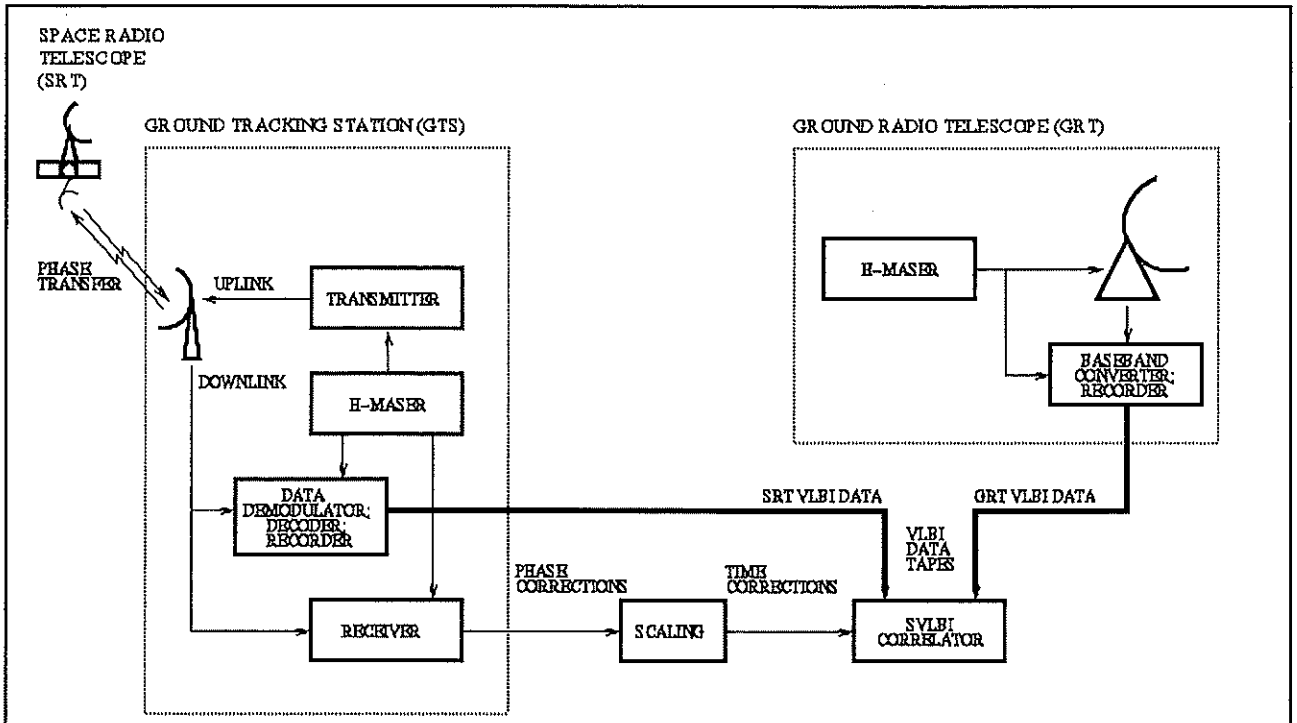

Fig. 2.4: Space VLBI System Simplified Overview.

time during each VLBI observation to effectively create a stable frequency standard and accurate timing system for the SRT in the correlation process.

In the broadest sense, the end to end Space VLBI process may be divided into four distinct phases: "data acquisition," "data playback and correlation," "fringe detection," and "image formation". "Data acquisition" consists of the reception, down-conversion, digitization and recording onto magnetic tape of the wideband astronomical data for the two radio telescopes of each interferometer baseline. "Data playback and correlation" consists of all tapes for all stations, having been shipped to the VLBI correlator, being played back at the correlator to reproduce the data samples at the output of the radio telescope digitizer, followed by correlation of all interferometer baselines. The output of the correlator consists of measurements of the fringe amplitude and phase for each interferometer baseline as a function of time, frequency, and polarization. "Fringe detection" consists of searching the correlator output for fringes, generally after averaging correlator output data samples over time and frequency to build up sufficient signal to noise ratio (SNR) that exceeds an established minimum detectable SNR or fringe detection threshold. For a given observation there is a general maximum integration time beyond which further integration over time will result in fringe amplitude degradation. This is generally referred to as the (maximum) "coherent integration time". Data are thus generally averaged in the fringe detection/analysis phases over this coherent integration time. Averaged correlated data of amplitude exceeding the established detection threshold constitute detected fringes. The "image formation" phase follows fringe detection; it relies on use of specialized image synthesis software, such as the NRAO Astronomical Imaging Processing System (AIPS), whose basic role is to "invert" the measured interferometer (detected fringe) amplitude and phase so-called "visibility" or (u,v)-plane samples to "image samples" via two-dimensional Fourier transformation.

Figure 2.4 shows the basic elements involved in the wideband data acquisition process for the SRT and GRT. For the GRT, data acquisition consists of reception, down-conversion to baseband, digitization and recording. Similar roles are performed for the "effective SRT," but for the "effective SRT" these functions are distributed between the SRT proper and its serving GTS.

Based on the GTS uplink phase reference, data are received, down-converted to baseband, and digitized on the spacecraft. The digitized VLBI data are subsequently modulated onto an RF carrier system and "telemetered" (downlinked) to the GTS, where the modulated data carrier is demodulated and "decoded" to recover the VLBI data, and then recorded onto magnetic tape. The "transmitter" in Figure 2.4 implements the uplink phase transfer signal; the "receiver" is responsible for forming essentially a phase difference function which is converted to units of time to form the time-series of "time corrections" necessary to create the accurate SRT clock within the correlator. This "scaling" function includes the addition of timing offsets for the effective SRT, providing a more complex form of "clock offsets" provided by GRTs to the VLBI correlator. Further details of the individual components of the Space VLBI end to end system are given in Chapter 5.

2.3.2. Mission Operations Overview

In this section, we provide an overview perspective of the mission operations structure of a "generic" Space VLBI system. The primary mission elements of a Space VLBI system operational structure are shown schematically in Figure 2.5, with specific reference to the ARISE mission. A more detailed description of Space VLBI Mission Operations is presented in Chapter 8, including a more detailed version of Figure 2.5 in Figure 8.1.

From the perspective of the operation of a Space-to-ground radio interferometer, the two ends of the interferometer baseline are represented by the ground radio telescope (GRT) and the Space radio telescope (SRT). In practice, a network or networks of GRTs observe in concert with the SRT to form the ensemble set of baselines to the SRT necessary for image formation. It is the increased length of the Space-to-ground baselines that provide the increased angular resolution of Space VLBI compared to ground-based VLBI. The GRT functions are unchanged in the Space VLBI system compared to their usual functions in ground-based VLBI. Accepting a central schedule, each GRT tracks the scheduled radio source and records the collected wideband VLBI data for shipment to the VLBI correlator. For each observation, each GRT is also responsible for delivering a log file to the correlator for correlation and VLBI calibration files to the appropriate Regional Server (as described in Section 8.8).

By contrast, the Space radio telescope (SRT) is significantly more complex than its GRT complement. Operation of the SRT requires a diverse set of world-wide distributed mission elements for SRT control, monitor, and tracking. We refer to this distributed set of mission elements as comprising an "effective Space radio telescope" or "effective SRT". The effective SRT elements consist of both Space and ground based components. Although considerably more complex, the effective SRT, however, is governed by the same master schedule that drives all GRTs. The primary component of the effective SRT is the ARISE spacecraft which carries the Space radio telescope proper, in the case of ARISE a 25 m inflatable reflector. The SRT support system is divided into separate flight operations (F-OPS) and ground operations (G-OPS) sections, which are controlled by independent operations groups. The (F-OPS) Flight Operations Group is responsible for spacecraft operations, including uplink and health and safety functions: sequences of control commands are periodically (e.g. once per week) uplinked to the spacecraft, and during the same sessions, on-board system health and safety data are retrieved. These so-called telemetry, tracking and control (TT&C) sessions are accomplished at a relatively low frequency link (for ARISE at X-band) using an omnidirectional spacecraft antenna. Higher data rate telemetry data containing science instrument and health and safety data, and the wideband VLBI data are obtained during communication sessions with the network of ground tracking stations. These sessions are indicated by the "Phase-Link" connection in Figure 2.5, and occur over a relatively high frequency link (for ARISE at Ka-band, near 37 GHz) using directional spacecraft and ground tracking station antennas. The (G-OPS) Ground Operations Group is responsible for the network of ground tracking stations (GTS) that communicate with the spacecraft during all scientific observations. By

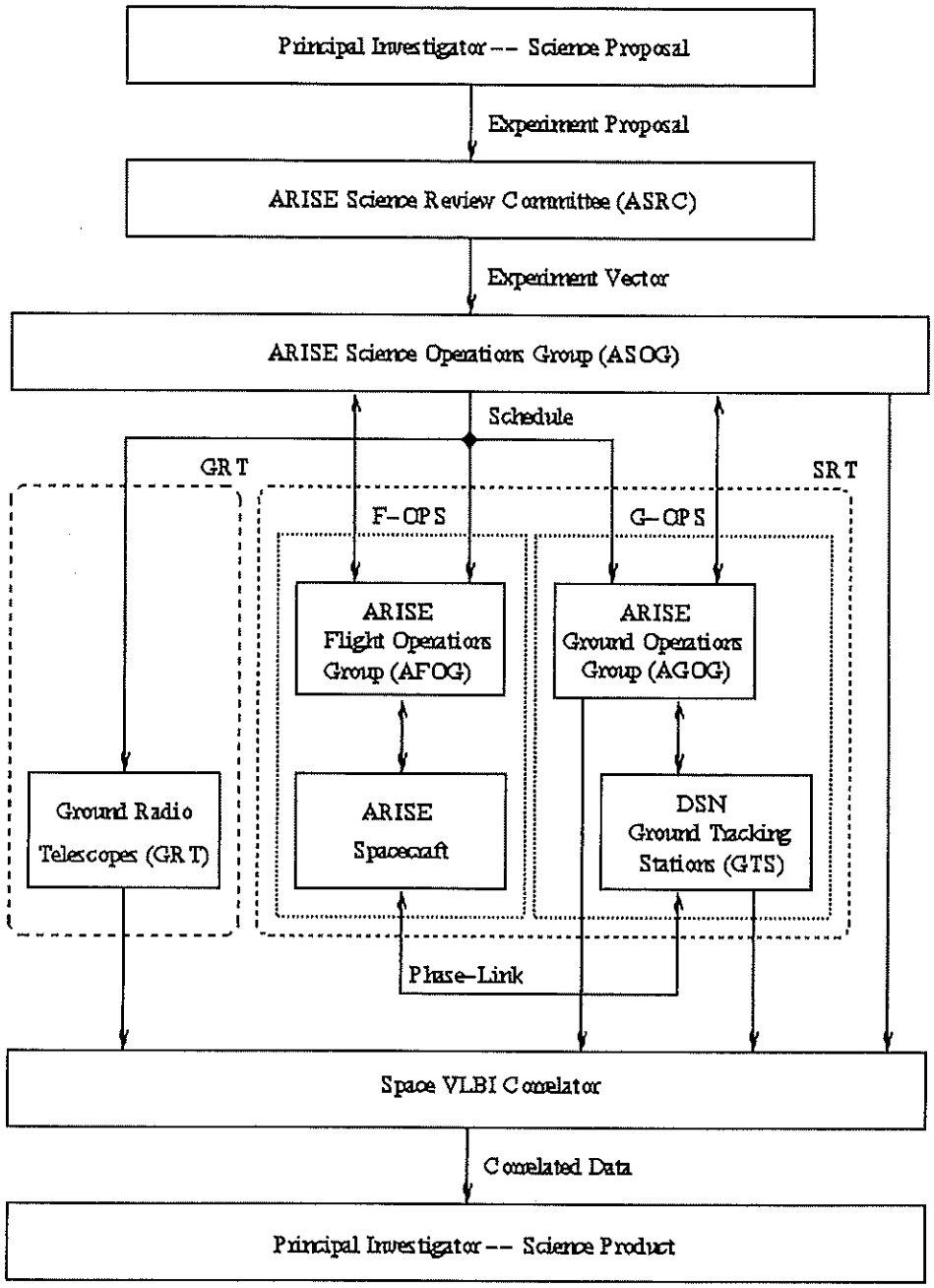

Fig. 2.5: ARISE VLBI Mission Operations Simplified Overview.

virtue of a high Earth elliptical SRT orbit, a network of GTSs is required for near continuous two-way phase link contact with the SRT during all scientific observation sessions. The NASA Deep Space Network (DSN) stations at Goldstone (California), Madrid (Spain), and Tidbinbilla (Australia), are used to support the Space VLBI missions. Other tracking stations, such as the Green Bank station in West Virginia, operated by NRAO, may also be used to provide additional coverage.

The primary functions of each GTS are to record the wideband VLBI data on magnetic tape for shipment to the correlator, and to record the spacecraft telemetry data for delivery to the flight and

operations groups (AFOG/ASOG). It also provides an uplink phase-stable frequency standard reference to the orbiting SRT, in the absence of an on-board frequency standard. This reference is used by all components of the spacecraft science and telecommunications subsystems. Additionally, in real-time the GTS measures a phase difference quantity based on the transponded SRT signal to provide a so-called time corrections file to the Space VLBI correlator to create an effective accurate and stable SRT clock to enable Space VLBI correlation. Wideband VLBI data gathered by the network of GRTs, and the GTSs on behalf of the SRT, are shipped to the Space VLBI correlator, where correlated data are sent to the principal investigator for each scheduled scientific observation. As stated earlier, ancillary files (log files, calibration files, and time correction files) are also sent to the correlator to enable correlation, fringe detection and image analysis.

The effective SRT flight (F-OPS) and ground (G-OPS) operations groups are responsible to the Science Operations Group, which is the primary scientific and operational authority. Day-to-day operations focus around the Science Operations Group in conjunction with its flight and ground operations groups. The network of GRTs function autonomously from the effective SRT. As described above and shown in Figure 2.5, overall Space VLBI operations is driven by a central "master schedule." This schedule is the end result of a scientific peer-reviewed process of proposals submitted by members of the astronomical community. As shown in Figure 2.5, this process is started with submission by principle investigators (PI) of scientific proposals to an international body known as the Science Review Committee (SRC), whose role it is to gauge the scientific and technical merit of all proposals and ultimately provide to the mission Science Operations Group a list of scientifically-ranked experiments known as the "experiment vector". The "experiment vector" results in the ultimate "master schedule" file, which as described above drives the GRT and SRT mission operations systems that support each scheduled scientific observation. The activities of experiment proposal, peer-review, and "experiment vector" generation are performed in Announcement of Opportunity (AO) cycles nominally at eight (8) to 12 month intervals. The delivery of an "experiment vector" to the Science Operations Group signifies the logical commencement of the operations phase for each AO cycle.

2.4 ARISE Mission Concept

ARISE will take advantage of the existing infrastructure in ground radio telescopes and systems used around the world for VLBI, including new instruments such as the Millimeter Array, and will explore a domain different from that studied by ground radio telescopes. Since Space VLBI depends on both the Space and ground elements, ARISE exemplifies the potential scientific gain from close cooperation between NASA and the National Science Foundation (NSF). The mission will be based on a 25 m Space-borne radio telescope operating at frequencies between 8 and 86 GHz, roughly equivalent to an orbiting element of the Very Long Baseline Array (VLBA). In an elliptical orbit with an apogee height of 40000-50000 km, ARISE will provide resolution of 15 microarcseconds or better, 5-10 times better than that achievable on the ground. At frequencies of 43 and 86 GHz, the resolution of light weeks to light months in distant quasars will complement the gamma-ray and X-ray observations of high-energy photons, which come from the same regions near the massive black holes. At 22 GHz, ARISE will image the H_2O maser disks in active galaxies more than 15 Mpc from Earth; those disks are not adequately resolved from the ground. Gas motions in the disks will be measured on scales of light months, several orders of magnitude smaller than the velocity fields sampled by optical telescopes, probing accretion physics and giving accurate measurements of black-hole masses. ARISE also will study gravitational lenses at resolutions of tens of microarcseconds, yielding important information on the dark-matter distribution and on the possible existence of compact objects with masses of $10^3 M_o$ to $10^6 M_o$.

The critical technology for ARISE is the 25 m aperture. Inflatable structures technology, under development for a variety of applications and users, is the current strawman choice for the main reflector, although other concepts also are being explored. On-board low-noise amplifiers and cryogenic coolers are being produced for missions such as MAP, Planck, and FIRST; MAP will be launched in 2000, carrying amplifiers in the same frequency range needed for ARISE. Advances in recording and correlation systems, to increase the VLBI data rate to Gigabits per second (Gbps), are under development. Given sufficient funding for the antenna and data systems technology, ARISE could be ready for launch by 2008 for a total cost under $400 million. It is anticipated that ARISE would be the forerunner of future missions that would improve the resolution and imaging capability by orbiting multiple spacecraft simultaneously, and observing at higher (mm and sub-mm) frequencies.

Chapter 3

Observational Capabilities of the ARISE Mission

3.1 Science Requirements

The science requirements for ARISE derive primarily from its main science goal of "Zooming in on Black Holes," which has been discussed at length in Sections 1.1-1.2. The requirements and their origins are discussed below.

3.1.1 Frequency Coverage

The baseline VLBI observing frequencies selected for ARISE are 8, 22, 43, and 86 GHz. All are standard VLBI frequencies. Almost all ground radio telescopes (GRT) (about 50) are equipped at 8 and 22 GHz, while some do not have sufficiently accurate surfaces for 43 or 86 GHz observations. We expect there to be about 20 separate GRTs at each of 43 and 86 GHz, spread among the U.S., Europe, Australia, and Japan, available in the ARISE era.

The two highest frequencies, 43 and 86 GHz, will supply the highest angular resolution, and are needed to observe "blazars" in the region of the spectrum where their cores are optically thin. At lower frequencies, these objects are optically thick, so that we see only to the surface where the optical depth is unity, rather than getting the full picture of the radio components. The 22 GHz frequency is required because it includes the spectral line in which water megamasers emit (22.235 GHz); these are among the key targets for ARISE. (Four transitions of the SiO maser at 42.820, 43.122, 85.640, and 86.244 GHz, also are present in late-type stars and may be observed by ARISE.) Finally, 8 GHz is the most sensitive VLBI frequency available on GRTs, including the large 70 m antennas of NASA's Deep Space Network (DSN), and will provide the best detection threshold. This enables studies of weak gravitational lenses, as well as other weak VLBI sources such as supernova remnants and stellar coronae. 60 GHz is an optional frequency which will be included if there is no significant additional cost. This is not a VLBI frequency, because the Earth's atmosphere is opaque to 60 GHz radiation. However, it does include a complex of lines emitted by molecular oxygen, and can be observed by ARISE in single-dish mode in order to map out the temperature and density structures in galactic star formation regions.

The total instantaneous bandwidth that will be observed is no more than 2 GHz. This may be observed in one polarization or may be split between polarizations. At the 86 and 43 GHz bands,

the VLBA will have standard bandpasses of (approximately) 80-95 GHz and 40-45 GHz, respectively, so having tunability over this range is adequate. At 22 GHz, sufficient tuning capability must exist to observe water megamasers at distances up to redshifts of z=0.2, requiring that tuning to frequencies as low as 18 GHz must be possible. Wideband 18-26 GHz receivers will be available in the ARISE era, and would be a good choice. At 8 GHz, a 2 GHz bandwidth is a minimum, in order to permit single-polarization observations at the full 8 Gbps data rate[1]. This also will provide a significant range of frequencies available instantaneously, in order to enable imaging by multi-frequency synthesis and studies of Faraday rotation. Reaching the methanol line at 6.6 GHz is highly desirable. Indeed, reaching 5 GHz either simultaneously with 8 GHz or with a separate feed is highly desirable in order to make continuum images using multi-frequency synthesis and to map spectral indices in jet sources.

3.1.2 Sensitivity

The desired detection threshold for a continuum radio source, using ARISE on a baseline to a 25 m telescope, is near 1 mJy at the lowest frequencies, ranging upward to 10 mJy at 43 GHz and 100 mJy at 86 GHz. At frequencies from 5 to 22 GHz, this detection threshold is driven by the need to observe weak gravitational lenses and supernovae in external galaxies. For the main spectral-line targets, namely the galaxies with water maser lines at 22 GHz, the requirement is to detect a 50 mJy line spread over 1.3 km/s at a significance of at least 3-5 times the noise, on an ARISE baseline to a large GRT such as the 100 m Green Bank Telescope (GBT). This will allow observations of all known water masers and those that are likely to be discovered over the next few years.

At 43 GHz, the detection threshold is driven by the need to have a selection of over 1000 blazars (highly variable, core-dominated radio sources), whose inner jets can be imaged. It is anticipated that at least this large a sample of gamma-ray blazars will be available from the Gamma-ray Large Area Space Telescope (GLAST) [3.1]. The 100 mJy threshold at 86 GHz is driven by the requirement that there be at least 100 detectable blazars with brightness temperatures near 10^{12} K. Source counts indicate that there are more than 200 blazars with total 86 GHz flux densities greater than 500 mJy. Assuming brightness temperatures of 10^{12} K (or, equivalently, a visibility of approximately 20% on a 50000 km baseline), this detection threshold enables the detection and imaging of over 100 objects with ARISE.

The RMS noise, and hence the detection threshold, on a baseline between antennas A and g (ARISE and ground) is proportional to:

$$\sqrt{\frac{Ts_A \times Ts_g}{Ae_A \times Ae_g \times df \times dt}}$$

where Ae_i is the effective area of antenna i (product of the physical area and the total aperture efficiency), Ts_i is the system temperature of antenna i, df is the total bandwidth (proportional to the data rate), and dt is the coherent integration time. Often, we characterize the sensitivity of a single telescope by its System Equivalent Flux Density, or SEFD, in Jy. This is given by:

$$SEFD_i = 2.76 \times 10^3 \frac{Ts_i}{Ae_i}$$

where Ts_i is in Kelvin and Ae_i is in square meters.

[1] Throughout this document, note that "8 Gbps" really means 8.192 Gbps or 8192 Mbps, "4 Gbps" really means 4.096 Gbps or 4096 Mbps, and so on.

Assuming a detection threshold of 7 times the RMS noise, the resulting fringe-detection threshold is given by:

$$S_{min} = 120 \text{ mJy} \times \sqrt{\frac{SEFD_A/3200 \text{ Jy} \times SEFD_g/4200 \text{ Jy}}{DR/8 \text{ Gbps} \times \tau/15 \text{ s}}}$$

where DR is the data rate and τ is the coherent integration time.

Tables 3.1-3.8 give the sensitivity results for the baseline ARISE mission design, which has a 25 m antenna with aperture efficiency ranging from 0.5 at the lowest frequency to 0.08 at the highest frequency, system temperatures of about 0.5 K x freq (GHz), and a data rate of 8 Gbps. Different quantities can be traded off against each other. For example, the same 86 GHz sensitivities as those given in the tables can be achieved if the aperture efficiency of the ARISE antenna at 86 GHz is doubled to 0.16 and the data rate is halved to 4 Gbps.

In order to meet the sensitivity goals, the antenna blind pointing accuracy must be within 10% of the full-width at half maximum (FWHM) of the antenna primary beam pattern. This corresponds to three (3) arcseconds at 86 GHz, six (6) arcseconds at 43 GHz, 11 arcseconds at 22 GHz, and 30 arcseconds at 8 GHz. Offsets of this magnitude will result in gain losses of more than 5% in the nominal pointing direction, so they must be known with sufficient accuracy to meet the 5% calibration goal (see Section 3.1.6).

Quantity	Nominal	Possible Range
Frequency Span	8 - 9 GHz	5 - 9 GHz
T_{sys}	12 K	8 - 15 K
Aperture Efficiency	0.50	0.4 - 0.6
SEFD	130 Jy	75 - 590 Jy
Coherence Time (C=0.9)	350 s	100 - 2000 s
Data Rate	4 Gbps	1 - 4 Gbps

Table 3.1: ARISE Sensitivity vs. Frequency - 8 GHz.

Quantity	Nominal	Possible Range
Frequency Span	21 - 23 GHz	18 - 23 GHz
T_{sys}	16 K	12 - 25 K
Aperture Efficiency	0.38	0.3 - 0.5
SEFD	240 Jy	130 - 1280 Jy
Coherence Time (C=0.9)	150 s	60 - 1000 s
Data Rate	8 Gbps	1 - 8 Gbps

Table 3.2: ARISE Sensitivity vs. Frequency - 22 GHz.

Quantity	Nominal	Possible Range
Frequency Span	42 - 44 GHz	40 - 45 GHz
T_{sys}	24 K	20 - 35 K
Aperture Efficiency	0.24	0.2 - 0.35
SEFD	560 Jy	320 - 2700 Jy
Coherence Time (C=0.9)	60 s	20 - 400 s
Data Rate	8 Gbps	1 - 8 Gbps

Table 3.3: ARISE Sensitivity vs. Frequency - 43 GHz.

Quantity	Nominal	Possible Range
Frequency Span	84 - 88 GHz	80 - 90 GHz
T_{sys}	45 K	30 - 80 K
Aperture Efficiency	0.08	0.08 - 0.2
SEFD	3200 Jy	850 - 16000 Jy
Coherence Time (C=0.9)	15 s	5 - 100 s
Data Rate	8 Gbps	1 - 8 Gbps

Table 3.4: ARISE Sensitivity vs. Frequency - 86 GHz.

Quantity	Nominal	Possible Range
8 GHz	1.9 mJy	0.6 - 15 mJy
22 GHz	4.5 mJy	1.3 - 46 mJy
43 GHz	15 mJy	4.4 - 162 mJy
86 GHz	120 mJy	25 - 1400 mJy

Table 3.5: ARISE 7-sigma Continuum Sensitivity to VLBA antenna (25 m).

Quantity	Nominal	Possible Range
8 GHz	0.4 mJy	0.1 - 3.6 mJy
22 GHz	0.8 mJy	0.2 - 8.3 mJy
43 GHz	2.5 mJy	0.7 - 28 mJy
86 GHz	26 mJy	5.5 - 300 mJy

Table 3.6: ARISE 7-sigma Continuum Sensitivity to GBT (100 m).

Quantity	Nominal	Possible Range
8 GHz	0.2 Jy	0.1 - 1.1 Jy
22 GHz	0.5 Jy	0.1 - 1.9 Jy
43 GHz	1.2 Jy	0.3 - 4.7 Jy
86 GHz	7 Jy	1.4 - 28 Jy

Table 3.7: ARISE 7-sigma Spectral Line Sensitivity to VLBA Antenna (1.3 km/s line).

Quantity	Nominal	Possible Range
8 GHz	0.05 Jy	0.02 - 0.25 Jy
22 GHz	0.1 Jy	0.03 - 0.35 Jy
43 GHz	0.2 Jy	0.05 - 0.8 Jy
86 GHz	1.5 Jy	0.3 - 6 Jy

Table 3.8: ARISE 7-sigma Spectral Line Sensitivity to GBT (1.3 km/s line).

3.1.3 Digitization

The observing and recording data rate must have a fixed maximum value due to limitations on the Space-to-Earth downlink and the VLBI recording system. The planned data rate for ARISE is 8 Gbps. For a fixed data rate and sampling of a baseband (IF) channel at the Nyquist rate, 1-bit and 2-bit quantization of the noise-like radio signals give approximately equal sensitivity, while higher-order quantization gives much poorer sensitivity. However, 2-bit quantization gives much higher

sensitivity for spectral-line sources, and also minimizes the requirement on the instantaneous bandwidth that must be observed. Therefore, the ARISE requirement is for 2-bit quantization, with a capability for 1-bit quantization. The *maximum* sample rate required per baseband (IF) channel is 512 Msamples/s (see Section 3.1.4), or 1024 Mbps per baseband (IF) channel at 2-bit quantization.

3.1.4 IF Channelization

The primary channelization requirements are described below. These requirements must be met by both the Space radio telescope (SRT) and all participating ground radio telescopes (GRT), and drive engineering requirements on the Space and ground acquisition systems as well as the VLBI correlators.

(1) ARISE must cover a total bandwidth of 2 GHz (either 2 GHz in a single, selectable (circular) polarization, or 1 GHz in each of two polarizations).
(2) ARISE must have velocity resolution of 0.1 km/s at 22 GHz, or a spectral resolution of 8 kHz, in order to have several channels across the line features seen in water megamasers. This resolution must be achieved over a total spanned bandwidth of 256 MHz at each polarization, but can be used over portions of the bandwidth where the spectral lines actually exist.
(3) The line features must be observable simultaneously with *continuous* wide-bandwidth continuum coverage in order to permit simultaneous detection of spectral-line and continuum features.

Implementation Options

Here we present implementation options for the wideband VLBI data processing which would satisfy the scientific requirements presented above. One option to satisfy the first requirement is with the use of eight (8) 256 MHz baseband (IF) channels, each sampled at 512 Msamples/s at 2-bit quantization. This would satisfy the requirement of 2 GHz total bandwidth. It is required to sample at least four separate frequency channels for multi-frequency synthesis, so a logical choice is to have four independently tunable local oscillators (LO). This would enable the eight channels to be both upper and lower sideband at a single polarization, or upper-sideband at both polarizations.

Fulfilling the second requirement of dividing the 256 MHz baseband (IF) channels into 8 kHz channels for spectral-line work could be done in any of several ways. The final choice must depend on cost and technology tradeoffs for both the Space and ground systems. Three possible options are listed below; other variants on these also could be envisioned.

(1) Use a correlator with the capability of placing 32,768 spectral channels across each of two (2) 256 MHz baseband (IF) channels. This would result in large data volumes, and is four times the number of channels (with the same spectral resolution) planned for the NRAO "VLA Upgrade" correlator at the time of writing. The third requirement of wideband continuum coverage would be satisfied automatically.
(2) Use on-board filters to reduce the baseband (IF) channels to 16 MHz bandwidth, which might be sampled at the Nyquist rate of 32 Msamples/s or oversampled at 512 Msamples/s. In the former case, it would be necessary to have eight (8) independently tunable LOs, so that eight (8) frequency channels could be targeted in each polarization. Simultaneous sampling of two (2) 256 MHz channels at the Nyquist rate could be achieved in the latter case, automatically providing the simultaneous continuum coverage, although multiple correlator passes might be required.
(3) Downlink two (2) 256 MHz baseband (IF) channels, then digitally filter the data on the ground (e.g. at the correlator) to create eight (8) or sixteen (16) 16 MHz channels. The correlator

would then generate 2048 spectral points per filtered channel, providing the desired spectral resolution of 8 kHz. A second correlator pass with unfiltered data and coarser spectral resolution would provide the required wideband continuum data.

3.1.5 Polarization

Dual circular polarization observations must be possible at all VLBI frequencies, in order to enable polarization imaging of continuum sources. Circular rather than linear polarization is necessary for detection of sources with weak linear polarization and for prevention of a loss of SQRT(2) signal-to-noise ratio upon correlation with GRTs using circular polarized feeds. Linear polarization would be acceptable only if GRTs are similarly equipped, and still is not the preferred option because of the desire to detect weak linearly polarized signals.

Dual polarization is required for spectral-line sources in order to achieve the sensitivity requirement given in Section 3.1.2. Using a single polarization causes a degradation of SQRT(2) in the available sensitivity.

Isolation between the two polarizations should be 3% or better in voltage, to match the polarization purity available at most GRTs.

3.1.6 A-priori Calibration Accuracy

A-priori amplitude calibration of the ARISE antenna must have an accuracy of 5%; this includes the combination of antenna gain in the source direction and total system temperature (i.e., the SEFD of Section 3.1.2).

3.1.7 Sky Coverage and Duty Cycle

A Sun-avoidance angle no greater than 30 degrees and an Earth-avoidance angle no greater than five (5) degrees are required for the pointing direction of the Space radio telescope (SRT). These requirements ensure that individual radio sources are accessible for at least two (2) months per year.

ARISE should provide a capability for full mapping of a source within a single orbit, which will be the typical observation time (12-14 hours). Depending on the scientific goal, some observations will last only a few hours.

The observing duty cycle on a science source must average at least 70-80% of a full orbit (80% is the target). Imaging capability degrades for coverage less than 70-80%, with the amount of degradation highly dependent on the details of a particular observation. Coverage less than 60% opens large holes in the aperture-plane coverage which is unacceptable. The duration of the orbit in which science data is not gathered would include losses for reasons such as the following:

(1) Unloading accumulated momentum in the reaction wheels.
(2) Calibration activities (e.g. pointing).
(3) Unavailability of ground tracking stations (GTS).
(4) Other miscellaneous engineering causes.

This requirement arises from the need to adequately fill the (u,v)-plane for imaging.

3.1.8 Orbit

Apogee Altitude

The orbit must be highly elliptical in order to adequately sample the (u,v)-plane. The minimum apogee altitude is 40000 km, set by the requirement to achieve baselines of approximately four (4) Earth diameters (50000 km). The scientific drivers for this requirement are as follows:

(1) Resolution of six (6) light months at 86 GHz, and one (1) light year at 43 GHz, even for the most distant blazars, with a resolution of better than 100 light days at 86 GHz for more than 50 blazars.
(2) Resolution of 0.03 pc for a water megamaser galaxy at a distance of 100 Mpc, in order to have six (6) pixels across the inner diameter of a maser disk.
(3) Capability of measuring maser proper motions of 200 km/s over three (3) years in a maser disk at 20 Mpc distance.

At the time of writing, it is believed that the maximum apogee height should be well below 100000 km in order to enable detection of a significant number of blazars at brightness temperatures near 10^{12} K (see Section 3.3.1). If the ARISE aperture efficiency at 86 GHz were increased by a factor of four (4) to greater than 30%, with the data rate remaining at 8 Gbps, apogee heights near 100000 km would be permitted since a significant number of these blazars appear then to be detectable.

Perigee Altitude

The selection of the perigee altitude should allow for overlap between ground-ground and ground-Space telescope baselines for calibration purposes.

Inclination

The orbit inclination should be chosen to maximize the north-south interferometer baselines between ARISE and the ground, while maintaining a reasonably circular beam. An orbital inclination equal to or greater than 30° is acceptable.

Changes in Orbit Plane

In order to achieve good imaging capability for most of the sky at some time during the mission, it is required that in its lifetime the ARISE orbital plane rotate through nearly a full cycle in the node angle and in the argument of perigee. For an apogee height of 40000 km, if that rotation is generated by orbit precession alone, this implies a mission lifetime of five (5) years and a perigee height of 2000 km, or a lifetime of six (6) years and a perigee height of 3000 km. Apogee heights significantly above 50000 km would require a lifetime of 10 years or more for the orbit precession, and would be unacceptable. The lifetime requirements generated by the need to rotate the orbital plane may be relaxed if that plane can be rotated by "active" spacecraft propulsion (which could include acceleration by "solar sailing").

Orbit Determination Accuracy

An orbit determination accuracy of 10 cm is required. This accuracy is sufficient so that the orbit error does not limit the coherent integration time at any of the VLBI observing frequencies. It permits the possible extension of the integration time to as much as an hour by means of phase-referencing the GRTs in order to calibrate the local atmospheric propagation effects.

3.1.9 Mission Lifetime

The minimum required lifetime of three (3) years is derived from the need to monitor individual radio sources in blazars through the generation and early decay of relativistically moving radio components, and the need to measure proper motions in megamaser galaxies at distances up to 20 Mpc. If the orbit plane is rotated only by precession, the minimum lifetime is five (5) to six (6) years depending on the orbit, in order to permit high-quality imaging of sources in all directions during the lifetime of the mission (see Section 3.1.8).

3.2 ARISE Spacecraft Constraints

The ARISE orbit has a number of constraints which may make it impossible for the Space radio telescope (SRT) to observe a given source under certain conditions. The SRT observing constraints are summarized below.

3.2.1 Sun

ARISE cannot observe sources within an sun angle (SA) of 30° where the sun angle is defined to be the angle between the source and the sun (see Section 3.1.7).

3.2.2 Moon

ARISE cannot observe sources occulted by the Moon.

3.2.3 Earth

ARISE cannot observe sources occulted by the Earth, and has a five (50 degree maximum Earth avoidance angle.

3.2.4 Eclipses

ARISE cannot observe during eclipses and during a half-hour recovery period after each eclipse.

3.3 ARISE Orbit Trade-off Study

The ARISE orbit is one of the major factors in determining the science return from the ARISE mission. The final orbit selection will be made after a detailed trade-off between scientific goals and spacecraft design, and after the complete results from the first Space VLBI mission VSOP, on-going at the time of writing, are known.

However, a preliminary study of the ARISE orbit with regard to meeting the science goals outlined in Section 3.1 has been performed. A range of possible values for the orbital elements are provided in the science requirements and are summarized in Table 3.9.

To reduce the number of tradeoffs at this stage, the following orbit parameter options have been used:

(1) Apogee altitudes: 40000, 50000, 70000, 100000 km
(2) Perigee altitudes: 3000, 5000 km
(3) Inclinations: 30° , 60°

A preliminary analysis of the impact of the orbital elements on the science return performed in the following sections leads to the recommendation of a "nominal" orbit for ARISE. However, a more complete orbital analysis needs to be performed to verify this preliminary assessment.

Quantity	Possible Range
Semi-major axis	15000 - 50000 km
Eccentricity	0.25 - 0.75
Apogee Altitude	40000 - 100000 km
Perigee Altitude	1000 - 6000 km
Inclination	30 - 63.4 deg
Orbital Period	5 - 30+ hr
Perigee Precession	0 - 280 deg/yr
Node Precession	5 - 180 deg/yr

Table 3.9: ARISE Nominal Orbit Parameters.

3.3.1 Orbit Sensitivity

There are several different approaches to examining the ARISE sensitivity. The approach we adopt here is a quasi-physical approach. Given the 7-σ sensitivities from ARISE to a single VLBA (25 m) antenna of 1.9, 4.5, 15, and 120 mJy at 8, 22, 43, and 86 GHz, respectively, we may ask the following question: on a given ARISE baseline, what type of sources are we able to detect? In this analysis, a source is represented as a single Gaussian component of total flux density, S_o, and brightness temperature, T_o. In Figure 3.1, the detection limits for the four (4) ARISE observing bands for three (3) different values of baseline length (40000, 70000, and 100000 km) are shown. The straight line corresponds to when the visibility function reaches a value of 0.9. Thus, to the right of this line, even though a source might be detected, we would be unable to determine its size. With this simple Gaussian source model, the minimum brightness temperature that can be detected on a baseline of length D with a detection limit of S_d is given by:

$$T_{bmin} = 3.1 \times 10^8 \, (D/10^4 \text{ km})^2 \, (S_d/\text{mJy}) \text{ K}$$

This minimum detectable brightness temperature is for a source with a flux density of $2.7S_d$. From Figure 3.1, we can see which sources can be detected as a function of observing frequency and baseline length. As an alternative to representing a Gaussian source by its total flux density and brightness temperature, we can represent it by its total flux density and Full Width Half Maximum (FWHM) size. In Figure 3.2, we show what sources can be detected as a function of these two source parameters and baseline length. We can see from this figure the size scales that will be probed by the different ARISE observing bands. The 0.9 visibility straight line is different for each observing band.

These figures show that the major constraint on the apogee height is provided by the constraint to be able to detect a sufficient number of sources at 86 GHz on the longest ARISE baselines. Current understanding of the maximum brightness temperature possible in the cores of radio sources indicates that there are probably few sources with maximum brightness temperatures in excess of the 10^{12} K Inverse Compton (IC) limit in the emitting component rest frame. In our observational frame, the observed brightness temperature as plotted on the x-axis in Figure 3.1 exceeds the IC limit by the factor $\delta/(1+z)$, where δ is the Doppler factor of the component and z is the redshift of the radio source. Typically, values of these parameters are 10 and 1 respectively. Thus, the

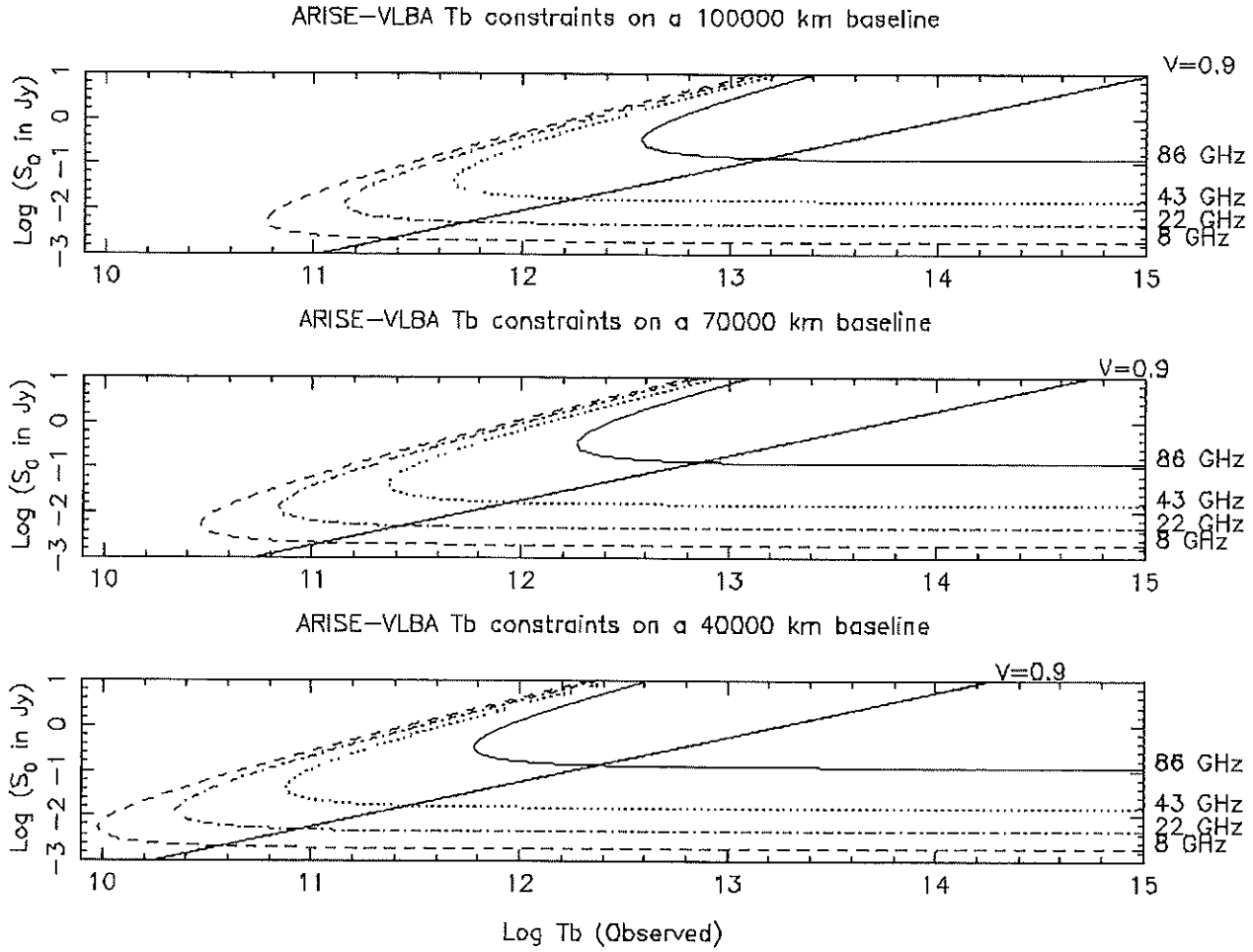

Fig. 3.1: Detection Limits for the Four (4) ARISE Observing Bands as a Function of Source Flux Density (*So*) and Maximum Brightness Temperature (*Tb*) for Three (3) Values of Baseline Length. Sources at the right of the curved lines are detectable, while sources to the left of the diagonal lines are resolvable.

observed brightness temperature limit is roughly 5 x 10^{12} K. Thus, as Figure 3.1 shows, orbits will apogee heights of 100000 km will only be able to detect sources at 86 GHz that have brightness temperatures in excess of the maximum expected observed brightness temperature. Thus, from a scientific perspective, orbits with apogee heights as large as 100000 km may produce a very low science return, since with this apogee height it may not be possible to detect any sources on the longest baselines. Thus, orbits with apogee heights of 40000 km or 50000 km are preferred over an apogee height of 100000 km.

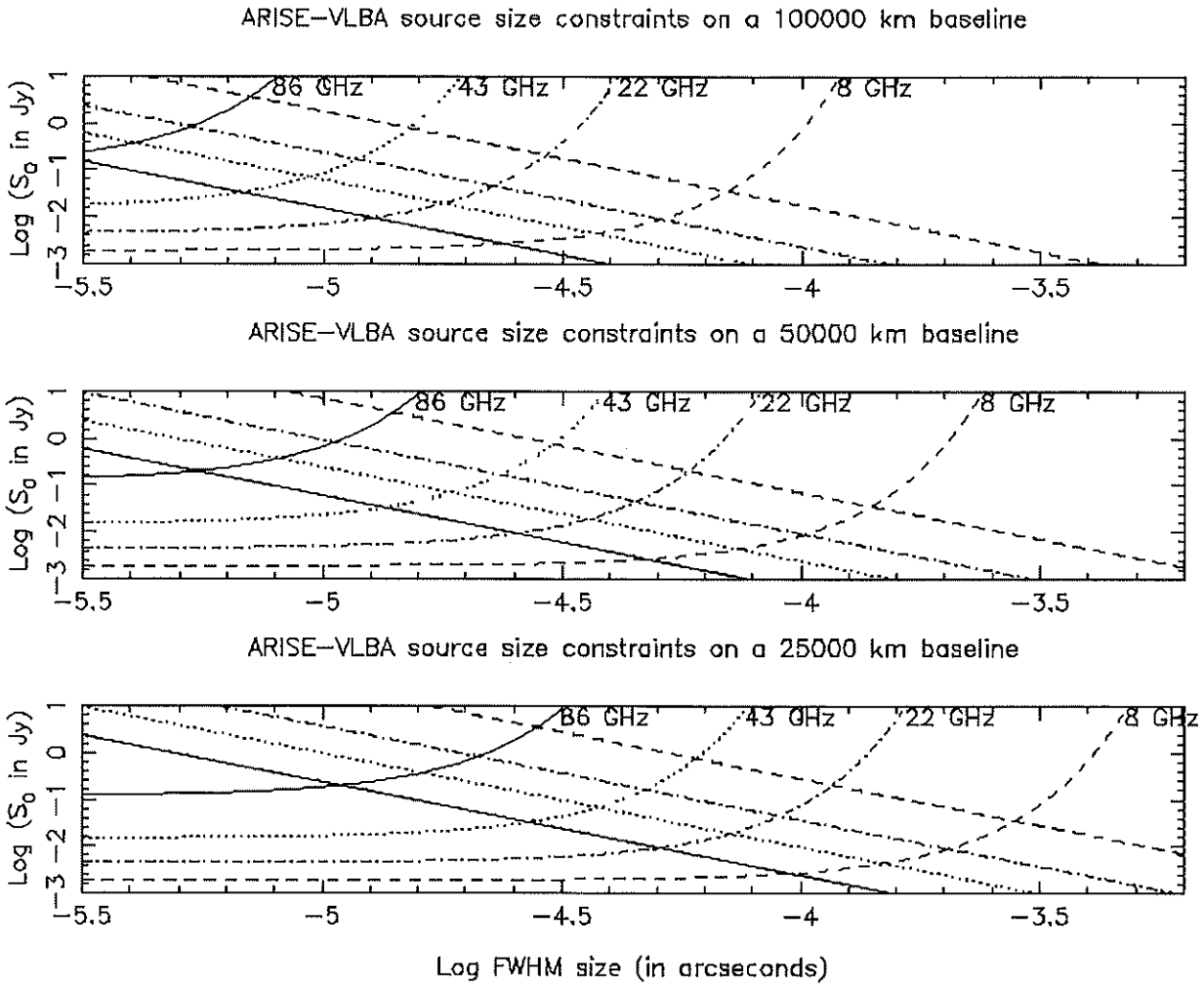

Fig. 3.2: Detection Limits for the Four (4) ARISE Observing Bands as a Function of Source Flux Density (*So*) and FWHM Size For Three (3) Values of Baseline Length. Sources above the curved lines are detectable, while sources below the diagonal lines are resolvable.

3.3.2 Orbit Normal and (u,v)-Coverage

One of the prime goals of the ARISE mission is to image sources with unprecedented angular resolution. In Figure 3.3, we show the (u,v)-coverage obtained for a 24 hour observation with ARISE (in its nominal orbit) and the VLBA, as a function of the equatorial coordinates of the source. The highest angular resolution (u,v)-coverage is obtained for sources that lie along the orbit normal and anti-normal directions (which are represented by the letters N in Figure 3.3). In equatorial coordinates (α, δ), these directions are given by (Ω - 6h, 90°-i) and (Ω + 6h, i-90°). Note that the (u,v)-coverage is essentially linear when the source lies in the orbit plane, shown as a sinusoidal curve in Figure 3.3, and where the apogee and perigee direction are labeled A and P, respectively.

In producing Figure 3.3, a simplified version of the nominal ARISE spacecraft constraints has been assumed. These simplified constraints are:

(1) ARISE cannot observe sources within 30 degrees of the Sun.
(2) ARISE cannot observe during eclipse.

(3) There is a limited field of view of the on-board telemetry antenna such that communication is only possible when a ground tracking station (GTS) lies within a cone of half-angle 120 degrees centered on an axis which is orthogonal to both the main antenna pointing axis and the solar panel axis.

The impact of the solar constraints is clearly visible on the plot with the 30 degree solar exclusion zone plotted. As the sun moves along the ecliptic throughout the course of a year, so does this exclusion zone. Poor quality (u,v)-coverages are obtained for sources south of the celestial equator because the VLBA is only able to observe these source for a limited number of hours a day (if at all). It is better for ARISE to observe these sources with GRT arrays in the southern hemisphere.

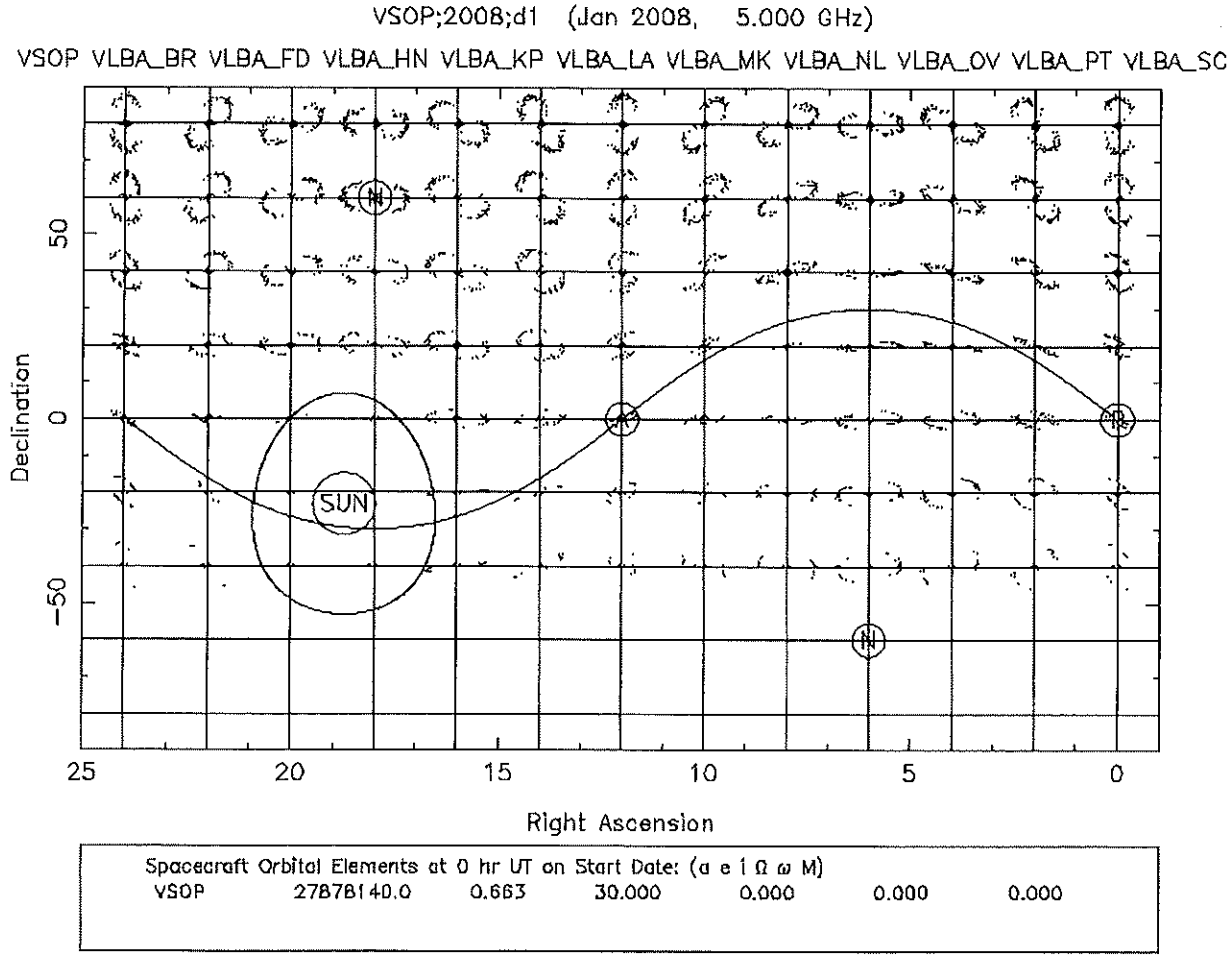

Fig. 3.3: All-Sky (u,v)-Coverages for a One (1) Orbit Observation with Nominal ARISE Orbit and the VLBA.

3.3.3 Precession of the Orbital Elements

Due to nodal precession ($d\Omega/dt$), the positions in the sky of the orbit normal and anti-normal directions precess with time. Since the orbit normal direction determines the (u,v)-coverage for a given source, the precession rate of the orbit normal is a critical factor in determining the science return from the ARISE mission. At the moment, both the injection argument of perigee, ω_o, and the right ascension of the ascending node, Ω_o, are free parameters.

It is instructive to examine how the derived orbital parameters P (orbit period), dΩ/dt (nodal precession), and dω/dt (perigee precession) depend on h_p, h_a, and i (perigee altitude, apogee altitude, and inclination, respectively). In Figure 3.4, we show how the orbital period (P) depends on h_p and h_a. Orbits with apogee heights of 40000 or 50000 km have periods which coincide nicely with the typical ground-based VLBI observation length. Increasing the apogee height, and hence the orbital period, much beyond these values has some disadvantages, since the typical imaging observation must last at least one orbit, and radio source structures may vary on time scales appreciably shorter than 24 hours.

In Figures 3.5 and 3.6, we show the nodal precession rate, dΩ/dt, for orbit inclinations of 60° and 30°, respectively. By lowering the inclination from 60° to 30°, we increase the nodal precession rate, for a given h_p and h_a, by a factor of sqrt (3) (dΩ/dt is proportional to cos i), as is shown in Figure 3.6. Even so, the nodal precession rate is only -58 degrees/yr for an orbit with a 3000 km perigee height and 40000 km apogee height and 30° inclination. By comparison, the nodal precession rate of the HALCA spacecraft of the VSOP mission is 228°/yr, for a mission lifetime of three (3) years. Thus, even with a perigee height as low as 3000 km, the nodal precession period is 6.2 years unless some non-gravitational force (e.g. ion-engine or solar sail) can be used to increase the nodal precession rate. Techniques to increase the nodal precession rate shall be examined in future ARISE studies.

One consequence of lowering either the perigee height or the orbit inclination is to increase the perigee precession rate (since dω/dt is proportional to $5\cos^2 i - 1$). At an inclination of 60°, dω/dt is very low since this inclination is close to i = 63.4°, where dω/dt = 0. In Figures 3.7 and 3.8, we show dω/dt as function of apogee and perigee for orbits with 60° and 30° inclination, respectively. For h_p = 3000 km, h_a = 40000 km, and i = 30°, one obtains dω/dt = 91°/yr. The major effect of perigee precession is to change the amount of time ARISE can be tracked with a ground tracking network such as the DSN. This issue is examined in Sections 3.3.4 and 3.3.5.

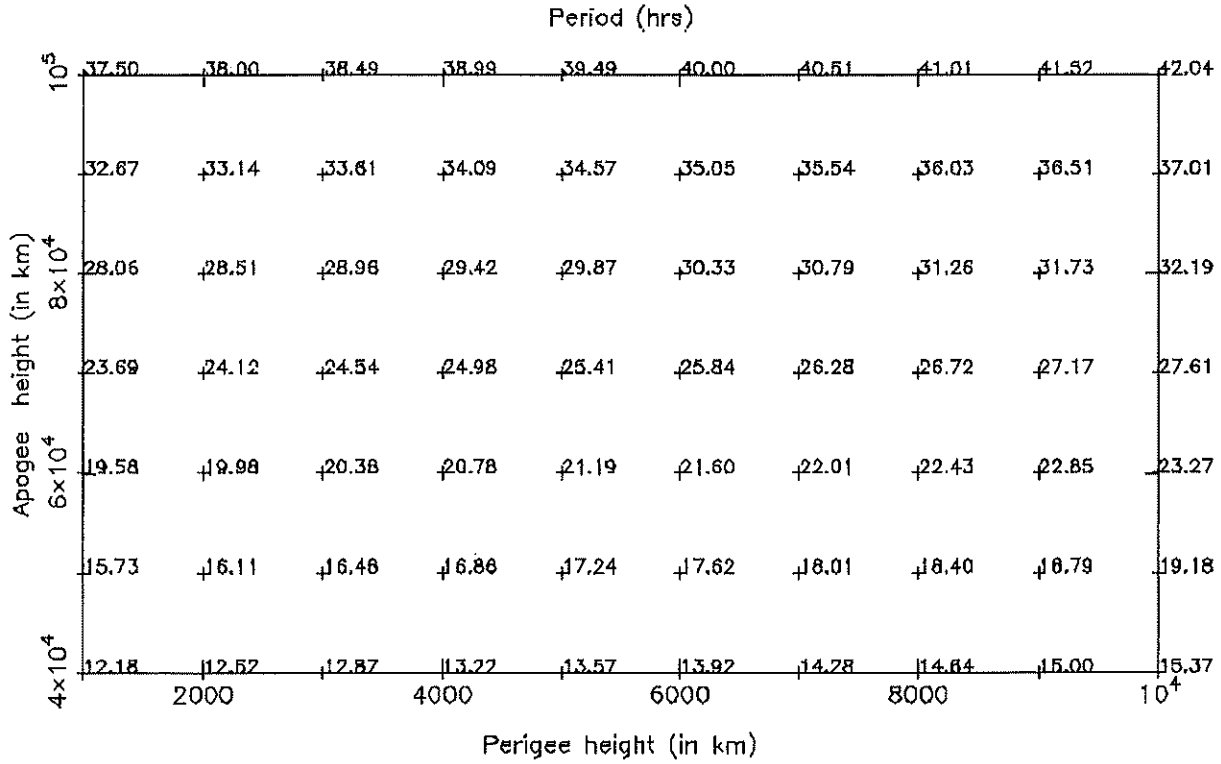

Fig. 3.4: Orbital Period as a Function of Perigee and Apogee Heights.

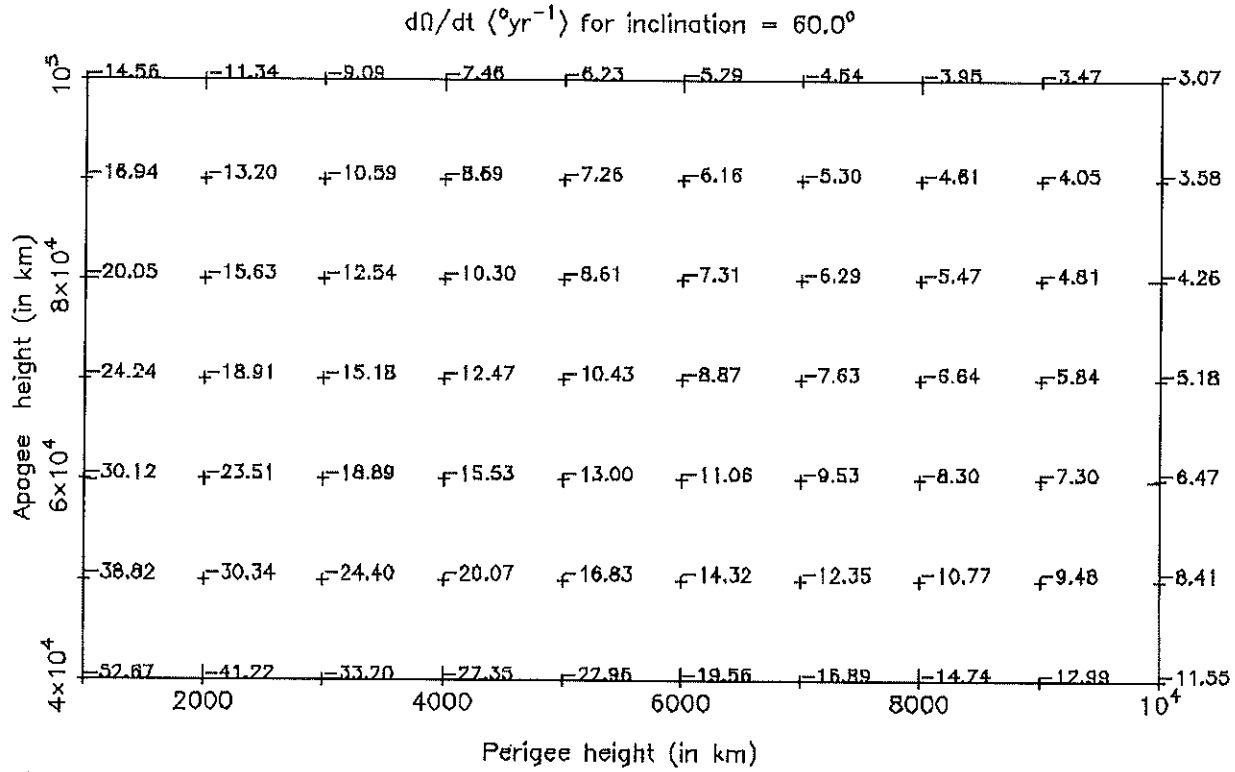

Fig. 3.5: Nodal Precession Rate dω/dt as a Function of Perigee and Apogee Heights for i=60°.

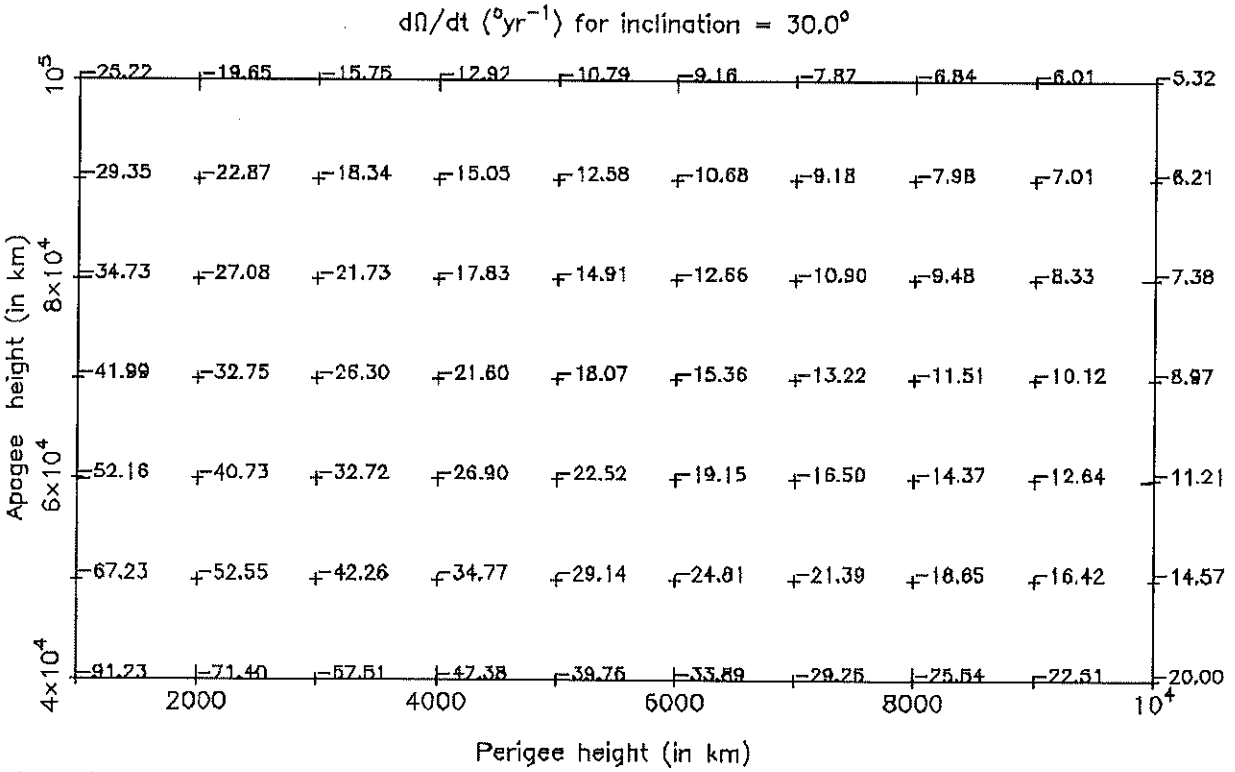

Fig. 3.6: Nodal Precession Rate dω/dt as a Function of Perigee and Apogee Heights for i=30°.

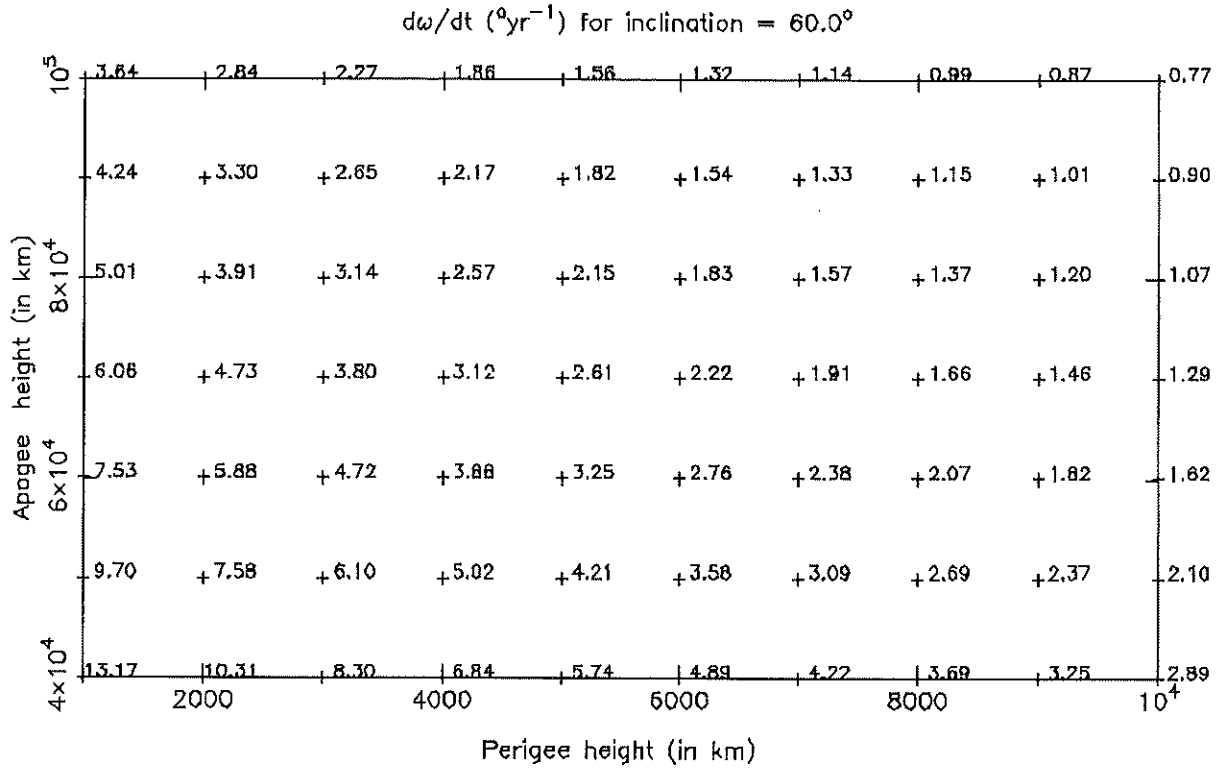

Fig. 3.7: Perigee Precession Rate dω/dt as a Function of Perigee and Apogee Heights for i=60°.

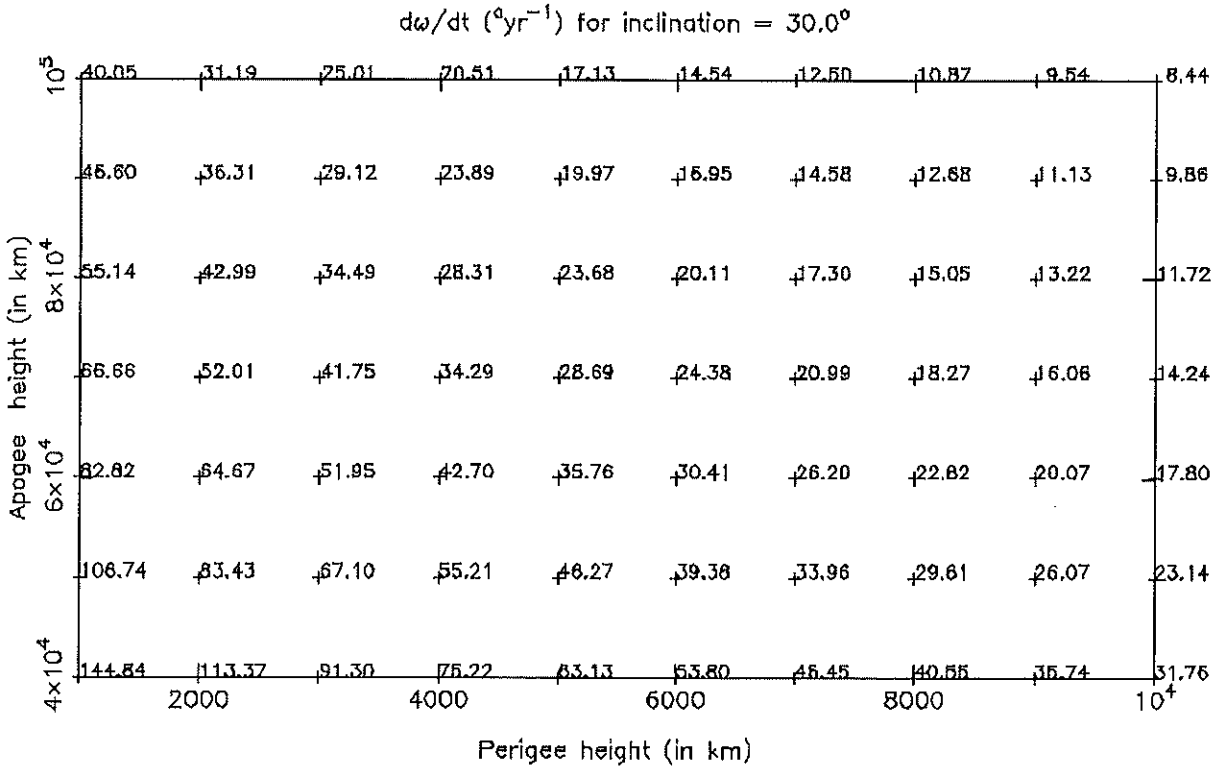

Fig. 3.8: Perigee Precession Rate dω/dt as a Function of Perigee and Apogee Heights for i=30°.

3.3.4 ARISE Tracking Coverage

We have studied the ground tracking coverage obtainable for ARISE as a function of the orbit apogee height h_a, the orbit argument of perigee ω, and various combinations of ground tracking stations (GTS). In Table 3.10, we show the percentage of time that ARISE can be tracked for various combinations of GTSs, and for two (2) values of h_a, three (3) values of ω, and for a fixed h_p of 3000 km. The default tracking network is assumed to be the three (3) DSN sites of Goldstone (GOLD-5), Madrid (MADR-5), and Tidbinbilla (TIDB-5), where the "5" indicates an elevation limit of 5°. In addition, the impact of adding GTSs at Green Bank (GBANK-5), Hartebeesthoek in South Africa (HART-5), and Santiago in Chile (SANT-5) is examined. As can be seen, even when the perigee is in the far south (ω = 90°), ARISE can be tracked for 84% of the time with the network of three (3) DSN sites, but *ignoring the effect of all spacecraft constraints*. For an orbit with (h_p, h_a, i) = (3000 km, 40000 km, 30°), the perigee precession rate is 91°/yr, which probably means that for at least the first 1.5 years of the mission, perigee will be in the southern hemisphere.

The results presented above are encouraging, as they seem to indicate that the requirement for 80% science data collection during a full orbit could be met with a tracking network consisting of the three (3) DSN sites alone, again provided that the spacecraft constraints have a minimal impact. However, some caution should be placed on this result. For example, in Table 3.11, we show the amount of tracking obtainable for an optional ARISE orbit given by (h_p, h_a, i) = (5000 km, 40000 km, 60°). For this orbit, the 80% science data collection requirement cannot be met with a tracking network consisting only of the three (3) DSN sites. For such an orbit, it would be very beneficial to have an extra GTS located in either South Africa or South America.

We also note that the percentage of time that ARISE can be tracked in a full orbit may not be the optimum way of expressing the science data acquisition requirement, since the spacecraft moves in its orbit at a non-uniform angular rate. An alternate requirement might be expressed in terms of the percentage of true anomaly in a given orbit that science data can be collected.

Orbit: h_p (km) = 3000, h_a (km) = 40000, i = 30°						ω = 0°	ω = 90°	ω= 270°
GOLD-5	MADR-5	TIDB-5				88.6	84.0	90.1
GOLD-5	MADR-5	TIDB-5	GBNK-5			89.3	90.1	90.6
GOLD-5	MADR-5	TIDB-5		HART-5		93.6	93.3	94.0
GOLD-5	MADR-5	TIDB-5			SANT-5	91.9	90.3	92.4
GOLD-5	MADR-5	TIDB-5	GBNK-5	HART-5		94.2	97.0	94.4
GOLD-5	MADR-5	TIDB-5	GBNK-5		SANT-5	91.9	90.4	92.4
GOLD-5	MADR-5	TIDB-5		HART-5	SANT-5	96.1	96.9	96.1
GOLD-5	MADR-5	TIDB-5	GBNK-5	HART-5	SANT-5	96.1	97.0	96.1

Orbit: h_p (km) = 3000, h_a (km) = 50000, i = 30°						ω = 0°	ω = 90°	ω= 270°
GOLD-5	MADR-5	TIDB-5				91.6	87.1	93.1
GOLD-5	MADR-5	TIDB-5	GBNK-5			92.3	91.7	93.4
GOLD-5	MADR-5	TIDB-5		HART-5		94.9	96.1	96.0
GOLD-5	MADR-5	TIDB-5			SANT-5	94.3	91.6	94.9
GOLD-5	MADR-5	TIDB-5	GBNK-5	HART-5		95.5	97.7	96.3
GOLD-5	MADR-5	TIDB-5	GBNK-5		SANT-5	94.4	91.7	94.9
GOLD-5	MADR-5	TIDB-5		HART-5	SANT-5	97.1	97.6	97.7
GOLD-5	MADR-5	TIDB-5	GBNK-5	HART-5	SANT-5	97.1	97.7	97.7

Table 3.10: ARISE Tracking for Orbits with Different Apogee Heights (i=30°).

Orbit: h_p (km) = 5000, h_a (km) = 40000, i = 30°						ω = 0°	ω = 90°	ω= 270°
GOLD-5	MADR-5	TIDB-5				88.6	87.3	90.4
GOLD-5	MADR-5	TIDB-5	GBNK-5			89.4	92.0	90.9
GOLD-5	MADR-5	TIDB-5		HART-5		94.4	95.4	94.8
GOLD-5	MADR-5	TIDB-5			SANT-5	92.3	92.0	93.1
GOLD-5	MADR-5	TIDB-5	GBNK-5	HART-5		95.2	97.3	95.3
GOLD-5	MADR-5	TIDB-5	GBNK-5		SANT-5	92.3	92.0	93.1
GOLD-5	MADR-5	TIDB-5		HART-5	SANT-5	97.1	97.3	97.1
GOLD-5	MADR-5	TIDB-5	GBNK-5	HART-5	SANT-5	97.1	97.3	97.1

Orbit: h_p (km) = 5000, h_a (km) = 40000, i = 60°						ω = 0°	ω = 90°	ω= 270°
GOLD-5	MADR-5	TIDB-5				85.2	69.3	89.6
GOLD-5	MADR-5	TIDB-5	GBNK-5			85.9	70.6	89.9
GOLD-5	MADR-5	TIDB-5		HART-5		92.7	91.6	93.6
GOLD-5	MADR-5	TIDB-5			SANT-5	92.2	94.1	93.3
GOLD-5	MADR-5	TIDB-5	GBNK-5	HART-5		93.2	92.7	93.9
GOLD-5	MADR-5	TIDB-5	GBNK-5		SANT-5	92.2	94.1	93.3
GOLD-5	MADR-5	TIDB-5		HART-5	SANT-5	96.1	97.2	96.4
GOLD-5	MADR-5	TIDB-5	GBNK-5	HART-5	SANT-5	96.1	97.2	96.4

Table 3.11: ARISE Tracking for Orbits with Different Inclinations (h_p = 5000 km, h_a = 40000 km).

3.3.5 Impact of ARISE Eclipses

Lowering the ARISE orbit inclination from 60° to 30° increases the frequency with which ARISE has eclipses. Since the ARISE spacecraft cannot observe during eclipses, and has a recovery time after eclipse of approximately half an hour, lowering the orbit inclination may provide serious limitations to the science return of the ARISE mission. Since the initial ARISE orbital elements are unknown at this stage, a set of eclipse histories have been produced so that this history could be determined as a function of the initial values of the argument of perigee ω_o and longitude of the ascending node Ω_o. A launch date of 1-Jan-2008 has been assumed, as well as a perigee height of 3000 km and apogee height of 40000 km. In the cases studied, there are seasons of long eclipses which occur near apogee and last more than 90 minutes. For reference, the orbital period is 12.9 hours. However, the number of short eclipses, which occur near perigee, is a strong function of the initial orbital elements. In Figure 3.9, we show a case (with $\omega_o = 0°$ and $\Omega_o = 90°$) where there are a relatively large number of short period eclipses. In contrast, in Figure 3.10, we show a case (with $\omega_o = 0°$ and $\Omega_o = 270°$) where there are relatively few eclipses. In the previous section, the percentage of time ARISE could be tracked was determined on the basis of ignoring any spacecraft constraints, including eclipse constraints. However, an eclipse of x minutes leads to a fractional loss of science data of $(x+30)/7.74$ percent. Thus, an eclipse of 100 minutes leads to a fractional data loss of 16.8%. However, averaged over three (3) years, the percentage of time in eclipse or recovery is 7.2% for the worst-case eclipse history shown in Figure 3.9, and only 3.4% of the time for the best-case history shown in Figure 3.10. Thus, a ground tracking network consisting only of the three (3) DSN sites may have difficulty meeting the 80% average science data collection requirement when the eclipse constraint is taken into account, since including the eclipse constraints reduces the average percentage of time that science data can be collected to very close to the 80% requirement. Furthermore, the average impact of any other spacecraft constraints (such as a limited field of view of the telemetry antenna or not being able to observe a source within 5 degrees of the Earth limb) are presently unknown and can only further reduce the effective science data acquisition time. Thus, it seems prudent to add an extra GTS to the network of three (3) DSN

sites to meet the 80% data collection requirement. The optimal location for an additional tracking station, from the three (3) sites studied, appears to be Hartebeesthoek (South Africa).

Tables 3.12 and 3.13 show the average percentage of time in eclipse for different values of ω_o and Ω_o. This average does not take into account the spacecraft recovery time after eclipses. We can

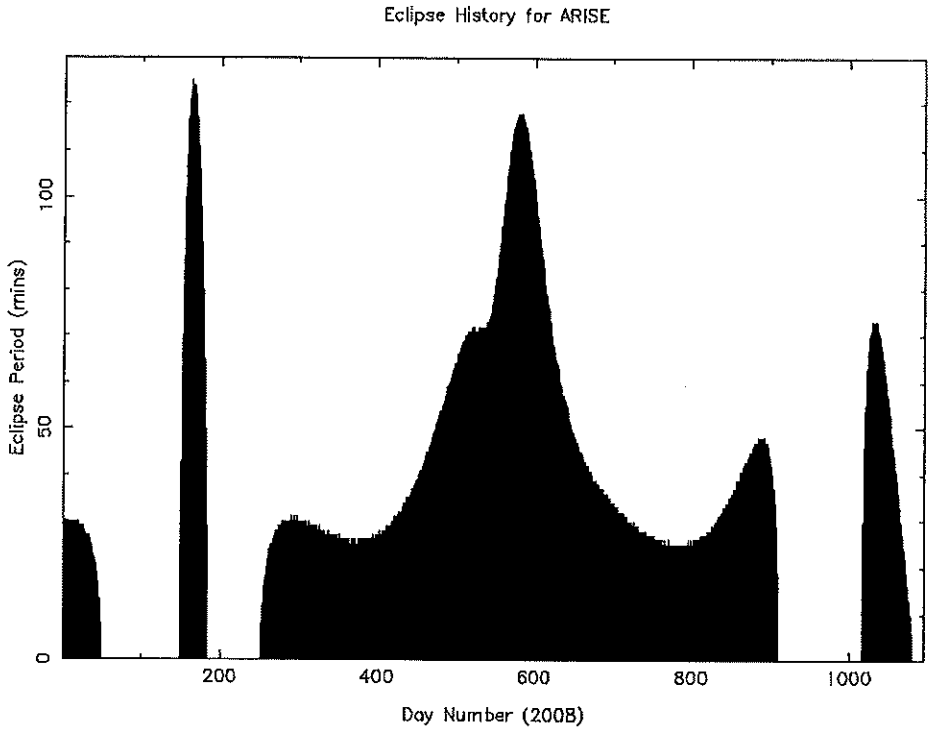

Fig. 3.9: Eclipse History for (h_p, h_a, i, ω_o, Ω_o) = (3000 km, 40000 km, 30°, 0°, 90°).

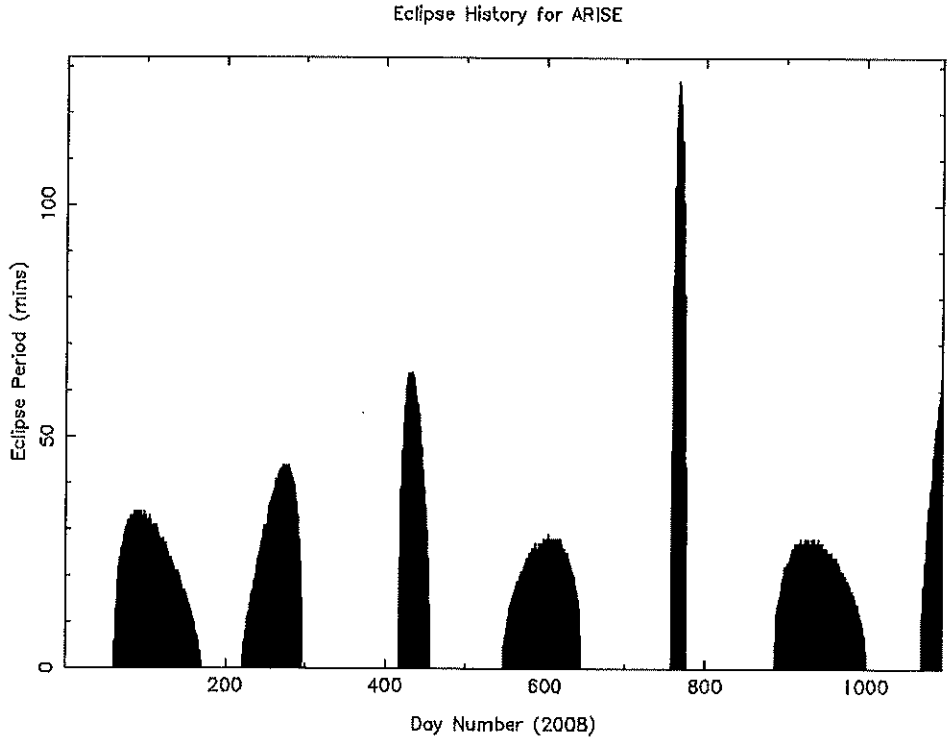

Fig. 3.10: Eclipse History for (h_p, h_a, i, ω_o, Ω_o) = (3000 km, 40000 km, 30°, 0°, 270°).

infer from these tables that an inclination of 60° has typically 0.5-2.5% better coverage than for inclinations of 30°. However, from the tracking coverage analysis, decreasing the inclination to 30° improves coverage by typically 1-3.5%. A ω_0 of 270° would increase tracking coverage and decrease time in eclipse compared to other values of ω_0. If choice was possible, the combination $(\omega_0, \Omega_0) = (270°, 270°)$ would be optimum.

ω_0 (°)	Ω_0 (°)	# of eclipses in 3 years	Average eclipse length (min)	% time in eclipse
0	0	1190	42.43	3.20
0	180	1415	35.90	3.22
0	270	899	29.75	1.70
0	90	1503	45.55	4.34
180	0	1201	33.91	2.58
180	180	1227	35.77	2.78
180	270	764	34.19	1.66
180	90	1663	36.53	3.85
270	0	1340	34.39	2.92
270	180	1111	38.22	2.69
270	270	857	30.34	1.65
270	90	1545	41.54	4.07
90	0	1224	41.17	3.20
90	180	1175	33.48	2.49
90	270	790	33.29	1.67
90	90	1667	39.05	4.13

Table 3-12: ARISE Average Eclipse Length for Different Orbits with Perigee Height 3000 km, Apogee Height 40000 km, and Inclination 30°, over 3 Years (1095 days).

ω_0 (°)	Ω_0 (°)	# of eclipses in 3 years	Average eclipse length (min)	% time in eclipse
0	0	795	35.66	1.80
0	180	676	31.62	1.36
0	270	552	33.32	1.17
0	90	798	32.76	1.66
180	0	885	32.17	1.81
180	180	595	36.09	1.36
180	270	554	33.21	1.17
180	90	761	33.87	1.63
270	0	989	31.14	1.95
270	180	668	33.27	1.41
270	270	563	33.18	1.18
270	90	1031	27.95	1.83
90	0	1008	29.99	1.92
90	180	652	33.81	1.40
90	270	554	33.65	1.18
90	90	1073	28.63	1.95

Table 3-13: ARISE Average Eclipse Length for Different Orbits with Perigee Height 3000 km, Apogee Height 40000 km, and Inclination 60°, over 3 Years (1095 days).

In summary, lowering the nominal ARISE orbit inclination from 60° to 30° has the effect of increasing the amount of time ARISE can be tracked with a ground tracking network such as the DSN. However, the number and frequency of eclipses is also increased, implying that the DSN tracking network alone is likely unable to meet the 80% average science data collection requirement. An additional ground tracking station is likely required with Hartebeesthoek (South Africa) being the preferred site from among the list of Green Bank, Santiago, and Hartebeesthoek.

3.3.6 Preliminary Orbit Selection

In view of the results presented in the previous sections (see Table 3.14), and also for the following practical reasons:

(1) Launch vehicle lifting capability and cost,
(2) Atmospheric drag concerns at 1000 km perigee altitude (with a 500 m^2 antenna), and Van Allen radiation intensity peak at 2000 km altitude,

it is recommended that the ARISE orbit have a perigee height of 3000 km, apogee height of 40000 km, and an inclination of 30° (see Table 3.15 and Figure 3.11). The optimum choice for ω_o and Ω_o cannot be determined since the launch constraints are unknown. However, once these constraints are known, the optimum values of these two parameters may be determined by the desires to maximize the tracking for a given ground tracking network over the mission lifetime, and to minimize the science data lost while the spacecraft is in eclipse or eclipse recovery. Once the science program has been further studied, additional orbit constraints may then be imposed by the requirement to observe major target sources with good (u,v)-coverage.

h_p (km)	h_a (km)	i (°)	Period (hrs)	ω_o (°)	Ω_o (°)	$d\omega/dt$ (°/yr)	$d\Omega/dt$ (°/yr)	NPP (yrs)	T_cov (%)	E_dur (%)
3000	40000	30	12.9	270	270	91.3	-57.5	6.3	94.0	1.6
3000	40000	60	12.9	90	270	8.3	-33.7	10.7	93.6	1.2
3000	50000	30	16.5	90	-	67.1	-42.3	8.5	96.1	-
5000	40000	30	13.6	90	-	83.1	-39.7	9.1	95.4	-
5000	40000	60	13.6	270	-	5.7	-22.9	15.7	93.6	-
3000	100000	30	38.5	-	-	25.0	-15.7	22.9	-	-

Where:
- h_p: Perigee altitude
- h_a: Apogee altitude
- i: Inclination
- ω_o: Argument of perigee (best case)
- Ω_o: Right ascension (longitude) of the ascending node (best case)
- $d\omega/dt$: Precession of the argument of perigee
- $d\Omega/dt$: Precession of the longitude of the ascending node
- NPP: Nodal precession period
- T_cov: Tracking coverage (assumes four (4) tracking stations, three (3) DSN plus Hartebeesthoek (South Africa))
- E_dur: Average eclipse duration

Table 3.14: Summary of ARISE Orbit Investigations.

We note that even with the above ARISE orbit, the nodal precession is still only -58 ° /yr. Future ARISE studies shall consider means of increasing this precession rate by either allowing lower perigee heights or by use of non-gravitational forces (such as the use of ion propulsion or solar sailing).

Quantity	Nominal
Semi-major axis	27900 km
Eccentricity	0.66
Apogee Altitude	40000 km
Perigee Altitude	3000 km
Inclination	30 deg
Orbital Period	12.9 hr
Perigee Precession	91.3 deg/yr
Node Precession	-57.5 deg/yr

Table 3.15: ARISE Selected Nominal Orbit.

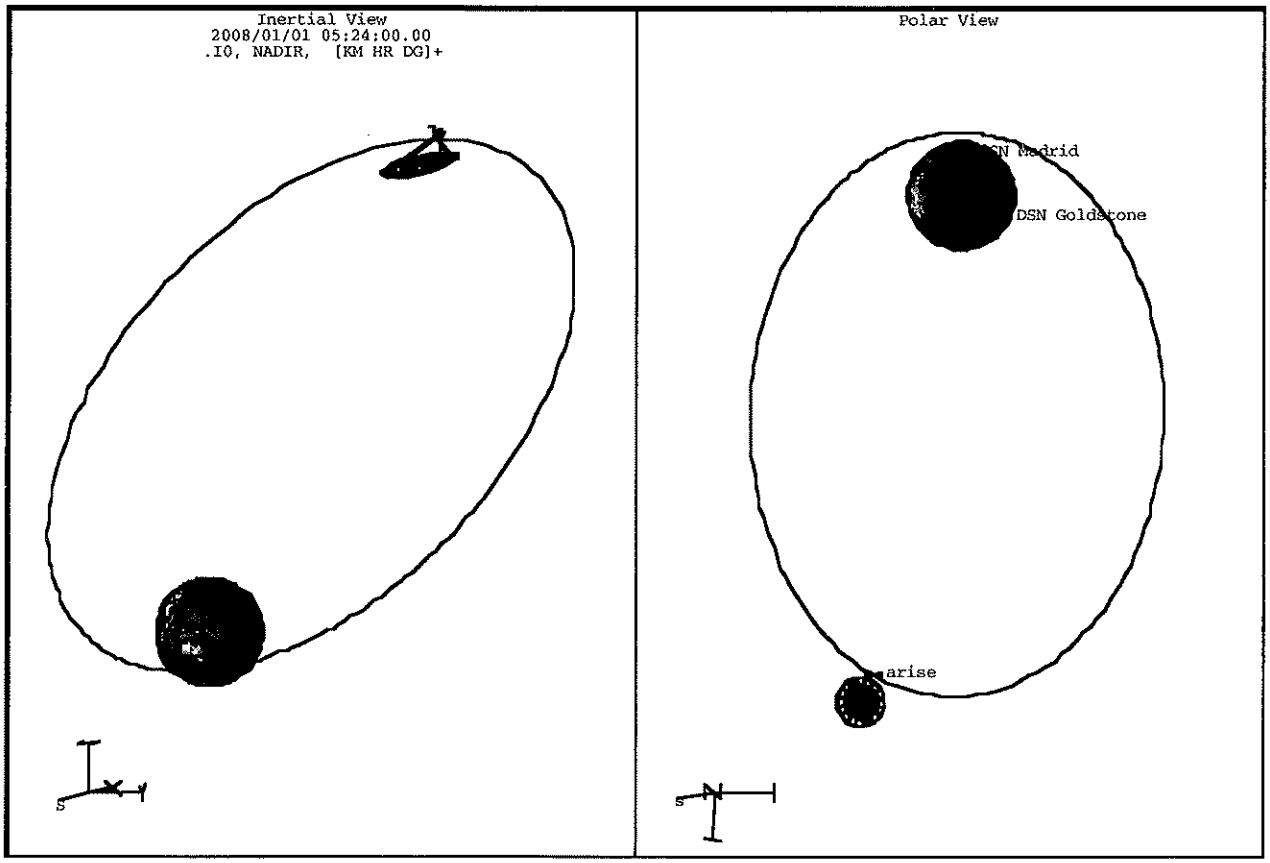

Fig. 3.11: ARISE Nominal Orbit: h_p = 3000 km Altitude, h_a = 40000 km Altitude, i = 30°.

3.3.7 Additional Note on Mission Lifetime Requirements

The orbit selected and the science requirements prescribe a mission lifetime of at least six (6) years. However, for technological and mission cost reasons, it was decided that a mission lifetime of three (3) years would be the baseline design. Further technology and cost analysis will review this assumption.

Chapter 4

Science Payload Front-end Description

4.1 Science Payload Requirements

Here we summarize the scientific requirements described in Section 3.1 that are applicable to the science front-end payload.

4.1.1 Frequency Coverage

Observing frequencies are at 8 GHz, 22 GHz, 43 GHz and 86 GHz. These frequencies correspond to wavelengths of 3.7 cm, 1.4 cm, 0.7 cm, and 0.35 cm, respectively. The maximum instantaneous bandwidth observed is 2 GHz.

Tunability of the instruments for the ranges 5-10 GHz, 18-26 GHz, 40-45 GHz, 80-95 GHz is desirable.

4.1.2 Sensitivity

The ARISE design should maximize the instrument sensitivity, within the bounds of technological constraints and mission cost. Antenna size, system temperature, bandwidth and coherent integration time must allow for a detection threshold for a continuum radio source of about 1 mJy at 8 and 22 GHz, 10 mJy at 43 GHz, and 100 mJy at 86 GHz.

4.1.3 Polarization

Dual circular polarization is required. Isolation between the two polarizations should be 3% or better in voltage.

4.1.4 Calibration Accuracy

Amplitude calibration of the ARISE antenna must have an accuracy of 5% including the antenna gain in the direction of the source and the total system temperature.

4.1.5 System Temperature

The receiver should be cooled so that total system temperatures are less than 12 K at 8 GHz, 16 K at 22 GHz, 24 K at 43 GHz, and 45 K at 86 GHz.

4.1.6 Sky Coverage and Duty Cycle

A Sun avoidance angle of less or equal to 30 degrees is required. The observing duty cycle on a science source must average at least 70-80% over the course of a full orbit. A typical imaging period is one (1) orbit.

4.1.7 Antenna Microwave Performance

The microwave performance of the antenna must be sufficient to meet the sensitivity requirements at all observing frequencies. A single antenna beam is necessary with on-axis aperture efficiencies as high as possible. Sidelobe levels are of secondary importance. The "effective" RMS surface error of the overall antenna system (including any correction method) should be 0.22 mm or better. (The required overall antenna efficiency at 86 GHz must be at least 8%).

4.2 Front-end Overview

The ARISE science front-end must fulfill the set of requirements described above. The front-end is composed of a main reflector (antenna) of aperture 25 m, a mechanically shaped subreflector of diameter 1.6 ms, and of a set of RF receivers (horns) located at the focal plane. The main reflector

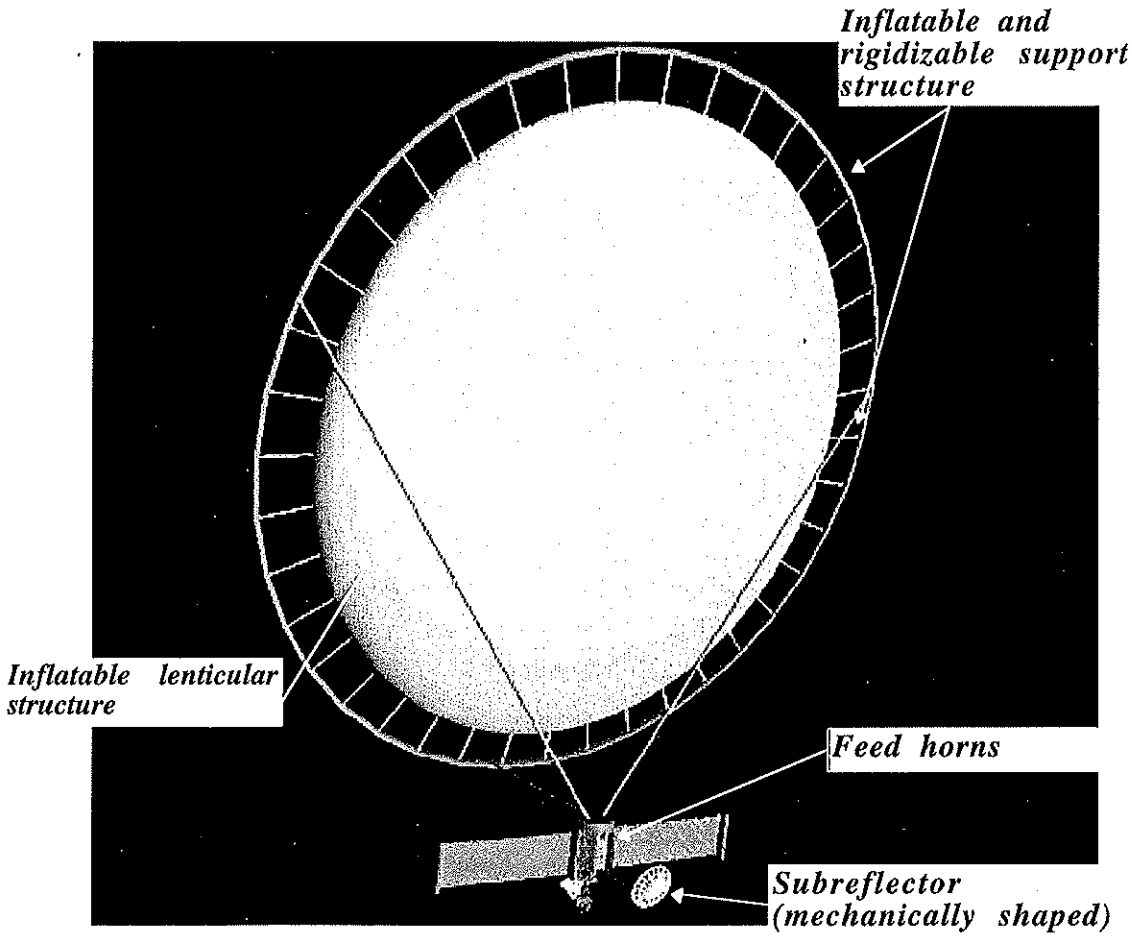

Fig. 4.1: ARISE Spacecraft Radio Antenna System Configuration.

uses inflatable structures technology (although other options are also being considered and described in Section 4.8), as it enables a low mass and low cost mission. The inflatable antenna is composed of a pressurized lenticular structure (one side is the reflector, the other an RF transparent canopy), and a Space rigidizable support structure (struts and torus), as shown in Figure 4.1. The current concept for the inflatable antenna has been developed by L'Garde, Inc., based in Tustin, California. Since at the time of writing the reflector RMS surface precision exceeds the specified requirement, a mechanically shaped subreflector is envisaged to adaptively correct for the main reflector surface distortions. This subreflector is composed of a thin composite sheet, whose shape is driven by a set of actuators. Operationally, the subreflector shape will be calibrated and set before each new source observation and in most cases after each eclipse. A metrology system will be used for calibration of the subreflector. The most promising technique for the metrology systems identified to-date is photogrammetry, involving a video mapping of the reflector surface. Photogrammetry utilizes two (2) or three (3) video cameras located at key points on the spacecraft, one or several light sources, and a surface reconstruction algorithm. Once the subreflector is calibrated, the signal is then focused onto four (4) receivers, one for each frequency band. Optionally, to improve the performance (antenna overall efficiency) at 86 GHz, an adaptive compensation feed array of 19 elements might be used to electronically compensate for remaining wavefront distortions.

The remainder of this chapter describes the hardware involved in the reception of the science data on the ARISE spacecraft to the point of the receiver output. Further signal processing is described in Chapter 5.

4.3 Main Reflector

4.3.1 ARISE Antenna System Configuration

The ARISE reflector configuration has been selected after evaluation of various reflector antenna geometries, and resulted from early trade-offs between on-axis and off-axis configurations. It was determined that an off-axis configuration offered better science performance (less obscuration) and fewer constraints on other factors in the spacecraft design.

Four different off-axis configurations were then evaluated: Prime Focus, Gregorian, Cassegrain, and Schmidt Cassegrain (Figure 4.2). The following criteria were employed: dynamics/structural stiffness, thermal stiffness, RF performance, mass, complexity, deployment reliability and alignment. It was determined that the Gregorian off-axis design uses a smaller and less complex structure than Cassegrain types. Furthermore, the Gregorian off-axis system offers the possibility of a mechanically shaped subreflector that is reasonably sized and controlled.

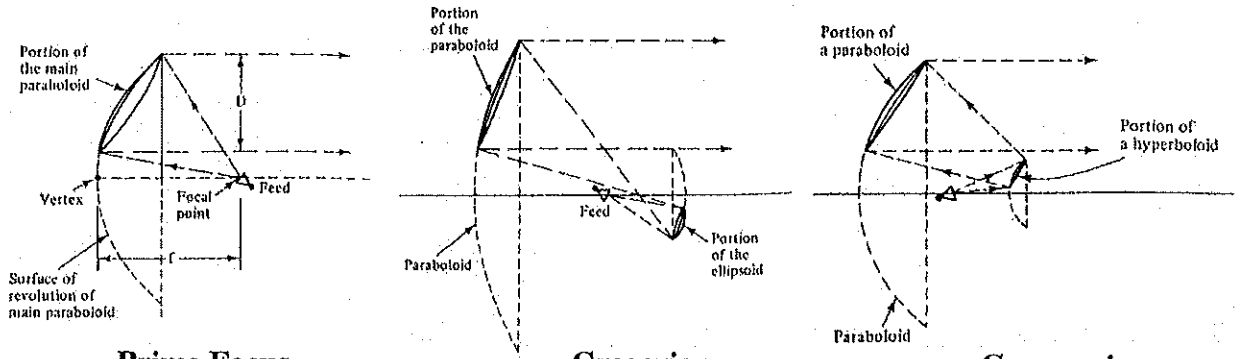

Fig. 4.2: ARISE Off-axis Radio Antenna System Configurations.

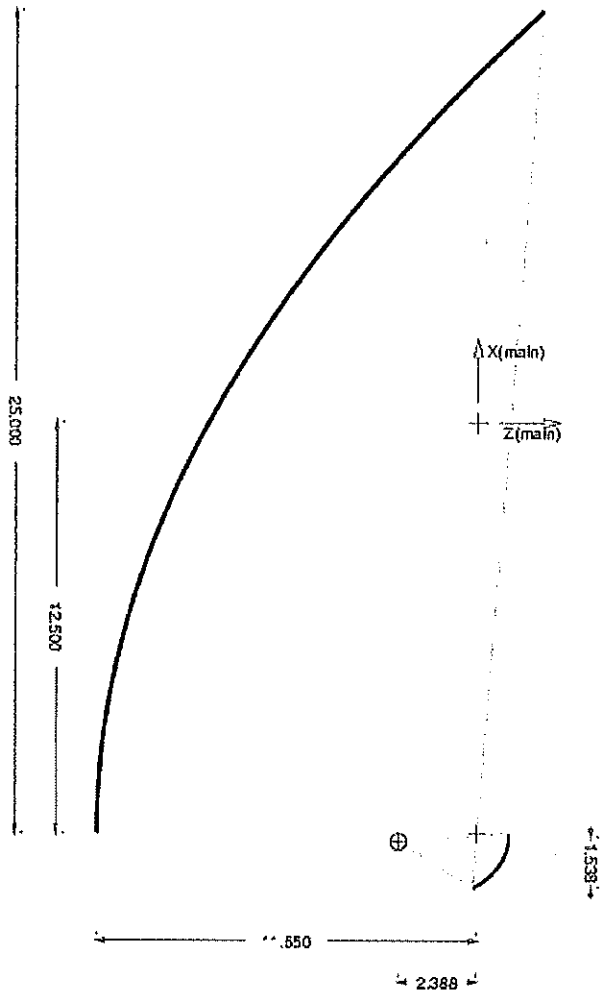

Fig. 4.3: ARISE Proposed Vertical Cross-section through the Dual Reflector Geometry.

Based on these arguments, a Gregorian dual-reflector antenna system has been selected for ARISE. Figure 4.3 displays a vertical cross-section through the reflector configuration. All the dimensions shown in this figure are in meters. The geometrical parameters, which fully define the reflector configuration as shown in Figure 4.3, are given below:

On-axis "mother" reflector diameter	D = 50 m
On-axis "mother" focal length	F = 11.55 m
Off-axis sub-aperture diameter	D = 25 m
Tilt angle between main reflector and subreflector axis	β = 5.67 deg.
Inter-foci distance	L = 2.4 m
Subreflector eccentricity	ε = 0.555

4.3.2 High Precision Inflatable Reflector

Description

The ARISE primary reflector concept has been developed by L'Garde, Inc. and is comprised of a reflective membrane with an RF transparent front canopy to complete the inflated lenticular envelope. The lenticular structure is combined with a tubular peripheral support torus forming a

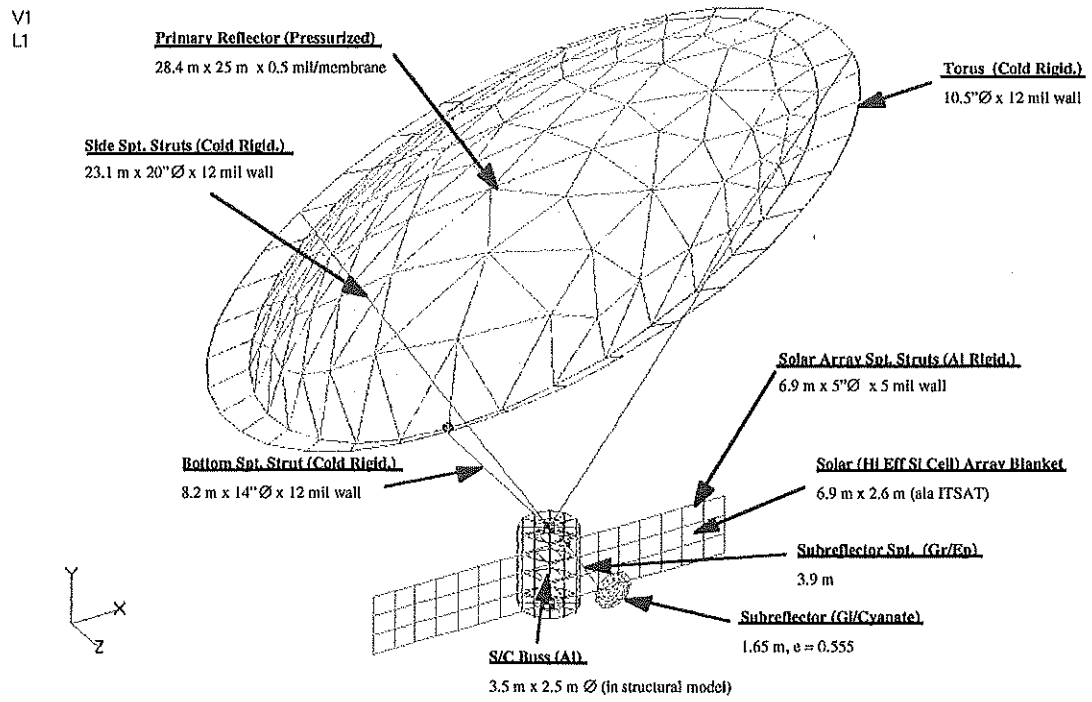

Fig. 4.4: ARISE Structural Configuration.

large, lightweight, yet relatively stiff Space structure. To minimize membrane stress, the lenticular structure is pressurized with less than 4×10^{-4} psi of N_2 and attached to the torus ring with constant force springs in a "trampoline" fashion.

The antenna assembly is aligned and attached to the spacecraft using three tubular support struts that are inflation-deployed from a stowage canister located at the top of the spacecraft bus. At the torus, the antenna support struts are kinematically attached at 120° intervals. They are designed with optimum diameters, wall thickness, and lengths to give mechanical rigidity (bending, torsion) yet minimal obscuration and shadowing of the primary (see Figure 4.4 and Table 4.1 for mass breakdown).

Components	Total Mass (kg)
Reflector/Canopy/Shield	32.4
Torus	13.3
Struts	30.9
Attachment hardware	10.9
Deployment hardware	6.0
Electronics	4.0
Inflation system	2.6
Canister	18.2

Table 4.1: ARISE Inflatable Antenna Mass Breakdown.

Rigidizable support structure technologies are used wherever possible on ARISE in order to minimize the need for "make-up" inflation gas. The primary reflector torus and antenna support struts maintain their mechanical stiffness and shape by using sub glass transition temperature (sub-Tg) rigidizable materials. SubTg rigidization utilizes composite fibers in an elastomeric matrix, which becomes rigid below a tailorable glass transition temperature (Tg). The elastomer is chosen such that its Tg is above the equilibrium temperatures of the deployed structure expected during the

entire mission. In this way, the structure will remain rigid through the mission. Generally, the spacecraft temperature before deployment is higher than the deployed equilibrium temperature due to the on-board electronics. Careful selection of the elastomer will place the structure above its Tg before deployment, and below it when deployed, enabling a totally passive rigidization method, requiring no heaters or specialized rigidization hardware. To minimize thermal gradients, these support members will be wrapped in Multi-Layer Insulation (MLI) blankets.

Reflector surface precision

An essential element of the ARISE design is the reflector precision. At the time of writing, L'Garde has built several inflatable reflectors under NASA and DoD development programs. Some of the larger reflectors included a 14 m IAE which was measured on the ground to have approximately 2 mm RMS surface accuracy. A 7 m reflector sponsored by DoD had a 1.7 mm RMS accuracy. Ground measurements have yielded surface shape accuracies between 0.67 mm and 1.3 mm RMS for gored 3 m diameter systems, with 0.8 mm to 0.96 mm as typical RMS values. This is the RMS deviation of the measured surface from a best-fit paraboloid. Measurements also demonstrate that surface slope errors of 1 milliradian or less are feasible. It must be noted that these surface accuracies and surface slopes were achieved using off-the-shelf materials with the reflector formed from flat gores. Although inflatable reflectors using current technology do not have the required accuracy for use as Space telescopes, L'Garde believes that the enabling technologies such as improved material properties, better material uniformity, and greatly-improved manufacturing processes are in the very near future. At present, inflatable reflectors are fabricated using flat gores joined together at the seams. The use of doubly-curved gores will yield better accuracy. A list of the 15 reflectors and their surface precision has been compiled by L'Garde. On the basis of current developments it is expected that submillimeter surface accuracy for a 25 m reflector is possible with appropriate development.

To generate a credible estimate of the magnitude and distribution of the 25 m ARISE antenna error, ground measurements from the 14 m Inflatable Antenna Experiment (IAE) reflector were utilized. The IAE reflector shape is shown in the top right of Figure 4.5. It was measured during a ground test in preparation for flight. During the test, one of the torus supports slipped and was not discovered until after the measurements were taken. Nonetheless, it is considered representative of the types of errors seen in this class of reflector, albeit somewhat exaggerated. As a projection of the type of errors that will be seen in future reflectors which are expected to be more systematic, a FAIM (Finite-element Analysis for Inflatable Membranes) software model prediction of the reflector shape has been utilized. FAIM predicts the shape of the inflated reflector analytically, but includes no random errors as seen in material properties and manufacturing errors. The two reflectors were interpolated together, resulting in the reflector shape representing the convolution of the theoretical global error generated by FAIM and the manufacturing errors scaled from the as-measured IAE.

Structural and thermal analysis

Of special concern were dynamic response, inertial static loading, and thermal distortion effects on antenna shape and alignment. Because of the "soft" nature of inflatable structures, and the temperature sensitivity of polymeric membranes, structural and thermal analytical models were created that had more resolution than simple static diagrams and lumped masses. The structural model consisted of over 700 elements (Appendix A) that closely approximated off-axis parabolic curvatures, strut orientation, subreflector alignment, solar array geometry, and spacecraft mass distribution. Special attention was given to membrane elements, polymer properties, and tubular geometries, all critical to inflatable structural behavior. The thermal model was based on the same nodal geometry and properties, allowing a direct one-to-one correspondence between temperature profiles and structural elements.

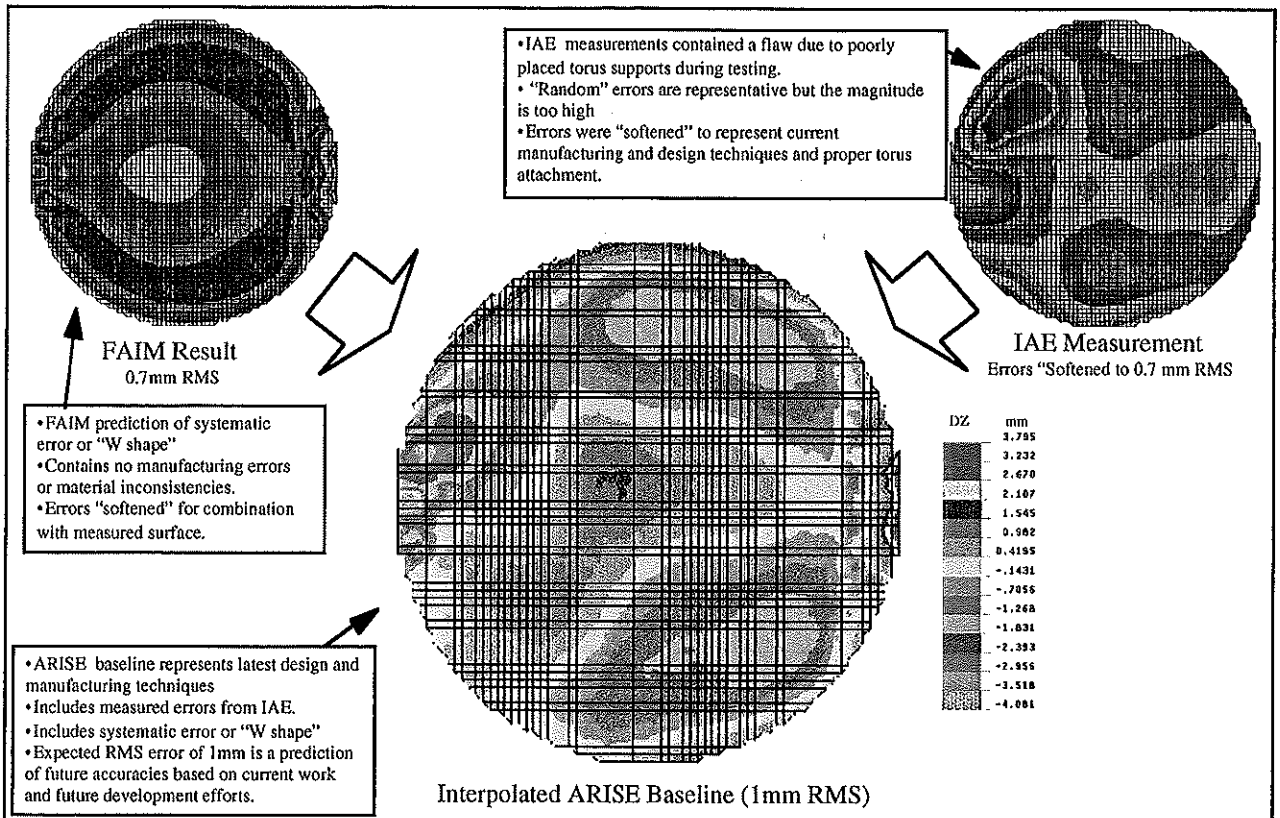

Fig. 4.5: ARISE Reflector Precision Projection.

Dynamics analysis

The ARISE reflector dynamic response has been analyzed using normal modes analysis (force-driven vibration stimuli have not yet been specified). Table 4.2 lists the first six non-rigid body normal modes for the off-axis Gregorian. In general, the modal frequencies were shown to be representative of large Space structures, and are within acceptable bounds given ARISE's operating scenarios. The resultant modal shapes are classic with tip displacements that are non-critical. (See Appendix A for coordinate references.)

Figure 4.6 shows the resulting structural displacements due to a conventional, static (without transients) thrust maneuver loading. A thrust vector of 0.015g at 2° off-axis was applied at the base of the spacecraft bus in order to study worst case asymmetric inertial loading. A maximum displacement of 4 mm was predicted. Since thrust maneuvers will not be performed during science observations, it was felt, based on these preliminary results, that thrust/slewing maneuvers would not create critical/castastrophic stress or strain conditions.

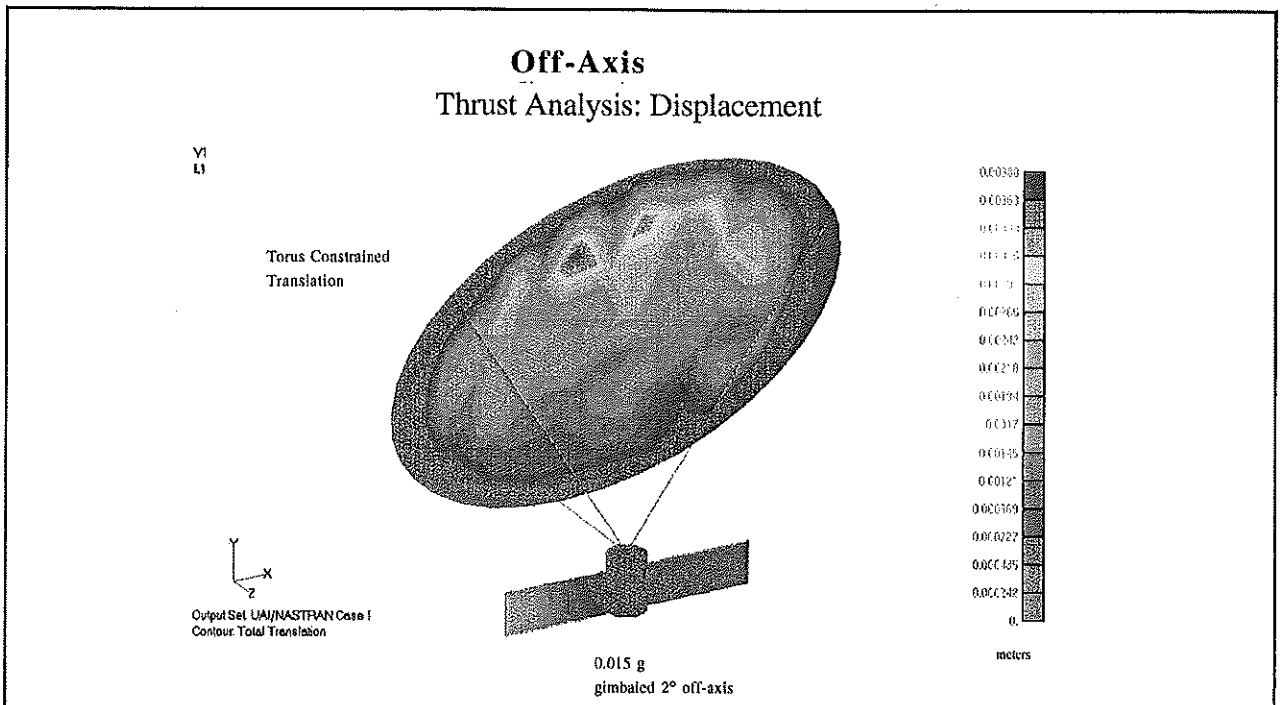

Fig. 4.6: ARISE Structural Displacements due to Static Thrust Maneuver Loading.

Mode #	Modal frequency (Hz)	Modal Shape	Max. *Tip* Displacement (cm)
1	0.3	Primary & S/C bus "nodding" to each other	12.5
2	0.5	Primary Y tilt	13.5
3	0.8	Subreflector Y cantilever	5.5
4	0.9	Subreflector Y tilt	5.8
5	1.0	Primary "trampoline" motion	6.1
6	1.2	Subreflector X tilt	2.5

Table 4.2: ARISE Normal Modes Analysis.

Thermal analysis

Another issue affecting on-orbit reflector surface precision is the thermal load expected during the mission. In the highly elliptic orbit seen by the ARISE spacecraft, and the unlimited pointing directions required for the mission, significant thermal gradients are endured by the reflector. In the elliptic orbit the equilibrium temperature of the spacecraft can vary quickly, and off-pointing sun angles and shadowing can cause dynamic thermal gradients. The effect on the reflector is to expand in hot regions and to contract in cooler regions, thus distorting the reflector shape.

A detailed worse case orbital thermal analysis was performed for the off-axis Gregorian configuration. One of the sub-solar points of the ARISE elliptical orbit was chosen for this test case. It was judged that the combination of solar heating at the bottom edge of the lenticular

antenna structure with the Earth's albedo/IR would generate large gradients across the reflector membrane (Appendix A, orbital configuration). For this temperature profile, the resulting induced thermal displacements, distorted shape, strains, and stresses are displayed in Appendix A, Thermal Distortion Analysis. The displacement magnitudes and vector directions are nodal, and represent the absolute displacement from the vertex of the primary reflector. They are cumulative, however, in the sense that they are a combination of rigid body motion and reflector distortion. A direct but qualitative indication of the primary reflector figure distortion are the membrane thermal strains. These strains are normalized local displacements giving rise to small membrane stresses. The thermal strains are also small, but because the ARISE has a large surface area, the net effect is a large movement at the top of the reflector of approximately 10 cm. The effect of the thermal loading of the primary reflector support struts is also a large contributor to the displacement of the primary.

An analysis is being performed at the time of writing to deconvolve the effective rigid body motion (corrected by control of strut/torus joints and subreflector orientation) from the primary reflector figure error (nulled by subreflector shaping and possibly feed phase correction). Another potential method for dealing with thermal distortion under investigation is a compromise of the primary and subreflector to the mid-range of possible distorted shapes that ARISE will see over an orbit, time, and operational orientation. As still another option, thermo-optical coatings might be used for passive control of membrane heat transfer to minimize thermal gradients.

Micrometeoroids

On-orbit debris presents a special hazard to the inflatable reflector. Fast moving particles can penetrate the lenticular membranes leaving holes in the structure and venting inflation gas. Since the reflector requires some internal pressure, leaks must be minimized and any lost inflatant must be replenished. Fortunately, the particle flux is quite small and the damage caused is minimal. However, over time the leaks compound, and for longer missions the make-up gas requirements can be significant. Micrometeoroid strikes are an annoyance to Space inflatables in general, but are not catastrophic.

L'Garde has conducted tests to quantify the damage caused by micrometeoroid particles on thin membranes. The tests were conducted at the Arnold Engineering Development Center in Tennessee. Particle sizes and velocities, representative of those expected in Earth orbit, were fired at membrane layers and the damage documented. It was found that the damage caused by these particles falls into three categories. High energy particles pass through the membranes and leave a hole about the same size as the particle (Figure 4.7). Low energy particles are completely shielded by the first membrane and are either deflected or become embedded. Particles with a certain combination of size and velocity in the medium energy category pose a different problem. The particles, upon impacting the first membrane break up and a series of particles spray out from the impact site. The resultant holes in the first layer are slightly larger than the particles themselves. The secondary particles then impact the second layer and can cause significant damage to the second film.

To minimize leakage caused by the medium energy micrometeoroids, another membrane is incorporated into the lenticular structure to act as the second film protecting the third layer from excessive damage. These protective layers or "whipple" shields can be incorporated as a flat membrane stretched between the lenticular membranes. This way, the second membrane impacted is inside the lenticular structure itself and supports no pressure difference, thus minimizing damage to the pressure-bearing membranes.

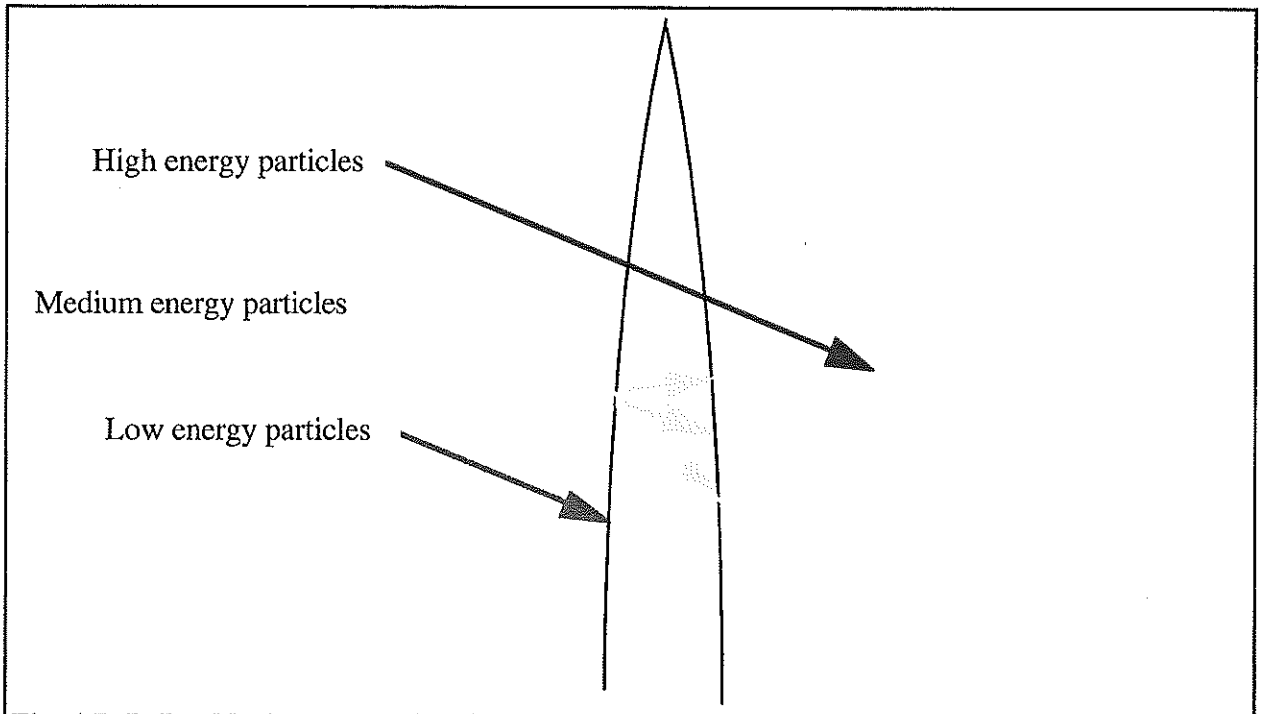

Fig. 4.7: Inflatable Antenna Thin Membrane Micrometeoroid Damage.

Make-Up Gas

L'Garde has developed analytic software to calculate damage on the membranes and the subsequent inflatant leakage over time. One set of software, ROID, given the expected flux of particles at the given orbit, calculates the damage to the membranes over the mission duration. The calculations are based on a compilation of the micrometeoroid impact data gathered during impact testing. Another set of software, GASFOR, calculates the loss of inflatant through the damaged membranes. These software tools were utilized in calculating the gas loss for the ARISE configuration, where one whipple shield was assumed.

No exact micrometeoroid flux was available for the highly elliptical ARISE orbit. An average flux was chosen, interpolated between Low Earth Orbit (LEO) and Geostationary Earth Orbit (GEO). LEOs typically experience the worst micrometeoroid flux, due to particles trapped by Earth's gravity and the ever-increasing debris caused by man's efforts in Space. GEOs have a much lower micrometeoroid flux, similar to deep Space. Future ARISE efforts shall include more detailed analyses of the flux experienced by the ARISE orbit.

Deployment

The inflatable structure antenna deployment sequence is shown in Figure 4.8. L'Garde has developed a new flexible enclosure canister. The concept promises significant weight savings over the solid canister designs. The lenticular structure and torus are stored inside a membrane container designed to withstand the increased internal pressure during ascent of the payload. Upon deployment, the top portion of the membrane is released by a pyrotechnic event. The petals open, releasing the lenticular structure and torus. Some residual gas in the lenticular structure is possible (as was experienced in the IAE flight experiment) and the lenticular structure is expected to billow out slightly to relieve any internal pressure. After initial deployment, the L'Garde Deployment Devices (LDD) are initiated. The next picture in the sequence shows the LDDs deploying the struts.

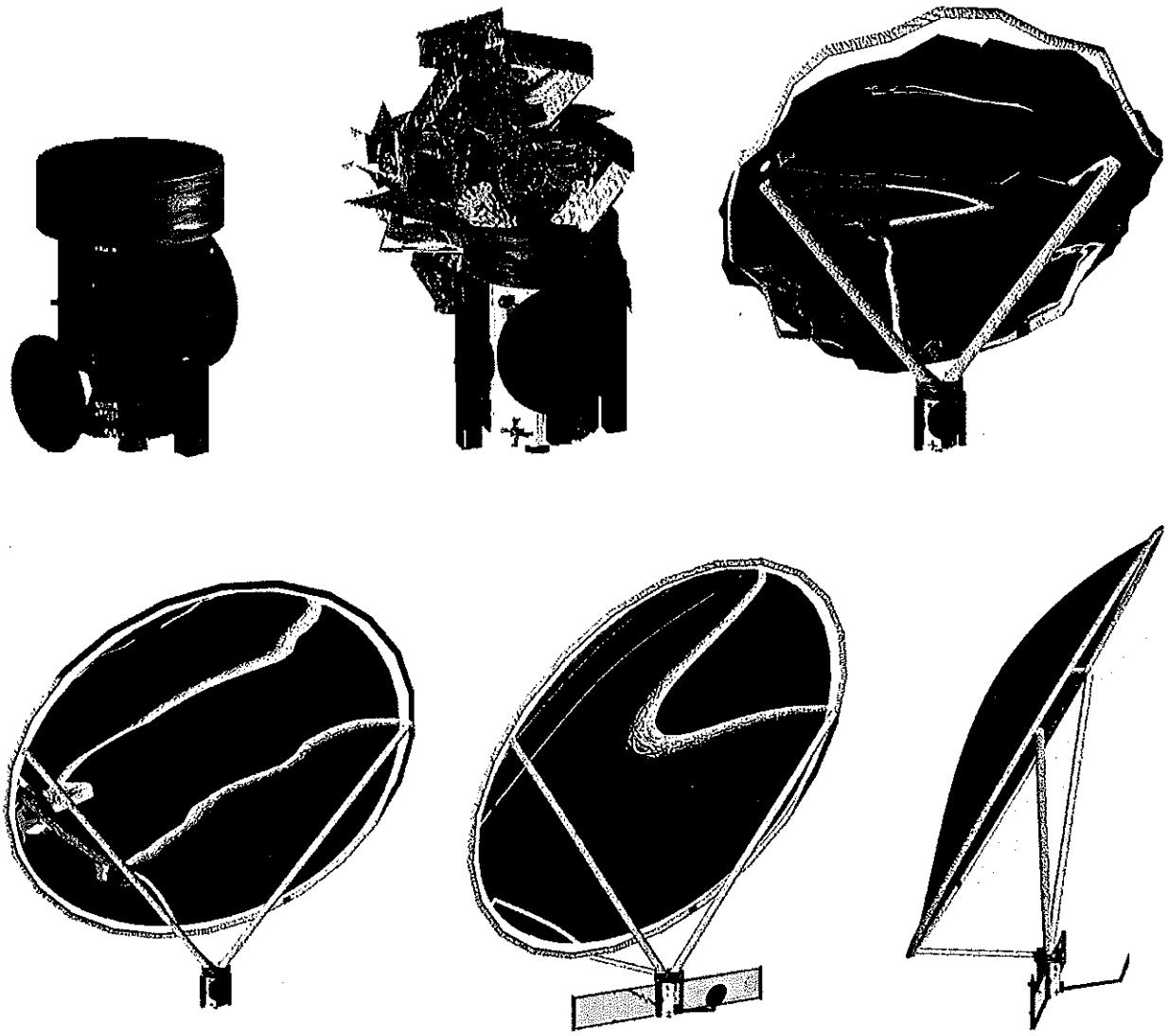

Fig. 4.8: Inflatable Antenna Deployment Sequence (by TDM Inc.).

Note the torus and lenticular structure are still uninflated and suspended between the extending struts. The next pictures show the struts at full deployment and the torus partially inflated. The lenticular structure is still not inflated. The inflatable solar array then gets deployed (for a simpler combined inflation system), followed by the inflation of the lenticular structure. Development of the deployment sequence draws extensively on the lessons learned from the IAE flight experiment.

Inflation system

The inflation system for the ARISE mission must provide gas for initial inflation of the struts, torus, envelope (reflector/canopy assembly), and solar array booms (inflatable solar arrays are used), and make-up gas for the envelope over the life of the mission. A range of options has been considered, including tanked gas, chemical gas generation, and combinations of these. The baseline specifications for the inflatable antenna are 3.0 kg necessary for initial inflation plus the appropriate amount of make-up gas required over a three-year mission life (estimated at 20 kg), and a lenticular structure operating pressure of 10^{-4} psi.

The inflation system as designed utilizes tanked gas for initial inflation and catalytic hydrazine decomposition for make-up gas. The gas tank is 0.24 m in diameter, T-1000 aluminum-lined graphite-epoxy, initially contains 0.4 kg He gas at 6000 psi, and has a mass of 1.4 kg. The hydrazine tank is common to the main propulsion tank. The estimated mass of the catalyst, valves, regulators, filters, orifice, and associated plumbing is 1.2 kg. The catalyst of 0.2 kg is estimated to be sufficient to provide a gas flow rate of 0.6 kg/min. The components are essentially off-the-shelf items, although some development of the catalyst bed is anticipated to minimize the ammonia content of the products, to provide the minimum molecular weight possible. (The masses listed here assume 100 percent decomposition of the N_2H_4 into N_2 and H_2.)

Operation of the system begins by actuating the pyro-valve (or latch valve) at the exit of the gas tank (Figure 4.9). Regulated helium gas is then introduced into the struts and torus (controlled by a series of solenoid valves), with the cooling of the gas over the duration of the fill being within acceptable parameters for the cold-rigidized portions of the structure. The initial inflation of the structure is assumed to have a 5 min duration (worst case). The next operation is pressurization of the solar array booms to sufficient internal pressure (8 psia) to extend and rigidize, followed by inflation of the antenna envelope to operating pressure. The isolation valve between the hydrazine tank and gas tank is then opened, allowing the gas tank to serve as a reservoir for the products of the hydrazine catalyst bed. The gas tank is of sufficient volume to maintain an approximate one-day supply of make-up gas at nominal conditions, at 5 atm tank pressure.

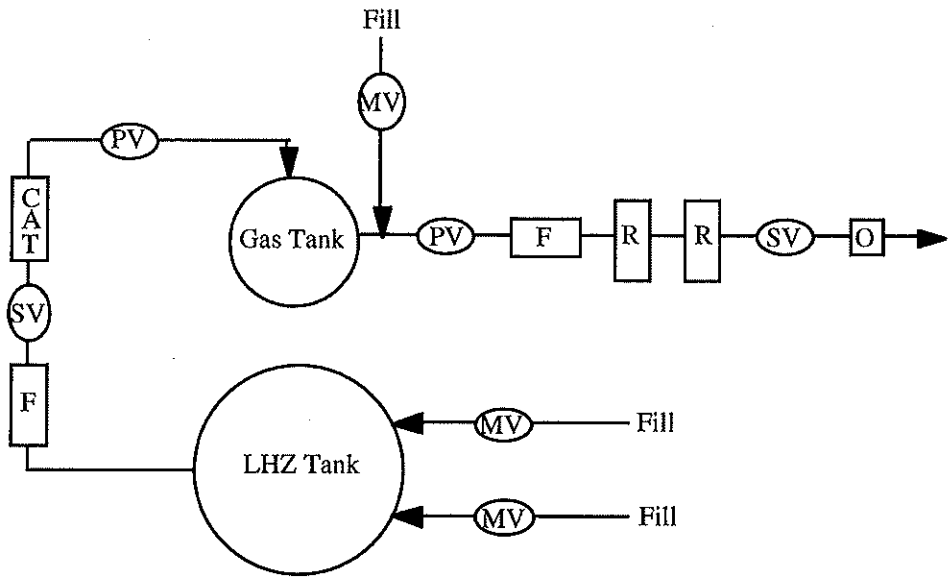

Fig. 4.9: ARISE Inflation System: MV = manual valve; SV = solenoid valve; PV = pyro valve; F = filter; R = regulator; O = orifice; CAT = catalyst bed; LHZ = liquid Hydrazine.

4.4 Subreflector (Mechanically Shaped)

The subreflector design is adaptive to compensate for reflector distortions in the primary reflector and RF-mechanical structure system. The inflatable primary reflector may require compensation for two different types of distortions. The first of these are those distortions that are relatively stable with respect to time. These errors will be seen at the time of the first inflation of the primary, and to a certain degree can be predicted by modeling. The second group of reflector deformations are those time-varying deformations resulting from thermal effects such as solar heating of the primary or its support structure, dynamic effects relative to spacecraft pointing, or structural creep and relaxation of strains in the structure.

This second group of deformations in the system is time-varying. However, these variations are very slow relative to the rate of response of contemporary "adaptive" systems. The responsiveness of "adaptive optics," in the sense in which the term is normally used, is in the 10's of kilohertz regime. These contemporary adaptive systems respond to rapid phenomena, such as the movement of the atmosphere in a high-energy laser beam. The adaptive optics system for ARISE responds to changes which occur at a frequency around a hundredth of a Hz or less. Therefore the "adaptive" aspect of compensating for these errors is a relatively simple one, given there is over six orders of magnitude difference between what is required for ARISE relative to other contemporary adaptive systems.

Adaptive secondaries for radio telescopes have been investigated by the NRAO, the MIT/Haystack Observatory, and elsewhere. The goals of these activities have been primary reflector gravity-sag compensation schemes, which permit a lower cost primary. Composite Optics, Inc. (COI) of San Diego has been working with radio telescope surface adjustment technologies for several years. This COI effort has been highly successful, and has demonstrated surface adjustment on surfaces as large as 3.3 m, using software to define adjustment changes that reduce the surface RMS deviations. Given a defined surface goal, the adjustment process can be utilized to change a given surface into the desired corrected surface. Moreover, the predictive models for these changes in surface are sufficiently accurate that the mechanical surface adjusters may be run open loop. This present device demonstration at COI establishes that a flight version may be engineered as an extension of technology in existence at the time of writing.

4.4.1 Subreflector Description

The proposed subreflector design has a lightweight reflective surface comprised of graphite composite. This reflector surface, supported by a backup structure or "strongback," will form the secondary reflector surface. The reflective surface will be fabricated to a shape that compensates for the known primary surface errors, and will be fitted with adjusters between the backup structure and the surface to permit precise regulation of the subreflector shape. A subframe behind the strong back will permit solid body motion of the subreflector in tip, tilt, and piston directions, as shown in Figure 4.10.

Design of Subreflector Support

The actuators must be attached to a relatively rigid support structure in order to generate the reaction force used to adjust the secondary reflector surface. Thermal distortion, weight and volume are of concern. Therefore, an isogrid graphite composite support structure with near-zero thermal expansion properties is proposed. The control modeling approach will be to characterize the stiffness of the support structure and include that stiffness in the adjustment algorithm.

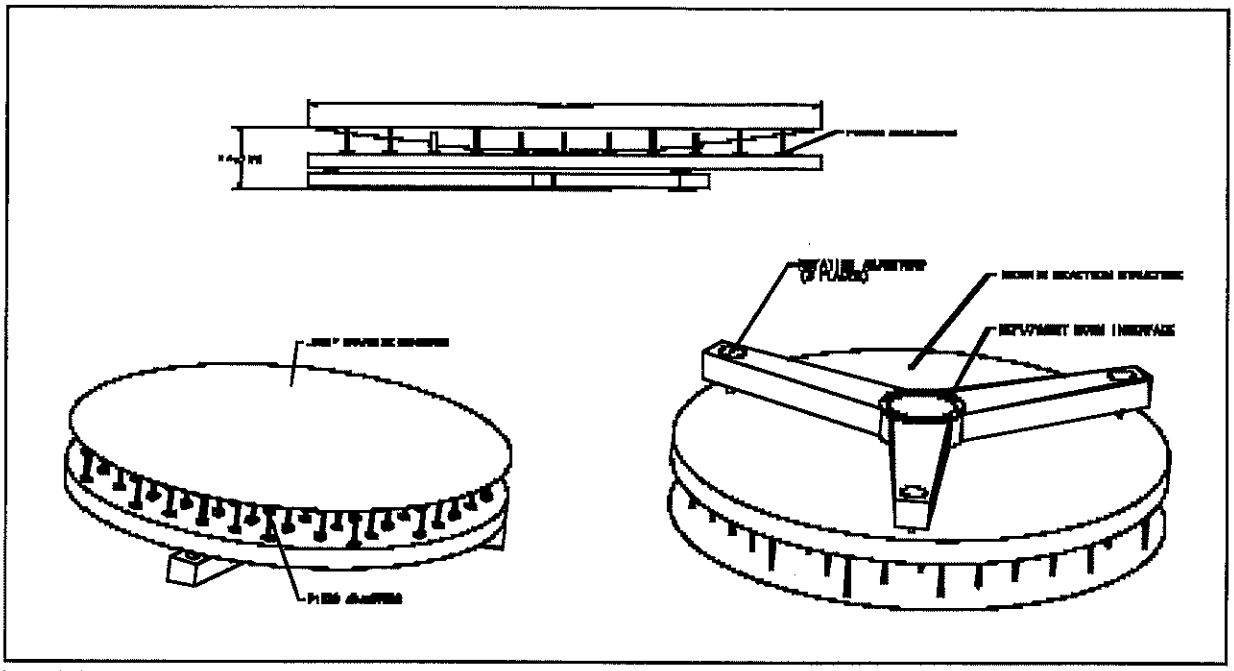

Fig. 4.10: Antenna Subreflector with Adjustable Surface Figure. Technology Demonstration Concept with Picomotors™.

Should additional stiffness or greater packing density be desired, an inflatable "cure on-orbit" structure could be utilized behind the isogrid structure. This inflatable reinforcement system can be inflated on-orbit to add cross sectional area to the structure and be permitted to rigidize before operation.

Surface Subreflector Adjustment

The shaping of the subreflector surface in Space requires around 50 long-travel (2 cm), medium-resolution (1 micron) actuators, which function at cryogenic temperatures (50 K), in order to maintain a 1.6 m subreflector with a surface figure resolution of 60 microns RMS. The greater the number of actuators the better the potential resolution. Algorithms for determining the correct number of actuators for a given quality of surface figure have been established analytically and verified in hardware tests. Figure 4.11 shows this basic, empirical relation between the number of adjusters and achievable RMS for an existing 3.3 m ground based system.

While the necessary cryogenic actuators are presently not available as off-the-shelf products, they will be required for a number of missions such as the Next Generation Space Telescope (NGST). NGST and other missions have active development programs to produce these actuation systems. A room temperature technology involving the Picomotor™, a piezoelectric-driven micrometer actuator with submicron resolution, has been demonstrated. The motors presently being developed for application on NGST will provide lightweight adjusters that can operate in vacuum over the operating temperature range required for ARISE.

Surface Control Software

The current adjustment program written at COI operates in terms of a surface definition that is defined in terms of Zernike polynomials. Although powerful in defining and correcting a standard set of optical surface distortions, this program may require development for a secondary surface that is adjusted for errors in a primary surface. COI has demonstrated that adjusters induce higher order error terms into the surface, requiring very high (greater than 37) Zernike terms to represent

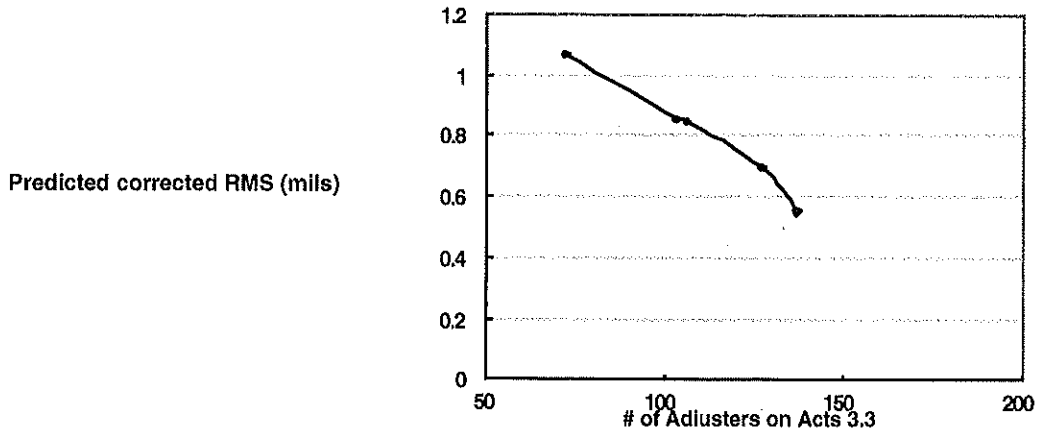

Fig. 4.11: Influence of Number of Adjusters on a 3.3 m Reflector.

the surface errors. The adjustment analysis should operate directly on a set of defined errors to a surface relative to an ideal surface definition.

On-going work at the time of writing (see [4.1] and Section 4.4.3) demonstrates the ability to define the desirable secondary surface to correct for a primary surface. Given knowledge of the actual secondary surface, the differences between the current surface and the desirable surface can be provided for the adjustment analysis. This is a relatively simple modification to present adjustment algorithms.

Projected Subreflector Performance and Current State of the Art

The ability to correct for surface errors with reflectors has been demonstrated in full scale test hardware at COI on a Phase II SBIR program. That program has utilized a 3.3 m parabolic reflector with mechanical adjusters attached for demonstration purposes. The initial surface had an RMS exceeding 8 mils (0.2 mm). Through the use of surface measurement and software written at COI, the adjustment system was able to demonstrate a "corrected" surface error of 1.5 mils RMS (0.04 mm RMS). The remaining RMS error was composed of significant gravity effects plus measurement error.

The accuracy of real-time surface adjustment for on-orbit applications has yet to be demonstrated. However, it has been shown at COI that motions on the order of 10 mils (0.25 mm) can be achieved easily with a 0.2-inch (0.5 cm) thick membrane surface. The surface planned for the ARISE secondary reflector will be on the order of 10-30 mils (0.25-0.75 mm) thick, such that applied forces will be very low to achieve motions on the order of +/- 100 mils (2.5 cm) in the membrane surface of the secondary.

For Earth-based systems, there is a design trade-off between distortions due to gravity, thickness of the reflector skin, and the number of adjusters. Figure 4.12 shows the correction of the gravity-induced RMS for the 3.3 m reflector. For Space-based applications, the absence of gravity loading permits a lighter structure. However, the trade-off exists between the number of adjusters, the stiffness of the strongback, and the degree to which a surface can be manipulated to achieve the necessary corrections.

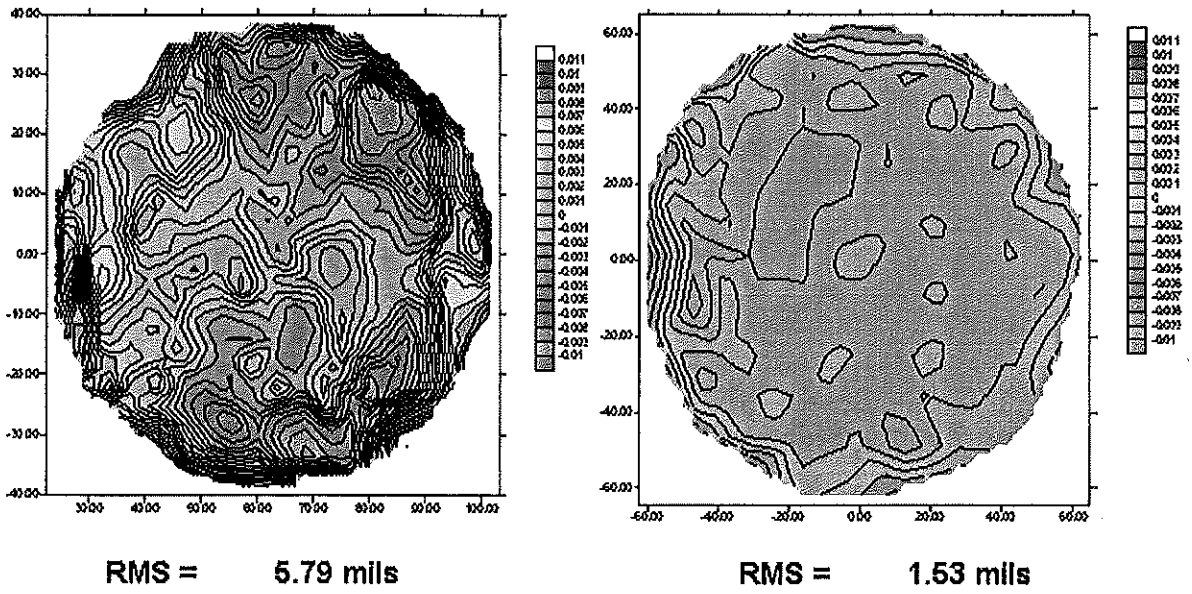

Fig. 4.12: Antenna Before/after Surface Adjustment Demonstration.

4.4.2 Present Tunable Subreflectors and Flight Technology Development Tasks

The development work required before demonstrating flight readiness of an active adjustment scheme based on present COI designs is relatively straightforward. Several topics must be addressed, and fortunately these tasks can proceed in parallel.

Adjuster Analysis Task, Accounting for Support Stiffness and Failed Actuators

The lightest-weight design permits some flexibility in the support structure. The adjustment analysis scheme handles this flexibility if the appropriate influence coefficient model is developed, which accounts for a sub-structure and its flexibility. In addition, the analysis should incorporate a method of "locking out" specific adjusters and still attempting to achieve surface tuning. This will be necessary when one considers the likelihood that one or several adjuster motors may malfunction during a mission. Rather than assume that the adjuster can be moved, it would be substantially more accurate to fix the adjuster at its current location during the analysis so that the balance of the adjusters may be moved to an optimum position accounting for the malfunctioning adjusters.

Adjuster Speed Analysis Task

The cycling times required for on-orbit operation will dictate the computational efficiency required of the adjustment algorithm. A sequence of steps is necessary to provide accurate surface compensation:

(1) Surface measurement through signal reception and other forms of metrology must be made to define subreflector surface figure, and image plane flatness.
(2) Distortion levels must be supplied to an analysis system that defines the desired secondary reflector surface shape.
(3) The desired subreflector shape must be subtracted from the "current" secondary adjuster shape and the adjustment analysis algorithm utilized to define adjuster changes.

(4) The adjusters must be changed and the surface response re-measured when all adjustments are complete for a given cycle.

These steps must occur within the on-orbit cycling time available for adjustment. The current adjustment algorithm requires approximately three (3) minutes to execute. However the adjustments, once defined, can be executed open-loop for every actuator in the system. This can be improved greatly with modifications that account for the fact that only one surface is being adjusted and the influence coefficients will not change for that surface.

"Flexible" Surface Demonstration Task

Once the adjustment code has been modified and an initial support structure designed, the adjustment process should be demonstrated using a surface of greater flexibility than present ground versions. This will permit a greater range of surface variations as may be required given the results of recent, conservative estimates for solar heating of the primary reflector.

Surface Compensation for Primary Reflector Figure Task

In principal the adjustment of a primary surface through a secondary surface can be performed. However, this should be demonstrated experimentally by taking a specific primary surface and adjusting a secondary surface and then coupling the two to determine overall performance.

Mass vs. Cost vs. Accuracy Trade Task for Detail Design Selection

Numerous variables influence the final design, cost and performance of the secondary reflector. Lower mass will induce more flexibility in the support structure and will place heavier burdens on the adjustment analysis algorithm. Fewer adjusters will reduce weight and cost, but will not permit as full a range of surface changes to be made. These variables must be quantified and optimized such that a system level design trade can be understood prior to determining a flight design.

An adaptive secondary reflector will be used to compensate for surface deformations in the primary inflatable reflector surface. It is understood that an inflatable surface will possess surface errors on-orbit that must be compensated for in the measurement system. Once the deformations are measured on-orbit, analytical methods exist which can define the shape of the secondary surface such that the combined surfaces produce an optimized RF signal. The ability to make these kinds of corrections has been demonstrated at COI on surfaces as large as 3.3 m, using algorithms to define adjustment changes to reduce the surface RMS. Given a defined surface goal, the adjustment process modifies a given surface to the desired new surface, permitting continuous, iterative correction for changes in primary reflector surface figure and elsewhere in the entire RF-mechanical system.

4.4.3 Antenna System Projected Performances

To compensate for the reflector surface distortions and to achieve the utmost performance for ARISE, a deformable subreflector has been studied. In the following, the results of numerical simulations of subreflector corrections in a dual reflector system are outlined.

Introduction

To study the performance characteristics of the most suitable subreflector surface shape, efficient numerical techniques are needed in the course of the optimization process, which necessitates repeated computation. As shown in Figure 4.13, three different techniques can be envisioned. First, Physical Optics (PO) on both the main and the subreflector (PO/PO) is used for complete

diffraction analysis. Especially for electrically large reflectors, PO/PO takes a prohibitively large amount of computer time. Second, Geometrical Optics (GO) traces an optical ray from the feed to the subreflector and the main reflector (GO/GO), and then minimizes the RMS of the phase in the main reflector aperture plane. While this technique is very fast, no diffraction analysis of the main reflector is involved. To overcome the disadvantages of the previous techniques, a hybrid shaping technique (GO/PO) is employed in this work. While this technique does not incorporate the diffraction losses of the subreflector during the shaping process, complete PO/PO diffraction analysis subsequently yields the radiation characteristics of the dual reflector antenna. Especially if it is desired to use the reflector antenna over a wide frequency band, an optical shaping technique yields a more frequency independent result. Also, for the ARISE reflector configuration, GO/PO is faster than PO/PO by orders of magnitude. The shaped subreflector surface is described through the coefficients of a Fourier-Jacobi (similar to Zernike expansion) surface expansion. For shaping applications, this GO/PO technique is incorporated into an optimization algorithm to iteratively attain the subreflector surface expansion coefficients. Next, the implementation of a Fourier-Jacobi surface expansion into a GO/PO reflector analysis is discussed and some unique features of this implementation are detailed.

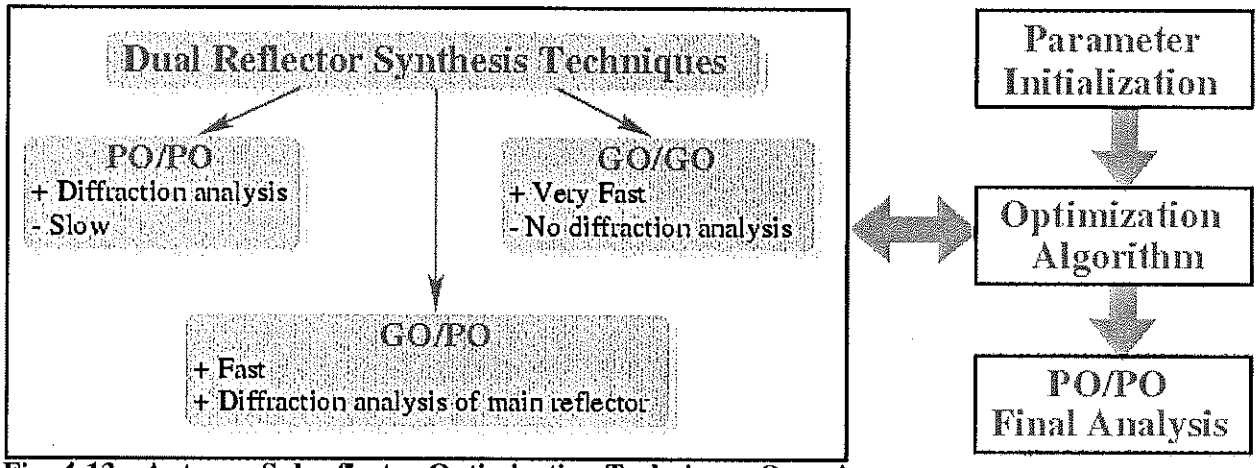

Fig. 4:13: Antenna Subreflector Optimization Techniques Overview.

GO/PO Implementation and Verification

The radiation characteristics, such as directivity or far-field patterns, of a dual reflector antenna are calculated from the main reflector PO currents. To determine the PO currents at a point on the main reflector, a Newton-Raphson iterative technique finds the reflection point based on Fermat's principle for a GO ray emanated from the feed. At the reflection point, the field strength of the incident ray, the curvature matrices of the incident ray, the surface, and the reflected ray are calculated. Once the divergence factor of the reflected ray is determined, the vector field of the reflected ray at the observation point on the main reflector is determined. For this GO/PO procedure, a surface description in terms of surface height, plus first and second derivatives is determined. To verify the derivation made above, the radiation characteristics for the ARISE dual reflector configuration were calculated for the analytical and the expanded subreflector surface. The far-field pattern of ARISE at 22 GHz, with both an analytically described subreflector as well as with the Fourier-Jacobi expanded surface, are shown in Figure 4.14. Both the surface accuracy of the Fourier-Jacobi expansion as well as the radiation performance comparison, as implemented into the GO/PO analysis technique, showed very good agreement with the analytical equivalent.

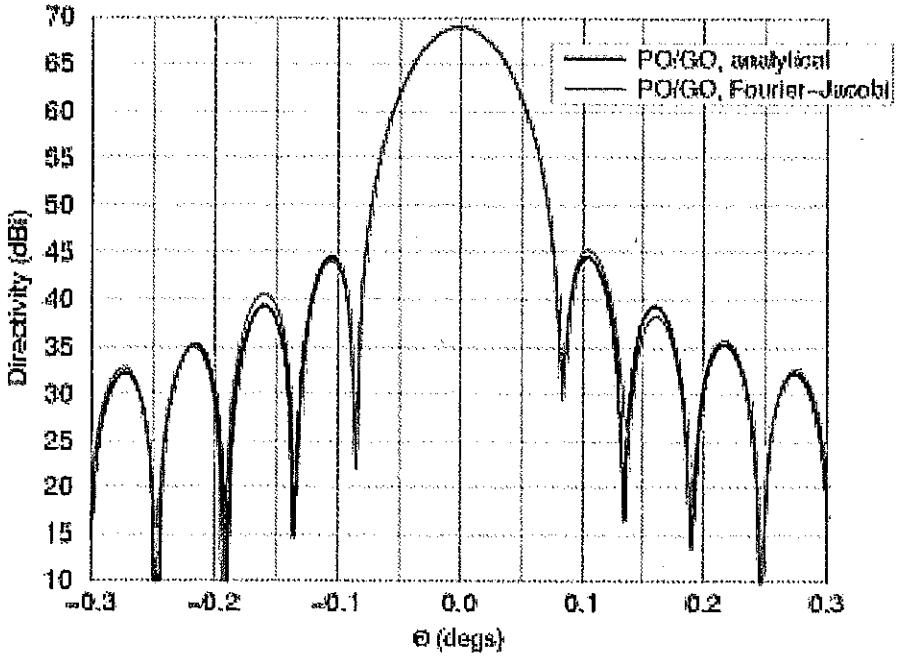

Fig. 4:14: ARISE 22 GHz Dual Reflector Far-field Pattern.

Performance for the 1mm RMS Surface Distortion

For the 1 mm RMS main reflector surface distortion as displayed in Figure 4.15 (left), the GO/PO procedure was applied at an operating frequency of 22 GHz. The most suitable surface shape of the correcting subreflector was found iteratively through a Simplex optimization algorithm. The subreflector surface shape difference to the ideal shape is displayed in Figure 4.15 (right). Clearly, the characteristics of the main reflector surface distortions have been recovered.

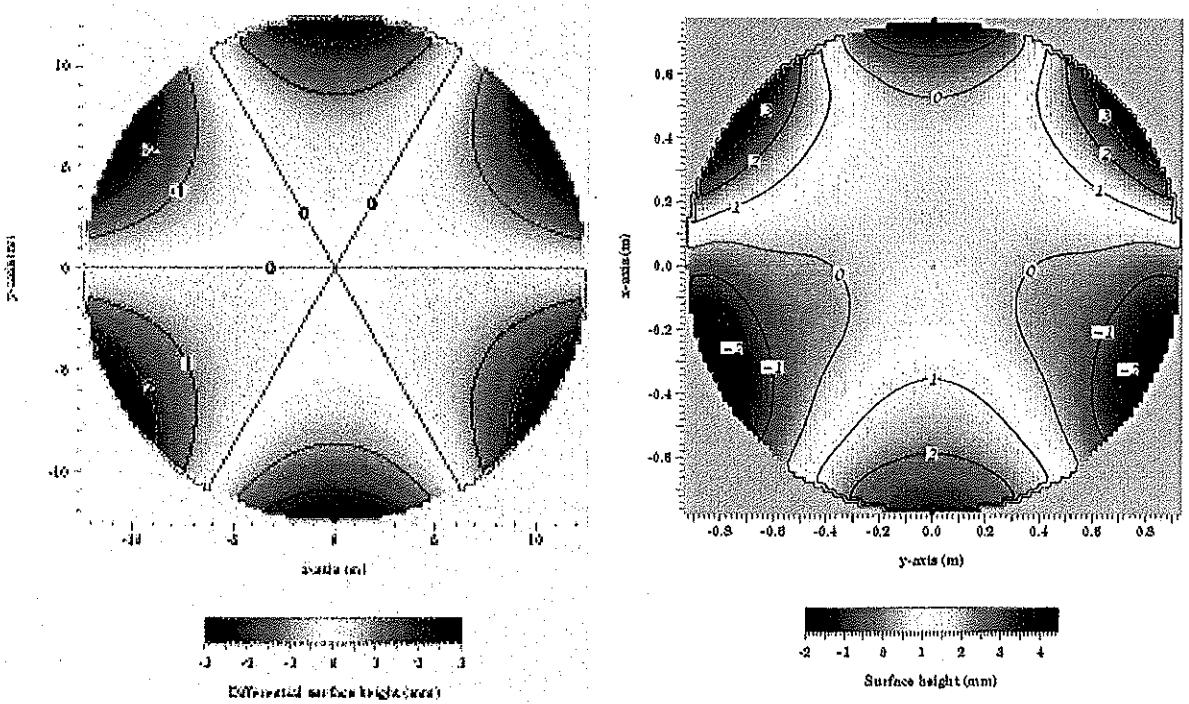

Fig. 4:15: (left) ARISE 22 GHz Main Reflector Surface Distortions; (right) Subreflector Surface Shape Difference to Ideal Shape.

In Figure 4.16, the ideal far-field pattern of ARISE at 22 GHz is displayed. Assuming the 1 mm RMS main reflector surface distortions, the far-field pattern of ARISE at 22 GHz is shown in Figure 4.17 (left). The sidelobe and cross-polarization level is significantly increased, and the directivity is decreased by 1.4 dB. Next, the corrective subreflector, as shown in Figure 4.15 (right), is applied. The far-field pattern with corrective subreflector at 22 GHz is shown in Figure 4.17 (right). The boresight directivity is increased by 1.3 dB with respect to the uncorrected result, and differs by only 0.1 dB relative to the ideal performance.

Next, the same corrective subreflector, shaped at 22 GHz, and displayed in Figure 4.15 (right), is applied to the operating frequencies of 43 GHz and 86 GHz. In Figure 4.18 (left), the distorted far-field pattern at an operating frequency of 43 GHz is displayed. The boresight directivity is reduced by 4.2 dB. With subreflector correction, the directivity recovers 4.0 dB and differs by only 0.2 dB from the ideal value. The respective corrected far-field pattern at 43 GHz is shown in Figure 4.18 (right). At 86 GHz, the distorted and corrected far-field pattern are displayed in Figures 4.19 left and right, respectively. For this configuration, the boresight directivity reduces from the ideal value by 7.7 dB, and recovers 7.0 dB to 0.7 dB below the ideal directivity.

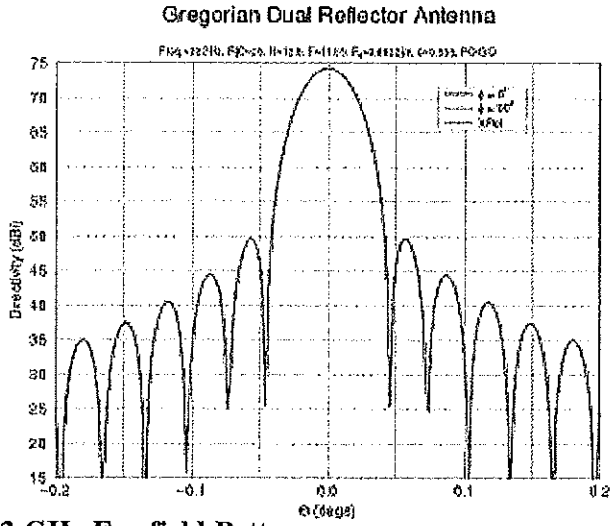

Fig. 4:16: ARISE Ideal 22 GHz Far-field Pattern.

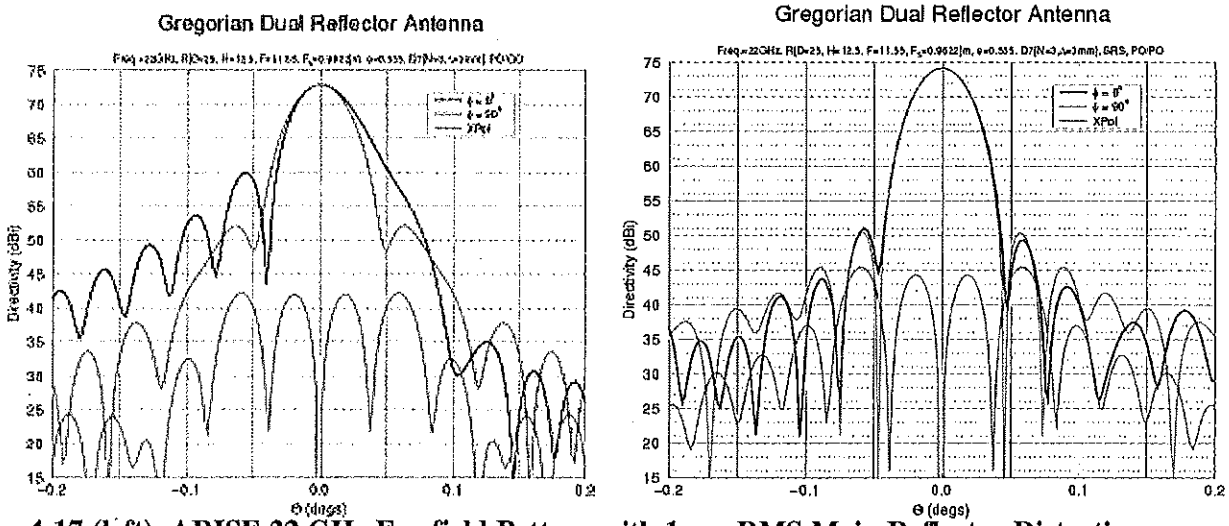

Fig. 4:17 (left) ARISE 22 GHz Far-field Pattern with 1mm RMS Main Reflector Distortions. (right) ARISE 22 GHz Far-field Pattern with Corrective Subreflector.

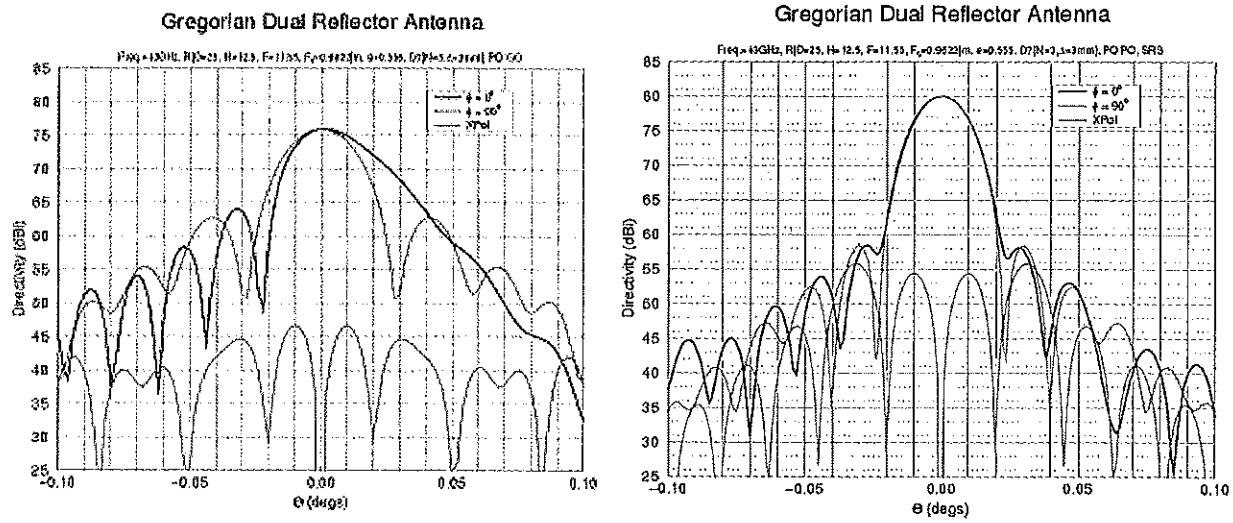

Fig. 4.18 (left) ARISE 43 GHz Distorted Far-field Pattern.
(right) ARISE 43 GHz Far-field Pattern with Corrective Subreflector.

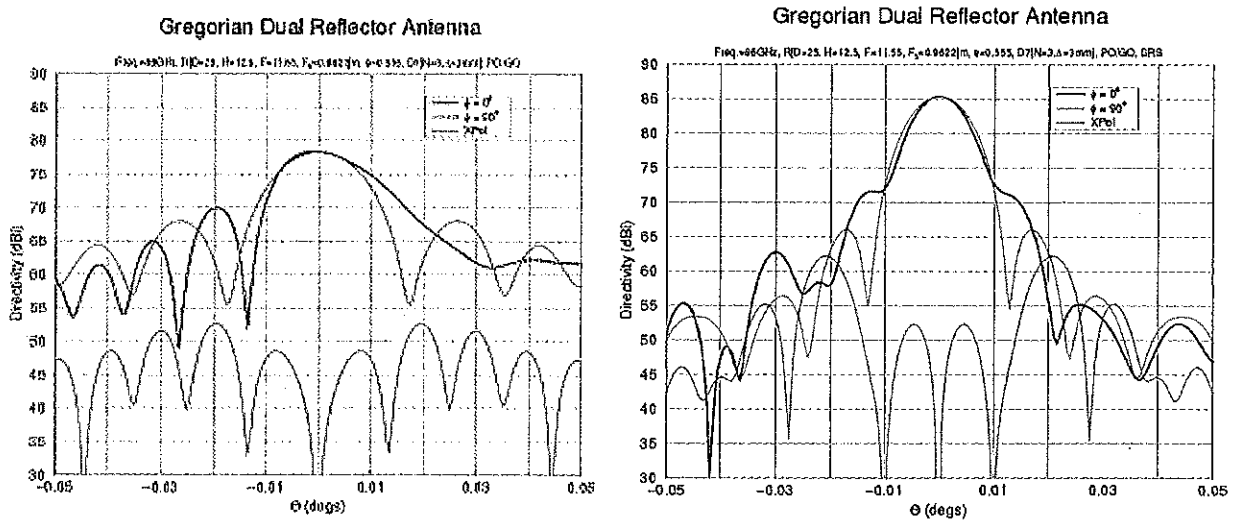

Fig. 4.19 (left) ARISE 86 GHz Distorted Far-field Pattern.
(right) ARISE 86 GHz Far-field Pattern with Corrective Subreflector.

In Table 4.3, the radiation performance of ARISE at 22 GHz, 43 GHz, and 86 GHz is shown in terms of the boresight directivity and the antenna efficiency. At each frequency, the ideal, distorted, and subreflector corrected radiation performance is displayed.

	F = 22 GHz		F = 43 GHz		F = 86 GHz	
	D [dBi]	AE [%]	D [dBi]	AE [%]	D [dBi]	AE [%]
Ideal	74.3	81	80.2	81	86.1	81
Distortions (1mm RMS)	72.9	58	76.0	31	78.4	14
Corrective subreflector (shaped at 22 GHz)	74.2	79	80.0	79	85.4	68

Table 4.3: ARISE Radiation Performance.

Overall System Efficiency

One of the most critical parameter to assess on ARISE is the overall antenna efficiency. For a 25 m diameter aperture, the science requirements ask for a 7 σ sensitivity of about 1 mJy at 22 GHz, about 10 mJy at 43 GHz and about 100 mJy at 86 GHz. It is then desirable that the antenna efficiency be at least 0.38 at 22 GHz, at least 0.24 at 43 GHz, and at least 0.08 at 86 GHz. The subreflector compensation scheme described above allows for an increase in antenna efficiency that includes distortions of the main reflector, aperture taper, feed spillover and polarization efficiencies. However, other losses should be taken into account. A preliminary assessment of these other system efficiencies is summarized in Table 4.4 for each frequency of interest. A major factor is the canopy transmittance, which is based on actual testing of a 0.5 mil CP-1 sheet coated with 100 Ang. of ITO (currently the candidate material for the canopy). The reflector material is a 0.5 mil sheet of Kapton coated with aluminum. The pointing error is an estimate from the spacecraft and antenna ADCS analysis.

Moreover, the above analysis has been performed for an "ideal" 1 mm RMS (i.e. the distortion patterns are very symmetric and might be simplistic compared to the real reflector distortion) surface shape and did not take into account the reflector distortions due to thermal effects. Thus the results presented in Table 4.4 are to be considered preliminary and should be treated as such. It is, however, expected that the thermal distortions, being by nature global and not local, should be relatively easy to correct with a re-focussing of the subreflector (through piston translation and tilt) and with the subreflector shape correction.

Efficiency	**22 GHz**	**43 GHz**	**86 GHz**
Subreflector correction (computed, includes antenna distortions, aperture taper, feed spillover, polarization)	0.79	0.79	0.68
RF path attenuation			
Shadowing (struts + S/C)	0.94	0.94	0.94
Canopy transmittance (twice)	0.91^2	0.88^2	0.85^2
Meteoroid shield (twice)	0.95^2	0.95^2	0.95^2
Reflector reflectance	0.98	0.98	0.98
Surface local rms (specular)	0.98*	0.98*	0.98*
Feed displacement	0.98*	0.98*	0.98*
Pointing error	0.98*	0.98*	0.98*
Surface ohmic efficiency	0.99*	0.99*	0.99*
Feed network loss	0.95*	0.95*	0.95*
Total efficiency	**0.48**	**0.45**	**0.37**

Table 4.4: ARISE Projected Overall Aperture Efficiency (preliminary) *: estimated efficiency

Future Work

Proposed future work includes the characterization of the realistic surface distortion in terms of its impact on the radiation characteristics. Additionally, the capability of the deformable subreflector to

correct for these surface distortions must be assessed. Moreover, the combined corrective performance of both shaped subreflector and array feed must be assessed.

As proposed, the subreflector surface is adaptively shaped in Space for main reflector surface distortion compensation. The minimum number of actuators, their location on the subreflector surface, and the resulting surface shape will have to be compared to the most suitable shape obtained through subreflector shaping. Furthermore, the radiation characteristics have to be assessed for the various cases.

4.4.4 Metrology System

As stated earlier in this document, the reflector shape (distortions) will vary during the mission. At every new source observation, the orientation of the spacecraft with respect to the Sun and the Earth will be different, and thus the thermal loads. In order to know the new subreflector position and shape to implement, a metrology system is used. The main objective of this system is to map and reconstruct the reflector shape. From the knowledge of the reflector surface, algorithms calculate the optimum (implementable) shape and position of the subreflector. This mapping will take place at each new source targetting and if necessary after each eclipse.

Several options for metrology systems have been investigated. The most promising system identified is photogrammetry. Its main advantages are its simplicity and its heritage. Photogrammetry is a technique that uses photographs for mapmaking. For ARISE, it involves three (3) cameras (one on each end of the solar array wings and one on the spacecraft), three (3) light sources positioned close to the cameras, and small optical reflectors (tape) positioned at key locations on the main RF reflector. Three pictures taken sequentially from the three cameras are combined to deduce the surface shape of the reflector. This activity is rather computationaly intensive, but not outside the limits of the selected spacecraft computer capabilities. Further definition of this system will be undertaken in future work.

4.4.5 Other Current Activities in the Subreflector Correction Area

Towards an application of the ARISE antenna development, here we describe a test and calibration of a fully actuated deformable flat plate (DFP) for compensating the gravity-induced structural deformations in the 70 m and 34 m DSN antennas. The most significant cause of performance degradation of the large DSN antennas at Ka-band (32-GHz) is the gravity-induced deformation of the main reflector surface occurring at the low and high elevation angles. This reduction in antenna performance at Ka-band at the low and high elevation angles for the 34 m beam waveguide (BWG) antennas is measured to be approximately 1 dB, while for the R&D BWG antenna, it is approximately 2.3 dB, and for the 70 m it is estimated to be more than 6 dB. Experiments performed at Goldstone (DSS-13) demonstrated that a deformable reflector could recover almost all of the gain lost due to the gravity deformation. A fully controllable surface would provide the capability of nearly completely compensating for the gain loss due to gravity induced structural deformations over the entire range of elevation angles. The deformable reflector would provide the lowest cost technology for providing this capability.

In 1998, all the analytical/computational tools were developed to enable near-real-time derivation of the optimum actuators displacements over all elevation angles (look-up table) from a measured holography data set at three elevation angles. This computational tool is critical for the success of this task since holography is the most direct and suitable technique for the calibration of the DFP and since in general an a priori knowledge of the exact deformation of the antenna at the low (high) elevation angles is not available and the gain loss due to sub-optimum setting is high at Ka-band. A demonstration of the DFP on the 70 m at Goldstone is underway at the time of writing.

For this demonstration, the DFP has been installed inside the Holography-Cone. Using the Holography-Cone (as opposed to mounting the DFP on top of an existing cone) offers many advantages including improved environment and increased space that allows for multi feed testing. It provides for easy compliance with noise abatement and provides easy access to the R&D equipment. The following has been accomplished to date.

A full set of holography maps has been derived from the measured data at 12.7, 36.7 and 46.7 degree holography maps. Using ray optics, the reflector shape that compensates for the calculated surfaces has been determined. Using a total power radiometer, the efficiency vs. elevation angle has been measured and the incremental improvement of the DFP measured by alternating between setting the surface flat and setting the surface for distortion compensation. Improvements range from 0.2 dB at the rigging angle (where the gravity induced loss is minimum) to nearly 4.0 dB at the high elevation angles (where the gravity induced loss is the maximum).

Further tests are planned with the monopulse feed providing the ability to track the spacecraft DS-1. Direct measurements of the improvement to the SNR will then be possible.

4.5 Adaptive Feed Array (Optional)

To improve the antenna efficiency at 86 GHz, an array feed is being contemplated to compensate for surface distortions and beam pointing errors. This array is currently carried as an option and does not appear in the baseline design. The geometry of this array feed is displayed in Figure 4.20. The actual number of feed array elements is a subject for future research.

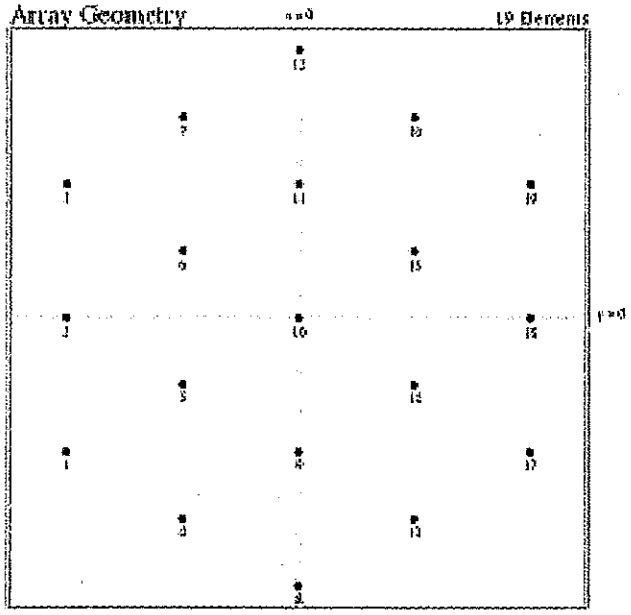

Fig. 4.20: ARISE 86 GHz 19-element Corrective Array Feed.

Analytic surface distortions as displayed in Figure 4.21 (left) are considered on the main reflector. In Table 4.5, the radiation characteristics of the three cases "ideal" (no surface distortions), "distorted" (analytic, 1 mm RMS, surface distortion model) and "compensated" (using corrective feed array excitation) are shown. Figure 4.21 (right) displays the far-field patterns of ARISE at 86 GHz with the analytic, 1 mm RMS, main reflector surface distortion, and a 19-element array feed

compensation. Note that in those cases, no subreflector shaping is used and only the array compensation is applied.

	F = 86 GHz	
	D [dB]	AE [%]
Ideal	86.2	82
Distorted (1mm RMS)	76.7	9
Compensated	78.63	14

Table 4.5: ARISE RF System Performance at 86 GHz, with 19-element Corrective Feed Array.

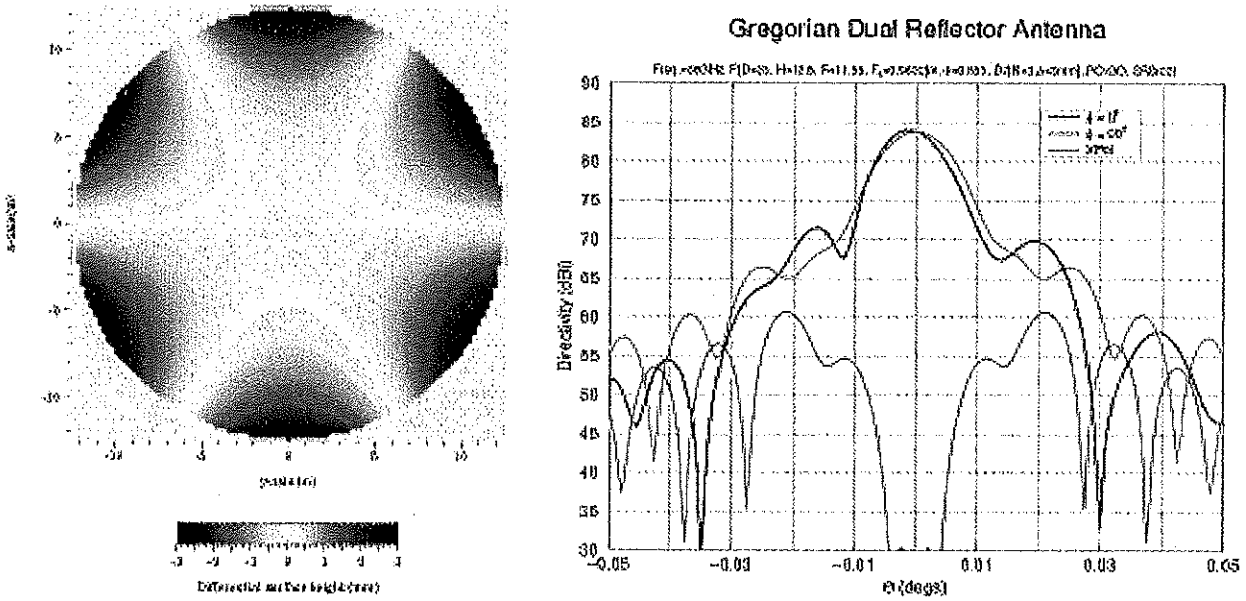

Fig. 4.21 (left) ARISE 86 GHz Analytic 1 mm RMS Surface Distortions;
(right) ARISE 86 GHz Far-field Pattern with 19-element Array Feed Compensation.

4.6 Receivers/Amplifiers/IFs

The ARISE receiver design is critical to the final performance of the instrument. By providing the lowest noise possible, requirements on the size and performance of the primary reflector can be bound to achievable goals. Cryogenic InP High Electron Mobility Transistors (HEMT) provide the lowest possible noise for receivers from 1-100 GHz operating at temperatures above 4 K. In addition, InP HEMT transistors operate with the lowest power dissipation of any three-terminal device, which is critical for thermal load on the cryocooler.

The baseline ARISE receivers are at the 8, 22, 45 and 86 GHz bands, with an optional band at 60 GHz. The receiver front end is cooled to 20 K. The front end comprises a horn, polarization splitter, and an InP HEMT amplifier (LNA). The front end is nominally designed to have a noise figure of five (5) times the quantum-limited noise at all observing bands. This noise temperature has already been achieved at 8, 22, and 44 GHz using InP HEMT amplifiers with discrete transistors. A noise figure of 31 K has been achieved at 100 GHz, or six (6) times the quantum-limited noise, via InP MMIC amplifiers manufactured for NASA by TRW [4.2]. The use of InP monolithic microwave integrated circuit (MMIC) technology allows for state-of-the-art

performance and ease of integration at 86 GHz. This will be crucial should the adaptive array be utilized on ARISE.

The sensitivity of the VLBI receiver system improves as SQRT(T_{sys}), thus continued development in the area of low noise receivers could pay a large dividend in achieving the ARISE performance goals.

Parameter	8 GHz	22 GHz	44 GHz	86 GHz
Noise (K)	8	12	19	39
Bandwidth (GHz)	2	2	2	2
Cryo power (mW)	64	23	15	8

Table 4.6: ARISE Receiver Performance.

A cryogenic gain of 30 dB is adequate for all frequency bands to minimize the effect of back-end noise. The cryogenic portion of the radiometer front end is connected to a warm back end via stainless steel waveguide or coaxial cable. The signals are then passed through an image rejection filter and mixed down to an IF band from 2-3 GHz. Warm RF amplification may be used to further reduce the impact of noise in the warm back end. All microwave reference synthesizer frequencies will be derived from the ground tracking station (GTS) uplink frequency reference. Further signal amplification will occur in the IF band.

The IF signals are selected by frequency and polarization, down-converted to a nominal baseband (IF) bandwidth of 256 MHz and digitized. The digitized data are formatted, modulated onto multiple frequency division multiplexed (FDM) carriers and transmitted to the ground tracking station. Further details are provided in Chapter 5.

The option for a 60 GHz channel operating in single-dish total power mode is intended to provide a first glimpse for a large aperture at this frequency, which is opaque from the Earth. Because the signals cannot be correlated with other ground radio telescopes, the ARISE 60 GHz channel must be stable for long integration times. Dicke-switching through telescope motion is not feasible for the large reflector. The alternatives for ARISE are frequency switching for spectral line measurements and spatial Dicke-switching in the focal plane for continuum stability.

4.7 Instrument Thermal Control

The 20 K temperature requirement for the HEMT amplifiers in the science instrument can be met by a 20 K hydrogen-sorption cooler coupled to a mechanical precooler. Sorption cooling has been demonstrated for flight aboard STS-66 in 1996. A 20 K continuous hydrogen sorption cooler is presently in development at JPL for the Planck Surveyor mission, and will be available around the expected start of ARISE. The sorption cooler requires a precooling stage of about 60 K or less, which can be supplied by any of a number of mechanical coolers that are expected to be available in the ARISE time frame. The complete cryocooler system will have a mass of 25-50 kg and require input power from 200-350 W, depending on the combination of cryocoolers that is ultimately chosen. The following paragraphs detail the performance requirements of the cooler system and some of the design options that are available.

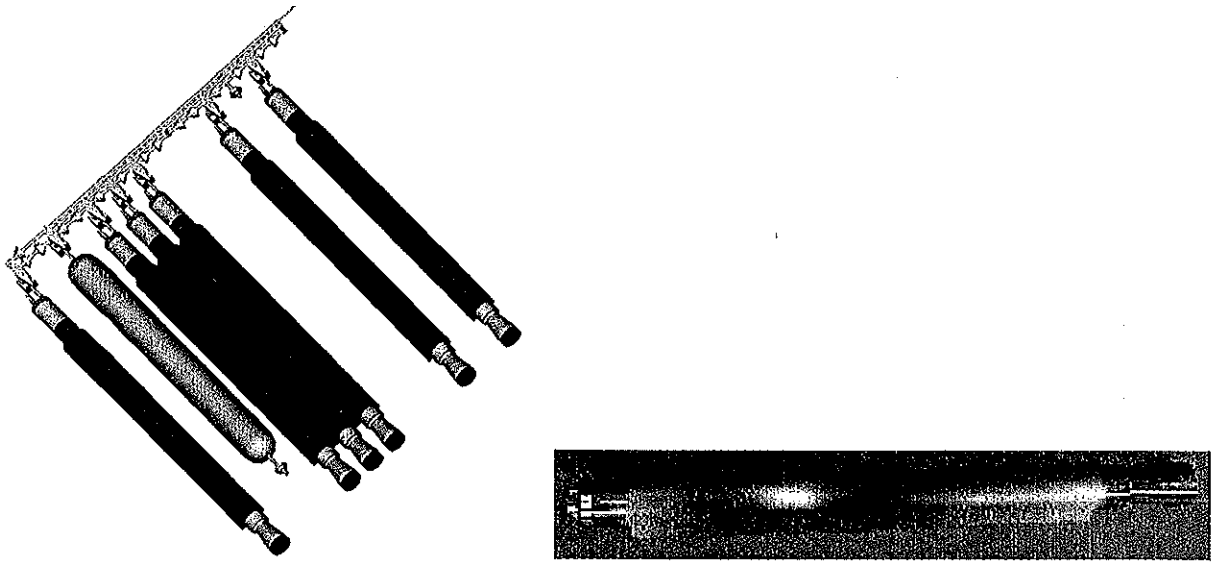

a) b)

Fig. 4.22: a) Mechanical Drawing of the Planck Surveyor Compressor Assembly. Each compressor bed for the Planck cooler is 45 cm long. The total compressor assembly mass is 35 kg. b) Photograph of a Single Compressor Bed. This length can be reduced to 2 cm for a 35 K precooled ARISE cooler, or 18 cm with a 60 K precooler.

The expected load on the 20 K cold-stage is between 170 mW and 210 mW, depending on the base temperature of the precooler selected. The sorption cooler in the Planck spacecraft is passively precooled to 53 K and is capable of providing about 1.3 W at 20 K with a total input power of 520 W. This design can be readily scaled to meet the lower load of the ARISE instrument by reducing the length of the compressor beds, shown in Figure 4.22, resulting in a corresponding decrease in mass and input power. The mass and power can be further reduced by providing a lower precooling temperature. Simply scaling the existing design to meet the ARISE requirement with a 35 K first stage leads to an input power of 110 W for the 20 K sorption cooler. Because the cooler becomes very efficient when the hydrogen is precooled to 35 K, the required metal hydride mass is very small, and the mechanical structure supporting the compressor can be reduced, resulting in even lower mass and input power. If the precooling requirement is relaxed to 60 K, the required input power is increased to 246 W. At both precooling temperatures most of the input power is supplied to the compressors as heat for desorbing hydrogen from the compressor beds, which cycle between 300 K and 423-480 K. The compressors are cooled from their high temperature back to 300 K, in order to reabsorb hydrogen, by passive radiators (0.6 to 0.9 m^2) at 290-300 K.

A number of mechanical coolers with sufficient heat lift in the 35-60 K range will be available for use as the precooling stage. Because of differences in the sets of coolers available, it is convenient to choose the endpoints of this range, 35 K and 60 K, for analysis. The load on the precooling stage will be dominated by parasitics (conduction and radiation) and at either temperature will be about 1.0 W. Flight, proto-flight, and engineering models of coolers for both temperatures already exist, and substantial development is expected to occur by the time ARISE enters phase C/D. Table 4.7 summarizes the characteristics of some coolers that are likely to be available. The Creare reverse-Brayton coolers are closely related to the 70 K cooler flown on STS-95 in October 1998. The TRW 55 K cooler shown in Figure 4.23 has been delivered and will fly as part of the Atmospheric Infrared Sounder (AIRS) on the Earth Observing System (EOS PM-1) in 2000; the 35 K TRW cooler is closely related to the AIRS cooler.

The ARISE baseline carries two (2) Creare reverse-Brayton coolers (one (1) in cold redundancy) and one (1) scaled sorption cooler for a total mass of 50 kg and power of 350 W.

Manufacturer	Cycle	Temp (K)	Input Power (W)	Mass (kg)	Maturity
Creare	Reverse Brayton	35	105	15	PF
Raytheon	Split-Stirling	35	112	18.5	PF
Lockheed Martin	Split-Stirling	35	198	29.4	FM
TRW	Pulse-Tube	35	288 (est)	32	EDM
Creare	Reverse Brayton	60	100 (est)	13.7	EDM
Lockheed Martin	Split Stirling	60	130	17.9	FM
TRW	Split Pulse-Tube	55	102	12.7	FM

Table 4.7: ARISE Mechanical Cooler Technology (adapted from [4.3]). Abbreviations for maturity levels: FM=flight model, PF=Proto-Flight, EDM=Engineering Development Model. All input powers are normalized for 1 W heat lift at the cold tip.

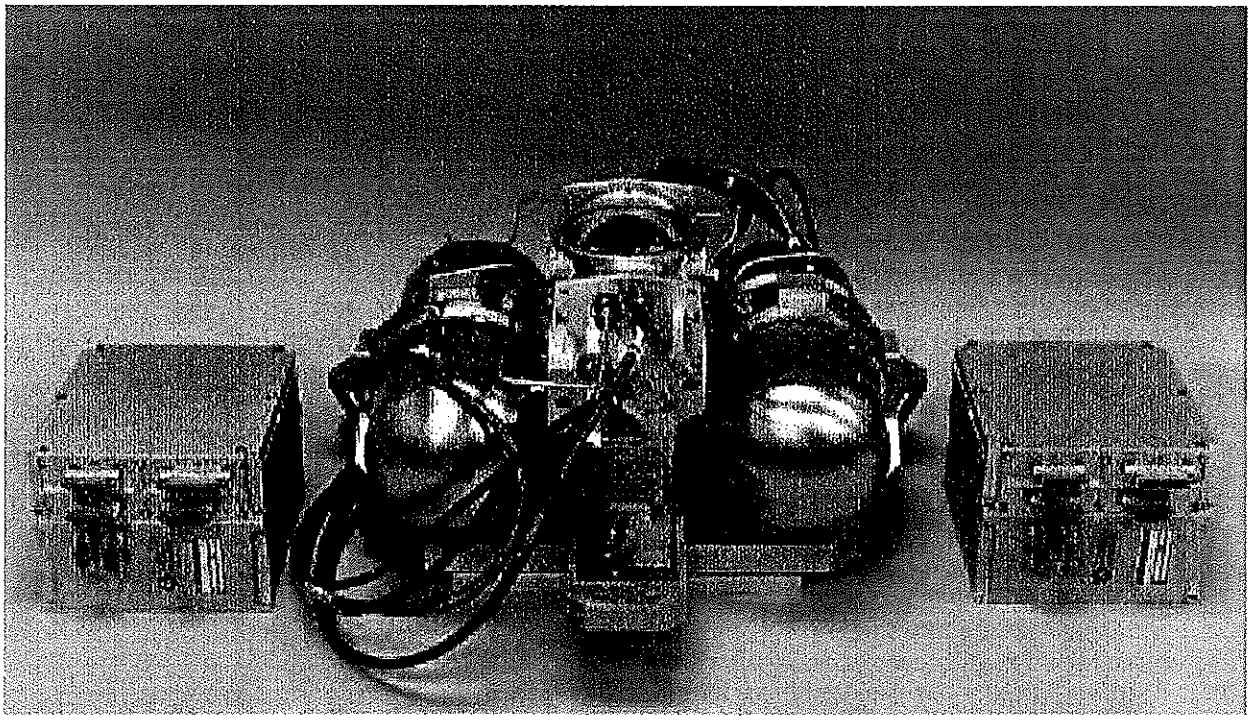

Fig. 4.23: The AIRS 55 K Cryocooler and Electronics [4.4].

4.8 Main Reflector: Non-Inflatable Options

Since the 1960's, deployable mesh reflectors that are autonomously deployed have been pursued for their potential to fill mid-sized (< 15 m) antenna apertures with extremely lightweight reflectors. Because of their relatively complex mechanical nature, they are usually expensive and present bulky stowed profiles for launch. Reliability, mesh management, and extreme thermal environments have also been issues of prime concern, especially as communications, imaging, and scientific satellite missions demand ever larger reflector apertures.

Recent developments in deployable mesh reflector designs, however, have made it possible to build antennas with larger diameters, increased deployment precision and figure accuracy, and longer orbital lifetimes. Many of these designs have been demonstrated at different levels of development while still others have been recently flown. The following discussion highlights representative mesh antenna concepts from two of the antenna Industry's leading manufacturers (TRW and Harris Corp.) that have the potential of being applied to the ARISE Mission with its high frequency and extreme temperature environment performance requirements. There is general agreement in the industry that while existing mesh technologies can meet the frequency requirements up to 43 GHz, 86 GHz antenna performance will require some near term technology development.

4.8.1 Harris Concept

Harris Corporation offers an alternative concept for ARISE based on their extensive deployable reflector heritage. Harris has flown over 14 reflectors for the government market including the twelve (12) 5 m diameter TDRSS reflectors, shown in Figure 4.24 (left), which operate up to 15.5 GHz. Harris has also flown multiple units of a classified 15.2 m diameter reflector whose existence has recently been declassified.

Most recently, Harris has delivered two, qualified, 12 m diameter commercial reflectors which operate at 2 GHz. These reflectors, shown in Figure 4.24 (right), are scheduled for launch late this year on the ASEAN Cellular Satellite (ACeS).

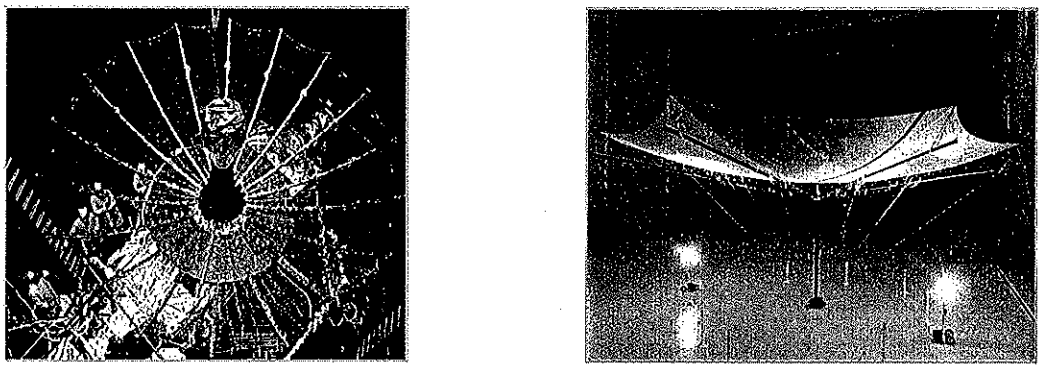

Fig. 4.24: (left) Harris TDRSS Antennas Operate up to 15.5 GHz; (right) Harris 12 m L-Band Commercial Reflectors.

Harris' ARISE concept involves the combination of an advanced mesh surface with a "solid deployable" graphite spline surface in one 25 m diameter deployable structure (see Figure 4.25). The inner 8 m diameter surface consists of a foldable solid graphite spline surface that will operate at 86 GHz. Initial testing on solid graphite spline surfaces demonstrated excellent reflectivity up to 90 GHz, which addresses the ARISE maximum frequency of 86 GHz. The remaining aperture

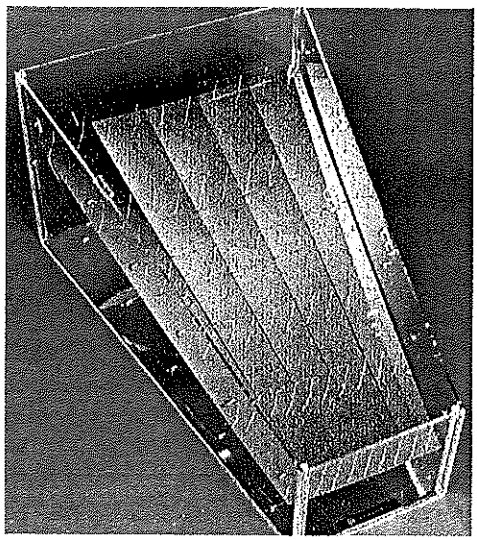

Fig. 4.25: Solid Deployable Graphite Spline Technology for High Frequency Applications.

consists of a high frequency mesh for operation up to 43 GHz. The deployment approach utilizes deterministic motor controlled motion to assure very high reliability deployment and mission success. The RF reflective gold plated molybdenum mesh surface and solid graphite spline surface are supported by a precision graphite structure and shaped using a low distortion cord network. These surfaces can be shaped to very accurate contour with less than 10 mils (0.25 mm) roughness. The reflector stows on top of the ARISE spacecraft and is attached to the spacecraft via a folding boom as seen in Figure 4.26. The current concept fits into a Delta 2 or equivalent low cost launch vehicle. The concept weighs approximately 450 kg and has an expected life on-orbit of over 10 years.

In order to reduce the program risks for ARISE, the following technology development studies are recommended:

- Surface Technology,
- Structure Technology,
- Manufacturing,
- Interfaces.

In the surface technology area, Harris envisions refining the design of the compound mesh and spline surface and then producing a subscale breadboard model to prove the concept. The breadboard will be used to evaluate surface stowage, interfaces, contour shaping, RF performance and surface management. This breadboard will prove the overall performance and functionality of the ARISE reflector design.

The structural technology study involves trading various concepts to achieve minimum stowed volume and assure compatibility with a low cost launch vehicle. This is primarily an analysis and design study with limited hardware models.

The third area is a manufacturing study. In order to make ARISE weight efficient, the reflector will be designed to be counterbalanced during deployments. This study will involve evaluating counterbalance schemes such as balloons and mechanical counterbalances. In addition, the manufacturing study will develop plans for aligning the RF system at the spacecraft level to assure full system performance on-orbit.

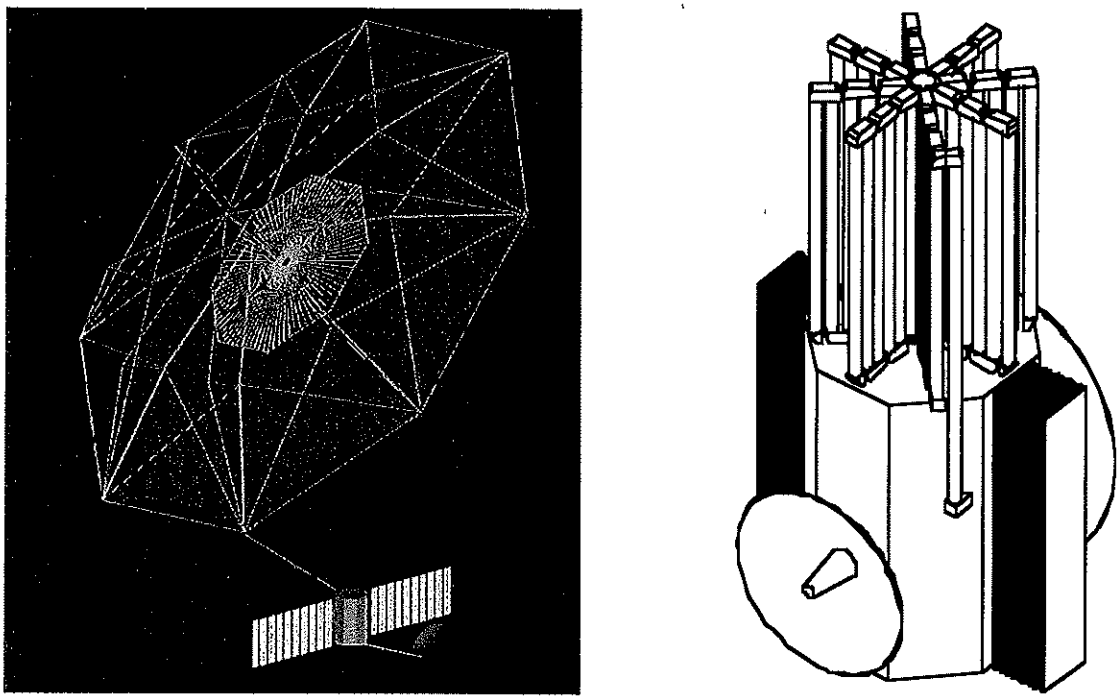

Fig. 4.26: (left) Harris 25 m Deployed Reflector Concept for ARISE; (right) Harris 25 m Stowed Reflector Concept for ARISE (1.3 m diameter and 2 m High).

Lastly, the interface study will refine and establish interfaces between the spacecraft and the stowed/deployed reflector. These include restraint locations, structural loads, and stowed and deployed frequencies.

4.8.2 TRW AstroMesh

TRW has three (3) mesh deployable antenna concepts that have potential for ARISE: the PAMS, the ASTROMESH, and a new "perimeter truss" configuration concept. The PAMS is a double articulated radial rib that has been developed to the point of a 10 m diameter prototype flight unit, but could be extended to 25 m. The ASTROMESH antenna concept, which is now owned by TRW, has been developed as two 12.25 m diameter flight units to be flown in 2001. TRW's new perimeter truss concept, similar in configuration to the ASTROMESH, has been demonstrated at the 2 m diameter size. According to TRW both perimeter truss approaches can be scaled to 25 m diameters.

The AstroMesh perimeter truss reflector is a mature technology that, in particular, has potential for application to the ARISE mission. It is a mature technology that has been demonstrated and fully qualified for Space flight through a comprehensive environmental testing program. The 12.25 m design (Figure 4.27) is now in production for geosynchronous mobile communications satellite missions. The AstroMesh uses a simple and efficient structural approach. It is, therefore, particularly suited to large sizes and off-axis antenna configurations. When deployed, it is significantly stiffer and more precise, thermally stable, and lower mass than most deployable mesh reflectors. In the stowed configuration, it requires less than the typical package volume. Apertures between 6 and 25 m can be integrated with existing spacecraft buses and yet be launched aboard a number of medium-sized boosters available worldwide. Reflector areal densities of 0.37 kg/m^2 have been demonstrated using flight-quality hardware in the 12 m class. All indications suggest

that for the larger reflectors, the areal density goes down due to an economy of scale in structural efficiency.

TRW has outlined a number of approaches to meeting the high frequency requirements (but maintaining low density), such as using a membrane, and/or solid/flexible composite panels near the central hub of the reflector structure. Although scaling diameters to the 25 m class will probably require a minimal re-design of existing mechanical technologies, increasing surface reflectivity at 86 GHz over a large aperture will require materials and mechanical research of packaging, deployment reliability, thermal and long term dimensional stability, and RF reflectivity.

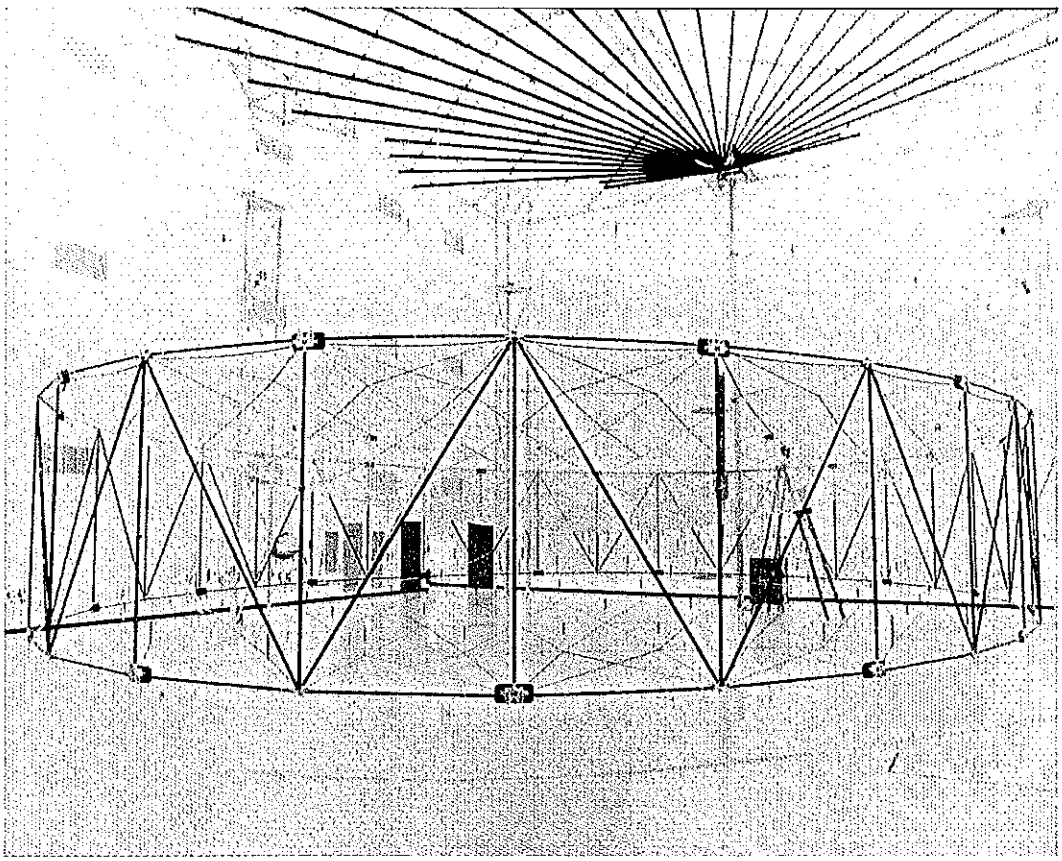

Fig. 4.27: TRW's 12.25 m AstroMesh Reflector.

Chapter 5

ARISE VLBI Data System and Ground Support System

Here we present an overview of the space VLBI system from the wideband data acquisition at the space and ground radio telescopes to the correlation and image formation phases. This overall process is shown in schematic form in Figures 5.1-5.3. In the broadest sense, wideband VLBI data from the two radio telescopes are recorded on magnetic tapes, shipped to the space VLBI correlator, played back at the correlator, and correlated. The correlated data are then searched for fringes and analyzed. Following fringe detection, the scientific images are created. The space radio telescope (SRT) is unique in that it unlike the ground radio telescope (GRT) does not have an on-board H-maser frequency standard and thus receives an uplinked coherent reference from its serving ground tracking station (GTS); furthermore, its wideband data must be downlinked for recording in the GTS. From the perspective of the GTS, it should produce wideband data samples for recording to tape that "resemble" tape recordings made by the array of GRTs; in particular, the "scientific/VLBI" channelization must be identical. In Figure 5.1, we present the two radio telescopes for a space-to-earth baseline, where the SRT as a system includes the SRT proper (in space) and its serving GTS (on the ground). It also presents the two-way phase transfer to the spacecraft, and the general requirement for time corrections of SRT data to effectively create a stable frequency standard and accurate timing system for the SRT in the correlation process. In Figure 5.2, we present the main components of the spacecraft science and telecommunication systems, and in Figures 5.3 and 5.4 in greater detail. In this chapter, we emphasize SRT VLBI data transfer/processing; similar functions, less the space-to-earth telecommunication data transmission system, are performed in the GRT.

Before proceeding to discuss the various systems in detail, in this paragraph we first provide an overall description of the wideband VLBI data processing, which is a logical extension of the architecture successfully exploited for the 1997 Japanese VSOP space VLBI mission [5.1]. As shown in Figure 5.2, this description divides the overall SRT data processing stages into three subsystems: the space radio telescope (SRT) spacecraft, ground tracking station (GTS), and VLBI Processing Center. The spacecraft and GTS processing may each be divided into so-called "science" and "telecommunication" subsystems. On the spacecraft, the role of the SRT radio astronomy science subsystem is to collect, receive, and convert to digital form the radio source signals from selected observing bands. The wideband VLBI science data in digital form is passed to the telecommunication subsystem which forms the "transmitter portion" of the data

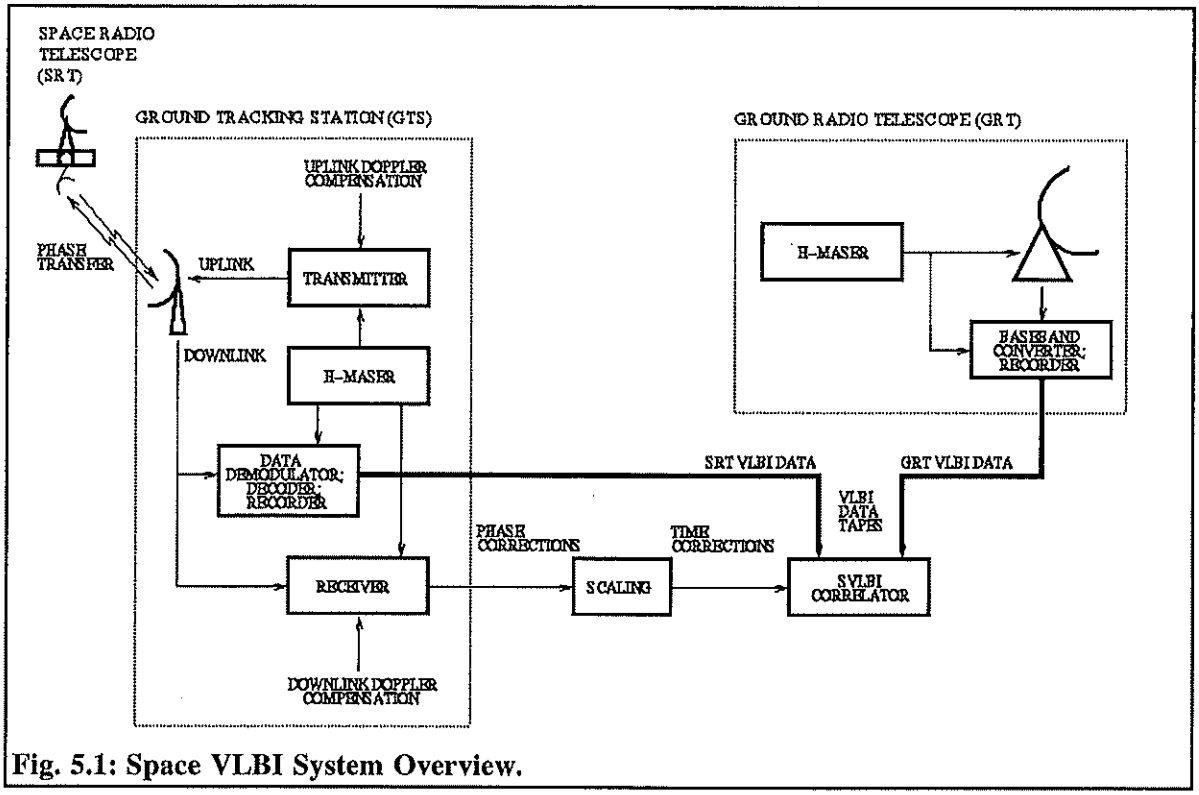

Fig. 5.1: Space VLBI System Overview.

transmission system to the GTS, modulating the science data onto the downlink Ka-band link. In the GTS, the telecommunication subsystem forms the data transmission system "receiver" and delivers the astronomical data as it appeared to its spacecraft counterpart at the output of the radio astronomy digitizers. This astronomical data is then recorded onto video tape in the VLBI tape recorder for shipment to the correlator, which processes the SRT data against data from all other GRTs. Implicit in this discussion is the necessity for a stable H-maser quality frequency reference on board the spacecraft. In the absence of an on-board (H-maser) frequency standard, a reference uplinked from the GTS is used to drive the science subsystems that deliver the wideband data to the spacecraft telecommunication subsystems, as well as the telecommunication downlink. The spacecraft telecommunication system and science subsystems are shown schematically in Figures 5.2-5.4. The telecommunication antenna, in conjunction with a diplexer is used for both uplink reception and downlink transmission. For ARISE, this communications link is at two frequencies at Ka-band (near 37 GHz for downlink, and 40.0 GHz for uplink).We note that the most critical requirement of the spacecraft telecommunication and science systems is that all required microwave reference frequencies are synthesized from the carrier voltage controlled crystal oscillator (VCXO) source derived from the GTS uplink. This function is implemented in the Multi-frequency Tunable Synthesizer module.

The transponded signal is received in the GTS and used to derive spacecraft navigation (orbit determination) and time corrections information. As shown in Figures 5.1 and 5.2, the GTS employs both uplink Doppler compensation to provide a spacecraft reference at its nominal frequency in the spacecraft frame, and downlink Doppler compensation to narrow the GTS receiver frequency window.

In Sections 5.2-5.7, we shall briefly describe each of the end to end signal processing components shown in Figures 5.2-5.4, with emphasis on the transport of the VLBI

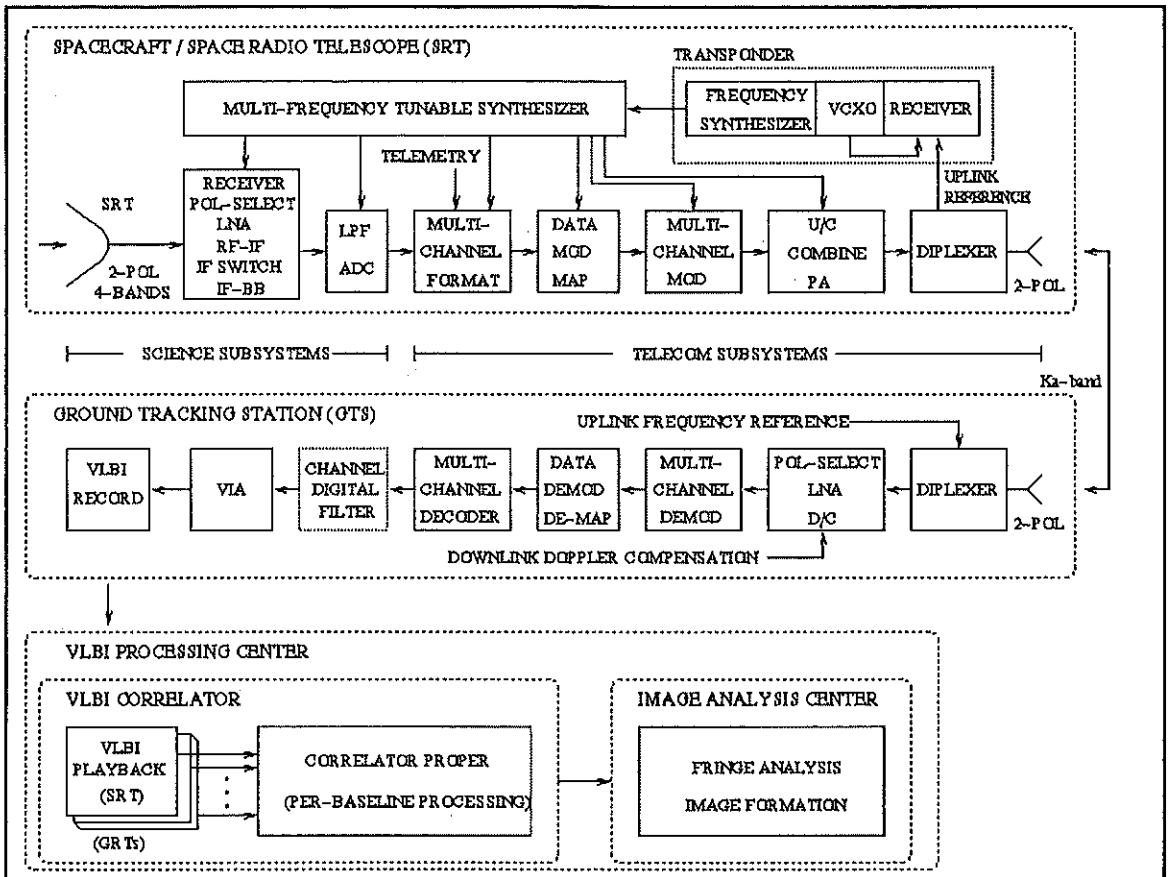

Fig. 5.2: ARISE VLBI System Data Flow Overview.

wideband data to the correlator input. In Section 5.1, we first review the scientific requirements that are appropriate for this discussion.

5.1 Spacecraft and Ground System Data Processing Requirements

Here we summarize the requirements described in Section 3.1 that are applicable to the spacecraft and ground system VLBI wideband "science" data processing, and of the offered implementation suggestions in Section 3.1 present those which shall be described in some detail in subsequent sections in this chapter. In particular, we summarize the frequency coverage, bandwidth, data rate, polarization, and IF channelization requirements.

(1) Observing frequencies shall be at 5 GHz, 22 GHz, 43 GHz and 86 GHz. (For these bands, frequency tunability over the ranges 5-10 GHz, 18-26 GHz, 40-45 GHz, 80-95 GHz, respectively, shall be supported.)
(2) A maximum of 2 GHz instantaneous bandwidth shall be supported.
(3) Two (2) GHz observations in a single, selectable polarization or 1 GHz in each of two (2) polarizations shall be supported.
(4) At Nyquist sampling and 2-bit quantization, the 2 GHz bandwidth corresponds to a maximum data rate of 8 Gbps.
(5) Quantizations of 1 and 2-bits per sample shall be supported.

(6) Simultaneous observations at different frequency bands and at single (selectable) or dual polarizations shall be supported.
(7) Eight (8) baseband (IF) channels with individually selectable bandwidths of 256 MHz and 16 MHz shall be supported.
(8) Sampling of individual baseband (IF) channels shall be at the Nyquist rate for the maximum channel bandwidth, and is to be fixed. The sample rate therefore shall be 512 MHz for the assumed maximum bandwidth 256 MHz channel, and the 16 MHz channel shall thus be oversampled.

5.2 Channelization and Telecommunication System Assumptions

To support the requirements described above requires a flexible data processing system for the space radio telescope (SRT) through the spacecraft science and telecommunication subsystems to the ground tracking stations (GTS). Similar functions are to be performed in the ground radio telescopes (GRT). The SRT and GRT functions are fundamentally the same with regard to scientific observations support, but the SRT function is complicated by the additional telecommunication data transmission system from space to earth. As described above, we assume a maximum of eight (8) maximum bandwidth 256 MHz baseband channels, sampled at the Nyquist rate of 512 MHz, and quantized to 2 bits per sample, yielding a total data rate of 8192 Mbps (8 Gbps). Present telecommunication technology, and even technology likely available at the time of ARISE system implementation, will not support multi-Gbps (e.g. 4 or 8 Gbps) transmission on a small number of (e.g. 1 or 2) downlink modulated carriers. The state of the art at the time of writing supports a 512 Mbps QPSK modulated carrier. Support for a single 256 MHz radioastronomy channel, which at 2-bit quantization and Nyquist sampling generates 1024 Mbps, would require two modulated 512 Mbps carriers. The requirement for eight (8) such 256 MHz channels (or its equivalent 8 Gbps data rate) would thus require 16 modulated carriers, frequency division multiplexed (FDM) on the downlink. To conserve link spectrum, the downlink is organized into eight (8) pairs of carriers operating in opposite circular polarizations. In the discussion below, we shall also assume the use of 512 Mbps SRT Formatters and GTS Decoders, which are also readily implementable at the time of writing. It is with these assumptions that we proceed with the system descriptions which follow. While we assume 512 Mbps rate Modulators/Demodulators and Formatters/Decoders, which are feasible at the time of writing, it is expected that rate increases (by at least a factor of two) which optimize the space to earth data transmission system by reducing the number of carriers and downlink transmission internal channels will be obtainable with advances in technology by the time of implementation.

5.3 Spacecraft Science Subsystem: The Digital Telecommunication Link Option

5.3.1 Space Radio Telescope (SRT)

The electromagnetic signal from two circular polarizations are collected by the ARISE space radio telescope (SRT). The SRT is specified to operate at some highest observing frequency at a given efficiency, and at higher efficiencies at lower frequencies.

We note that the SRT is often referred to as the High Gain Antenna (HGA), but this should not be confused with two other spacecraft to ground communications antennas: the omni-directional low gain antenna operating at X-band for telemetry, command, and control (TT&C), and the directional antenna operating at Ka-band for the two-way phase link and wideband VLBI data downlink.

5.3.2 Receiver, Pol-Select, LNA, RF-IF, IF Switch, IF-BB

There is support for four (4) observing band receivers (feed horns), at frequencies of 8, 22, 43, and 86 GHz. Each receiver is sensitive to both hands of circular polarization. The signals from the Polarization Selector (Pol-Select) are fed to Low Noise Amplifiers (LNA) for each polarization, and undergo two down-conversion (D/C) steps from RF to a common wideband IF, and subsequently from different selected IF bands (channels) to baseband (BB). Eight (8) IF to baseband down-converters are available to generate up to eight (8) analog baseband (or IF) channels, each of maximum 256 MHz bandwidth. The eight (8) 256 MHz baseband (IF) channels for 2 GHz total bandwidth may be allocated to a single polarization or divided between the two polarizations. This flexibility is provided in the IF Switch, which has frequency and polarization select controls.

5.3.3 LPF, ADC

The analog baseband signals are (nominally) low-pass filtered (LPF) to 256 MHz and digitized. The sampling clock is fixed at the Nyquist rate of 512 MHz, and quantization occurs at 2 bits per sample. The eight (8) 256 MHz channels at 512 Msamples/s and 2 bits/sample (1 Gbps per channel) generate the maximum data rate of 8 Gbps. Lower data rates of 4, 2, and 1 Gbps may be supported in numerous ways, such as use of fewer baseband channels requiring fewer downlink carriers. Additionally, the ability to switch the default 256 MHz low pass filters to 16 MHz bandwidth is provided to permit higher spectral resolution in the correlator. Such a mode, or in general any mode that reduces the "information" data rate from the maximum rate per modulated carrier (i.e. less than the default 512 Mbps), may require a form of "data randomization" to maintain a suitable symbol transition density on the modulated downlink to facilitate synchronization in the GTS. This randomization function may be performed as part of the telecommunication Modulator subsystem, but equally well in the spacecraft VLBI Formatter.

5.3.4 Multi-Channel Data Formatter

The Data Formatter imposes a framing signature for downlink data and timing recovery within the GTS Decoder, and multiplexes the complete spacecraft telemetry into the wideband data stream. The Formatter is multi-channel in that it operates separately on each digitized baseband channel bitstream. In our baseline scenario of 256 MHz baseband channels, a 16-channel Formatter operating on 512 Mbps rate input bitstreams provides for the 8 Gbps maximum rate. The digitizers in the "ADC" block always provide 2-bit quantized samples to the Formatter; the selection of 1 vs. 2-bit quantization at the Formatter output is performed within the "Data Modulator Mapping" block. For simplicity, the Formatter is of the so-called "data replacement" design type, whose output data rate is the same as the input rate and whose formatting simply overwrites the original astronomical data. Its primary functions are the inclusion of framing (sync words, frame counter, and Formatter channel identification) and spacecraft telemetry embedded within the wideband VLBI data samples at a nominal frame rate such as 200 Hz.

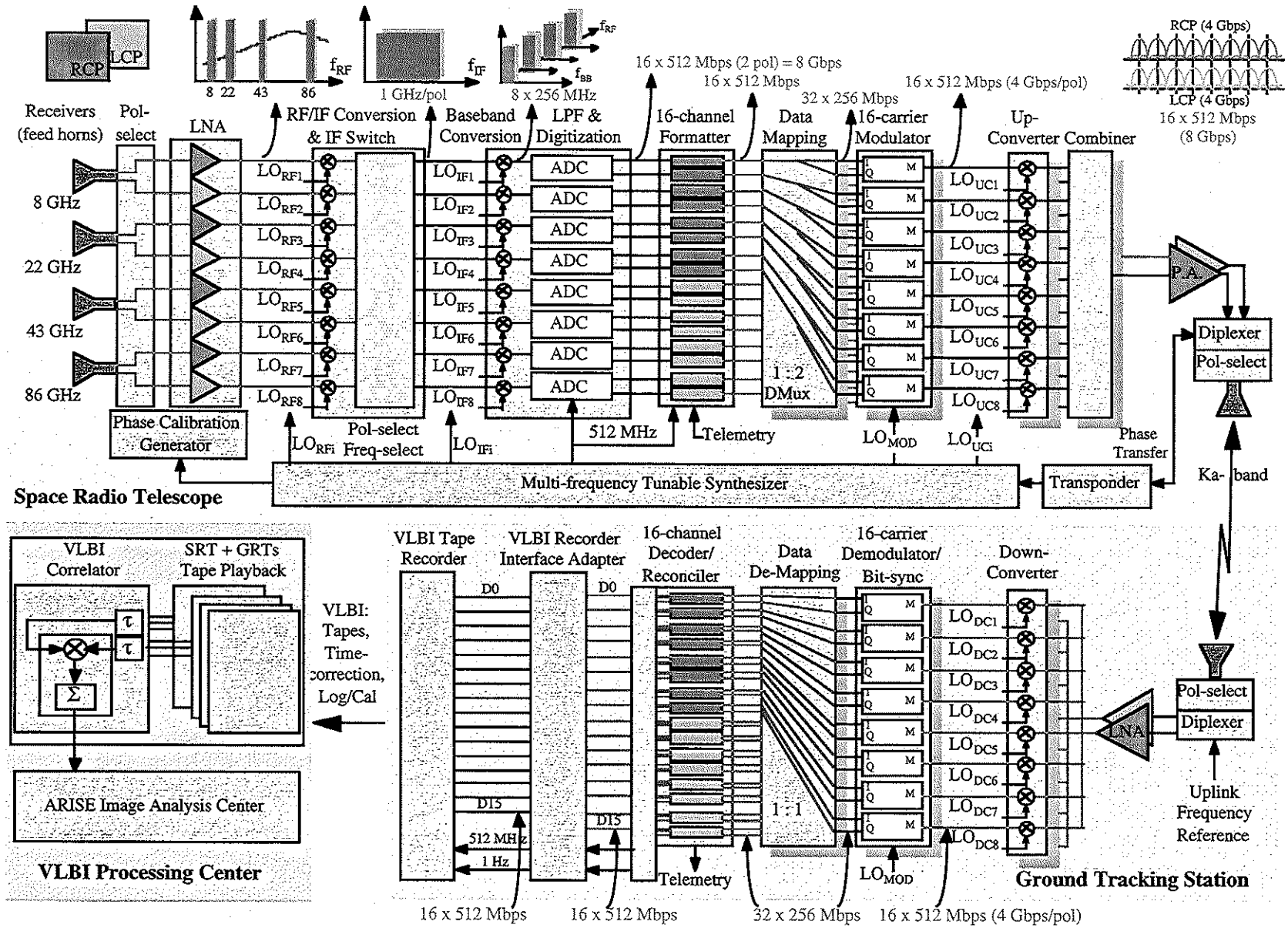

Fig. 5.3: ARISE VLBI System Data Flow.

All spacecraft health and safety monitoring telemetry (that is transmitted at X-band as part of the conventional TT&C services), as well as the science calibration data telemetry, are to be included in the wideband data path of each Formatter channel. This unifies the design of each channel within the Formatter subsystem, and provides for independent and redundant telemetry decoding in the GTS Decoder. An optional phase transfer downlink (using a Ka-band carrier separate from the data carriers) could also be modulated with spacecraft telemetry, allowing an additional or alternate path for this data independent of the GTS data Decoder.

As alluded to above, in support of effective "information" data rates less than the maximum rate of 512 Mbps per modulated carrier (e.g. if a 16 MHz filter is employed in place of the 256 MHz filter), a frame-synchronized "data randomization" function in the Formatter provides adequate data downlink transition density for data detection in the GTS. This randomization is removed in the GTS Decoder following frame synchronization. Additionally, "safe-guarding" of individual baseband channels from faults or degraded performance in individual downlink carrier streams may be provided by Formatter data interleaving (or "barrel-rolling") over a number of formatted data downlink frames; the interleaving would be synchronously removed in the GTS Decoder.

5.3.5 "Data Modulator Mapping"

The formatted VLBI data bitstreams pass through a "Data Modulator Mapping" block, whose function is to reconcile the data rate of the Formatter output bitstreams to bitstream rates required by the Modulator. This is necessary if the spacecraft digitizer (ADC) or Formatter bitstream rates are different from those required by the Modulator inputs. This block performs the required data rate conversion via simple multiplexing or demultiplexing, and may also provide input and output switching. We note that this block may be physically implemented within the preceding Data Formatter block, but is logically a separate data processing step. As an example, for the baseline 256 MHz baseband channel at 2-bit quantization, which corresponds to two 512 Mbps bitstreams (a total 1024 Mbps data rate), and assuming a 512 Mbps Modulator, each 512 Mbps formatted bitstream is split into two 256 Mbps bitstreams (as a "data mapping" function) which interface directly to the 512 (2x256) Mbps QPSK Modulator ("I" and "Q") inputs. In this example, a future 1024 Mbps Modulator (desired to minimize the number of separate downlink carriers) requires no demultiplexing, the Data Modulator Mapping block becomes a transparent path, and the two formatted 512 Mbps bitstreams for each radioastronomy channel directly feed the two Modulator inputs.

5.4 Science Data Downlink: The Digital Telecommunication Link Option

5.4.1 Baseline Multi-Gbps Modulation Scheme

The ARISE wide-band VLBI science signal will be transmitted in real-time from the spacecraft to ground tracking stations (GTS) for digital recording and subsequent shipment to the correlator for final processing. This section presents a configuration which meets the mission requirements presented in Section 3.1.

The ARISE spacecraft will rely on an on-board, highly directional and steerable, telemetry antenna to direct the digitized science data streams to the GTS. This is necessary in view of the bandwidth of the science streams to avoid large transmitters on-board. Experience with the 1997 Japanese VSOP space VLBI mission has shown that a single telemetry antenna can provide the specified coverage, if a 180 degree field-of-view is provided for the telemetry antenna, and a sufficient number of GTSs are provided. Under these conditions the loss of coverage when a GTS is in

view, but the telemetry antenna is blocked by the spacecraft, can be maintained at low levels by careful choice of sources to be observed.

The ARISE mission will rely on several geographically distributed GTSs to provide the high percentage of coverage specified. Although the precise set of stations has not yet been determined, it is expected to include at least the three sites of the NASA/JPL Deep Space Network (DSN) near Barstow (California), U.S.A., Madrid, Spain, and Tidbinbilla, Australia. Viable added sites under consideration, both to meet coverage requirements and to provide excess coverage to allow for station outages, are Green Bank (West Virginia), U.S.A., Usuda, Japan, and Santiago, Chile. The precise set will be determined by the final selection of the space-to-ground link frequency band and the distribution of sites necessary to meet the coverage requirements for that frequency band, the availability of suitable GTS, and quid-pro-quo agreements with other agencies for non-NASA GTS implementations and operations. The NASA GTSs are currently planned to be upgraded versions of the existing DSN Space VLBI Subnet of 11 m GTSs being used to support the VSOP mission at the time of writing.

The ARISE baseline plan relies on the 37 GHz Space Research band for transmission of the wideband science data streams to ground. The primary frequency allocation of this 1 GHz band (37.0 to 38.0 GHz) is nearly sufficient for transmission of 2 GHz analog bandwidth required as per Section 3.1 using dual-polarized carriers (see Section 5.6), but insufficient for transmission of a digitized 8 Gbps data stream except by use of unconventional modulation schemes. Fortunately, the adjacent frequency band from 38.0 GHz to 39.5 GHz, although not allocated to Space Research, is allocated to the exact same set of users as share the lower band.

The wideband science data streams will be modulated onto dual-polarized telemetry carriers and transmitted over the telemetry antenna to the GTS. Two options are possible: digitization on-board or digitization in the GTSs. If the science signal is digitized on-board and then transmitted, most modulation techniques require more than the 1 GHz allocated. On the other hand, this digital transmission will avoid signal degradation and other losses which the analog streams suffer. If the science streams are transmitted as analog streams, then digitized in the GTS, the 1 GHz frequency allocation is sufficient, but the science stream suffers some added degradation.

The baseline plan is that the ARISE telemetry stream will employ on-board digitization. A particular form of spectral shaping of the digital stream, known as Square Root Raised Cosine (SRRC), will be used in conjunction with conventional Quadrature Phase Shift Keying (QPSK) modulation. The spectral shaping relies on digital filters to introduce controlled amounts of inter-symbol interference into the digital stream, which effects a fairly sharp spectral cut-off of the RF spectrum (in order to satisfy governmental frequency allocation constraints on out-of-band interference). But the use of dual (orthogonal, circular) carrier polarization, along with good spectral-shaping practices, still requires a total RF bandwidth on the order of 2.5 GHz. This ARISE baseline plan assumes that the mission will be able to obtain a waiver to allow use of the whole 2.5 GHz band on a non-interference basis. The argument is that the combination of very wide-band noise-like signals, focused into a narrow beam by the spacecraft Ka-band antenna, should result in interference-free operation to all band-sharing services not located in the narrow illumination footprint at any particular GTS. Also being considered is the use of a sharp cutoff post-power amplifier filter to limit the total spectrum extent, but at the expense of some extra cost and signal loss. Alternatively, an analog transmission scheme is being examined in more detail as a within-band allocation approach since it requires no waiver.

The technology of spectral shaping and Modulators capable of handling multi-Gbps data rates is limited; hence the low-risk approach of multiple-carriers (Frequency Division Multiplexed) is incorporated into the ARISE link. The ARISE 8 Gbps data are sub-divided to either 512 Mbps or 1024 Mbps carriers. The lower rate requires sixteen (16) carriers (8 carriers per polarization) but is consistent with the technology feasible at the time of writing [5.2]; the higher rate requires only

eight (8) carriers but requires added technology advances. The exact choice is not critical so the lower-risk (but more cumbersome) 512 Mbps/carrier option is used here.

In summary, in the ARISE baseline plan, the spacecraft transmits up to 2 GHz radioastronomy bandwidth to the GTS in the 37 GHz Ka-band by use of dual-polarized multiple frequency-multiplexed carriers modulated with spectrally-efficient digital streams using conventional QPSK modulation, but relies on waivers and secondary allocations to use a full 2.5 GHz bandwidth. Alternate options, in terms of transmission frequency, on-board or ground (GTS) digitization, and/or modulation schemes are discussed in the next section.

5.4.2 Advanced Multi-Gbps Modulation Schemes

There are at least three different frequency band options for transmitting the wide-band VLBI science data from the spacecraft to ground: the Space Research band at 37 GHz, the Space Research band at 71 GHz, and optically (in the range from 500 to 1550 nm).

Within the 37 GHz band, there are at least two options for "squeezing" 8 Gbps through the 1 GHz limited frequency allocation there: on-board digitization coupled with bandwidth compressive, spectrally-efficient, quadrature amplitude modulation (QAM), or a novel form of "constant envelope" analog modulation. The 71 GHz option would be expected to rely on dual polarized digital data streams using conventional QPSK modulation, as it uses less than the 3 GHz band allocated for Space Research. The optical approach offers solutions at 500 nm, 900 nm, or 1550 nm.

None of the several options mentioned above has a clear advantage at the time of writing. But conventional QPSK modulation with dual polarization at 37 GHz offers the least risk (and, therefore, has been selected here for the ARISE baseline plan), but will require a frequency allocation waiver and involve a secondary use status (comparable to what the 1997 VSOP mission has relied on successfully). The QAM technique has not heretofore been used in space links, as it requires a much advanced technology, and substantially more on-board RF and prime power. For these reasons, it has been dropped from further consideration. The analog "constant envelope" modulation scheme also has not been used in space links, but it requires little new technology, and uses about the same on-board power as that needed for conventional QPSK modulation.

The 37 GHz options rely on well-documented and tested space link technologies, since it is adjacent to the Deep Space allocation at 32 GHz which has been under development for two decades. Spacecraft transmitters and antennas, and ground antennas and receivers are well-understood and offer little added risk by movement to 37 GHz. Existing 34 m tracking stations provide for experimentation at 32 GHz (and 37 GHz), and the Deep Space Network is slowly migrating to this higher frequency.

The 71 GHz option, although it would rely on traditional modulation techniques, is not well documented nor tested within the U.S. No data is available at the time of writing on the performance of DSN antennas at this frequency. However, 86 GHz radio astronomy systems planned for mounting on the DSN 34 m antennas in the near future should provide substantial data over the next few years. Also, the Millimeter Array (MMA) planned by the National Radio Astronomy Observatory (NRAO) for location in Chile, will rely on 10 m antennas with excellent performance at 71 GHz. Thus, although this band offers a potentially straightforward solution to the issue of 8 Gbps science data to ground, it is not considered in the ARISE baseline plan at the time of writing as it deemed greater risk than the 37 GHz option.

The optical approach is also not considered because of the lack of sufficient data on which to base a low-risk solution to the ARISE telemetry link. Nonetheless, NASA/JPL has conducted two

successful system-level demonstrations for optical communications over space-ground links, albeit at much lower data rates [5.2]. The virtue of optical links is the lack of frequency allocation constraints and the low likelihood of interference because of the smaller beamwidth than the RF options. On the other hand, pointing and reception are more difficult than with the RF solutions, and the GTS implementation would lack prior examples on which to build. Nevertheless, this approach is rapidly maturing, and the evolving technology necessary to meet the ARISE 8 Gbps rate requirements should be watched as a possible alternative.

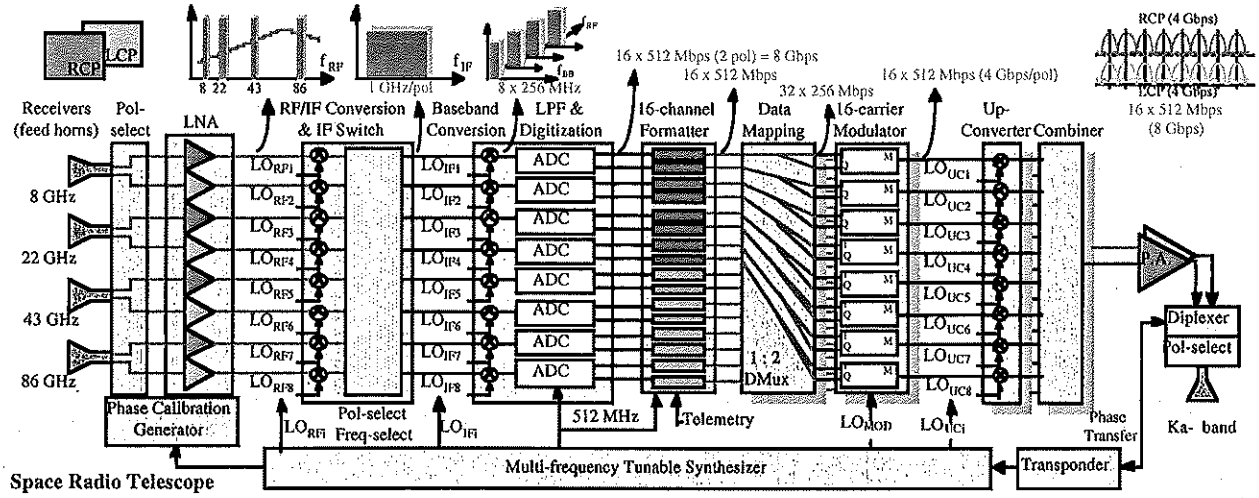

Excerpt from Fig. 5.3.

5.4.3 Multi-channel Data Modulator

The output of the Data Modulator Mapping block consists of signals which may be directly applied to the Modulator. The outputs of all Modulators are at some common IF, which are up-converted to RF using independent tunable local oscillators (although the same LO frequency is used for oppositely polarized signals). The Modulator is "multi-channel" in that discrete modulated carriers are generated, separated in frequency after up-conversion to produce a frequency division multiplexed (FDM) signal. Multiple parallel carriers are employed to simplify implementation of the spacecraft Modulator and GTS Demodulator, which are limited in maximum data rate by technology available at the time of implementation. For a 512 Mbps QPSK Modulator (feasible at the time of writing), support for 8 Gbps requires 16 Modulators (eight (8) per downlink polarization sense); it is desirable to reduce this number by at least a factor of two by the time of implementation.

5.4.4 U/C, Combiner, PA

The individual modulated carriers at the nominal IF are individually up-converted (U/C) to the Ka-band RF, where they are combined, power amplified (PA) and radiated by the Ka-band transmitter to the GTS. For reasons of spectral efficiency, two orthogonal (circular) polarizations are used for space to ground transmission.

There are a number of alternatives to be considered for how the downlink VLBI data carriers should be combined and amplified in order to achieve the highest power efficiency. Each polarization requires its own power amplifier (PA) and combining network. The baseline approach is that all eight (8) carriers per polarization are combined (added) at low power levels, the

composite then being input to a single power amplifier (PA). Then, in order to minimize carrier inter-modulation products, it becomes necessary to linearize (back-off) the PA, with a resultant loss of (power supply, DC to RF) power efficiency. For a traveling wave tube amplifier (TWTA), the efficiency will be on the order of 25-30%. The telecommunication link budget for QPSK modulation indicates that an RF power of 16 W per polarization (2 W per carrier) be provided, which places the DC power supply requirement at around 55 W.

On the other hand, if each carrier has its own saturated PA (perhaps 60% efficient), significantly better amplifier power efficiency is obtained, but the subsequent losses in combining necessitate higher individual PA output (possibly three (3) rather than two (2) W per carrier). Also, the use of individual PAs could result in the use of solid-state power amplifiers (SSPA), rather than a TWTA.

Another consideration is physical placement of the PA packages. The baseline design is to locate them within the main spacecraft structure, and supply the RF signals to the antenna feed via waveguide. Because the telecommunication antenna has a 1.2 m diameter, and will be pointed over a wide range of angles by means of a hinged boom, the waveguide run will be lengthy and involve several rotary joints. In the telecommunication link budget, a modest 3 dB loss has been allowed for this waveguide run, but it could prove greater. As a result, it may be expedient to locate the PAs on the backside of the antenna. By this means, the waveguide loss occurs at low power (mW) levels, with a considerable savings in both RF and prime (DC) power. It could also mean that the waveguide could be replaced by flexible cable. This, and other options, will be studied during the ARISE detailed design activities.

5.4.5 Diplexer

The spacecraft diplexer is used to pass the GTS uplink phase reference to the transponder's receiver, and transmit the spacecraft telecommunication system downlink carrying the wideband VLBI data and telemetry for transmission to the GTS, through a single antenna feed horn.

5.4.6 Transponder

Phase transfer at Ka-band will take place using an uplink frequency in the range 40.0-40.5 GHz, and the downlink frequency will be either one of the VLBI data QPSK carriers, or a separate carrier, in the 37.0-38.0 GHz range. These frequencies are in the allocated Space Research bands. The ground tracking station (GTS) uplink signal is an unmodulated carrier, which is slowly tuned (uplink Doppler compensation) over a frequency range of typically a few MHz with respect to the nominal carrier frequency.

The function of the spacecraft phase transfer transponder is to receive and phase-lock to the uplink carrier, and provide a local frequency "standard" output frequency (e.g., 100 MHz) to the on-board science and telecommunication subsystems. All spacecraft reference frequencies and downlink carrier frequencies are synthesized from this "standard" frequency in the Multi-frequency Tunable Synthesizer.

The principal performance requirement on the transponder is that it adds a minimum of non-reciprocal phase noise to the phase transfer process. Typically, this should be no more than 1.0 degree RMS of random phase noise in a 10 Hz bandwidth about the uplink carrier frequency, plus a systematic quadratic phase component (due to circuit phase drift) of less than 1×10^{-5} deg/s/s. Other requirements are that the receiver's phase-lock tracking bandwidth be on the order of 1000 Hz, and the receive dynamic signal range be 40 dB. The need for a larger dynamic range, plus a swept self-acquisition capability, are obviated by the fact that the GTSs precisely control the uplink EIRP and perform Doppler compensation (which places the carrier frequency received at the

spacecraft within the natural pull-in range of the phase-lock tracking loop). Basically, an uncomplicated, wide-band, design will suffice.

5.4.7 Phase Calibration Generator

As is customary in VLBI systems employing multiple, discrete science observing channels, phase calibration tones are injected via directional coupler into the wideband VLBI path as close to the point of external signal reception as possible. The injected tones, synchronized to the GTS uplink reference via the Multi-frequency Tunable Synthesizer, may be extracted either in the GTS or correlator, and play a critical role in "aligning" the individual baseband (IF) channels to realize the effective coherent 2 GHz bandwidth (8 Gbps) detection threshold.

5.5 Ground Tracking Station (GTS): The Digital Telecommunication Link Option

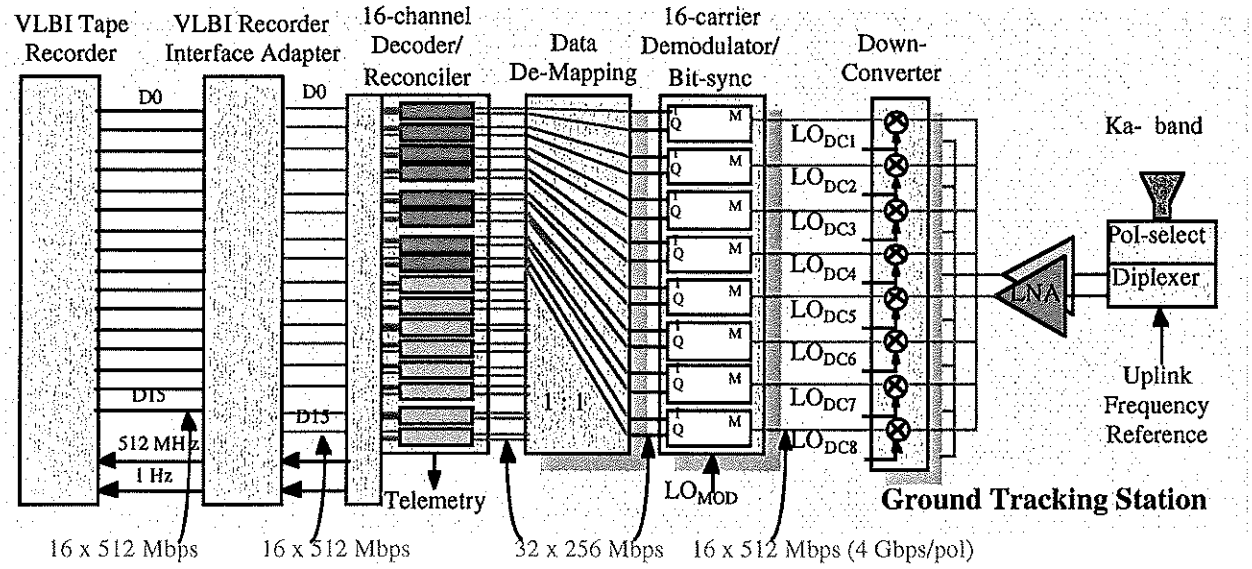

Excerpt from Fig. 5.3.

5.5.1 Diplexer, Pol-Sel

The GTS diplexer is used to pass the received spacecraft telecommunication system downlink, and transmit the GTS uplink phase reference to the spacecraft, utilizing a single antenna feed horn. The polarization selector provides separate signals to the two LNAs, one per polarization.

5.5.2 LNA, D/C

The two polarizations of the Ka-band downlink are simultaneously received, amplified (two LNAs, one per polarization), and down-converted (D/C) to a common IF for input to the GTS Demodulator. Separate filtering and down-conversion stages are necessary for each modulated

carrier within the multi-carrier composite downlink. However, only one selected down-converter needs to be provided with the downlink Doppler compensation signal.

5.5.3 Multi-channel Data Demodulator

The individual carriers are received to reproduce the data inputs to the spacecraft modulators. This involves carrier reconstruction for each QPSK channel (the original discrete frequency carriers are suppressed in QPSK modulation), coherent demodulation, data symbol synchronization, and data detection (hard decisions on whether data 1's or 0's are being received).

5.5.4 "Data Demodulator De-mapping"

This reproduces the bitstreams at the output of the spacecraft Formatter that feeds the Data Modulator Mapping block, and is implemented via multiplex/demultiplex circuitry with output switching.

5.5.5 Multi-channel Decoder

The individual Decoder channel inputs are "decoded" to reproduce the inputs to the spacecraft Data Formatter. There is no SNR-enhancing coding (e.g. convolutional coding) in the downlink data transmission system and a bit error rate of 1×10^{-4} is tolerable. The Decoder maintains frame and bit integrity, and recovers from detected timing (bit) slips. Furthermore, telemetry data are extracted from the wideband data stream and recorded. If data randomization and/or interleaving are employed on the spacecraft, e.g. in the Formatter, these functions are removed (reversed) in the Decoder following frame synchronization.

The multi-channel nature of the Decoder block implies that prior to VLBI recording, the individual Decoder channel (data, high-speed clock and 1 Hz reference) outputs must be reconciled to a common clock. The final outputs of the Decoder shall consist of the up to 8 Gbps data, suitably channelized, with the appropriate channelized data clock and 1 Hz reference. For eight (8) 256 MHz baseband channels, this may take the form of 16 bitstreams at 512 Mbps/bitstream, 512 MHz clock, and 1 Hz timing reference. This data/timing "reconciliation" is best implemented at the output of the Decoder proper, as shown in Figure 5.3.

5.5.6 Re-channelization Filter (optional)

The role of the re-channelization digital filter is to channelize the received spacecraft channels into channel bandwidths appropriate to those generated by the GRTs, should they be different, or for special observing modes requiring narrower processing bandwidths than the default 256 MHz (or 16 MHz) ARISE channel. In the event that spacecraft data re-channelization is required, maintenance of only two bits per sample at the re-channelization digital filter output introduces an additional digitization loss. We note this is an optional block as re-channelization is to be avoided if at all possible, or may alternately be employed at the correlator, where the re-channelization loss may be minimized with a more complex correlator. One advantage of the GTS implementation is to enable correlation at those correlators that do not support re-channelization, thus permitting sharing of the ARISE mission correlator load should this be necessary.

5.5.7 VLBI Recorder Interface Adapter (VIA)

The role of the VLBI Recorder Interface Adapter (VIA) is to provide the physical interface to different VLBI recording system types. It is possible that multiple recording system types will be supported at the GTSs. The VIA may also be required to perform a multiplex/demultiplex function to provide a specific data rate interface to specific VLBI recording systems.

5.5.8 VLBI Recorder

The VLBI recorder takes in the wideband data samples, synchronous clock and 1 Hz reference from the Decoder and records the data onto magnetic tape. For a maximum rate of 8 Gbps and eight (8) 256 MHz channels, the nominal interface may consist of 16 bitstreams at 512 Mbps/bitstream, 512 MHz clock and 1 Hz timing reference.

5.6 Science Data Downlink: The Analog Telecommunication Link Option

Analog transmission was successfully tested during the TDRSS VLBI demonstration in 1986, so some limited experience exists, although it is not nearly as extensive as that on digital transmission as used for VSOP. It is recognized that analog signal transfer has its own collection of difficulties, unprovens, and caveats, but its implementation, by comparison with the digital system outlined above, appears simpler, less costly (at least insofar as the hardware is concerned), and not as risky.

Figure 5.4 is the block diagram for the analog approach, and comparison with Figure 5.3 readily indicates the differences between the two implementations. All of the multi-channel functions needed to realize digital data transfer are gone, replaced by two, basically single channel, analog conduits (one for each RF polarization). In effect, the analog transmission scheme simply relays the wideband (1 GHz) outputs from the RF/IF Conversion & IF Switch unit to the GTS, where they become digitized by a VLBI Data Acquisition Terminal (DAT) like those used by cooperating GRTs. On the surface, this appears to be a remarkable simplification, requiring the following subsystems and features.

5.6.1 Space Radio Telescope (SRT)

Constant Envelope Converter – this unit takes a 1 GHz wide IF channel, and converts its Gaussian dynamic amplitude into a constant-envelope (sinusoidal) equivalent.

Telemetry Modulator & Combiner – this provides a reference or pilot carrier, which is modulated by the spacecraft telemetry data, and combined with the wideband constant-envelope signal.

Up-Converter – this unit functions to translate the wideband data plus pilot IF composite to RF (Ka-band).

Power Amplifier (P.A.) – by virtue of the constant envelope nature of the signal to be transmitted, this may be a saturated, relatively low power, solid-state power amplifier (SSPA).

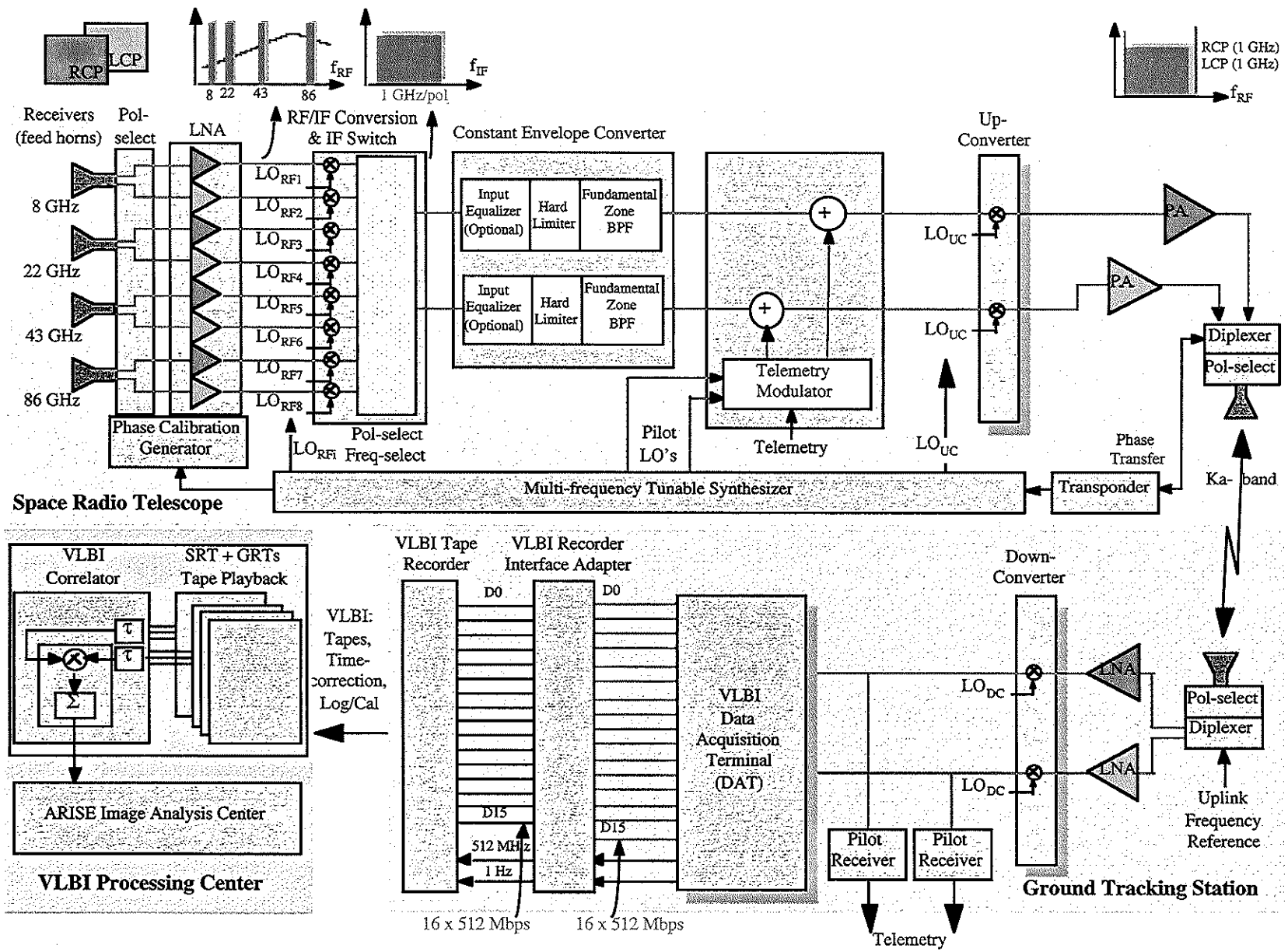

Fig. 5.4: ARISE Analog-downlink VLBI System Data Flow.

5.6.2 Ground Tracking Station (GTS)

Down Converter – this unit receives both RF signals (RCP & LCP), and translates each RF carrier to a common IF.

VLBI Data Acquisition Terminal (DAT) – this unit takes two 1 GHz wide IF channels, converts each to four 256 MHz baseband channels, filters, and quantizes, each baseband channel to 2-bits. The output consists of sixteen 512 Mbps data streams.

Pilot Receiver – acquires, coherently tracks, demodulates and detects the telemetry from, a modulated pilot.

5.6.3 Discussions and Technology Assessment

Contrasting the previous list with that for the digital architecture indicates a dramatic difference in complexity.

Strictly speaking, a 1 GHz wide analog VLBI signal can conceptually be transmitted directly without any modification to its amplitude characteristics. Ordinarily, since the signal is essentially broadband Gaussian noise, manifesting a dynamic random amplitude, a linear transfer system is needed to preserve waveform integrity. But considering the fact that, upon reception, the signal is quantized to one or two bits, absolute linearity is not essential. In fact, for one-bit quantization (retaining only the polarity or sign of the samples) it makes no difference how the amplitude is distorted as long as the zero crossings are preserved. However, two-bit quantization is usually based on the $\pm 1\sigma$ crossings of the signal's amplitude, and the perception or consonance of this breakpoint can be lost if the signal is passed through *uncontrolled nonlinearities*. The concern here is on uncontrolled nonlinearities, ones which are not precisely known or may be temporally changing. Therefore, whatever degree or type of nonlinearity is allowed, it must be definite.

This criterion may be met through hard-limiting (infinite clipping) of a Gaussian bandpass signal, followed by fundamental zone bandpass filtering. This produces a "sinusoidal" waveform, wherein the RF "carrier" becomes a wideband, constant envelope, phase modulation. (This transformation is hereafter referred to as "constant envelope conversion" – CEC). Because the CEC waveform has a constant envelope nature, subsequent nonlinearities, such as that introduced by an RF transmitter saturated power amplifier, do no harm. In fact, a saturated RF transmitter power amplifier should be used, rather than a linear amplifier that has lower efficiency.

The theory of bandpass hard-limiting or CEC is well understood for simple signal sets, such as a sinusoid plus additive Gaussian noise. For VLBI, the signal is made up of wideband observation "noise" plus wideband additive receiver noise. This particular mix has not been cogently studied (in the general literature), but many of its attributes are similar to the sinusoidal case. What is unique for its application to VLBI is that upon reception at the GTS, the DAT will channelize the 1 GHz wide CEC signal into four contiguous 256 MHz sub-channels. This process will again alter the nature of the sub-channel signal from constant envelope to something which is more Gaussian-like. Preliminary analysis and simulations have indicated that the principal effect on the quality of the CEC VLBI signal, relative to a linear VLBI signal, is a small loss (<1 dB) of SNR.

Another property of CEC is that it alters the spectrum of the original signal by means of non-uniform amplification across the frequency band. Specifically, the spectrum's bandedges are sharply accentuated relative to the bandcenter, the transition band is less steep, and stopband levels are higher. However, studies have shown this can largely be compensated for by using a bandpass filter, embodying antipodal characteristics, at the input to the CEC. It is expected that the equalized CEC spectrum should not be more than 20% wider than the input spectrum.

These performance uncertainties are judged to be minor issues, easily settled by some additional analysis and testing (including CEC experiments with GRTs). Hardware implementation of CEC seems quite straight forward, not requiring any new or advanced technologies. Notwithstanding, there are some more serious system issues which must be addressed. They included time synchronization, the effects of wideband signal Doppler shift, and propagation medium (troposphere) degradation.

Time synchronization is a formidable task whether the downlink is analog or digital. The basic problem is to establish and maintain a precise epoch for the spacecraft observed signal with respect to ground time in the presence of Doppler and highly dynamic spacecraft to GTS delays. For the digital link, the epoch is measured once each second as the time difference between the divided down data bit clock to "one Hz," and the local one-second time tick. This has been fastidiously worked out for VSOP, and is consequently proven. But analog transmission does not directly allow this measurement. As a solution, the use of a least two subsidiary "pilots" (separate carriers, one for each polarization) is envisioned. These carriers are required to provide a Doppler shift reference essential to proper CEC RF signal downconversion to baseband, and also become the downlink leg of the transponded phase transfer process.

Also, in lieu of digital modulations, some means must be provided for transmitting science and crucial spacecraft telemetry. Accordingly, the pilots not only provide a timing reference, but also become the vehicle for VLBI related telemetry information. Both of the pilots are used for this purpose. It is expected that formatting and modulation will be implemented in accordance with CCSDS standards.

The propagation medium has little effect on the digitally transmitted VLBI data (it slightly degrades the received data bit error rate). But for the analog link, the medium introduces signal degradations due to dispersion and scintillation. For ARISE, operating at Ka-band, only the consequences of the troposphere are significant. Of course, all GRTs also contend with the effects of the troposphere at the observing frequency. But for the ARISE SRT, it is not the observing frequency, but the downlink frequency which counts. Thus, if the observing frequency is higher than the downlink frequency, the tropospheric degradation of the SRT will be less than that for the GRT. Conversely, ARISE observing frequencies less than the downlink frequency sustain more relative loss. However, the SRT has a marked advantage in this regard over its GRT counterpart because of the phase transfer link, and injected phase calibration tones. The phase transfer link measures scintillation, and the cal-tones gauge the frequency selective effects of dispersion (as well as passband distortion introduced by the CEC transformation). Correspondingly, it should be possible to largely correct for the downlink tropospheric effects, e.g. at the VLBI correlator.

VLBI signal level calibration for an analog downlink is more difficult than for the digital downlink. Once digitized on the spacecraft, the VLBI data sent digitally is invariant to all subsequent transfer related (especially amplitude) variations. By contrast, the analog downlink must contend with the continually changing path attenuation between the spacecraft and ground receiver. It therefore becomes necessary to provide appropriate automatic level control of the received analog signal up to the input to the ground DAT. This may be readily accomplished by continual measurement and adjustment (AGC), based on a combination of the VLBI signal and pilot levels, prior to the DAT.

5.6.4 Analog versus Digital Tradeoff Summary

Analog space-to-earth VLBI data transfer offers a viable alternative to sophisticated digital modulations. Its implementation does not require beyond current state-of-the-art apparatus. The RF bandwidth needed is essentially that of the VLBI observation bandwidth (about 1 GHz, in each of two transmission polarizations), while the downlink signal, using the CEC technique, is able to

make use of a transmitter saturated power amplifier. Overall, significant simplifications are obtained for both spacecraft and ground systems, and cost is greatly reduced by perhaps $10M. However, continued theoretical and implementation/test studies are required to fully validate this technique.

5.7 VLBI Processing Center

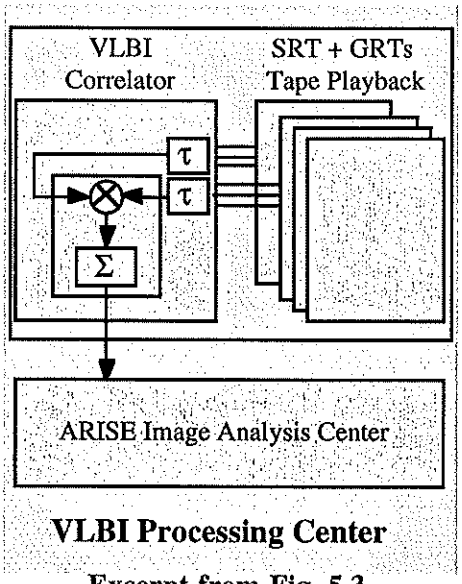

Excerpt from Fig. 5.3.

5.7.1 VLBI Correlator

The VLBI correlator consists logically of two separable blocks: the VLBI playback recorder that reproduces its radio telescope channelized data, and the "correlator proper" which correlates data for all pairs of telescopes (baselines). The correlator reduces the 8 Gbps data for each station down to total output data rate levels at the MByte/s level. All correlated data are archived onto commercial standard tape media/formats such as Digital Audio Tape (DAT).

5.7.2 Image Analysis Center

The roles of the image analysis center are fringe detection and analyses, and image formation. Fringe detection and analysis are necessary before image formation can proceed. Scientific wideband data calibration is also performed.

Chapter 6

Mission Analysis

6.1 Launch Vehicle and Injection Capabilities

The ARISE nominal orbit has the following characteristics:

Quantity	Nominal
Semi-major axis	27900 km
Eccentricity	0.66
Apogee Altitude	40000 km
Perigee Altitude	3000 km
Inclination	30 deg.
Orbital Period	12.9 hr
Perigee Precession	91.3 deg/yr
Node Precession	-57.5 deg/yr
Orbit Knowledge	10 cm

Table 6.1: ARISE Nominal Orbit.

We note that these characteristics alone have been used in the mission analysis and spacecraft design presented in this document. This decision was motivated by the desire to have at least a single point design within the tight funding level allocated for this proposal. During pre-Phase A and Phase A of the mission, a broader perpective will be taken and trade-offs performed to improve the overall science return.

The launch vehicle selected for the ARISE mission is the McDonnell Douglas Delta II 7925. The 7925 version features nine (9) solid rocket motors, and a Star 48B spinning third stage. Figure 6.1 shows the injected mass as a function of apogee altitude and fairing type for the 3-stage 7925 vehicle at 28.7 deg. inclination. For ARISE, the 2.9 m diameter (9.5 ft) fairing was selected since it allowed sufficient space for the stowed spacecraft, and since the injected mass was greater than that allocated for the 3 m fairing, it left more margin for spacecraft mass growth. Figure 6.2 shows the performance capability of the 2.9 m diameter fairing as a function of inclination. The injected mass at 40000 km and 30° inclination is 1810 kg.

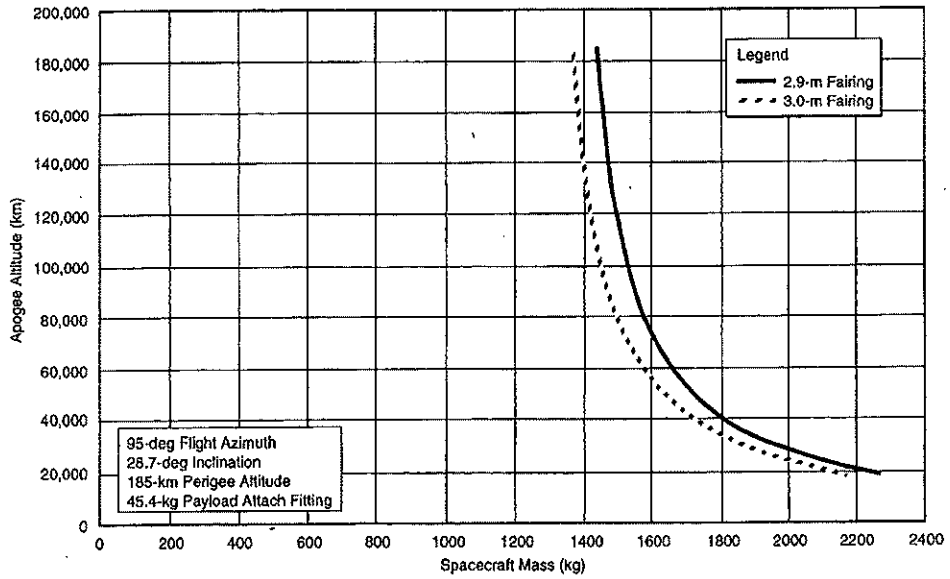

Fig. 6.1: Delta 7925 Three Stage Launch Vehicle Capability.

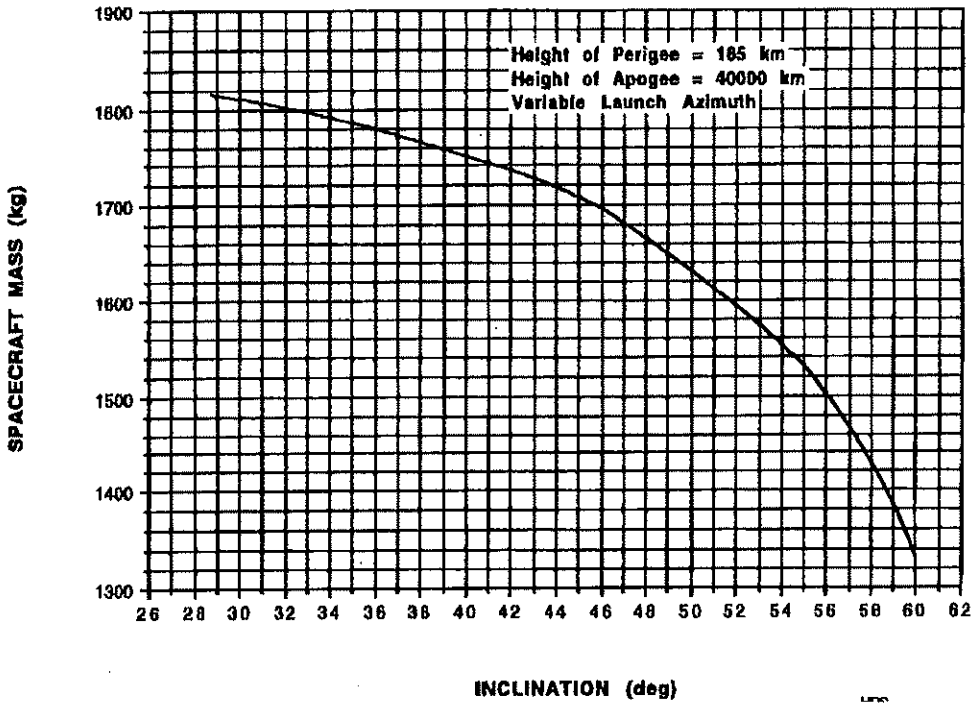

Fig. 6.2: Injected Mass as a Function of Inclination for Delta 7925 2.9 m Fairing.

6.2 Launch and Orbit Transfer

Once launched, the spacecraft will go through a de-spin and stabilization mode. About 6.9 hours after insertion, a perigee raise maneuver will occur at the GTO (Geosynchronous Transfer Orbit) apogee. This perigee raise maneuver will be done with a NTO/Hydrazine 450 N Leros 1-C, which features an Isp of 325 s. A ΔV of about 380 m/s will be achieved in about 24 minutes. Eight (8) 22

N thrusters will be used for main burn trajectory correction, and eight (8) 0.9 N thrusters will be used for coarse attitude control maneuvers.

6.3 Deployment Sequence

After the perigee raise maneuver, five (5) sequences of deployment will occur. First, due to its large size, the inflatable antenna will be deployed. This deployment will be controlled and will take between 5 and 20 minutes. The antenna support structure is inflated first. To simplify the inflation system, the inflatable solar arrays will be deployed (on 2 wings) next. This scenario enables the combination of the antenna inflation system, solar array inflation system, and the attitude control/propulsion system, thus reducing system dry masses. Third, once the solar arrays are in place, the reflector/canopy assembly get inflated. The spacecraft will be running on batteries until solar array deployment, and will be telecommunicating with the Earth at X-band with two omnidirectional antennas. The fourth deployment will involve the subreflector. A rigid astro-mast type arm will be used to carry the subreflector to about 3.6 m from the spacecraft. A gimbal system at the end of the mast will then align the subreflector with the main reflector. The last deployment will be that of the 1.2 m diameter telecommunication antenna. This antenna needs to be deployed downward with respect to the spacecraft bus in order to get a clear half-space field of view and also to minimize coupling of Ka-band telecommunication antenna with the main reflector. A gimbaling system will allow the antenna to rotate and cover a whole half space. The spacecraft will be then ready for additional checkout (In Orbit Checkout, IOC).

6.4 Space Environment

The radiation environment for two different inclinations and two different arguments of perigee (at 40000 km apogee and 5000 km perigee) has been assessed. In summary, the trapped magnetospheric charged particles (electrons and protons) dose behind 100-mils of aluminum has been estimated to be:

- 105 krad[Si]/yr @ $i = 30$ deg., $\omega = 0°$.
- 40 krad[Si]/yr @ $i = 60$ deg., $\omega = 0°$.
- 102 krad[Si]/yr @ $i = 30$ deg., $\omega = 90°$.
- 60 krad[Si]/yr @ $i = 60$ deg., $\omega = 90°$.

The solar flare proton dose has been calculated to be on average about 10 krad[Si] for three (3) years, which is small compared to the trapped magnetospheric particles. The requirement for the reflector radiation material resistance has been assessed. The surface dose on the reflector has been estimated at about 130 Mrad/yr, while bulk dose adds up to about 40 Mrad/yr.

The electrical surface charging of the ARISE main reflector has also been investigated. In summary, differential static potential between the two thin Kapton sheets (one Al coated) forming the main reflector could reach about 20 kV under worst conditions, which could lead to self-sustained arcs. Although the use of an Indium Tin Oxide (ITO) coated Kapton sheet for the canopy might be satisfactory, electrostatic discharge (ESD) still remains a materials issue until appropriate tests are done. Details on the radiation and ESD environment can be found in [6.1].

Chapter 7

Spacecraft System Description

7.1 Spacecraft Requirements

Here we summarize the requirements described in Section 3.1 that are applicable to the spacecraft design.

7.1.1 Mission Lifetime

For an apogee height of 40000 km, if the orbit plane is rotated by precession generated by orbit precession alone, this implies a mission lifetime of six (6) years and a perigee height of 3000 km. However, as per Section 3.3.7, the mission lifetime has been set to three (3) years.

7.1.2 Sky Coverage and Duty Cycle

A Sun avoidance angle no greater than 30° and an Earth avoidance angle no greater than 5° are required. The observing duty cycle on a science source must average at least 70-80% over the course of a full orbit. A typical imaging period is one (1) orbit.

7.1.3 Orbit Determination Accuracy

An orbit determination accuracy of 10 cm is required.

7.1.4 Pointing Requirements

The absolute pointing accuracy of the electrical axis (boresight) of the antenna must be less than or equal to three (3) arcsec at 86 GHz, six (6) arcsec at 43 GHz, 11 arcsec at 22 GHz, and 30 arcsec at 8 GHz. The attitude reconstruction accuracy of this axis shall be TBD arcsec. The spacecraft should be capable of slewing of 180° in less than 1 hour.

7.1.5 Launch Vehicle

For cost reasons, the spacecraft should be launched from a Delta II.

7.2 Spacecraft Configuration

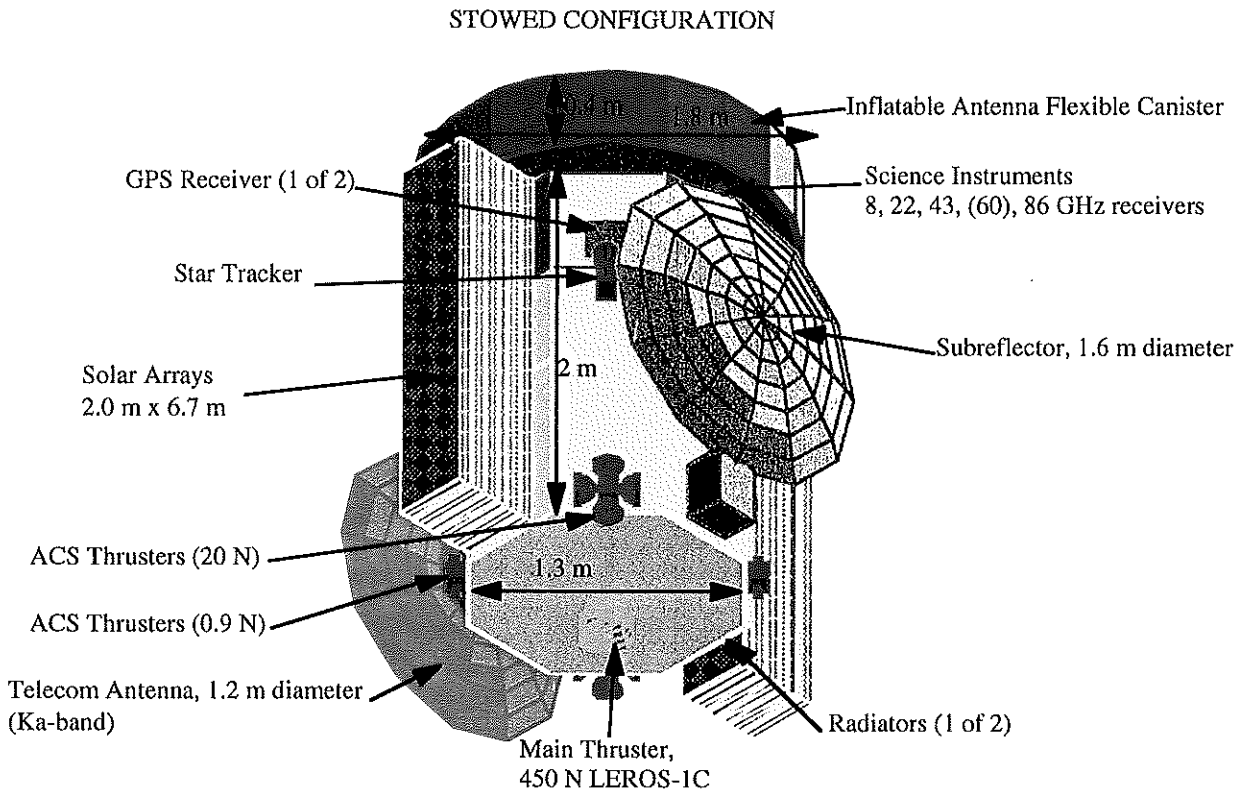

Fig. 7.1: ARISE Spacecraft in the Stowed Launch Configuration.

The ARISE spacecraft design is based on an octagonal shaped bus 1.3 m large and 2 m high. Figure 7.1 shows a conceptual external configuration of the ARISE spacecraft. Figure 7.2 shows the conceptual layout of the interior of the spacecraft bus. The octagonal structure supports the inflatable antenna canister on the top, as well as the inflatable solar arrays on two of the side panels. The other panels support a deployable 1.2 m diameter RF Ka-band telecommunication antenna, a deployable 1.6 m diameter subreflector, and various other spacecraft equipment (ACS thrusters, GPS receivers, star tracker, radiators, omni-directional antennas, etc.). The science receivers described in Section 4.6 are located at the focal plane, on the same panel as the subreflector and below the canister in a manner that no blocking of the receivers occurs. The canister has been designed to be part of the bus structure as much as possible (to reduce its structural mass) and to minimize blocking/shadowing of the main reflector.

The spacecraft volume and maximum dimensions were driven by the Delta II 7925 2.9 m diameter three-stage configuration fairing. The interior dimensions of the fairing are 2.5 m diameter at the base (same diameter for a height of 2 m) and about 4.6 m high. The canister diameter was constrained by the width of the shroud. In the current design, there is about a 0.3-0.4 m radial margin with respect to the shroud for the lower part of the spacecraft (everything below the canister).

The interior layout of the spacecraft was driven by the Delta II 7925 center of gravity (Cg) requirement, which must be located about 1.2 m above the separation plane. The fairing separation plane corresponds to the top of the launch vehicle payload attach fitting. The lower third of the spacecraft bus contains mainly the propulsion module with the Hydrazine, Nitrogen Tetroxide,

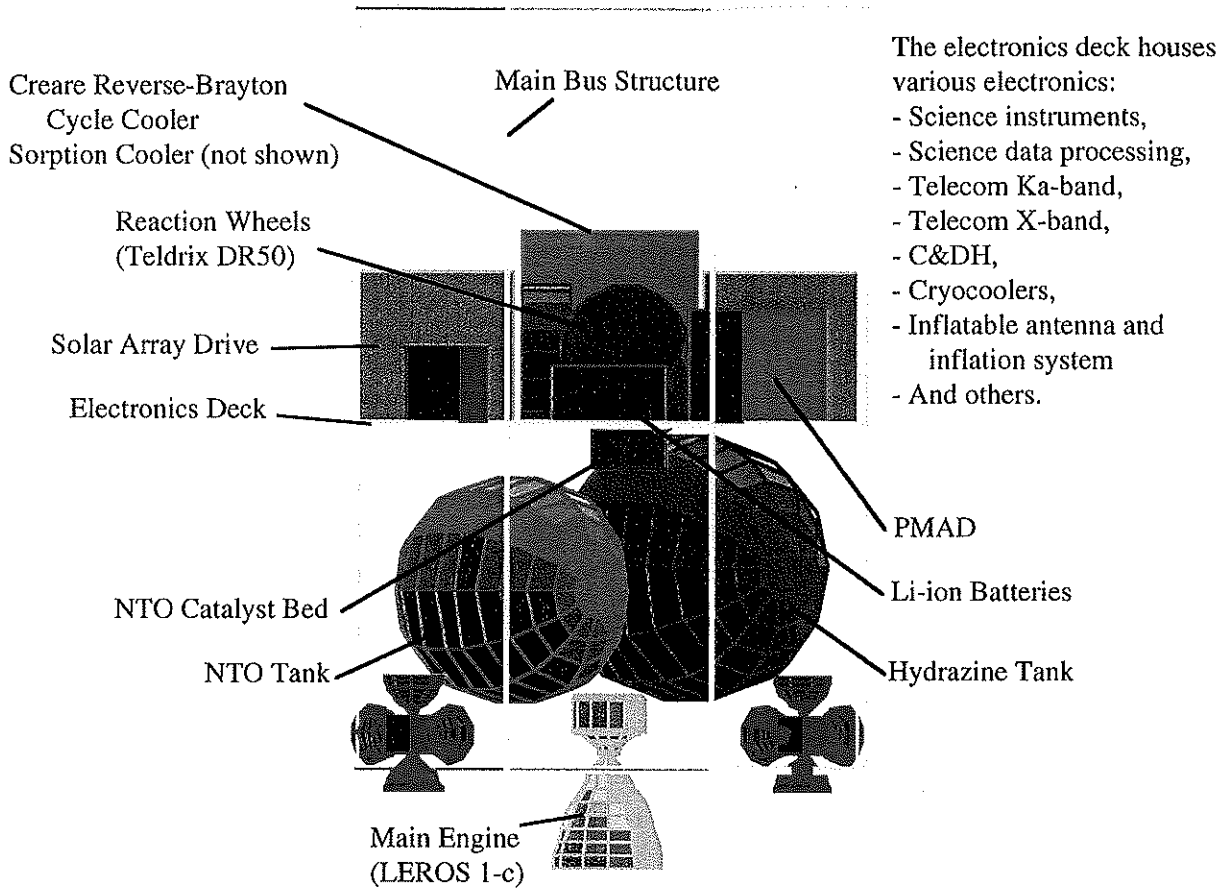

Fig. 7.2: ARISE Spacecraft Inside Layout.

Xenon (high Isp Thrusters propellant), and pressurant tanks, feed systems, main engine and mounting, inflation catalyst bed, and various hardware associated with the inflation system. About 223 kg of fluids are initially loaded, and about 152 kg of propulsion dry mass (with contingency) are mounted in this first third of the spacecraft bus. The middle third houses the electronics deck, with the Telecommunication, Data System, Power, Attitude Control, and Science System hardware and electronics. This deck also includes the two cryocooler stages, with the Sorption cooler mounted at the bottom of the inflatable antenna canister. Little or no effort has been made to integrate the electronics with the structure, as per the Lockheed Martin Multifunctional Structures bus design. By the time of spacecraft final design, it is to be anticipated that such an integrated bus will be current technology and thus the spacecraft design will have to be revisited to take this technology into account (a projected 20% reduction in total spacecraft mass could be applicable then). The top third of the spacecraft bus holds the inflatable antenna canister which is integrated with the bus structure.

A challenge in the spacecraft configuration design has been to take into account all pointing and field of view requirements. During science observations, the main reflector can be pointed anywhere in the sky except for a 30 deg. cone around the Sun. At the same time, the solar arrays must be pointed toward the Sun to provide the 2.3 kW needed (see power budget in Section 7.4.2), and the Ka-band telecommunication antenna must be pointed toward the Earth for near-continuous science data downlink. To achieve these requirements, the solar arrays are one-axis gimbaled and the telecommunication antenna deployed and two (2) degree-of-freedom gimbaled to

cover a least a half-space (targetted at 120 deg. half cone angle). At the time of writing, it is believed that this configuration should permit almost near-continuous coverage of the ground tracking stations, although a more thorough analysis is warranted to evaluate the effective coverage.

7.3 System Functional Description

A high level system functional block diagram of the ARISE spacecraft is shown in Figure 7.3. The key functions are provided by the following subsystems:

(1) A standard X-band RF subsysten for TT&C and emergencies, comprising:

- two (2) body mounted hemispherical patch antennas to provide near 4π steradian coverage,
- two (2) X-band transponders (one (1) in cold redundancy),
- two (2) 0.5 W RF solid state power amplifiers (one (1) in cold redundancy),
- one (1) set of X-band microwave components (diplexer, cables, connectors, etc.).

(2) A Ka-band RF subsysten for science data and telemetry transmission and phase transfer, including:

- one (1) 1.2 m diameter Ka-band antenna deployed on a boom,
- two (2) 512 Mbps modulators with Square-Root Raised Cosine shaping filters (one (1) per polarization) to downlink the wideband VLBI science data at a rate of 8 Gbps,
- two (2) 16 W RF TWTA power amplifiers (one (1) per polarization),
- two (2) up-converters and combiners (one (1) per polarization),
- two (2) Ka-band (37-39.5 GHz) transponders (one (1) in cold redundancy),
- one (1) set of Ka-band microwave components (diplexer, cables, connectors, etc.).

(3) The Command and Data Handling (C&DH) subsystem, which consists of:

- one (1) internally redundant Central Data Management Unit (CDMU) for uplink command processing, time-tagged command storage, spacecraft fault protection control, spacecraft time distribution, and health data collection,
- two (2) redundant low power serial busses to provide an interface for control and monitor of the health of other subsystems.

(4) The Power subsystem comprising:

- a two (2)-wing 2.3 kW inflatable solar array for main power generation,
- two (2) solar array drive mechanisms to keep the array Sun-pointing,
- one (1) set of primary Li/SO_2 batteries for post-launch activities (about 5 kWhr),
- one (1) set of secondary Li-ion batteries (about 350 Whr, with 126 W of recharge power) for power generation during eclipses,
- one (1) Power Managment and Distribution Unit (PMAD),

- one multiple high Isp thruster processing unit.

(5) The Attitude Determination and Control (ADCS) subsystem, which includes:

- two (2) star trackers for attitude measurements during stabilized phases (one (1) in cold redundancy),
- one (1) Sun sensor with five (5) heads used in the coarse acquisition phase and for back-up and safe modes,
- one (1) Inertial reference Unit (IRU) providing attitude information during slewing phases,
- actuator drive electronics for solar array, telecommunication antenna pointing, reaction wheels and propulsion system control,
- four (4) reaction wheels to execute slew maneuvers and to compensate for disturbance torques for fine pointing (one (1) in cold redundancy),
- two (2) GPS receivers.

(6) The Propulsion subsystem consisting of:

- one (1) Nitrogen Tetraoxide tank and one (1) Hydrazine tank and corresponding feed systems for perigee raise maneuver, ADCS propellant, and main reflector make-up gas,
- eight (8) 22 N thrusters for main burn trajectory correction,
- eight (8) 0.9 N thrusters for coarse attitude control maneuvers,
- three (3) high Isp thruster clusters for solar torque compensation,
- one (1) high Isp propellant tank and feed system,
- one (1) catalyst bed for Nitrogen Tetraoxide decomposition into Nitrogen for main reflector make-up gas,
- one (1) gas tank and corresponding feed system for the main reflector and solar array inflation system.

(7) The Mechanisms subsystem comprising:

- a subreflector boom, gimbal and deployment mechanism,
- a Ka-band antenna boom, gimbal and deployment mechanism.

(8) The spacecraft bus Thermal Control subsystem including:

- a 2 m^2 radiator,
- multilayer insulation (MLI) blankets for thermal control between the spacecraft and space, as well as between spacecraft elements,
- a set of electric heaters and controllers for temperature sensitive elements such as batteries and propulsion elements,
- a variable conductance heat pipe system and associated pumps.

The Science, Antenna System and Science Instruments Thermal Control have been described in detail in Chapter 4.

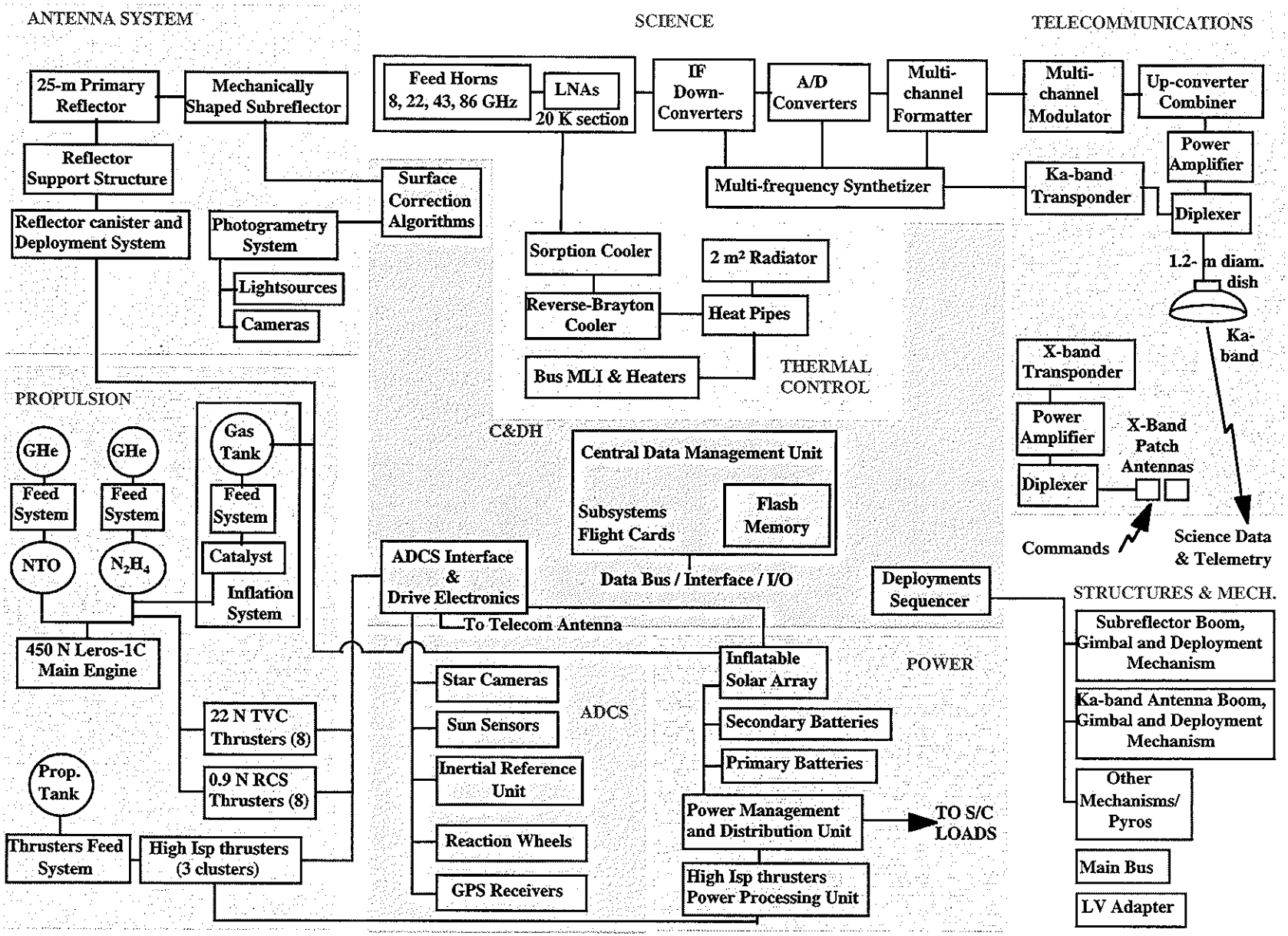

Fig. 7.3: ARISE Spacecraft High Level System Functional Block Diagram.

7.4 System Budgets

7.4.1 Mass

A top level mass budget of the ARISE spacecraft is summarized in Table 7.1. A 30% mass contingency has been applied to the spacecraft dry mass, except to the solar array mass which has an intrinsic contingency due to the power budget contingency. No launch vehicle margin has been added since it is believed that the launch vehicle capabilities will have increased by the time of launch.

Subsystem	Mass (kg)
Inflatable antenna	192.3
Subreflector and metrology system	105.6
Telecommunications (X-band)	8.2
Telecommunications (Ka-band)	36.3
C&DH	25.4
Power	105.1
Solar arrays	31.4
ACS	82.1
Thermal Control	125.5
Structures/Mechanisms	287.3
Propulsion system	116.7
Science instruments	51.0
Spacecraft dry mass	**1166.8**
Contingency (30%)	340.6
Propellants/Fluids	222.8
Launch Vehicle adapter	45.4
Total spacecraft mass	**1775.6**
Launch vehicle capability (i=30 deg.)	**1810.0**
Additional margin	**34.4**

Table 7.1: ARISE Spacecraft Mass Budget.

7.4.2 Power

The power demand as a function of mission modes is summarized in Table 7.2. A 30% power contingency has been used for all modes.

Power mode / Subsystem	Launch + post-launch	Orbit insertion	All deploy-ments	Science	Slews, calibra-tions	Eclipses
ACS	139.5	139.5	139.5	228.5	228.5	139.5
Propulsion	60	60	70	520	10	10
C&DH	9	15	15	15	15	9
Inflatable antenna	82	82	82	5	5	5
Power	20	20	20	72	40	40
Mechanisms	0	0	80	80	80	50
Telecom	34	34	34	216	34	34
Thermal control	70	70	70	450	70	70
Science	0	0	0	100	0	0
Subtotal (W)	**415**	**421**	**511**	**1659**	**605**	**358**
Contingency (30%)	124	126	153	498	181	107
Battery recharge				126	126	
Total (W)	**539**	**547**	**664**	**2283**	**912**	**465**
Source	Primary battery	Secondary battery	Primary battery	Solar array	Solar array	Secondary battery
Duration (hrs)	6.4	0.5	2			0.75

Table 7.2: ARISE Spacecraft Power Budget per Mission Mode.

7.4.3 Propellant

The propellant budget is based on the launch vehicle injected mass. The main perigee raise burn ΔV is about 240 m/s. There is an additional 30 m/s contingency. Table 7.3 summarizes the propellant budget:

Propellant budget:	Mass (kg)
Spacecraft dry mass	1420.3
Total spacecraft mass	1810.0
Perigee raise maneuver	147.6
Residuals	4.3
Pressurant (He)	2.8
ACS fluids (Hydrazine)	20.0
ACS fluids (Xenon)	24.8
Inflation gas (He)	0.4
Make-up gas (Hydrazine)	23.0
Total	**222.8**

Table 7.3: ARISE Spacecraft Propellant Budget.

7.4.4 Pointing Budgets

Potential perturbation sources include the ACS reaction wheels, cryocoolers, thermal and dynamic effects, lenticular structure pressure maintenance, and ESD Lofting.

7.4.5 Observation Timeline

To address the requirement of 70-80% science data acquisition, a list of spacecraft functions during routine operation has been established in Table 7.4. The orbit period is 12.9 hours, or about 774 minutes.

Task	Frequency (per orbit)	Maximum Duration (min)	(%)
Tracking station efficiency (95%)	1	38.7	5%
Tracking station coverage (95%)	1	38.7	5%
Eclipses (3% average loss)	1	23.2	3%
Target source slewing and coarse pointing	1	19	2.5%
Antenna calibration			
Antenna stabilization	2	2 x 10	2.6%
Antenna distortion mapping	2	2 x 10	2.6%
Subreflector focusing & shaping	2	2 x 10	2.6%
Pointing calibration	1/60	1/60 x 60	0.1%
Ground tracking station switching and link establishment	3	3 x 5	1.9%
Star tracker calibration	1	30	3.9%
Reaction wheel unloading	TBD	TBD	
Cryocooler set-up	TBD	TBD	
Antenna gas maintenance	TBD	TBD	
Effective total		**225.6+**	**29.1%**
Maximum required	20% of orbit	**155**	**20.0%**
RF data acquisition	80% of orbit	**619**	**80.0%**

Table 7.4: ARISE Mission Functions Resulting in Loss of Science Data Collection.

The estimated durations will depend on the observing band set for the selected source and should be lower at the lower frequency bands. Not included here are the ground functions (e.g., tape change). This table is a starting point for a more elaborate analysis of the coverage to be performed in the future.

7.4.6 Slew Time and Settling

When changing observing source, the ARISE spacecraft can slew at a rate of 3 deg/min. However, slewing is a two-stage process which means that the total angle the spacecraft slews through is greater than or equal to the angle between the two sources. The spacecraft slews around one (1) or two (2) of its principal axes of rotations (antenna boresight, solar-arrays rotation axis, and

spacecraft longitudinal axis) before reaching its final position. Thus, under the worst case scenario, it takes 19 minutes to slew the spaceraft to a new source (90° apart). Furthermore, the antenna is estimated to take about 10 minutes to settle.

7.5 Command and Data Handling

7.5.1 Requirements and Assumptions

The Command & Data Handling Subsystem (C&DH) for the ARISE spacecraft is required to operate for a primary mission life of three (3) years. The dual string block redundant design acts as a bent pipe to control the gating of VLBI data within the science instrument. The bi-level switch controls are changed at a low data rate. The C&DH receives periodic X-band uplink commands at a rate of 2 kbps when in contact with the DSN Ground Command Station (GCS). The electronics must operate through an equivalent radiation environment of 315 krads behind 100 mils of aluminum. The mass storage device in the C&DH is not required to store or process the high speed science data, which is telemetered to the ground in real-time.

7.5.2 Design Implementation and New Technology

The C&DH required functions are performed by either (one of two) C&DH block-redundant string. Redundancy provides a high level of reliability to meet the primary and extended mission life requirements. We note that all key elements of the CDS design are new technology. The C&DH avionics interfaces are summarized in Figure 7.4.

The Lockheed Martin PowerPC 750 processor verifies and processes uplink commands, stores time tag commands & GPS data, controls the spacecraft fault protection, configures the science data path, distributes the spacecraft time and collects State-Of-Health (SOH) data. The flight code and packetized SOH data are stored in FLASH non-volatile memory. Redundant low power serial busses provide an interface to control and monitor the health of the other subsystems. The flight software code is expected to be written in ANSI C or C++. VxWorks (a commercial real time operating system and development environment) is recommended. The ADCS pointing and control algorithms, the metrology system algorithms, the subreflector correction algorithms, and various other flight algorithms are supported in the C&DH software.

The size of the volatile DRAM memory will be 128 Mbytes. The spacecraft and instrument flight code will be stored in 8 Mbytes of EEPROM non-volatile memory with EDAC monitoring. The 12 Multi-Chip Modules (MCM) in the C&DH design have a mass of approximately 6 kg. Each C&DH string dissipates 8 W.

During critical maneuvers the watchdog timer within the active C&DH string will monitor C&DH performance. If a performance fault is detected by the watchdog timer a (Power On Reset) POR will be performed on the active C&DH string. If the active C&DH String continues to malfunction, the watchdog timer circuitry will autonomously switch the C&DH String off and turn on the redundant C&DH String. During non-critical maneuvers, ground commands can be sent to the spacecraft to override the autonomous feature regarding the power switching of C&DH strings.

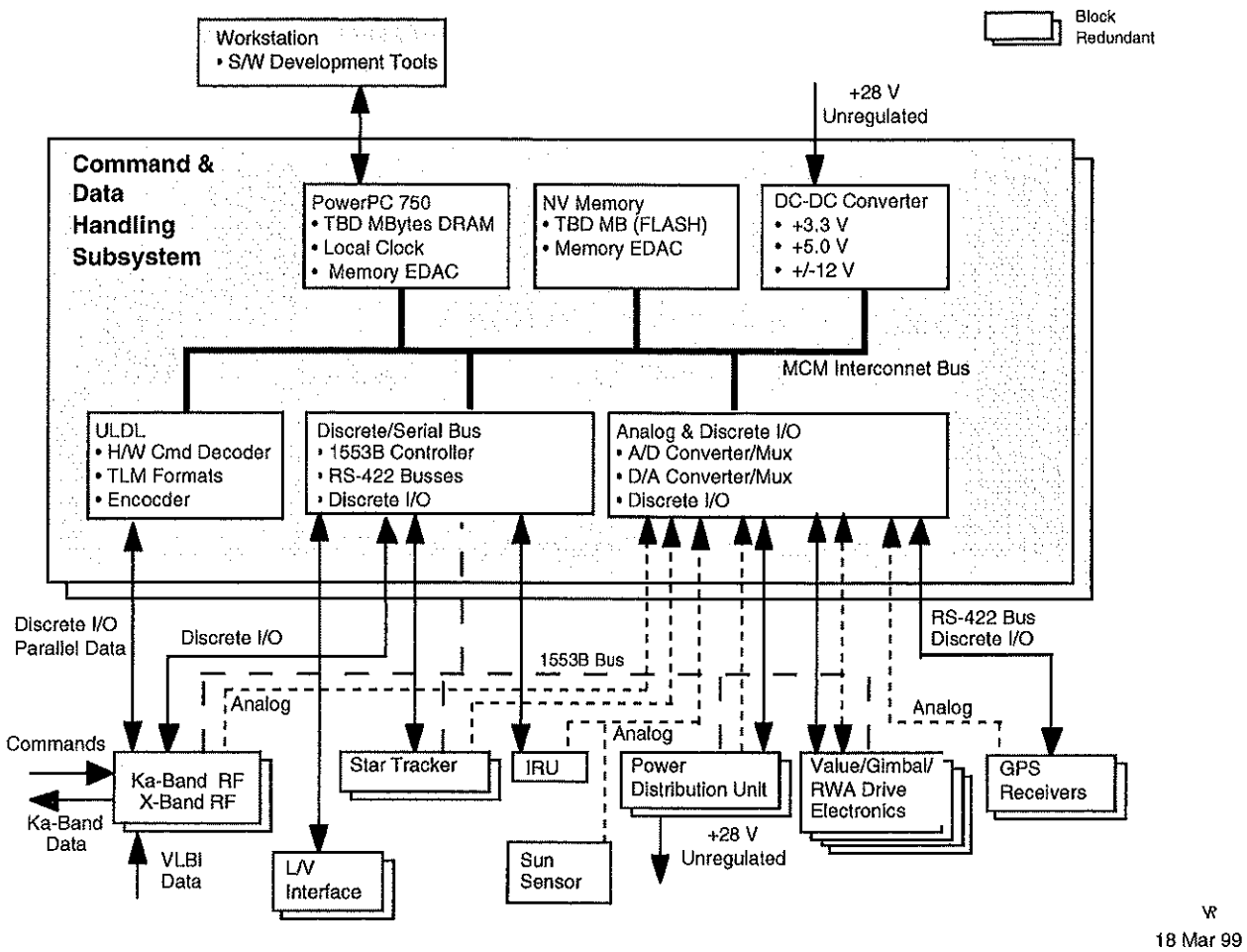

Fig. 7.4: ARISE Command & Data Handling (C&DH) Block Diagram.

The C&DH is required to perform many critical spacecraft functions. Several examples are shown below:

- Uplink command processing and distribution
- Sequence storage and control
- Maintenance and distribution of spacecraft time
- Collection and formatting of engineering spacecraft sensor data
- Bulk storage of engineering data
- Subsystem control and services
- Spacecraft fault protection
- Attitude Estimation
- Attitude Control
- RCS Delta-V / Translational Control
- Solar and / or HGA Articulation Control

The baseline radiation environment is 315 krads[Si] Total Ionizing Dose behind 100 mils of aluminum. A tantalum enclosure is recommended. Commercial rad-tolerant electronic devices can

be shielded behind 270 mils of Tantalum. The shielding mass is 8.7 kg. The effective radiation environment inside the enclosure is 19.8 krads[Si] TID. The electronic devices should be selected to have immunity to Single Event Latch-up (SEL) and immune to Single Event Upset (SEU) to 75 MeV/mg-cm^2.

7.6 Telecommunication Subsystem

The ARISE telecommunication system includes an X-band command subsystem and a Ka-band telemetry and science subsystem.

7.6.1 X-band Subsystem

The X-band subsystem performs command, telemetry, and control (TT&C) functions interfacing with the DSN Ground Command Station (GCS), as shown in Figure 8.1. It consists of a Spacecraft Transponding Modem (STM), a diplexer, a solid-state power amplifier (SSPA), an ultra-stable oscillator (USO), two X-band patch antennas, and an RF switch, as shown in Figure 7.5. The baselined 0.5 W SSPA provides sufficient downlink margin to the (assumed) 34-m DSN GCS. The baseline ovenized USO is manufactured by Applied Physics Laboratory (APL) and is similar to the USO used on the Cassini spacecraft. The required warm-up DC power for the oscillator is 4.5 W and the operating DC power at 25 C is 2.3 W. Two X-band patch antennas are placed strategically on the ARISE spacecraft to provide near 4π steridian coverage. An RF switch is used to select which antenna to communicate with the DSN GCS.

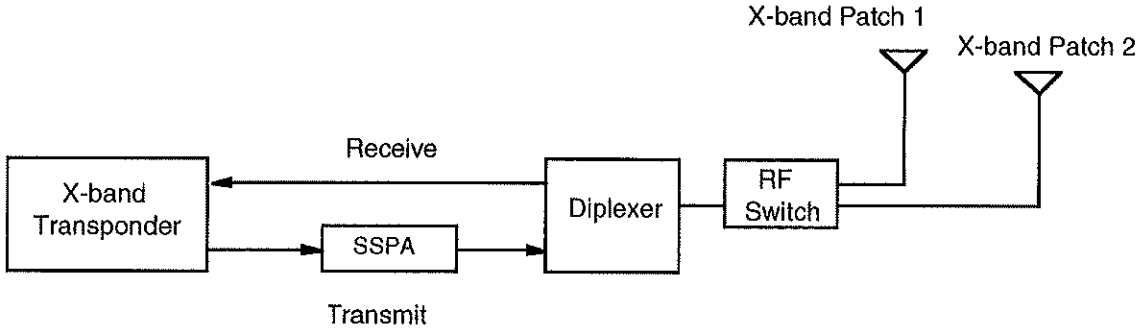

Fig. 7.5: ARISE X-band Telecommunication Subsystem Block Diagram.

7.6.2 Ka-band Subsystem

The Ka-band telecommunication subsystem is composed of an 8 Gbps downlink transmitter and a Ka/Ka transponder. The high rate downlink is used to transmit the science wideband VLBI data. The Ka/Ka transponder provides a stable phase reference for the on-board scientific instrumentation uplinked from an H-maser frequency standard at the ground tracking station (GTS).

The details of the 8 Gbps science data downlink Ka-band subsystem have been described in Chapter 5. The baseline plan is to divide the 8 Gbps data into sixteen (16) 512 Mbps channels, with eight (8) channels transmitted using left circular polarization (LCP) and the remaining eight using right circular polarization (RCP). Each 512 Mbps channel is modulated using Square-Root Raised Cosine (SRRC) filtered quadrature phase shift keying (QPSK) at a symbol rate of 256 Msample/s (512 Mbps per modulator). The SRRC filter operates at 25% excess bandwidth (α = 0.25) and introduces controlled intersymbol interference (ISI) that improves the spectral efficiency (total bandwidth occupancy) of the QPSK modulation. While the bandwidth allocation of this

scheme occupies approximately 2.5 GHz of bandwidth, which exceeds the 1 GHz bandwidth allocated to Space Research, a waiver for its use is required. A more aggressive design using quadrature amplitude modulation (QAM) has been investigated for ARISE in the event that FCC restricts the space VLBI spectral allocation to the original 1 GHz. Compared to a more advanced eight 1024 Mbps channels approach, the current sixteen channel baseline is considered to be a lower risk option at the expense of higher system complexity. It is foreseeable that advances in high speed electronics can support 1024 Mbps modulated carriers in a few years. At that time, the selection of the sixteen or eight (8) channel design will be re-evaluated.

Figure 7.6 shows a block diagram of the ARISE Ka-band telecommunication subsystem. Each of the 512 Mbps channels is modulated and up-converted to a different RF frequency, resulting in adjacent non-overlapping carriers. The eight (8) channels for each polarization are then collected and amplified by a TWTA. Since the SRRC-filtered QPSK modulated signals do not have constant envelopes, the TWTA is backed-off from its saturated mode and operated in the linear region with reduced power efficiency.

Table 7.5 shows the nominal link budget of the 8 Gbps downlink. The signal from each polarization is amplified by a 16 W TWTA and transmitted via a 1.2 m high gain antenna (HGA). The maximum pointing loss is assumed to be 0.3 dB for the spacecraft HGA, and is assumed to have 60% efficiency at 37-39.5 GHz. The power amplifiers are assumed to be near the HGA so that the length of the waveguide is no more than 1.5 m with approximately 3 dB of loss. The maximum slant range of the link is 46800 km (assuming a 40000 km nominal orbit apogee), and we have assumed a minimum elevation angle of 7°. Atmospheric attenuation is assumed to be 1.9 dB using the DSN standard model. A more comprehensive search of propagation data is needed to provide a better estimate of the atmospheric attenuation. The efficiency of the 11-m DSN GTS antenna is estimated to be about 38%, pointing and polarization losses are assumed to be no more than 0.4 dB and 0.3 dB, respectively, and the estimated system temperature is 145 K for a cryo-cooled system. The ground receiver should include an equalizer to remove the intersymbol interference and distortion introduced by the non-ideal filtering of the SRRC filters. The nominal link margin is nearly 8 dB. This margin is sufficient for three joint sigma deviations to provide a highly reliable link.

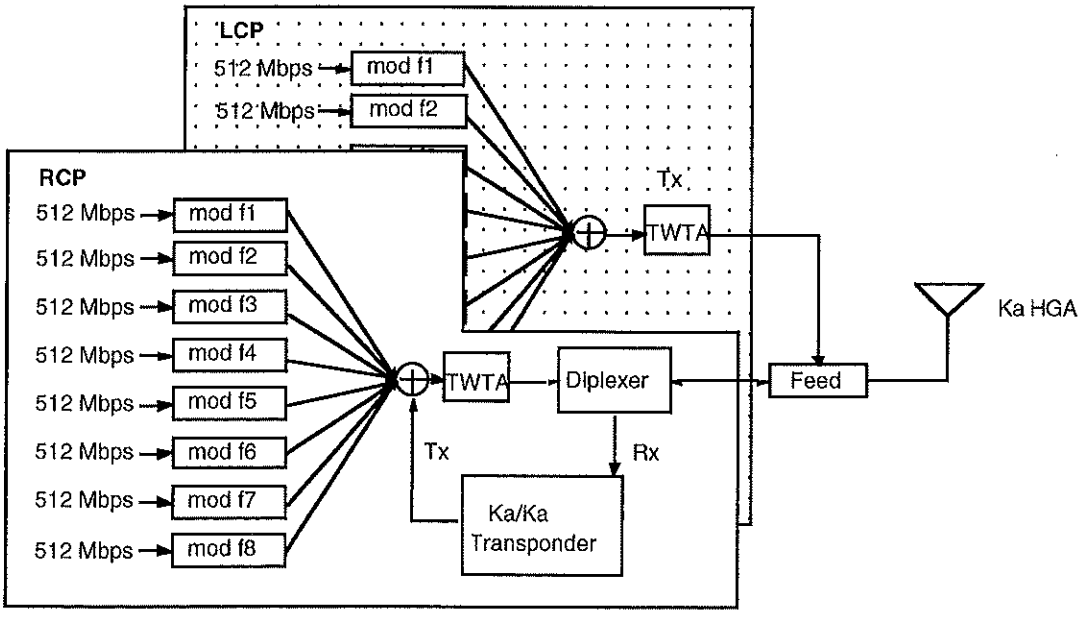

Figure 7.6: ARISE Ka-band Telecommunication Subsystem Block Diagram.

The Ka/Ka transponder is used to receive the phase reference tone from a GTS and downlink the transponded tone and the 8 Gbps multi-carrier data. The transponder has an uplink frequency of 40 GHz and a downlink frequency range of 37-39.5 GHz (QPSK modulation with SRRC filtering) in the bands allocated to Space Research. A small portion of the 37-39.5 GHz spectrum is employed for the transponder downlink tone within the 8 Gbps spectrum, likely at a modulated carrier null. The exact transponder turn-around ratio is yet to be determined. The loop bandwidth of the transponder is expected to be about 1000 Hz and the dynamic range of the received signal is expected to be about 40 dB. The baseline tranponder does not include a power amplifier. Its output power is expected to be about 10 dBm. The downlink tone is summed with the high rate carriers and amplified by the TWTA as shown in Figure 7.6.

Transmitter power	16.00	Watts
Transmitter power	42.04	dBm
Transmitter cable losses	-3.00	dB
Antenna gain	53.00	dBi
Antenna Efficiency	-2.22	dB
EIRP	89.82	dBm
S/C Pointing loss	-0.30	dB
Max. Range	4.68E+04	km
Link Frequency	3.70E+10	Hz
Atmospheric attenuation	-1.90	dB
Space losses	-217.21	dB
Ground receiver parameters		
Receive antenna gain	72.59	dBi
Antenna efficiency	-4.20	dB
Ground pointing loss	-0.40	dB
Polarization losses	-0.30	dB
System Noise Temperature	145.00	K
Noise spectral density	-176.99	dBm/Hz
Received power Summary		
Received total power	-61.90	dBm
Received Pt/No	115.09	dB-Hz
Data Rate	4.10E+09	bps
Eb/No	18.96	dB
Eb/No Threshold (uncoded)	11.00	dB
Eb/No Margin	**7.96**	dB

Table 7.5: ARISE Link Budget for 8 Gbps Data Downlink.

7.7 Thermal Design

The thermal control system for the ARISE spacecraft consists of two specific elements: the cryo-cooler stages, and the bus thermal control. The cryocooler stages have been described in Section 4.7 and therefore we describe here the bus thermal control.

The spacecraft systems that affect the Thermal Control System (TCS) are: the Power System, due to battery and solar array requirements; the Propulsion System, due to temperature requirements of the propellants; and the systems that require electronic components, due to their operating temperature requirements. Furthermore, the thermal design requires knowledge of the structure

because its material (thermal conduction) and configuration (radiation) affect the thermal exchange between spacecraft elements.

The TCS must control the temperature of the spacecraft elements within allowable limits for this spacecraft, which has an electrical power level of about 2300 W, and which has a cold zone which must be maintained at 20 K. The design uses standard passive thermal control elements, and will use technology available at the implementation cutoff date. Multilayer Insulation (MLI) blankets will control the thermal radiation between the spacecraft and space, as well as between spacecraft elements. Thermal surfaces will be used to control the thermal balance between the spacecraft and the environment. Thermal conduction control will be used to maintain thermal gradients as required. Also required are electric heaters and controllers for temperature sensitive elements such as batteries and propulsion elements.

To maintain the science subsystem horn/LNA at 20 K, a two-stage cryogenic cooler system is required. The design must incorporate thermal isolation between the spacecraft bus elements and science subsystem, which will require thermal conduction and radiation isolation. The thermal energy from the cryogenic coolers will be transferred to thermal radiators with looped heat pipes that are mounted on the spacecraft bus. The thermal radiators will be constructed from high performance composite material and will also incorporate heat pipes.

The thermal control of the inflatable elements will use passive means, plus heaters, if necessary, for storage, deployment and rigidization. Several optional rigidization techniques are being evaluated. One technique under consideration is cold rigidization. This technique requires that the inflatable elements be kept below 225 K. An initial analysis indicates that, with the correct external thermal surface, in this case FEP-Aluminum or FEP-Silver, this temperature level can be achieved. To provide the uniformity required, a simple 5-layer MLI blanket is necessary. The inflatable elements must be kept above the rigidization temperature during launch and prior to deployment; this is to be accomplished with a MLI cover and a small heater. The deployment must be accomplished rather rapidly, as the inflatable elements will cool to 225 K in 5-20 minutes.

7.8 Attitude Determination and Control Subsystem (ADCS)

The ADCS system (in conjunction with the propulsion system) has to perform changes in velocity (delta-V). In addition, it must determine and control spacecraft attitude and rate to allow science observations. It must do this in the presence of various external and internal disturbances. To verify performance, models must be built for both static and dynamic analysis. Below we discuss the requirements, choice of components, cost, and analysis, including modeling.

7.8.1 ADCS Requirements

The science driven ADCS requirements are described as follows:

(1) The spacecraft should be capable of slewing of 180 deg. in less than 1 hour.
(2) The telescope boresight shall always be more than 30 deg. from the Sun.
(3) Stability must be maintained during science observations. The required stability and duration are given in Table 7.6, and depend on the observing frequency.
(4) The absolute pointing accuracy of the electrical boresight during observations shall be 3 to 30 arcseconds, depending on the observing frequency. This is given in Table 7.6.

While meeting these requirements, the ADCS must also counteract external disturbance torques consisting of the Earth's gravity gradient forces and moments, and solar pressure forces and

moments. In addition, there are internal disturbance sources such as the ADCS components themselves (thrusters or reaction wheels) and other devices such as coolers.

Frequency [GHz]	Motion [arcsec]	Time Scale [sec]	Stability [arcsec/sec]
8	**30**	**350**	**0.086**
22	**11**	**150**	**0.073**
43	**6**	**60**	**0.1**
86	**3**	**15**	**0.025**

Table 7.6: ARISE Spacecraft Stability Requirements.

7.8.2 Components

To satisfy these stringent requirements and perform routine ADCS operations, one set of reaction wheels and two sets of thrusters with different thrusting capabilities are envisioned as the actuators. One star tracker, one Sun sensor, one Inertial Reference Unit, and one GPS receiver are envisioned as on-board attitude sensors. These may be redundant for reliability as desired.

The ACS design is driven by the tight requirements and low structural frequencies of the antenna, which dictate reaction wheels for fine pointing. These are sized by the torque and momentum capabilities required for slewing and counteracting environmental torques. Vibration isolation components may be necessary depending on the design of the cooling system and the results of more detailed dynamics simulations. These can either be passive, as the isolation used for the Hubble Space Telescope (HST) reaction wheels, or active, as for STRV2.

These components can meet the accuracy requirements for the spacecraft bus itself. However, to point the optical boresight to the same accuracy will require calibration of the alignment between the optical axes and the bus axes. In addition, the stability of this calibration is an issue since it may not be possible to calibrate during observations. Thermal variations and material aging may cause significant perturbations requiring periodic re-calibration. This issue will require a close interaction between the RF and ACS subsystems.

If a sufficiently bright source is targeted, it may be possible in real time to use the onboard image centroid to determine the calibration between the basebody and the boresight. If the target is too weak (likely) then we must depend on the previous calibration performed for a bright source, and either assume it stays constant, or measure the current shape (metrology) and then calculate the changes in the calibration. Analysis of this type of problem will obviously require extensive high fidelity modeling of the structure, it's thermal characteristics, it's dynamic characteristics, the interaction with the attitude control system and any disturbance sources, and the RF performance. This will require development of integrated analysis tools, as current tools such as IMOS (Integrated Modeling of Optical Systems) are only just now developing the capabilities needed to handle inflatable structures, and extensive experience with these will be necessary to handle the ARISE analysis problem.

7.8.3 Spacecraft Model

An analysis has been performed to size the disturbance environment. A finite element model of the ARISE spacecraft has been built in Matlab using the IMOS software. This model has been refined by using NASTRAN data for consistency with the structural design. The finite element model features all the structural dynamic components of the spacecraft, with the exception of the bus and the subreflector, which are assumed to be rigid. The solar panels and the subreflector boom are, however, modeled using finite elements. See Figure 7.7 for the model. Therefore, there are beam

elements for the support struts and the hard truss, and membrane elements for the reflector and the canopy. The inflatable torus, modeled as a circular ring, is connected to the reflector/canopy through a set of pre-tensioned constant force springs. The membrane elements are linear, with no pretension. All material properties are homogeneous and isotropic. The finite element model has 1876 degrees of freedom (132 beams, 72 constant force springs, 396 membranes, 24 multi-point constrained degrees of freedom, 472 mass-less degrees of freedom obtained through Guyan reduction), of which 1382 are retained for the dynamic analysis. A model for the reaction wheels, including saturation at 0.2 Nm, is included in the structural model. The model also describes input forces and torques, such as those derived from gravity gradient, solar pressure, thruster forces, and reaction wheel torques. Static and dynamic deformation under open loop or closed loop control were produced.

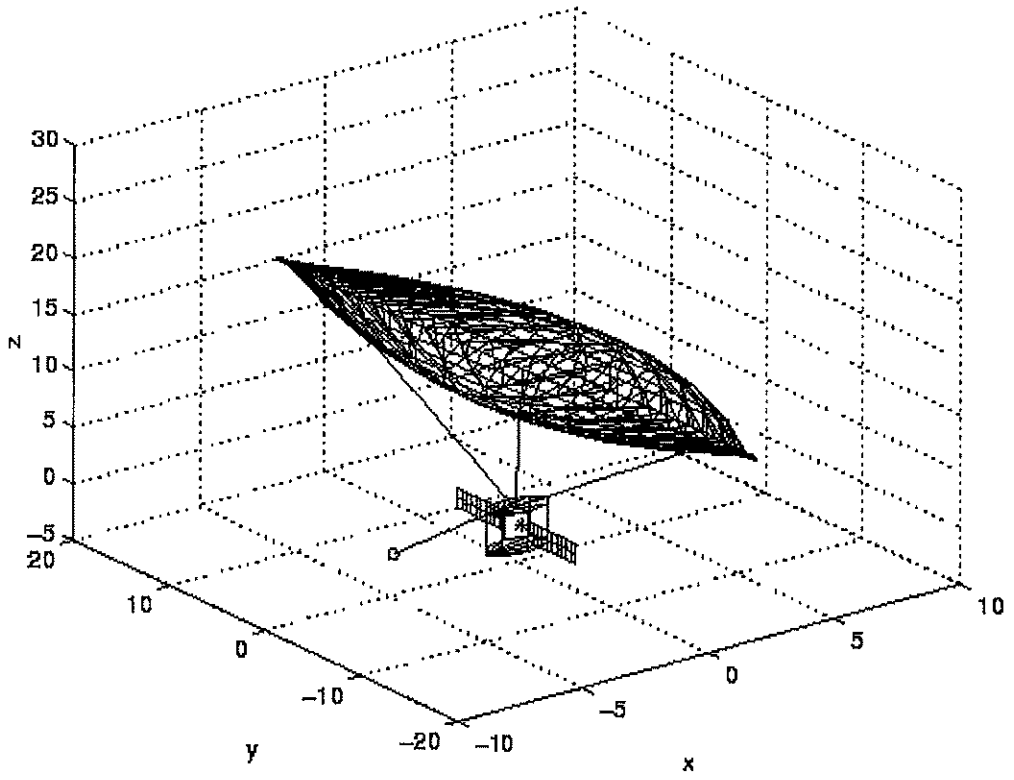

Fig. 7.7: ARISE Spacecraft and Antenna Finite Element Model.

7.8.4 Disturbances

Given the inertia matrix, we can determine the gravity gradient torque for arbitrary spacecraft orientations. IMOS also has the capability of determining the gravity deformation forces that result from gradients. The solar force direction in the spacecraft frame of reference has an angle with the boresight (theta), and an angle of rotation around the boresight (alpha). The impact of the solar force and torques on the antenna can be determined for various geometries.

Preliminary analyses show that the solar force is less than 3.7×10^{-3} N, the solar torque is less than 0.05 Nm, the gravity gradient force is less than 4.5×10^{-4} N, and the gravity gradient torque is less than 5.12×10^{-3} Nm. Of interest is the distance between the center of pressure and the center of

mass, equal to [-6;-7.5;-14.0] m. Figures 7.8 and 7.9 show the solar torque magnitude as a function of theta and alpha.

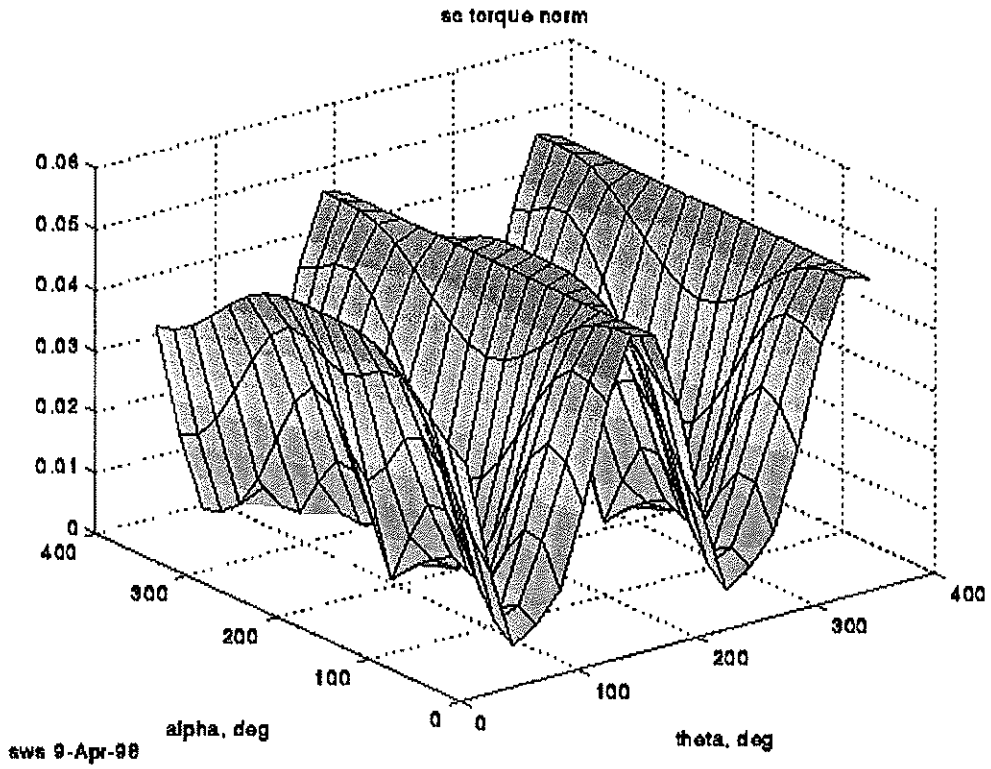

Fig. 7.8: Solar Torque Magnitude as a Function of Theta and Alpha.

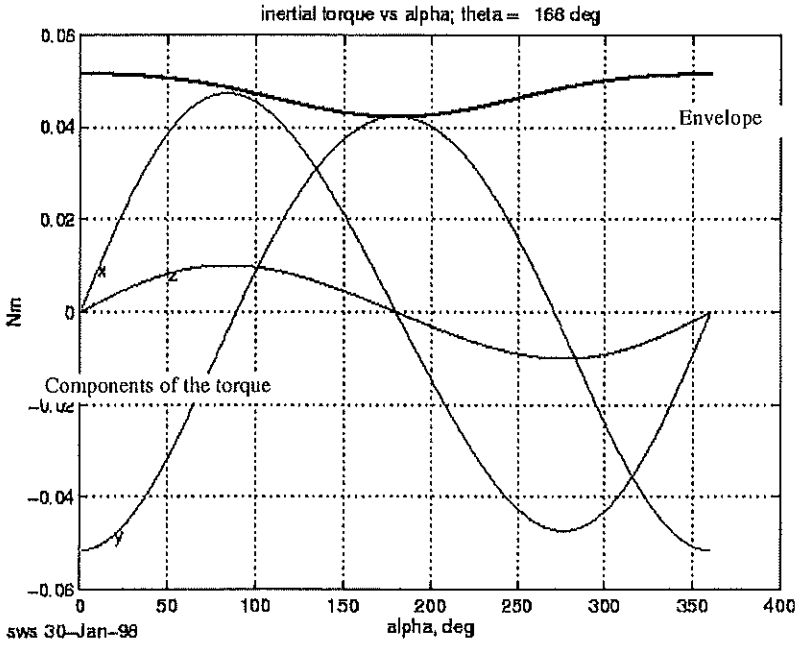

Fig. 7.9: Solar Torque Magnitude as a Function of Theta and Alpha.

Cooler disturbance data are not available at the time of writing, but an example of the possible magnitude of the disturbance is given by STRV2. In that case, a 1W TI cryogenic cooler was used. It produced forces of about 5 N at various harmonics of the 55 Hz drive frequency. If the ARISE cryocoolers produces forces of this magnitude, it is very likely that they will have to be isolated at least by a passive system similar to that used on the HST.

7.8.5 Momentum Management

After examining various options for reaction wheels, the following wheel was chosen:

Teldix DR 50:
- torque: 0.3 Nm,
- max momentum: 300 Nms,
- max wheel speed: 6000 RPM,
- power: 150/15/3 W,
- mass: 12 kg,
- size: 0.15 m x 0.5 mD.

Given the maximum torque, one option is to wait as long as 99 minutes before unloading the wheels, which certainly is longer than required. The wheels will then be spinning at maximum speed (6000 RPM) and drawing maximum power. Another option would be to unload the wheels when they reach about 1/4 of their momentum capability (1500 RPM), which requires much less power. This option also leaves a large margin for observational flexibility. In addition, the reaction wheel disturbances are functions of the square of the wheel speed, so minimizing the speed improves the pointing performance.

The power usage, considering all solar angles is given in Table 7.7. The maximum power is the power required for all three wheels just before unloading, minimized over all solar incidence angles. This assumes all wheels are unloaded at once. The maximum average power is the power for all three (3) wheels, averaged over one cycle, taking the maximum over all solar incidence angles.

Option	Time before unloading (min)	H at unloading (Nms)	Maximum power (W)	Maximum average power (W)
A	99	300	314	180
B	26	80	117	81

Table 7.7: ARISE Spacecraft Power for Reaction Wheels during Observations.

The wheels can perform a two (2) degree slew in about 118 seconds, and a 180 degree slew in about 19 minutes.

Solar Torque Compensation

The magnitude of the solar pressure force is about 3-4 mN, translating to a torque of about 0.05 Nm at the spacecraft bus. However, unloading the solar torques even with high Isp (specific impulse) thrusters located at the spacecraft bus would require a significant amount of propellant (calculations show that it requires on average 350 kg/year of Hydrazine at 220 s Isp and 50-80 kg/year of Xenon for a 2000 s Isp thruster). Several options have been considered to passively and actively compensate for the solar torques. The passive option consists of rotating the whole spacecraft about the boresight, but this maneuver would affect the power collection, the

telecommunication antenna pointing, and the quality of the science data. The passive option has thus not been considered as a viable option. Active compensation options have focused on using high-Isp low-thrust thruster located at the main reflector torus/struts intersection to take full advantage of the moment arm. There are three (3) candidate electric propulsion systems [7.1]:

(1) Field emission thrusters
(2) Colloid thrusters
(3) Micro-ion thrusters

Field emission thrusters, or Field Emission Electric Propulsion (FEEP), have very high specific impulses (typically 8000 s), provide thrust level between 10^{-6} and 10^{-3} N, and have a compact size, which includes the propellant storage. They are going to be tested soon for about 1500-2000 hours and are technologically mature compared to the two other thruster options. Typical power requirement is about 60 W/mN. Disadvantages of FEEPs are the potential contamination issues (especially on the main reflector canopy surface) since they use liquid metal as propellant (Cs), a high operating voltage, and a narrow operating temperature range.

Colloid thrusters have been designed to produce thrust levels of 0.2-0.5 mN at power levels of about 4.4 W/mN. Their specific impulse ranges from 450 s to 700 s, although some designs provide up to 1350 s. They use glycerol propellants. Colloid thrusters were studied extensively during the late 1960s and early 1970s for spacecraft attitude control, but fell out of favor due to their low thrust levels. Recent developments in micro-spacecraft are bringing back interest in colloid thrusters, although the technology is still at the laboratory model level.

Mini-ion thrusters are scaled models of the 30-cm diameter NSTAR ion engine flying at the time of writing on the Deep-Space One (DS-1) spacecraft, with improved and miniaturized components. Still at a conceptual level, it is estimated that a 3-cm ion engine would provide 1 mN of thrust with an Isp of about 2500-3000 s. Ion thrusters use Xenon as propellant, which is stored in a supercritical state. Their power requirement would be about 80 W/mN (assuming a 20% efficient thruster). Lifetime and actual performances are still of concerns for these devices.

A high level mass and power trade has been performed between these three technologies to assess a mass and power allocation for such a system, and the mini-ion thrusters appeared the most promising. Thus in the current spacecraft concept, three mini-ion thruster clusters are mounted on the inflatable antenna torus/struts joints to correct for solar pressure torques. However, more thorough analyses and trade-offs of these three options will need to be performed. Further analysis is also required to determine the implications of having thrusters on the inflatable antenna torus, both from the ACS and structures points of view. A more thorough analysis of ways to overcome the solar torques should also be performed at this stage.

If high Isp thrusters are used to counteract the solar torques in subsequent designs, smaller reaction wheels may be selected to obtain the fine pointing required.

7.8.6 Dynamic Analysis and Control

We wish to quantify here the consequences of the reaction wheel unloading on the inflatable antenna dynamics.

Thruster firing impact

Preliminary analysis of a two (2) second firing of a pair of 0.9 N thrusters resulting in a torque about the vertical axis of the spacecraft (z) shows that the maximum relative deformation at the joint between the torus and a rigidizable strut never exceeds 20 mm, and the residual vibration rapidly

dampens due to the high structural damping present in the inflatable structure (3% structural damping). See Figures 7.10, 7.11 and 7.12.

Reaction wheel impact

Figure 7.13 presents the results of open loop simulations performed with the HST reaction wheel model at 2000 RPM. The quantity shown is the angle due to deformation at the torus-strut attachment point when the wheels are operating. Based on test data, the wheels produce disturbance forces and moments due to imbalance, motor cogging, and ripple. However, the results show that the requirements can be satisfied. This indicates that isolation of the wheels may not be needed. Note that we may obtain additional margin by keeping the wheels at a lower speed by unloading more often, which is quite possible as the observation (coherent integration) times for the radio frequencies requiring the highest precision are only about 6 minutes (at 86 GHz).

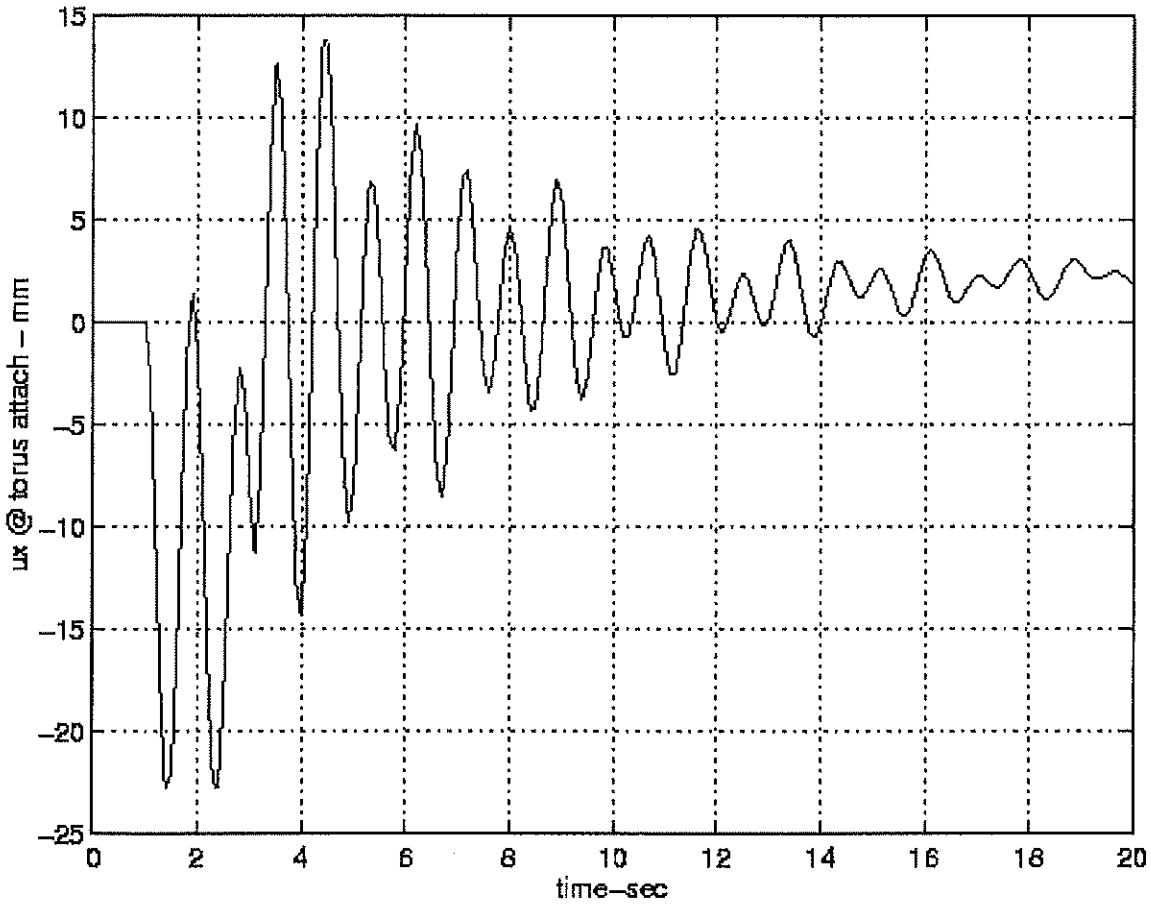

Fig. 7.10: X-displacement at Strut/Torus Joint Resulting from 2 s Firing of Pair of 0.9 N Thrusters about the z Axis.

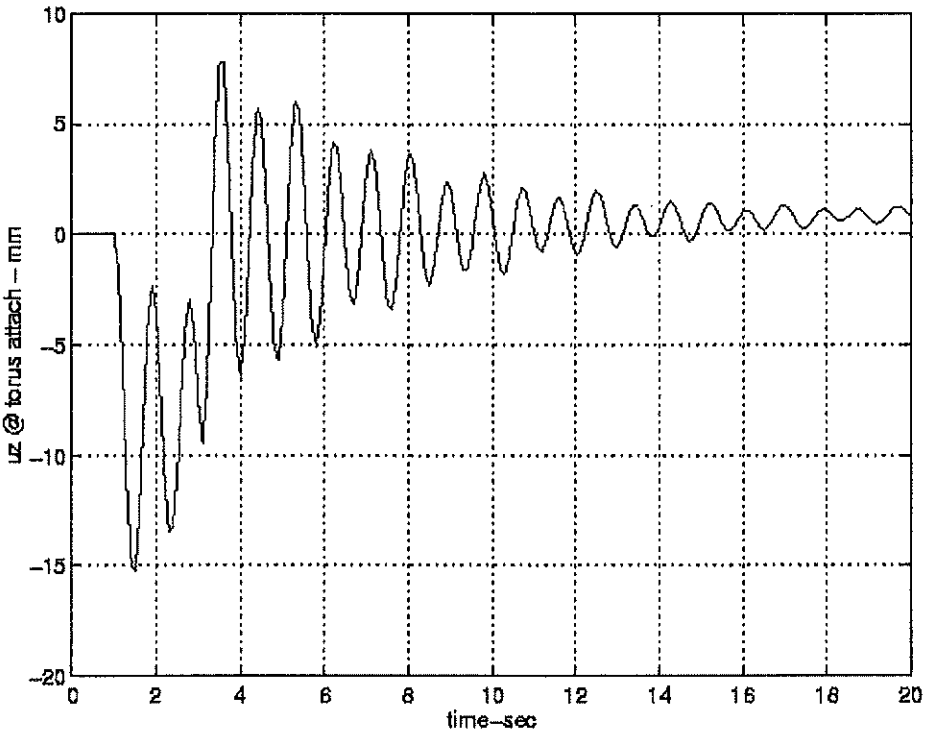

Fig. 7.11: Z-displacement at Strut/Torus Joint Resulting from 2 s Firing of Pair of 0.9 N Thrusters about the z Axis.

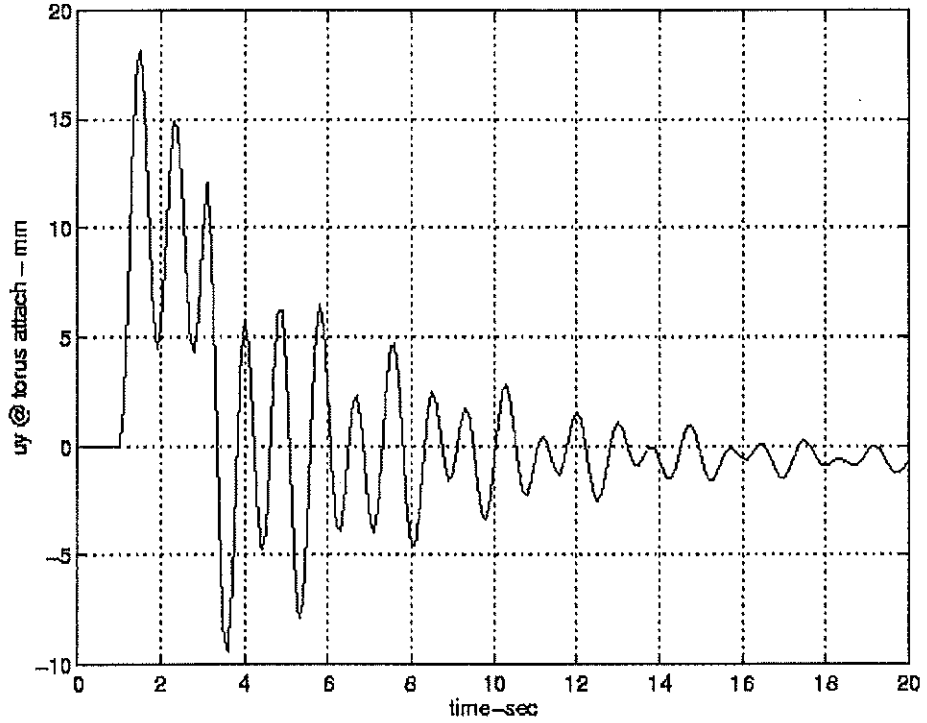

Fig. 7.12: Y-displacement at Strut/Torus Joint Resulting from 2 s Firing of Pair of 0.9 N Thrusters about the z Axis.

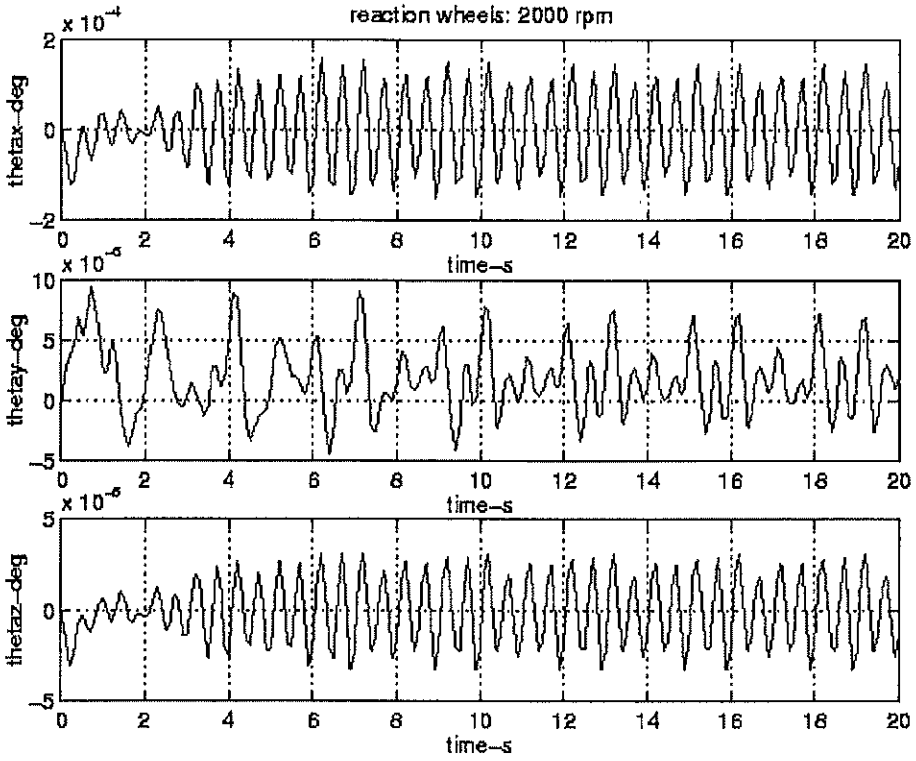

Fig. 7.13: Deformation at Strut/Torus Attachment Point with Reaction Wheel at 2000 rpm.

7.9 Structure and Mechanisms

The ARISE structure is composed of a primary structure withstanding the launch loads and a secondary sustaining lighter loads. However, we have not attempted in this study to define and design the material and thicknesses for both structures. A mass of 10% of the spacecraft dry mass, less propulsion and inflatable antenna subsystem masses, has been allocated for both bus structures, which rounds up to about 75 kg. Cables and connectors were taken as 7% of the spacecraft dry mass, less propulsion and inflatable antenna subsystem masses. An allocation of 40 kg has also been made for additional radiation shielding of sensitive parts of the spacecraft (C&DH shielding has been bookkept separately).

Several booms and mechanisms are used in the current baseline. The subreflector is deployed on a 3.6-m boom. At the end of this boom, where the subreflector is located, a gimbal and actuator system permits piston and two (2) Degree of Freedom (DOF) tilt motions. The solar arrays are one (1) DOF (rotation) gimbaled. The telecommunication antenna is deployed on a 0.5-1-m boom, and gimbaled for at least a full half-space coverage. Mass and power for these booms and mechanisms have been estimated based on current and flown boom and mechanism technologies.

7.10 Power Subsystem

The power subsystem has three major parts. The solar array provides power during sunlit periods. The battery provides power during eclipses, supplements the solar array during peak power periods, and provides power during the immediate post-launch period, before the solar arrays are deployed. The Power management and Distribution Unit (PMAD) system provides power management and distribution. It includes the peak power tracker; distribution, regulation and control electronics; and pyrotechnics.

The larger spacecraft power loads are the cryocoolers, the reaction wheels, the 8 Gbps downlink telecommunication system, and the mini-ion engines. Also, since the power requirements are large during science observations, no science will be performed during solar eclipses.

Calculations of the estimated solar array area and mass have been based on spacecraft requirements of 2160 W EOL, which includes 30% contingency. Until further details are available on the spacecraft power profile, it was assumed that the solar array would handle all power needs during sunlit periods. Adding an estimated 126 W to recharge the Li-ion secondary battery, the overall array sizing assumed a net 2300 W EOL requirement. The results for six (6) of the leading cell candidates are detailed in Table 7.8. These mass and area numbers include the cells and thin coverglass (3 mil), with the exception of the copper indium diselenide (CIS) cells which do not include coverglass, wiring, terminals, connectors, and substrates. As is customary, they do not include additional contingency (this is carried at the system level), nor do they include the support structure (connection to the spacecraft), deployment, drive or housing. Overall, the most reasonable compromise between area, mass, cost and availability was projected to be the inflatable array (ITSAT type) using high-efficiency Si cells at a specific power of 86 W/kg BOL. The array area would be 15.6 m^2 and the array mass would be 31.4 kg. Because of high temperature conditions, the ARISE solar array blankets will be supported by thin-walled polymer struts laminated with aluminum foil. The strut tubes are initially over-inflated past the aluminum foil yield point. Once the pressure is removed, the stressed aluminum maintains much of the strut's rigidity and shape.

	Area (m^2)	Mass (kg)
GaAs	14.3	44.4
2-junction (GaInP/GaAs)	12.7	39.4
3-junction (GaInP/GaAs/Ge)	10.6	31.2
CIS (LMA est.)	35.4	32.9
CIS (L'Garde est.)	35.4	24.2
High efficiency Si	15.6	31.4

Table 7.8: ARISE Spacecraft Calculated Solar Array Area and Mass for 2300 W EOL.
GaAs = gallium arsenide on Ge substrates
GaInP/GaAs = two junction cell on Ge substrate
GaInP/GaAs/Ge = three junction cell on Ge substrate; includes active Ge junction
CIS = copper indium diselenide

Calculations of the estimated secondary battery mass and volume have assumed that the battery would be used only during eclipses (465 W for 45 min, or 349 Whr). The primary battery requirements cover a 9.0 hr period immediately post-launch (4803 Whr). Until further details are available on the spacecraft power profile, it has been assumed that the solar array would handle all active power needs during sunlit periods. It was assumed that neither science data collection nor

telecommunication would take place during eclipse. It was also assumed that the mission lifetime would be limited to about three (3) years, in order that a Li-ion battery could handle the required number of cycles. The calculations do not include battery mass or battery volume contingency, which would be carried at the system level. The required 25 Ahr Li-ion secondary battery would have a mass of 7.3 kg and a volume of six (6) liters. It is evident that a large mass and volume penalty would result if a Ni-based battery were to be substituted.

Calculations of the estimated Power and Distribution Management Unit (PMAD) mass were based on extrapolations from the Phase A Light SAR calculations performed at JPL in 1996. It was assumed that the ARISE EOL solar array power would be 2300 W, and the secondary battery capacity would be 25 Ahr. The calculated mass of the peak power tracker would then be 13.3 kg, and the mass of the distribution, regulation and control electronics would be 63.9 kg, for a total PMAD mass of 77.2 kg. The corresponding EOL PMAD specific power would be about 30 W/kg. This corresponds favorably to the 30 W/kg anticipated for the JPL X-2000 PMAD second delivery. The results are detailed in Table 7.9.

Several key technology challenges for the power system have been identified. First, the advanced solar array technologies (multi-junctions and CIS) must be scaled up without appreciable efficiency loss if they are to compete effectively with Si and GaAs. Second, deployment mechanisms for ultra-lightweight solar arrays need to be flight qualified. Third, Li-ion secondary batteries require a flight demonstration, as well as a need to be demonstrated in large sizes (over 20 Ahr). Fourth, the PMAD mass can only be reduced if the projected parameters of the X-2000 third delivery (approximately 200 W/kg) can be demonstrated and scaled up. The X-2000 third delivery is planned for a very small (10 W) power system.

	LightSAR	**ARISE**
Solar array power (EOL)	782 W	2400 W
Battery capacity	44 Ahr (Ni)	25 Ahr (Li)
Peak power tracker	6.4 kg	13.3 kg
Dist, Reg & Cntrl Electronics*	15.0 kg	63.9 kg
Total PMAD mass	21.4 kg	77.2 kg
PMAD specific power (EOL)	36.5 W/kg**	30 W/kg***

Table 7.9: ARISE Spacecraft Calculated PMAD Mass.
*Estimate based on EOL array power corrected for environmental degradation only (EOL/0.85)
**LightSAR assumed a very bare-bones system
***30 W/kg is approximate value for X-2000 PMAD 2nd delivery

In summary: size estimates, including mass and area, have been generated for the ARISE solar array. Size estimates, including mass and volume, have been generated for the ARISE battery. A ROM estimate of power electronics mass and specific power has been calculated. Several key needs were identified. First, more data on the planned orbit and eclipses are needed to refine the power system sizing. Second, more data on the spacecraft power profile vs. time are needed to determine the proper role of the battery in supplementing the solar array. Third, the calculations assume a moderately benign radiation environment, which may not hold true for the planned ARISE orbit; more data is needed on the radiation environment to properly size the power system, particularly the solar array which is relatively difficult to shield. Further studies shall include: updating the power system design in accord with evolving system requirements, continuing to reduce the power system mass, refining the PMAD mass and cost estimates, and establishing a power system design and fabrication schedule.

7.11 Propulsion subsystem

The propulsion module is a bi-propellant dual-mode propulsion system that is used to perform a 270 m/s periapse raise, reaction control during the periapse raise, and attitude control for the duration of the mission.

The bi-propellant dual-mode propulsion system uses nitrogen tetroxide (NTO) and hydrazine (N_2H_4) as the oxidizer and fuel, respectively. The periapse raise is performed using a 445 N Royal Ordinance LEROS-1c main engine that is qualified for these propellants exclusively, and which features an Isp of 325 seconds. Two titanium tanks (one for the oxidizer and one for the fuel) are used to store the propellant. The oxidizer and fuel tanks are pressurized via separate high-pressure helium feed systems (two pressurant tanks). The separate feed systems eliminate any possibility of propellant migration. Eight (8) 22 N and eight (8) 0.9 N mono-propellant (hydrazine) thrusters are assumed for thrust vector and roll control. Conventional technology components are assumed.

This design has two possibilities for combining the inflation system with the propulsion system. One option is to have an NTO inflation system feeding off a line downstream of the oxidizer tank. Liquid NTO decomposes into gaseous N_2 and O_2 through a two-step reaction. Another option is to have an N_2H_4 inflation system feeding off a line downstream of the fuel tank (feeding off the RCS system). Liquid N_2H_4 decomposes into gaseous NH_3, N_2, and H_2 through a two-step reaction. Since there are separate pressurization feed systems for both the oxidizer and the fuel, both tanks remain pressurized for the entire mission. No pyrotechnic firings are necessary after the periapse raise.

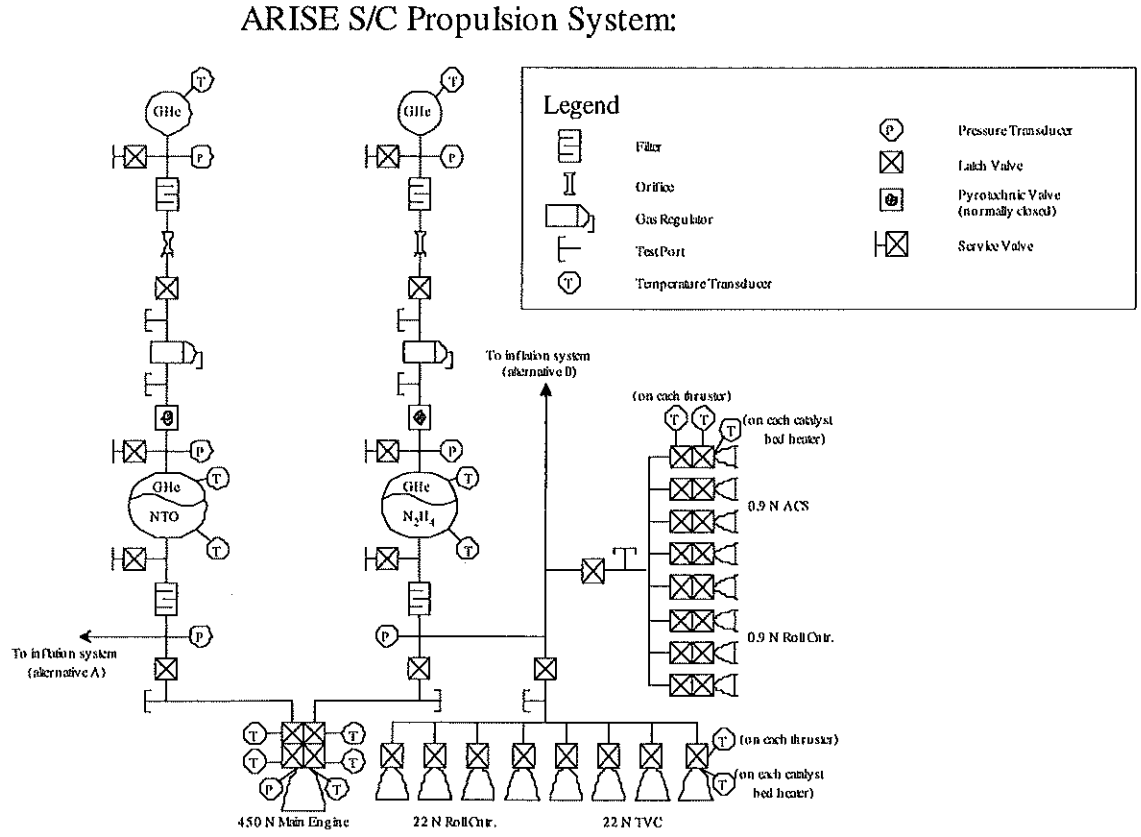

Fig. 7.14: ARISE Spacecraft Propulsion System.

Chapter 8

Flight and Science Mission Operations

8.1 Mission Operations Overview

In this section, we provide a description of the mission operations structure of a "generic" space VLBI system, but in the context of the ARISE mission, from the scientific proposal and peer-review phase, to the ground and space control, monitor, and data collection phases, to the VLBI correlation and interferometer fringe analyses phases, and ultimately to the end science product. Although this description is "generic" it shows only the DSN ground tracking stations providing the spacecraft tracking coverage, but we note that incorporation of other tracking stations outside the DSN is a simple extension within the overview scheme presented.

The space VLBI system mission operational structure is shown schematically in Figures 8.1 and 8.2. We identify eighteen (18) "mission elements" (ME) involved in the space VLBI mission, and in this section briefly describe each of these in turn. In the text below, the MEs are individually enumerated ME-1 through ME-18 and in Figures 8.1 and 8.2 as simply 1 through 18. While Figure 8.1 concentrates on the identification of the space VLBI mission elements, Figure 8.2 concentrates on the file interchange products between mission elements, with emphasis on those involved in the scientific ground support system for the space radio telescope. In the sections below, the mission element "Primary Communications" input and output space VLBI system data products are identified in Figure 8.2 as itemized numbers in parentheses. For example, the input data products for the Correlator (ME-17) shown in Figure 8.2 as "(1)" through "(9)" are also enumerated in the "Primary Communications" text at the end of Section 8.9.

We note that in Figures 8.1 and 8.2, a one-way arrow denotes the (one-way) "delivery" of a particular ME deliverable, in the form of one or more files or data products, whereas a double-arrow designation denotes a more general two-way communication process between two MEs, generally involving file deliverables/transfers and inter-ME verbal or "ad hoc" electronic communication. In these figures, "narrow" lines identify file deliverables, and "wide" lines are reserved for the transfer of the wideband VLBI data on magnetic tapes. In the context of space VLBI system file "delivery," we note that file "availability" is a more appropriate term: as a general rule, an operational file (data product) to be exchanged between mission elements is placed on a specific file server by the appropriate ME generating the data product and is made available for general "data-get" access by all other MEs, not only the one to which it is primarily intended. This "all data available to all" scheme implicitly improves overall space VLBI mission communications.

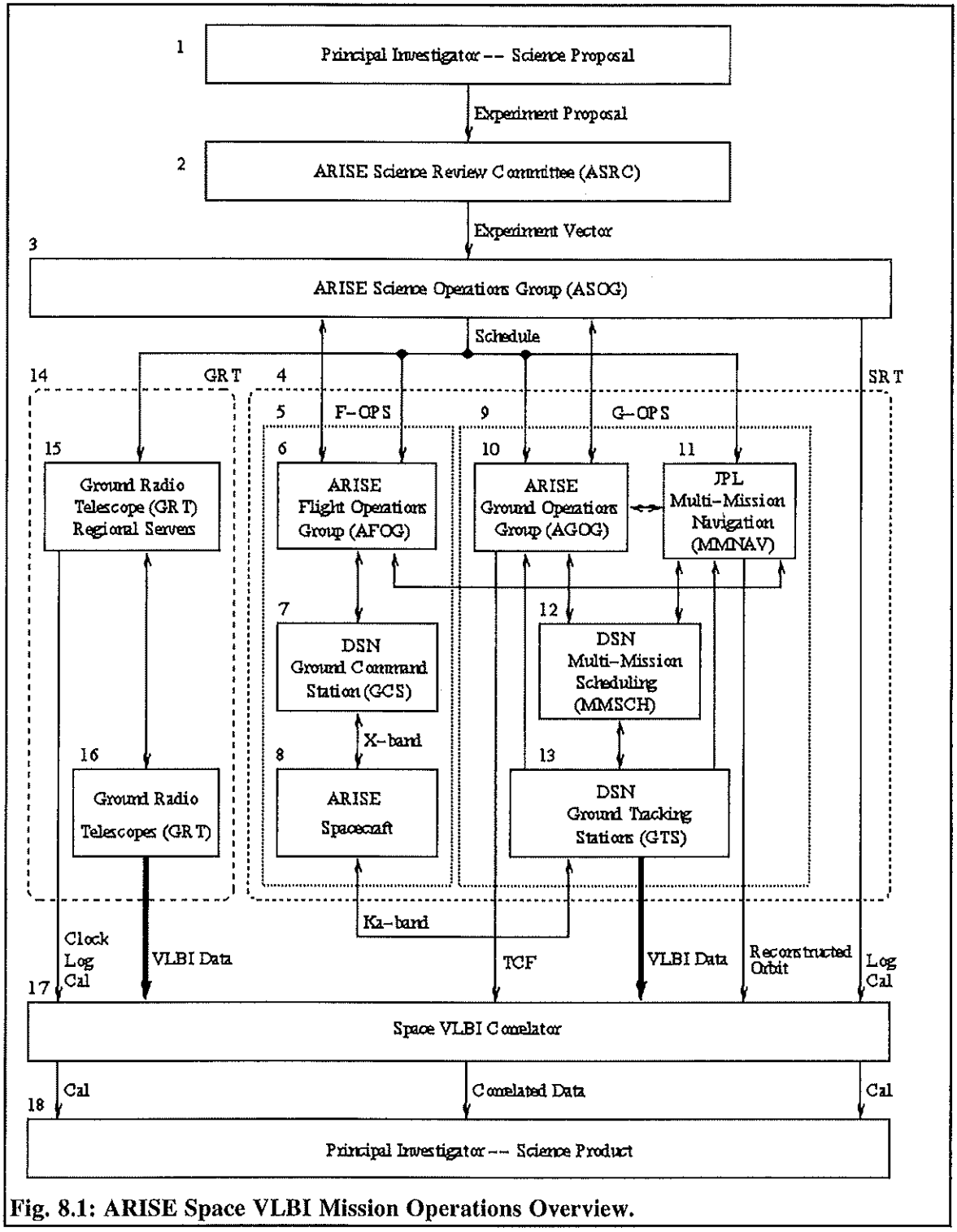

Fig. 8.1: ARISE Space VLBI Mission Operations Overview.

We note that the space VLBI mission provides a number of distributed data servers which provide overall mission data/data products. In particular, the ground radio telescope (GRT) Regional Servers (ME-15) provide data on the space VLBI mission "ground segment," and the ARISE Flight Operations Group (AFOG, ME-6), ARISE Ground Operations Group (AGOG, ME-10), and ARISE Science Operations Group (ASOG, ME-3) individually maintain file servers for their respective data products for the mission "space segment." In addition to the electronic exchange of

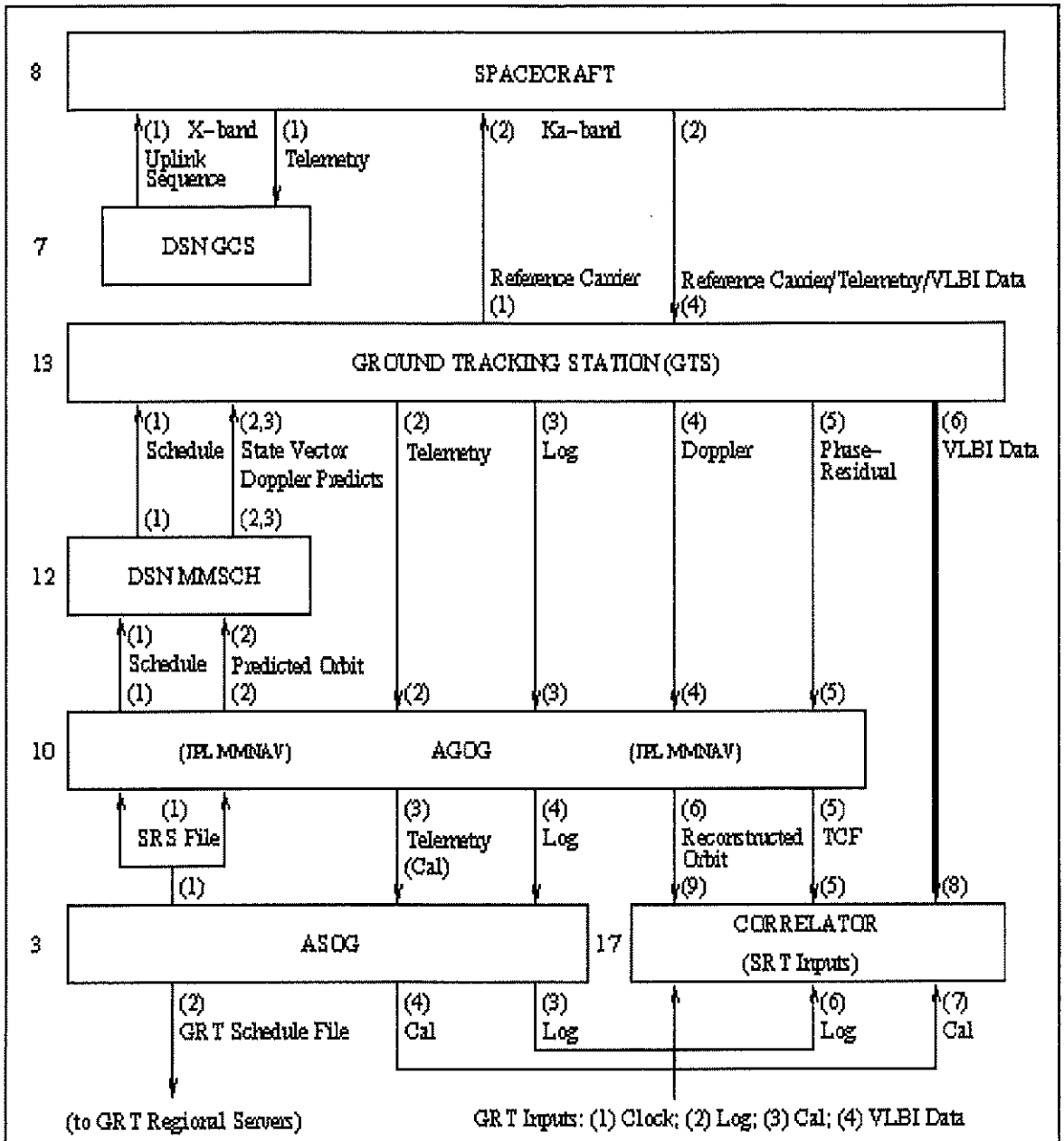

Fig. 8.2: ARISE Space VLBI Mission Operations Science Data Flow.

data files for routine operations as described above, each mission element sends periodic weekly or bi-weekly e-mail status reports to all other mission elements.

In the space VLBI system, all electronic communication between mission elements occurs via the (global) Internet. To be contrasted with the electronically exchanged data communications of what are often generally known as space VLBI "ancillary data," the wideband VLBI data recorded on magnetic tapes are exchanged between the VLBI correlator and the recording mission element (ground radio telescope, or space radio telescope via its serving ground tracking station) by physical mailing of tapes.

The AFOG, AGOG, and ASOG individually maintain file servers for their respective data products, which are made available to all mission elements. To provide a single point of external access for the effective space radio telescope via the ASOG server, it is possible that the AFOG and AGOG data products are placed on the ASOG server.

It is important to recognize that the ASOG is the central governing authority in overall mission operations and analyses. Its ground support groups in the ARISE Flight Operations Group (AFOG) and ARISE Ground Operations Group (AGOG) support the ASOG's activities. The AFOG and AGOG generally operate independently from one another with both reporting their respective mission operations status and performance monitoring to the ASOG. Although the AFOG and AGOG operate generally independently, all information is available and shared between the AFOG, AGOG, and their controlling body in the ASOG.

8.2 Principal Investigator -- Science Proposal (ME-1)

Principal Investigators (PI) submit proposals to the ARISE Science Review Committee (ASRC) in Announcement of Opportunity (AO) cycles of the ARISE mission. An AO period might be of duration eight (8) to twelve (12) months for an expected mission lifetime of three (3) years. Proposals are submitted by electronic mail in a standard form to a data server maintained by the ARISE Science Operations Group (ASOG).

ME-1 (PI) Primary Communications:

Outputs: *Scientific Proposals to ASRC.*
Inputs: *Feedback on proposals from ASRC.*

8.3 ARISE Science Review Committee (ASRC) (ME-2)

For each Announcement of Opportunity (AO) period, the ARISE Science Review Committee (ASRC) reviews the submitted scientific proposals, gauges their technical and scientific feasibility, and ultimately passes the final "experiment vector" to the ARISE Science Operations Group (ASOG), which schedules the mission based on the ranked proposals.

ME-2 (ASRC) Primary Communications:

Inputs: *Scientific Proposals from Principal Investigators (PI).*
Outputs: *"Experiment vector" to ASOG.*

8.4 ARISE Science Operations Group (ASOG) (ME-3)

The ARISE Science Operations Group (ASOG) is responsible for the operation of the mission, including both space and ground segments. The mission "space segment" or "effective space radio telescope (SRT) segment" (ME-4) deals with operation of both the spacecraft itself and the commanding and ground tracking stations (GTS) that support it, namely Flight Operations (F-OPS, ME-5) and Ground Operations (G-OPS, ME-9). The mission "ground segment" (ME-14) deals with the operation of the network of ground radio telescopes (GRT) participating in each scientific observation. We note that the mission "space segment" is active for all scheduled modes of tracking, whether they be "experiment support" or "navigation support" tracking passes. The former passes coincide with scheduled GRT resources involving the mission "ground segment". The latter passes do not involve the "ground segment" and are intended primarily for maintenance

of the spacecraft orbit or to obtain spacecraft telemetry data. We note that spacecraft navigation and telemetry information are available for both types of scheduled tracking supports.

Based on the "experiment vector" from the ASRC, the ASOG generates so-called "long-term" and "short-term" schedules for the mission network of GRTs and for the effective SRT. Long-term schedules are generally required primarily for planning purposes, in particular to: (1) optimize the allocation of observing (data collection) resources (GRTs and SRT) to maximize the scientific return for each scheduled observation; (2) satisfy the long lead-time requirement for GRTs whose time must be generally allocated months in advance of a particular scientific observation; (3) satisfy the long-lead time requirement for correlators which must manage the VLBI tape pool and redistribution of tapes for future observations. Based on these requirements, the long-term schedules are sent out generally three (3) months in advance of a particular scientific observation. By contrast, short-term schedules, oftentimes referred to as "detailed schedules," are derived from the long-term schedule and are used operationally for detailed control (schedule and configuration) of the network of GRTs and the effective SRT. The GRT and SRT short-term schedules are included in the "master schedule" file referred to as the Space VLBI Radio Telescope Schedule (SRS) file.

The SRS file is generated by the ASOG as the mission primary schedule source. There is no explicit scheduling in the SRS file for the VLBI data processing (correlation/analysis) or other processes such as inter-mission-element file deliveries/exchanges, as these schedules follow mutually agreed time lines outside the scope of the SRS file. These practices are agreed to on an international basis by all space VLBI mission elements and are documented in an ARISE Mission Operations Handbook (AMOH). The AFOG is responsible for the generation of the spacecraft component of the SRS file, as the AFOG is the body most familiar with overall spacecraft functions. However, close interaction is required with the ASOG which is most familiar with the scientific instrumentation and overall goals. The ASOG is responsible for the scheduling of the scientific GRT resources. We thus refer to the SRS file generation as a joint ASOG/AFOG function. Below we briefly describe the SRT and GRT scheduling functions.

The ASOG/AFOG are responsible for mission scheduling, in the form of the generation of the SRS file. There is one SRS file generated per week, commencing at 0-hour UT Monday. The SRS files are generally produced on a monthly basis for the four (4) upcoming weeks, although they may be subsequently updated if necessary. A given SRS file contains information on the scheduling of the control and data acquisition resources of the effective SRT, and is made available to the control groups of the effective SRT, namely the AFOG (ME-6) and the AGOG (ME-10), as well the JPL Multi-Mission Navigation (MMNAV) group (ME-11). Additionally, the SRS file contains information related to GRT scheduling. The AFOG communicates with the spacecraft via the Ground Command System (GCS, ME-7), serving as the ASOG to spacecraft interface. The AGOG communicates with the spacecraft ground support system, primarily the ground tracking stations (GTS, ME-13), serving as the ASOG to ground system interface.

The ASOG is responsible for the generation of the ("detailed") GRT schedule files. The GRT schedule files are based on the SRS file, and take into account specifics related to individual GRTs or GRT networks. Unlike practices in ground-only VLBI, where individual PIs supply schedules to the GRTs, in space VLBI it is most efficient for a central agency, namely the ASOG, to perform this function. The ASOG sends the GRT schedules to the appropriate GRT "Regional Servers" (ME-15), consistent with ground-only VLBI practice. It is the role of each GRT to obtain the latest version of its schedule file from its associated Regional Server.

Following the scientific observations, log and calibration information for the SRT and GRT must be provided to the space VLBI correlator and/or PI. Supply of SRT log (Log) and system calibration (Cal) information is the responsibility of the ASOG. Log information consists primarily of tape recorder related events necessary for tape playback at the correlator. After each scheduled

scientific observation ("experiment") tracking support, the wideband VLBI tapes from the involved GTSs (ME-13) are shipped directly to the VLBI Correlator. Information related to the SRT log (Log) and system calibration (Cal), however, is sent by the GTSs to the AGOG (ME-10) for forwarding to the ASOG, and it is the role of the ASOG to supplement the SRT Log/Cal information before making the "final" Log information available to the Correlator (ME-17) and the "final" Cal information available to the Correlator and/or Principal Investigator (PI). In a similar fashion, for the GRTs, VLBI tapes are sent directly to the Correlator, and it is the role of the GRTs to send the GRT Log/Cal information to their Regional Centers, which post this information for retrieval by the Correlator and/or Principal Investigator (PI). Information related to "UT clock offsets" for the SRT and GRT, necessary for correlation, are also made available to the Correlator. For the SRT, this is in the form of the so-called "time corrections file" (TCF) for each experiment tracking support and is provided by the AGOG from information provided by the GTS; for the GRT, this is in the form of a "Clock" file provided by the GRT Regional Servers from information provided by each GRT.

8.4.1 Mission Analysis

The ASOG conducts overall mission analysis. Mission analysis in space VLBI is particularly critical due to the distributed nature of its mission elements. The overall mission analysis consists of a periodic assessment of flight (F-OPS) and ground (G-OPS) operations carried out through the following activities:

(1) The immediate analysis of short-term problems that were identified by instrument, spacecraft, or ground systems monitoring or analysis, but cannot be isolated to one of those systems.
(2) The identification and analysis of long-term system problems from a global, end-to-end perspective.
(3) The assessment of the past and prediction of the future performance of the ARISE end-to-end system.

Response to this mission analysis of problems may require a high-level coordination effort to oversee and optimize the planning and control exercised by the elements of the flight and ground systems and the establishment of plans for configuration controlled upgrades to the flight software or ground system upgrades to improve the performance of the ARISE end-to-end system.

8.4.2 Calibration and Instrument Analysis

The ASOG calibrates the ARISE instrument and data produced by it and analyzes the instrument performance. Instrument analysis is an extension of instrument monitoring. The major difference resides in that instrument analysis requires a detailed engineering knowledge and expertise about the instrument. Instrument and data calibration is based on data collected from several sources, such as pre-launch calibration data (a set of calibration data is taken on the ground during pre-launch testing), and in-flight calibration data (calibration data are collected by the instrument as a normal, on-going part of its science data acquisition). Calibration and instrument analysis includes the following activities:

(1) Determination of the relationship between the instrument data and the physical parameters sensed by the instrument (radiometric calibration).
(2) Determination of the relationship between the instrument data and the spatial coordinates of the physical parameters (geometric calibration).
(3) Interpretation of instrument engineering data and quick-look data to determine instrument health.

(4) Long-term trend analysis of instrument engineering data, calibration results, quick-look data, and data quality assessment results to determine instrument system and subsystem performance.

ME-3 (ASOG) Primary Operational Communications:

Inputs: *"Experiment Vector" from ASRC.*
Outputs: *(1) SRS file (jointly produced with AFOG).*
(2) "GRT schedule file" to GRT Regional Servers.
(3) SRT log (Log) information to Correlator.
(4) SRT system calibration (Cal) information to Correlator and/or Principal Investigator (PI).
Other: *Miscellaneous communications with the effective SRT, i.e. F-OPS (AFOG) and G-OPS (AGOG), and on an "as-needed" basis with GRTs.*

8.5 ARISE Space Radio Telescope (SRT) (ME-4)

The effective ARISE Space Radio Telescope (SRT) is made up of a distributed diverse set of ARISE mission elements, including the spacecraft and its space radio telescope proper, and its ground support system. The operation of this "effective SRT" is divided into separate Flight Operations (F-OPS) and Ground Operations (G-OPS) sections. F-OPS is controlled by the AFOG and G-OPS is controlled by the AGOG. The AFOG and AGOG are responsible to the ASOG.

The primary output products of the effective distributed-element SRT resemble those of a conventional GRT from the perspective of the VLBI data processing (correlation and analyses) phases, namely the VLBI wideband data and associated SRT log (Log) and system calibration (Cal) files, and implicitly or explicitly including best estimates of the telescope position and UTC clock offset. In this context, GRT clock offsets (Clock) are periodically posted by each GRT to its respective GRT Regional Server (ME-15) from measurements made typically by GPS receivers at each GRT; by contrast, SRT clock offsets are posted for each tracking support in the form of a so-called "time corrections file" (TCF) derived by the ARISE Ground Operations Group (ME-10) from measurements provided by the GTSs (ME-13) in real-time. GRT (and GTS) positions are maintained in Correlator (ME-17) data bases and are updated very infrequently; by contrast, SRT positions (ephemerides) are periodically derived (typically every 1-2 weeks) by the JPL Multi-Mission Navigation (MMNAV) group (ME-11) from measurements provided by the GTSs in real-time, as well as information available from other sources such as spacecraft orientation, solar radiation pressure model, etc., as a function of time.

ME-4 (SRT) Primary Operational Communications:

Inputs: *(1) SRS file from ASOG/AFOG.*
Outputs *(1) Spacecraft predicted orbit ("integrated trajectory") file to DSN MMSCH.*
(2) Spacecraft Ka-band telemetry, including preliminary SRT system calibration (Cal) information from GTS to ASOG.
(3) Preliminary SRT log (Log) information from GTS to ASOG.
(4) Time corrections file (TCF) to Correlator.
(5) Reconstructed orbit file to Correlator.
(6) Wideband VLBI tapes to Correlator.
Other: *(1) Miscellaneous communication with AFOG and AGOG regarding spacecraft orbits and orbit determination improvement.*
(2) Miscellaneous communication regarding overall mission operational issues.

8.6 ARISE Flight Operations (F-OPS) (ME-5)

ARISE Flight Operations (F-OPS) is divided into the ARISE Flight Operations Group (AFOG), the DSN Ground Command Station (GCS), and the ARISE spacecraft. F-OPS is controlled by the AFOG, which communicates with the GCS, which in turn communicates with the spacecraft. The AFOG serves as the interface between the spacecraft flight operations system (F-OPS) and the ASOG.

ME-5 (F-OPS) Primary Operational Communications:

Inputs:	*SRS file from ASOG/AFOG.*
Outputs:	*Spacecraft X-band telemetry, tracking, and control (TT&C) information via GCS to ASOG and AGOG.*
Other:	*Miscellaneous communication with ASOG and AGOG regarding overall mission operational issues.*

8.6.1 ARISE Flight Operations Group (AFOG) (ME-6)

The ARISE Flight Operations Group (AFOG) is responsible for all aspects related to Flight Operations (F-OPS). In particular, it is responsible for the scheduling and configuration, and health and safety (H&S) monitoring of the ARISE spacecraft and science sub-systems. Its functions may be divided into engineering and scientific operations, for which there are generally separate operations teams. Engineering operations deals primarily with spacecraft telemetry, tracking and control (TT&C); scientific operations deals primarily with scientific instrument issues.

The AFOG generally operates independently from the ARISE Ground Operations Group (AGOG, ME-10), with both AGOG and AFOG groups reporting individually to the ARISE Science Operations Group (ASOG, ME-3). Certain data, however, in particular spacecraft telemetry, is of mutual importance to both AFOG and AGOG groups; this data is available to both groups via the ASOG central data server.

The AFOG functions may be divided into the following categories: Sequencing, Commanding, and Spacecraft Monitor/Analysis. Sequencing and commanding may be viewed jointly as representing a "spacecraft uplink" process, whereas spacecraft monitor/analysis may be viewed as a "spacecraft downlink" process. Sequencing and commanding is performed on a "prime shift" basis, and most activities are accomplished through periodic endeavor. An exception is the coordination of a team effort to diagnose an emergency situation. By contrast, spacecraft monitor/analysis is, in general, an on-going continuous process and is conducted with the aid of automated software.

Sequencing

The AFOG generates sequences of commands based on conflict-free mission profiles. Sequencing generally operates in a long-term turnaround mode to support observations planned far in advance. It must also support a short-term mode to support special situations such as scientific targets of opportunity and spacecraft activities such as orbit maintenance maneuvers. Sequencing produces a conflict-free sequence of commands for uplink to the spacecraft. This involves the following activities:

(1) Translating instrument and spacecraft activities in mission profiles into sequences of spacecraft commands.
(2) Identify and resolve conflicts in sequences.

(3) Translate commands into data streams to be loaded into spacecraft memories by command uploads.

Commanding

Commanding may be considered a joint function of the AFOG and the DSN Ground Command Station (GCS, ME-7) which radiates commands at X-band to the ARISE spacecraft (ME-8). Commanding by the AFOG is considered to involve checking command sequence validity and archiving command loads.

Spacecraft Analysis/Monitor

Spacecraft analysis/monitor includes the following activities:

(1) Verification of spacecraft command receipt and execution of planned activities.
(2) Detection of spacecraft alarm conditions.
(3) Display and interpretation of spacecraft engineering data to determine long and short-term performance and health and safety (H&S).
(4) Calibration of the spacecraft systems and subsystems.

We note finally that the AFOG is autonomously responsible for gauging its flight system operations (F-OPS) performance, which includes the spacecraft but also the Ground Command Station (GCS), and for feeding this information to the ASOG to supplement its broader-scoped overall mission analysis.

ME-6 (AFOG) Primary Operational Communications:

Inputs: *(1) SRS file from ASOG/AFOG.*
(2) Spacecraft downlink X-band telemetry from GCS.
Outputs: *(1) Uplink command sequences to GCS.*
(2) Spacecraft downlink X-band telemetry to ASOG.
Other: *(1) Miscellaneous communication with ASOG and AGOG regarding overall mission operational issues.*
(2) Miscellaneous communication with JPL MMNAV regarding spacecraft orbits and orbit determination improvement.

8.6.2 ARISE Ground Command Station (GCS) (ME-7)

The ARISE Ground Command Station (GCS) is a single telemetry, tracking and control (TT&C) station for the ARISE spacecraft. A single GCS is used at a given time, but this station may be drawn from the pool of DSN multi-mission command stations. ARISE TT&C is performed at X-band, and TT&C operations are expected to routinely occur on a weekly basis. The GCS accepts spacecraft uplink command and control sequences from the AFOG and uplinks these to the spacecraft. During TT&C operations, the GCS receives ARISE downlink telemetry acquired in real-time or from its on-board recorder, and transfers this data to the ASOG. We note that the complete set of spacecraft telemetry data is delivered to the GCS at X-band, but additionally to the network of Ka-band GTSs during each scheduled ("experiment" or "navigation") tracking support.

ME-7 (GCS) Primary Operational Communications:

Inputs: *Uplink sequence from AFOG.*
Outputs: *(1) Uplink X-band sequence from AFOG to spacecraft.*
(2) Spacecraft downlink X-band telemetry to AFOG.

8.6.3 ARISE Spacecraft (ME-8)

The ARISE spacecraft consists of an orbiting platform housing the space radio telescope (SRT) proper and its associated scientific package, and spacecraft engineering and maintenance systems. During telemetry, tracking, and control (TT&C) sessions, the spacecraft communicates with the ARISE Ground Command Station (GCS) at X-band. During scientific "experiment" tracking supports and "navigation" supports, the spacecraft communicates with the scheduled GTSs at Ka-band, receiving an uplinked Ka-band phase reference signal used to synchronize the on-board radio astronomy science and Ka-band communication packages. The spacecraft transponds the Ka-band reference to the ground tracking station for navigation purposes, as well as for inclusion into the derivation of "time corrections" required for space VLBI correlation. The on-board GPS receiver data may supplement the navigation data derived from the two-way phase link to the spacecraft.

We note that "telemetry sessions" for space VLBI missions are more stringent than those for "usual" space missions. To date, most space missions employ fairly infrequent TT&C sessions (e.g. ARISE will nominally operate at one TT&C session per week), while operating on-board tape recorders for recording health, safety, and the (to-date generally low rate) scientific data. Space VLBI differs primarily in that continuous contact must be made with a ground tracking station for all times of the scientific observation. This is primarily because the high rate VLBI data (e.g. 8 Gbps) must be downlinked for recording at the GTS. Secondarily, to minimize on-board data recording storage requirements, system calibration data which ultimately serves to calibrate the space interferometer fringe amplitude and phase must be downlinked in real-time for recording at the GTS.

ME-8 (Spacecraft) Primary Operational Communications:

Inputs: *(1) Uplink X-band sequence from GCS to spacecraft during telemetry, tracking, and command (TT&C) sessions.*
(2) Uplink Ka-band reference carrier from GTS to spacecraft during "experiment" or "navigation" tracking sessions.
Outputs: *(1) Downlink X-band carrier/telemetry to GCS.*
(2) Downlink Ka-band reference carrier/telemetry/VLBI data to GTS.

8.7 ARISE Ground Operations (G-OPS) (ME-9)

ARISE Ground Operations (G-OPS) is divided into the ARISE Ground Operations Group (AGOG), the JPL Multi-Mission Navigation (MMNAV) group, the DSN Multi-Mission Scheduling (MMSCH) group, and the network of DSN ground tracking stations (GTS). G-OPS is controlled by the AGOG, which communicates with JPL MMNAV, DSN MMSCH, and the GTS network. The AGOG operates a semi-automated data processing system known as the ARISE Data Oversight and Transfer System (ADOTS); the ADOTS is described in some detail below. The AGOG serves as the interface between the spacecraft ground operations system (G-OPS) and the ASOG.

ME-9 (G-OPS) Primary Operational Communications:

Inputs: *SRS file from ASOG/AFOG.*
Outputs: *(1) Spacecraft Ka-band telemetry data via GTS to ASOG.*
(2) Preliminary SRT log (Log) information from GTS to ASOG.
(3) Preliminary GTS system calibration (Cal) information to ASOG.
(4) Time corrections file (TCF) to Correlator.

(5) GTS wideband VLBI data to Correlator.
(6) Reconstructed orbits from JPL MMNAV to Correlator.

Other: *Miscellaneous communication with ASOG and AFOG regarding overall mission operational issues.*

8.7.1 ARISE Ground Operations Group (AGOG) (ME-10)

The ARISE Ground Operations Group (AGOG) is responsible for all aspects related to spacecraft Ground Operations (G-OPS). In particular, it is responsible for the operation of the GTSs, and communication with the JPL MMNAV and DSN MMSCH groups. The AGOG functions are largely implemented within a semi-automated data processing system known as the ARISE Data Oversight and Transfer System (ADOTS). Emphasis in the AGOG system ADOTS is on ground system operations (G-OPS) oversight/monitor and final data product transfer/delivery. The AGOG generally operates independently from the ARISE Flight Operations Group (AFOG, ME-6), with both AGOG and AFOG groups reporting individually to the ARISE Science Operations Group (ASOG, ME-3). Certain data, however, in particular spacecraft telemetry, is of mutual importance to both AFOG and AGOG groups; this data is available to both groups via the ASOG central data server.

The AGOG functions may logically be divided into "uplink" and "downlink" processes, although these are not to be confused with issues related to AFOG spacecraft communications described in Section 8.6.1. The AGOG "uplink" process is generally a "scheduling and predicts" function, passing schedules and predicted orbits to the GTS network: schedules via the MMSCH group and predicted orbits via the MMNAV group. The AGOG "downlink" process consists of GTS oversight/monitor, transformation of the "raw" GTS products to their final output form, and "transfer" or delivery of the GTS products to the final mission element(s). AGOG functions may be divided into "near-real-time" and "post-pass". "Near-real-time" refers to the collection of station monitor and spacecraft telemetry health and safety data in near-real-time for delivery to the ASOG, on generally 30-second report periods, and "post-pass" refers to collection, transformation, and data product delivery at some non-critical time after the end of each tracking pass, generally 24 hours. In particular, for each scheduled tracking support, this involves delivery of near-real-time spacecraft telemetry to the ASOG, and in the case of "experiment" supports delivery of post-pass data products required for space VLBI correlation and fringe analyses, including scientific instrument system calibration information (Cal), SRT log information (Log), and time corrections file (TCF). We note that the primary mission operations role of the AGOG is to transfer data, primarily spacecraft telemetry data, from the GTS network to the ASOG for overall mission analysis. However, the AGOG is autonomously responsible for gauging its internal ground system operations (G-OPS) performance, particularly for the GTS network, and maintaining smooth internal operations in support of overall mission operations.

ME-10 (AGOG) Primary Operational Communications:

Inputs: *(1) SRS file from ASOG/AFOG.*
(2) Spacecraft Ka-band telemetry data from GTS.
(3) Preliminary SRT log (Log) information from GTS.
(4) Two-way phase link-derived Doppler/navigation data from GTS to JPL MMNAV.
(5) Two-way phase link residual (Time corrections-related) file(s) from GTS.

Outputs: *(1) Schedule file to DSN MMSCH.*
(2) Spacecraft predicted orbit ("integrated trajectory") file to DSN MMSCH.
(3) Spacecraft Ka-band telemetry, including preliminary SRT system calibration (Cal) information from GTS to ASOG.
(4) Preliminary SRT log (Log) information from GTS to ASOG.
(5) Time corrections file (TCF) to Correlator.

(6) Reconstructed orbit file to Correlator.

Other: *Miscellaneous communication with ASOG and AFOG regarding overall mission operational issues.*

8.7.2 JPL Multi-Mission Navigation (MMNAV) (ME-11)

The JPL Multi-Mission Navigation (MMNAV) group is responsible for analyzing the trajectory of the orbiting spacecraft. In particular, during routine mission operations, the MMNAV group is responsible for providing so-called "predicted orbits" to the GTSs for the purpose of spacecraft tracking, as well as "reconstructed orbits" to the Correlator for the purpose of efficient SRT correlation. Predicted orbit information data is sent to the GTSs via the DSN Multi-Mission Scheduling (MMSCH) group that communicates directly with the GTSs. Orbit solutions are generally obtained from the network of GTSs in the form of radiometric tracking data derived from the two-way phase link to the spacecraft. This GTS data is a time series of apparent spacecraft radial velocity derived from the two-way phase link, and is often referred to as "integrated Doppler" data. This data may be supplemented with data from the on-board GPS receiver. Predicted orbit solutions are made available on a periodic interval (e.g. twice per week), and sent to the GTSs via the MMSCH for future tracking. Additionally, the MMNAV group is responsible for the generation of a more refined (accurate) "reconstructed orbit" for delivery to the space VLBI Correlator to enable correlation using an accurate model of the SRT position and velocity. This derivation is based on tracking data obtained during GTS supports, but also data related to other factors influencing the spacecraft position and velocity such as spacecraft orientation, solar radiation pressure model, etc. The reconstructed orbit files are made available approximately two weeks after a particular scientific observation and, using data encompassing the epochs of observations to be correlated, are designed to reduce the position and velocity errors of the spacecraft so as to facilitate fringe searching and minimize the Correlator total data volume produced. Finally, in addition to the support provided during nominal mission operations, the MMNAV group is responsible for support of special or unusual events such as spacecraft maneuvers and initial orbit injection.

We note that direct communication between the JPL MMNAV group and the AFOG, i.e. not via the ASOG or AGOG, may occur. This is for the purpose of exchanging information related to spacecraft maneuvers, etc. for the improvement of predicted and reconstructed orbit solutions, and generally occurs independent of the nominal MMNAV orbit deliverables to the GTSs or Correlator.

ME-11 (JPL MMNAV) Primary Operational Communications:

Inputs: *(1) SRS file from ASOG/AFOG.*
(2) Near-real-time navigation (radiometric Doppler) data from GTS.

Outputs: *(1) Predicted orbit file to DSN MMSCH.*
(2) Reconstructed orbit file to Correlator.

Other: *Miscellaneous communication with AFOG and AGOG regarding spacecraft orbits and orbit determination improvement.*

8.7.3 DSN Multi-Mission Scheduling (MMSCH) (ME-12)

The DSN Multi-Mission Scheduling (MMSCH) group is responsible for effectively merging the AGOG schedule and JPL MMNAV predicted orbit file ("P-file") with a computed "Doppler predicts" file to create a logically single transmission to the GTSs, from which the GTSs may derive local real-time events, antenna pointing (tracking) information, and two-way phase system uplink and downlink Doppler compensation terms. These last two GTS functions are often referred

to as "angle and frequency" tracking, respectively. The MMSCH implementation is, for DSN historical reasons, somewhat modified. In practice, at the time of writing, the MMSCH produces three not two outputs:

(1) AGOG "Schedule file" (effectively a "pass through" of the input schedule file).
(2) Spacecraft "State Vector" (or "integrated trajectory") file used for GTS antenna pointing ("angle tracking").
(3) "Doppler Predicts" file for GTS uplink and downlink Doppler-compensated control on the two-way phase link ("frequency tracking").

As stated, in other implementations, (2) and (3) above may be implemented locally at each GTS based directly on a predicted orbit file.

Unlike most mission supports, for ARISE the DSN has a dedicated network of three ground tracking stations, one at each of the DSN complexes in Australia, Spain, and California. Hence, the usual MMSCH function related to station conflict resolution is not required for the ARISE mission.

The MMSCH function is performed at each creation by the ASOG of a new "master schedule" (SRS file), and is nominally performed on a weekly basis, several days in advance of the upcoming support week commencing 0-hour UT on each Monday. However, updates are accommodated in special circumstances such as if a better orbit file is required, to serve scientific targets of opportunity, or in cases of emergencies.

ME-12 (DSN MMSCH) Primary Operational Communications:

Inputs: *(1) Schedule from AGOG.*
(2) Spacecraft predicted orbit ("integrated trajectory") file from JPL MMNAV.
Outputs: *(1) Schedule to GTS, for control of GTS real-time activities.*
(2) Spacecraft "State vector" file to GTS, for antenna pointing ("angle tracking").
(3) Spacecraft "Doppler predicts" file to GTS, for two-way phase system Doppler compensation ("frequency tracking").

8.7.4 ARISE Ground Tracking Station (GTS) (ME-13)

The network of ground tracking stations (GTS) is responsible for the Ka-band tracking of the ARISE spacecraft. Each GTS receives the schedule, spacecraft "state vector" (predicted orbit), and "Doppler predicts" files, and tracks the spacecraft in angle and Doppler-compensated frequency. The GTS measures a round-trip two-way phase/timing residual, which ultimately is converted in the ADOTS to a time corrections form for space VLBI correlation. Time corrections are required in the absence of an accurate frequency standard on the orbiting spacecraft, and to correct for any timing offsets within the GTS and in the downlink transmission path. The radiometric Doppler observable is also derived from the two-way phase residual for navigation purposes, and is generally sent back to the JPL MMNAV group in near-real-time for diagnostics; this data is used by the MMNAV group for predicted and reconstructed orbit derivation. The GTS delivers spacecraft telemetry and station log (Log) to the AGOG, which is passed on to the ASOG which further processes it to deliver the final SRT log (Log) and calibration (Cal) information to the Correlator.

VLBI data from the wideband spacecraft downlink is demodulated from the downlink data-modulated Ka-band carrier and recorded on wideband VLBI tape recorders for direct shipment to the Correlator. If the mission correlation load is to be shared amongst multiple correlator facilities,

this may require different tape recording systems at the GTSs, which implies scheduling of the recording system type and Correlator for each tracking pass.

ME-13 (GTS) Primary Operational Communications:

Inputs: *(1) Schedule from DSN MMSCH.*
(2) Spacecraft "State vector" file from DSN MMSCH.
(3) Spacecraft "Doppler predicts" file from DSN MMSCH.
(4) Downlink Ka-band reference carrier/telemetry/VLBI data from spacecraft/SRT.
Outputs: *(1) Uplink Ka-band reference carrier to spacecraft/SRT.*
(2) Spacecraft Ka-band telemetry data to AGOG.
(3) Preliminary SRT log (Log) information to AGOG.
(4) Two-way phase link-derived Doppler/navigation data to JPL MMNAV.
(5) Two-way phase link residual (Time corrections-related) file(s) to AGOG.
(6) SRT wideband VLBI data to Correlator.

8.8 Ground Radio Telescope (GRT) (ME-14)

The global ground radio telescope (GRT) resources may be divided into the ground radio telescopes themselves (GRT, ME-16), generally a set of telescopes managed independently by radio astronomy organizations world-wide, and a smaller set of GRT "Regional Servers" (ME-15) that serve as communication points for generally geographically-grouped telescopes. In routine ground-only VLBI practice, the Regional Servers serve as the repository for observing schedules and for the post-observation GRT data products, primarily the GRT (tape recorder) log (Log) and the system calibration (Cal) information, but also including the GRT clock offsets (Clock). This practice is generally unmodified for space VLBI mission operations. The primary exception is that in usual ground-only VLBI scheduling, it is the individual Principal Investigators that form the "detailed schedules" from a posted (GRT) "global schedule," whereas in the space VLBI case it is the central scheduling body, namely the ASOG, that performs the GRT "detailed scheduling".

ME-14 (GTS) Primary Operational Communications:

Inputs: *(1) GRT schedule from ASOG.*
Outputs: *(1) GRT clock offset (Clock) information to Correlator.*
(2) GRT log (Log) information to Correlator.
(3) GRT system calibration (Cal) information to Correlator/PI.
(4) GRT wideband VLBI data to Correlator.

8.8.1 Ground Radio Telescope (GRT) Regional Servers (ME-15)

The ground radio telescope (GRT) Regional Servers serve as "centralized data repositories" for telescopes in certain geographical regions of the world. In practice, there may be Regional Servers in Australia for southern hemisphere GRTs serving the Asia-Pacific Telescope (APT) consortium, in Europe serving the European VLBI Network (EVN), and in the United States serving the Very Long Baseline Array (VLBA) and other northern hemisphere telescopes. These Regional Servers serve as the repositories for GRT clock offset (Clock), tape recorder log (Log), and system calibration (Cal) information necessary for space VLBI post-observation data processing including correlation and scientific analyses. The GRT Regional Servers serve the equivalent function for the distributed network of GRTs as does the AGOG server for the distributed network of GTSs. We note that both GRT Regional Servers and the AGOG serve functions related to the handling of the so-called mission "ancillary data," i.e. those data (files) transferable electronically between mission

elements and in particular not including the high-data rate VLBI wideband data that is recorded on wideband tapes and sent directly from the GRTs and GTSs to the Correlator.

ME-15 (GRT Regional Servers) Primary Operational Communications:

Inputs: *(1) GRT clock offset (Clock) information from GRTs.*
(2) GRT log (Log) information from GRTs.
(3) GRT system calibration (Cal) information from GRTs.
Outputs: *(1) GRT clock offset (Clock) information to Correlator.*
(2) GRT log (Log) information to Correlator.
(3) GRT system calibration (Cal) information to Correlator and/or Principal Investigator (PI).

8.8.2 Ground Radio Telescopes (GRT) (ME-16)

The ground radio telescopes (GRT) comprise a world-wide network of telescopes that co-observe with the orbiting space radio telescope (SRT) and which jointly form the space-to-ground interferometer baselines. The GRTs are independent of the ARISE mission but contribute so-called "co-observing" time to the mission. The GRTs collectively, under the auspices of the Global VLBI Working Group (GVWG) and in collaboration with the ASOG, contribute blocks of co-observing time in support of the ARISE mission. These time blocks are generally negotiated and agreed to and assigned months ahead of a particular scientific observation. The GRTs receive schedules from the ASOG via their Regional Servers and observe the specified radio source in the specified station configuration. The wideband VLBI tapes are sent directly to the Correlator. GRT logs (Log) and system calibration (Cal) information are delivered to their Regional Servers for access by the Correlator and/or Principal Investigator (PI). We note that conventional (ground-only) VLBI practice is to have the GRTs "put" their data to the Regional Servers, although access to the Regional Server data follows the "data-get" principle of space VLBI. This practice is consistent with the space VLBI "data-get" principle if the communications between GRTs and their Regional Server is viewed as "internal".

ME-16 (GRT) Primary Operational Communications:

Inputs: *GRT schedule from ASOG.*
Outputs: *(1) GRT clock offset (Clock) information to GRT Regional Servers.*
(2) GRT log (Log) information to GRT Regional Servers.
(3) GRT system calibration (Cal) information to GRT Regional Servers.
Other: *GRT wideband VLBI tapes to Correlator.*

8.9 Space VLBI Correlator (ME-17)

The space VLBI Correlator is fundamentally responsible for the correlation of all pairs of baselines for the radio telescopes (space and ground) participating in each scientific observation. In the case of ARISE, data is correlated at a rate of up to 8 Gbps per station. The output of the Correlator is a set of correlated data in the MByte/s rate regime, following a large data reduction stage. This level of successful data reduction is possible only by virtue of the high accurary to which the radio telescope positions and time-varying clock offsets are known at correlation time, particularly for the SRT. The correlated output data is subsequently searched for fringes. Fringe searching is ultimately performed by the Principal Investigator (PI), generally at their home institution, as a distinct step following correlation. However, correlators are responsible for analyzing periods of data for a subset of observations for fringe verification to the orbiting SRT and reporting diagnostic

information related to fringe analyses to the ASOG and interested parties, particularly the AGOG. This diagnostic function is performed in the Image/Fringe Analysis Center of the VLBI Processing Center. A team of Correlator personnel is responsible for Correlator operations, including correlation, fringe analyses and diagnoses, and VLBI tape management. After the post-correlation fringe analyses phase, VLBI tapes are erased and returned to the mission tape pool for redistribution to the GRTs and GTSs as required. This tape return path is not explicitly shown in Figure 8.1. At the present time, the correlation output results are mailed to the Principal Investigator (PI) in the form of industry-standard computer tape storage formats such as Digital Audio Tape (DAT), although by the time of ARISE operations Internet networking speeds might have increased to the point that correlator output data might be made available electronically over the Internet as are other mission element data products.

ME-17 (Correlator) Primary Operational Communications:

Inputs: *(1) GRT clock offset (Clock) information from GRT Regional Servers.*
(2) GRT log (Log) information from GRT Regional Servers.
(3) GRT system calibration (Cal) information from GRT Regional Servers.
(4) GRT wideband VLBI tapes from GRTs.
(5) SRT time corrections file (TCF) from AGOG.
(6) SRT log (Log) information from ASOG.
(7) SRT system calibration (Cal) information from ASOG.
(8) Wideband VLBI tapes from GTS.
(9) Reconstructed orbit from JPL MMNAV.

Outputs: *(1) Correlated data to Principal Investigators (PI).*
(2) Diagnostic fringe analyses information to AGOG and ASOG.

Other: *Miscellaneous communication regarding overall mission operational issues.*

8.10 Principal Investigator -- Science Product (ME-18)

The Principal Investigator (PI) searches for fringes in the entire Correlator output data set for a particular scientific observation, generally using the National Radio Astronomy Observatory (NRAO) Astronomical Image Processing System (AIPS). It is followed by an image generation phase to create the final radio astronomical image. High resolution scientific images/interpretation/publications are generally the end scientific product of each successfully supported scientific observation or set of observations.

ME-18 (PI) Primary Operational Communications:

Inputs: *(1) Correlated data from Correlator.*
(2) GRT system calibration information from GRT Regional Servers.
(3) SRT system calibration information from ASOG.

Outputs: *Scientific products/publications.*

Chapter 9

ARISE Technologies and Roadmaps

9.1 ARISE Technologies Overview

The most challenging aspect of the ARISE mission is a large inflatable antenna. Inflatable structures technology, under development for a variety of users, is the current baseline choice for the main reflector, although other mechanically deployed reflector alternatives are being explored. On-board low noise amplifiers and cryogenic coolers are being produced for missions such as MAP, Planck, and FIRST. MAP will be launched in 2000, carrying amplifiers in the same frequency range needed for ARISE. Advances in recording and correlation systems, to increase the VLBI data rate to Gigabits per second (Gbps), are under development. Figure 9.1 shows the various ARISE technology requirements.

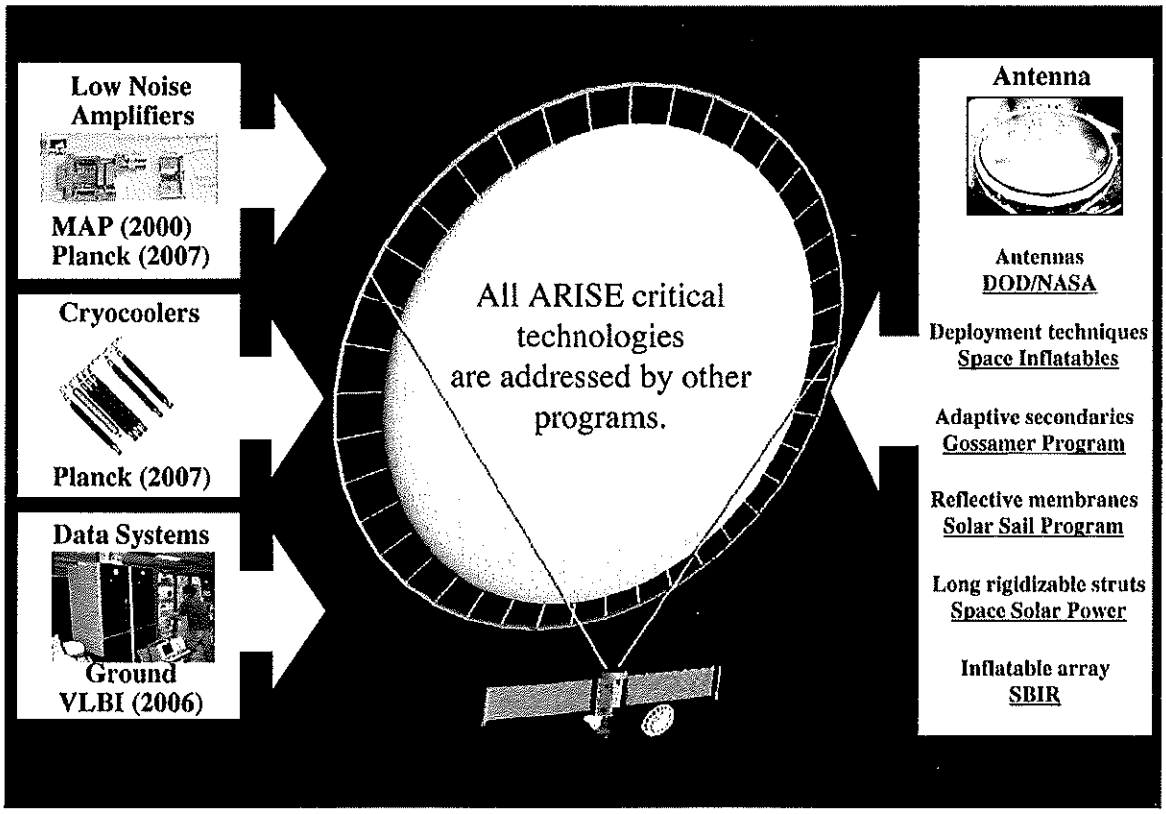

Fig. 9.1: ARISE New Technology Needs Met By Existing Technology Development Programs and Flight Projects Launched before ARISE.

ARISE, as a VLBI mission, is an international project by definition. ARISE will take advantage of the worldwide assets in systems and operations that have enabled VLBI, and even Space VLBI in the form of the VSOP mission, to become a routine observing technique. In addition to ground infrastructure, ARISE has initiated cooperation with the Canadian Space Agency (CSA) and the Joint Institute for VLBI in Europe (JIVE), which may result in a complete development of the recording systems as well as some on-board systems. Discussions are also underway with the Japanese to make ARISE a cooperative mission between NASA and ISAS/NASDA. On the American front, the biggest contributors to the project will be the Department of Defense sponsoring an extensive portion of the antenna development and NSF contributing ground assets and scientific expertise. This close partnership will make ARISE not only one of the most exciting and innovative missions of the first decade of the new century, but also affordable to NASA.

The status and current programs of each technology need are now described in more detail.

9.2 InflatableAntennaTechnology

Inflatable technology is well funded by NASA and DoD. Both agencies have embarked on a joint program to develop inflatable technology [9.1]. The year 2000 is extremely important from the ARISE inflatable structure point of view, due to the initiation of a multiyear NASA Space Science Gossamer Technology Program. The Gossamer Program will be focused on four areas, each beneficial to the ARISE antenna development: large ultra-light structures, large apertures, large antennas, and adaptive techniques.

The large ultra-light structures part of the Gossamer Program will assure that the inflatable rigidizable technology for the ARISE torus and struts is well characterized and flight-tested. The program will also validate the inflation system and controlled deployment techniques.

The large aperture and antenna portion of the Gossamer Program will develop technology aimed at improving surface accuracy of large reflectors. The long-term goal of the Program is to create not only a large 20-40 m class aperture operating in the microwave range, but a series of large apertures with applications to millimeter, sub-millimeter, infrared and eventually optical telescopes. The ARISE antenna, as difficult as it may seem to develop, is only at the beginning of this chain.

The final part of the Gossamer Program will address adaptive techniques. There are two aspects of adaptive techniques that are important in construction of the ARISE antenna. The long inflatable struts must be first deployed, then inflated to the appropriate shape and subsequently rigidized. This process may result in small deviations from the desired strut positioning. These deviations will be adjusted using adaptive strut techniques, such as adaptive membranes, shape memory foams, or other techniques. The other aspect of adaptive techniques pertains to the secondary optics shape control. The secondary reflector for ARISE is now envisioned as a 1.6 m semi-major axis ellipsoid. The surface of this ellipsoid will be made out of a thin graphite composite shell. The shell will be attached to a strong-back and its surface adjusted by means of approximately 40-60 actuators. Composite Optics Inc. recently tested a 3.3 m reflector built for the Millimeter Array Program.

The adaptive secondary reflector will be used regardless of the antenna choice. According to calculations conducted by UCLA the secondary can improve the aperture efficiency at 86 GHz from $< 10\%$ to $> 40\%$ by correcting large systematic errors common in inflatable antennas. The secondary might also be very beneficial to the mechanical antenna options. It would assure more robustness and lower sensitivity to environmental effects of the Harris antenna. The Harris antenna will use high density mesh spanning 25 m diameter to assure good antenna performance up to 43

GHz. The inner 8 m diameter will utilize precision graphite splines to give high antenna performance at 86 GHz.

9.3 L'Garde's Inflatable Antenna Technology Program

The following technology development effort has been planned at L'Garde to achieve the ARISE reflector precision goals of a 25 m reflector operating over a frequency range of 8-86 GHz. See Table 9.1. The tasks presented here will be executed by various NASA and DoD existing programs.

9.3.1 Reflector Manufacturing

Initially five (5) 3 m reflectors are planned. The first reflector will utilize current design, construction techniques, and materials, and will be used as a control. Subsequent reflectors will concentrate on improvements in materials, gore cutting, seaming, and support structure. Before construction, the material will be thoroughly surveyed to fully quantify the materials properties and statistical variations in the stock material. This will be done under strictly controlled environmental conditions with no pre-treatment or modified handling of the material. During construction, the gores, seams, and rim will be thoroughly surveyed for geometric accuracy. Once completed, highly accurate video-grammetry will be conducted to characterize the reflector shape. Concurrently this information will be used for an analytic sensitivity analysis documented in the design/analysis section. All reflectors will be mounted on rigid rings to isolate the reflector effects from the support structure effects. Later in the test program, as the structure develops and test articles are available, reflectors will be mated with a support structure.

Based on the sensitivity analysis, techniques will be proposed to improve design, manufacturing and materials, and will be used to improve the four (4) successive reflectors. Additionally the last three (3) reflectors will investigate the effects of lowering the reflector F/D to the 0.25 proposed for the ARISE configuration, and expand L'Garde's understanding of the F/D effects. Some of these technique improvements might involve: pretreatment of the materials, handling techniques, gore cutting compensation, adhesives and bonding techniques, seaming procedures, mandrel configuration, and increased rim precision.

Given the previous effort, aperture scaling will be addressed with two 7 m reflectors. The first will incorporate the most recent design and manufacturing techniques, and the second will address any unforeseen scaling issues. To further increase aperture and investigate non-linear scaling effects, two 14 m reflectors will be constructed using existing Inflatable Antenna Experiment (IAE) tooling, and finally a single 25 m demonstrator reflector will be constructed and measured.

9.3.2 Design/Analysis

Using the statistics gathered during construction and survey of the initial proposed 3 m reflector, an analytic sensitivity analysis will be conducted using L'Garde's FAIM (Finite Element Analysis of Inflatable Membranes) analytical tool. The errors will be characterized in a statistical sense to analytically represent the distributed errors. Once all the errors are characterized, a Monte Carlo analysis will be conducted using FAIM. This analysis will predict the major factors influencing the

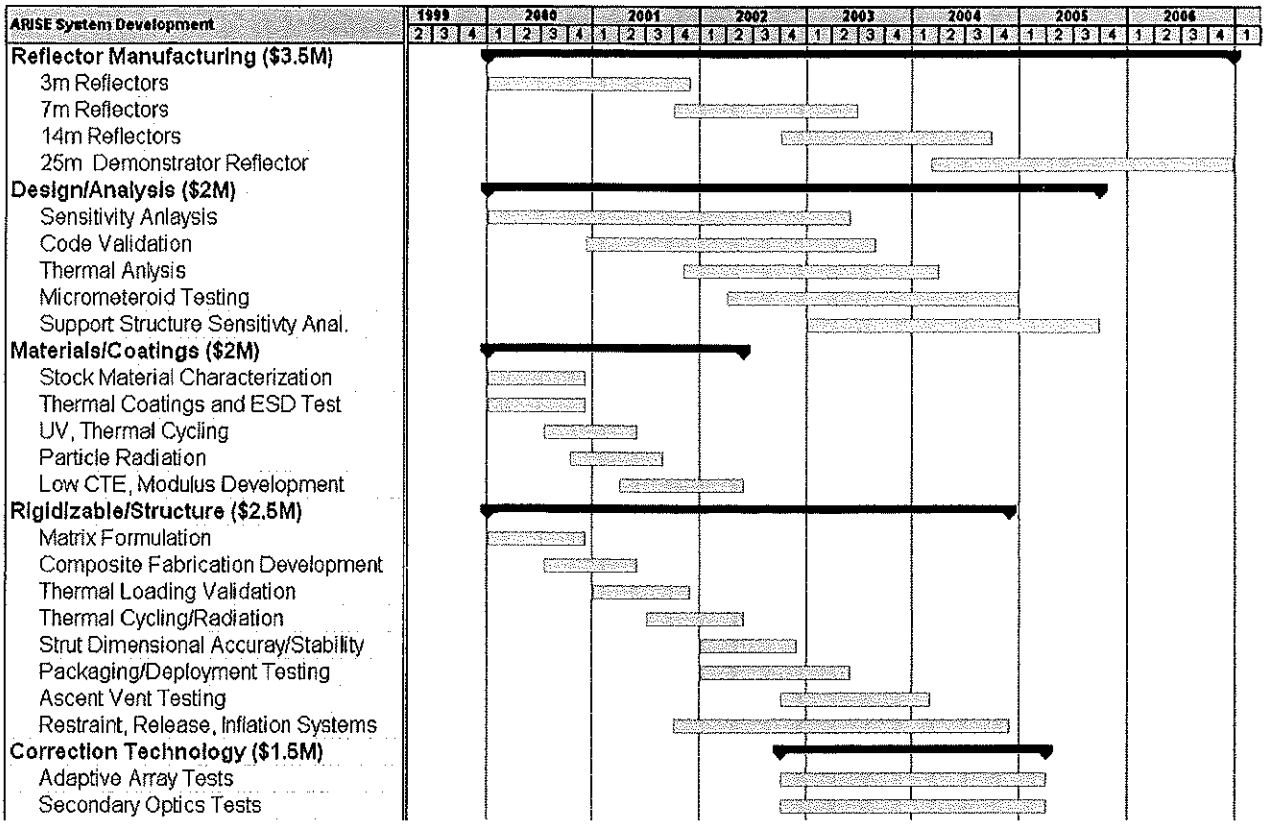

Table 9.1: ARISE Inflatable Antenna Development Program Schedule.

reflector surface accuracy. In this way resources will be applied to the appropriate design parameters in the reflector development program.

Once a finished reflector surface is fully mapped, FAIM will be run again using the measured manufacturing errors, and its output validated against the known surface shapes. Based on this analysis, minor modifications to the FAIM code may be warranted and undertaken. Previous validations have been performed with less complex shapes, this analysis is necessary to validate the code for manufactured reflector shapes.

Another component affecting reflector surface accuracies are thermal gradients and temperatures on the reflector membrane. Given the on orbit thermal loads, FAIM is capable of predicting the mechanical behavior of the reflector and subsequent surface accuracy. One of the 3 m reflectors will undergo thermal vacuum testing to simulate the expected on orbit thermal loads. This reflector will incorporate some of the latest thermal control coatings proposed by L'Garde to minimize thermal distortions. The surface accuracy under these loads will be precisely measured and the results used to validate the effectiveness of the thermal control coatings, and the FAIM thermal predictions.

To predict make-up gas requirements L'Garde's micrometeoroid damage model must be extended to include third film damage. Tests have been conducted using representative particle velocities on dual membranes. Theory predicts less damage on the third membrane but needs validating. Tests are planned to address these issues improving our make-up gas predictions.

9.3.3 Materials/Coatings

Material property variations are a significant factor in manufactured reflector accuracy. As discussed in the Reflector Manufacturing section, the material will be characterized in detail. Parameters of interest include uniformity and directionality of modulus, Poisson's ratio, thickness, creep, CTE, hygroscopic properties, packageability and wrinkle resistance to name a few.

Further development will be conducted in the area of high performance thermal coatings. These coatings absorb some of the incident energy on the exterior of the lenticular, while distributing the internal trapped energy as evenly as practical. Small samples will be tested to validate expected performance. These coatings will be concurrently evaluated for proper electrostatic discharge dissipation. These materials will be utilized in the thermal testing of the 3 m series reflector.

Lifetime issues such as UV resistance, particle radiation effects, and thermal cycling will be characterized and accounted for in the design. Atomic oxygen is not considered a threat in the high orbit occupied by the ARISE mission. Space environment testing of material samples is planned.

Investigation into new materials is ongoing. Low modulus materials may allow greater wrinkle resistance and lower internal pressures therefore lowering support structure and make-up gas requirements. Low CTE materials will reduce the negative effects of thermal loading, increasing reflector accuracy. Further material pre-treatment techniques will be investigated to stabilize and homogenize salient material properties.

9.3.4 Correction Technologies

Even with the expected surface precision improvements, some corrective technology will be required to achieve good RF performance at 86 GHz. Several corrective technologies are available which, used in conjunction with inflatable space reflectors, could achieve the apparent required surface accuracies. These technologies are:

Adaptive RF feeds: an array of RF transducers mounted at the focal plane of the reflector coupled with signal processing software and hardware are able to improve RF performance dramatically. Analytically this technology is very promising but lacks the ground testing that this program addresses.

Adaptive secondary reflectors: this technology utilizes an adaptive secondary reflector to correct the reflected energy focused on the feed. In it's simplest form it can be a fixed geometry to correct known standing errors in the reflector. Using active control of the sub-reflector shape it can be used to take out transient imperfections such as thermal distortions and distortions due to maneuvering loads.

L'Garde proposes to utilize some of the reflectors developed during the reflector development program to validate these technologies. The RF hardware and test facilities have yet to be identified.

9.3.5 Rigidizable Structure

For space missions of any significant duration it is not practical to have a constantly inflated structure. Over time small leaks develop in the high-pressure torus and strut support structure venting inflatant, which must be replenished. For longer missions this make-up gas mass becomes prohibitive, therefore the walls of the torus and struts must be rigidized after deployment. The low-

pressure reflector suffers far less inflatant loss and thus can practically remain pressurized for long periods.

L'Garde has proposed the use of SubTg rigidization for ARISE. This technique utilizes the glass transition temperature (Tg) of an elastomer to produce rigid structures at the deployed equilibrium temperatures expected during the ARISE mission. Other rigidization techniques are in development but the SubTg technique will produce the highest overall system strength to weight ratio.

Matrix formulations and composite fabrication techniques will be developed to meet or exceed the 10 Mpsi modulus goal at the peak operational temperatures endured during the ARISE mission. These temperatures will be predicted assuming the use of MLI, and will be validated during a thermal vacuum test plan of candidate materials. Additionally, the materials will be thermally cycled and subjected to particle radiation in order to determine long term effects. Fabrication techniques will be developed to produce as dimensionally accurate and thermally stable a structure as possible. The actual deployed shape of the torus under various thermal loadings will be predicted based on long test samples and fed back into the FAIM code to determine the sensitivity of reflector accuracy to structural geometry. The effect of the support system and the lenticular torus assembly procedure will be quantified in a similar manner.

Reflectors and structural elements will be subjected to packaging and deployment tests. The mandrel deployment devices are baselined for the ARISE configuration, the functionality of these devices and their effect on the strength of the struts will be tested. The key element in the reflector packaging is ascent venting. Building on previous experience gained during the AIE flight and subsequent development programs, packing techniques and hardware devices will be further developed to mitigate the effects of entrapped air. Low mass canisters, launch restraint and release systems are also desirable and will be further developed during the program.

9.4 Low Noise Cryogenic Amplifier Technology

Cryogenic low-noise amplifiers using discrete InP or GaAs HEMT devices have been built at 8, 22 and 43 GHz which meet the ARISE requirements. At 22 and 43 GHz, NRAO has built amplifiers for MAP which are flight qualified and meet the ARISE requirements. At 86 GHz, NRAO has built amplifiers using discrete InP transistors, which will also fly on MAP. These devices also meet the ARISE requirements. Furthermore, JPL has been working with TRW to develop InP MMIC amplifiers at this frequency. Such amplifiers have been measured with less than 40 K noise at 86 GHz. For the MMIC option, Planck will meet the ARISE requirements with flight qualification before 2003. Little or no technology development is required for either option and flight qualification merely requires chips and testing for the MMIC option.

However, the sensitivity of ARISE improves as the square-root of the receiver noise temperature or T_{sys}. The current state-of-the-art in cryogenic low noise amplifiers has demonstrated 5 x quantum limited performance at frequencies as high as 50 GHz. TRW and JPL have developed a low noise MMIC amplifier at 100 GHz which has demonstrated 31 K noise or 6 x times limited noise (see Figures 9.2 and 9.3). Continued development of cryogenic amplifiers geared towards another factor of 2 in performance could potentially ease the requirements on the primary reflector surface. A relatively small investment by NASA in this area could have a large return for ARISE as well as other NASA missions requiring the lowest possible receiver noise temperature.

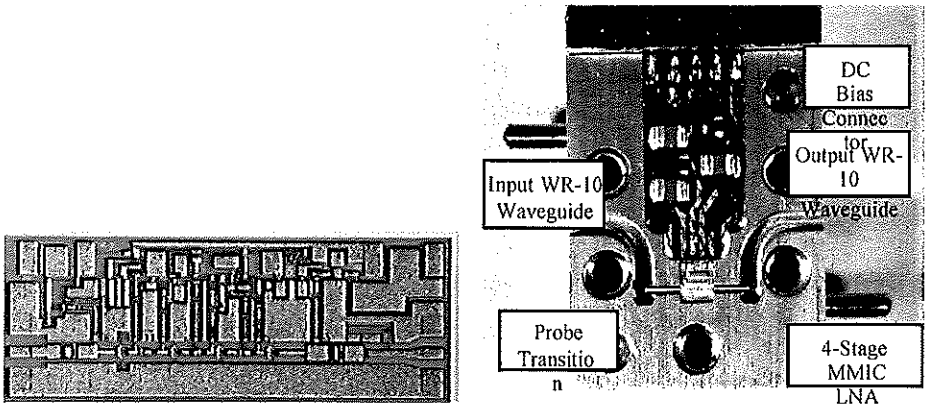

Fig. 9.2: 100 GHz MMIC Amplifier. Amplifier chip and amplifier module containing the chip.

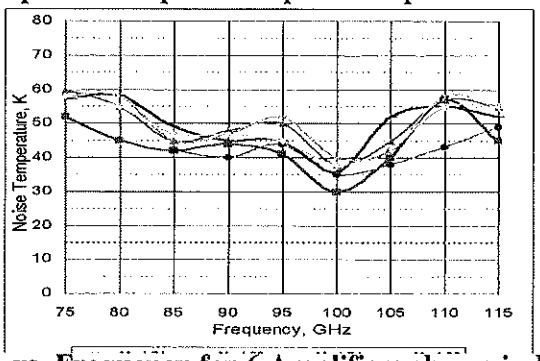

Fig. 9.3: Noise Temperature vs. Frequency for 6 Amplifiers shown in Figure 9.2.

9.5 Cryocooler Technology

The ARISE thermal requirement for the science instruments (receivers and LNAs) is that they need to be cooled at 20 K with a cooling load of 0.5 W. The cooling system that will satisfy these requirements consists of a pre-cooler stage followed by a sorption cooler. Flight, proto-flight, and engineering models of 35-60 K pre-coolers already exist and substantial development is expected to occur by the time ARISE enters phase C/D. Table 9.2 summarizes the characteristics of some coolers that are likely to be available at that time.

Manufacturer	Cycle	Temp (K)	Input Power (W)	Mass (kg)	Maturity
Creare	Reverse Brayton	35	105	15	PF
Raytheon	Split-Stirling	35	112	18.5	PF
Lockheed Martin	Split-Stirling	35	198	29.4	FM
TRW	Pulse-Tube	35	288 (est)	32	EDM
Creare	Reverse Brayton	60	100 (est)	13.7	EDM
Lockheed Martin	Split Stirling	60	130	17.9	FM
TRW	Split Pulse-Tube	55	102	12.7	FM

Table 9.2: ARISE Mechanical Cooler Technology. Abbreviations for maturity levels: FM=flight model, PF=Proto-Flight, EDM=Engineering Development Model. All input powers are normalized for 1 W heat lift at the cold tip.

The 20 K continuous hydrogen sorption cooler is presently under development at JPL for the Planck Surveyor mission and will be available at the start of ARISE. Sorption cooling has been demonstrated for flight aboard STS-66 in 1996. The design for ARISE will be a direct scaled-down version of the Planck sorption cooler.

9.6 Data Systems Technologies

The technology issues regarding the ARISE data systems are determined by the 8 Gbps systems requirement, implicating the space-to-earth telecommunication downlink, and the VLBI acquisition, tape recording and correlator systems, and are described here.

9.6.1 Telecommunication Link Issues

Two primary options exist regarding the necessary 8 Gbps telecommunications link: a traditional but more complex and costly digital approach similar to that used in the VSOP mission, and an analog approach which to-date is untested. Both options continue to be investigated. Both options assume the use of Ka-band. While there appears to be few technological unknowns with the analog approach, it is yet to be proven in VLBI applications, although it offers the advantages of cost as well as satisfying Ka-band spectral allocations. The digital option employs a high rate 512 Mbps QPSK receiver under joint development by JPL and GSFC at the time of writing, and is expected to be operational by 2001. This receiver, however, is not designed to receive a SRRC filtered QPSK modulated signal, necessary to limit the digital method spectral emissions, and this extension must be developed. A high speed equalizer is needed for the ARISE ground receiver to mitigate the effects of intersymbol interference caused by imperfect filtering and possible multipath fading due to low elevation angles, and study and implementation of this device is required. Additionally, a high speed SRRC filtered spacecraft modulator is required to complete the telecommunication system, and preliminary investigation on this design has begun. Assuming a waiver can be obtained for Ka-band transmission, both digital and analog telecommunications presently appear feasible. Developments involving more complex schemes employing QAM or optical transmission will be monitored but are not considered primary candidates for ARISE.

9.6.2 VLBI Acquisition, Tape Recording, and Correlator Systems

The ARISE 8 Gbps VLBI data rate requirement imposes the need for new-generation VLBI data acquisition, tape recording, and correlator systems. However, continuing improvements in VLBI systems technology appear promising and the evolving technologies could be in place to support these rates. This appears particularly true for the data acquisition and correlation systems. For example, multi-Gbps correlator designs in connected-element interferometers are under development (1-2 Gbps designs exist today even in VLBI applications), and experience with these broadband designs should be applicable to the ARISE application. There is perhaps further doubt regarding the availability of suitable recording systems, although developments are proceeding.

The MkIV (and related VLBA) recording systems hold promise in the development of thin-film head technology which may yield a ten-fold improvement in present data densities and thus support the 8 Gbps requirement. The Canadian S3/S4 systems, driven largely by consumer application (such as HDTV) helical-scan digital formats, also promise 4-8 Gbps systems and are under development. Both development paths, challenged by the 8 Gbps ARISE requirement, will be carefully monitored, as the tape recorder system appears to be the greatest VLBI-specific technological challenge, although all components of an 8 Gbps VLBI system present great technical challenges.

9.7 ARISE Technologies Summary

As shown throughout this document, the ARISE new technology requirements will be met by existing and emerging technology programs and flight projects launched before ARISE. The combined value of these programs, as direct savings to the ARISE project, will be at the tens of million dollar level. With these technology gains, the ARISE spacecraft will be lighter, higher performance, satisfying the challenging science goals, and present a total cost to NASA of about $400M (including an estimated $60M Delta II launch), yielding an affordable and most exciting endeavor.

Appendix A

ARISE Structures and Thermal Analysis

ARISE Finite Element Model

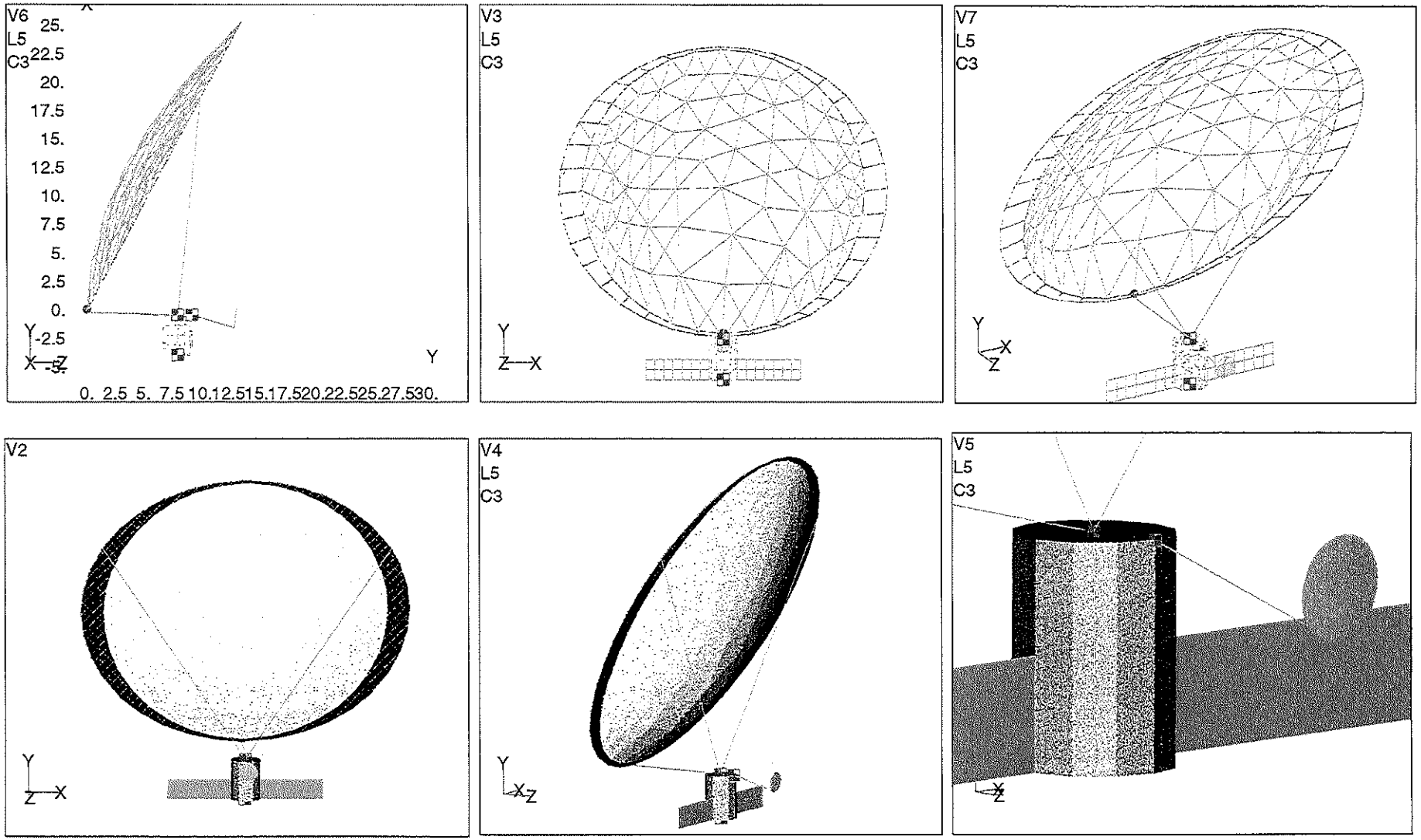

Off-Axis Gregorian, f = 11.55m, D = 25m, f#p = 0.23

OFF-AXIS GREGORIAN
Mass and Inertia
f = 11.55 m, D = 25 m, f#p = 0.23

UNIT	MASS (kg)	CENTER OF MASS (m)			MASS INERTIA at Local CG (Global C/S) (kg*m^2)		
		X	Y	Z	Ixn	Iyn	Izn
S/C Buss - Cylindrical 2.5m dia. X3.5m, Al 3/16" Misc S/C Equip. & Instr. - (Coolers, ACS, Strar Tracker/Sensors, Buss modules, Power, Telecom Elect., CDH,CCS, etc.)	1442.3	0.00	-2.25	8.00	2614.7	1415.2	2614.7
Feed Array	35.0	0.00	-0.50	9.25	0.0	0.0	0.0
Deployment Canister	57.3	0.00	-0.50	8.00	0.0	0.0	0.0
Telecom - Optical Com	15.0	0.00	-4.00	8.00	0.0	0.0	0.0
Primary - Reflector Surface Al - Kp (0.5 mil) - Au (300 psi membrane stress)	11.5	0.00	13.13	5.49	581.5	591.0	888.7
Primary - Canopy Surface CP-1 (0.5 mil)	10.5	0.00	11.77	7.99	532.7	530.4	825.2
Primary - Torus Inflatable Rigidized Al (10.5" dia, 12 mil thick)	18.3	0.00	12.50	6.77	1909.0	2341.6	3385.8
Primary - Spring Tensioners F = 0.5 lb	1.3	0.00	12.52	6.78	83.7	182.6	228.3
SubReflector - Eliptical Gl/Cyanate 1.2 x 1.65m, e = 0.555	11.0	0.00	-0.83	13.01	1.8	1.8	3.6
Truss - SubReflector Spt. 3.9m Gr/Ep Deployable	4.6	0.00	-1.08	11.12	5.8	5.3	0.5
Bottom Strut - Primary Spt. 8.2m Gr/Ep Deployable	8.4	0.00	-0.38	3.92	45.9	45.9	0.0
Strut - Primary Side Spt. Inflatable Rigidized Al (2 ea. - 16" dia, 14 mil thick) 23.1 m	15.0	0.00	9.07	9.04	464.1	819.2	1272.4
Solar Array	18.9	0.00	-2.69	8.00	11.0	589.5	600.5
TOTAL Global C/S at Reflector Vertex	*1793.3*	*0.00*	*-1.55*	*8.04*	*18791.7*	*7307.3*	*21857.4*

ARISE Thermal Distortion Analysis (Reflector Rear-View)

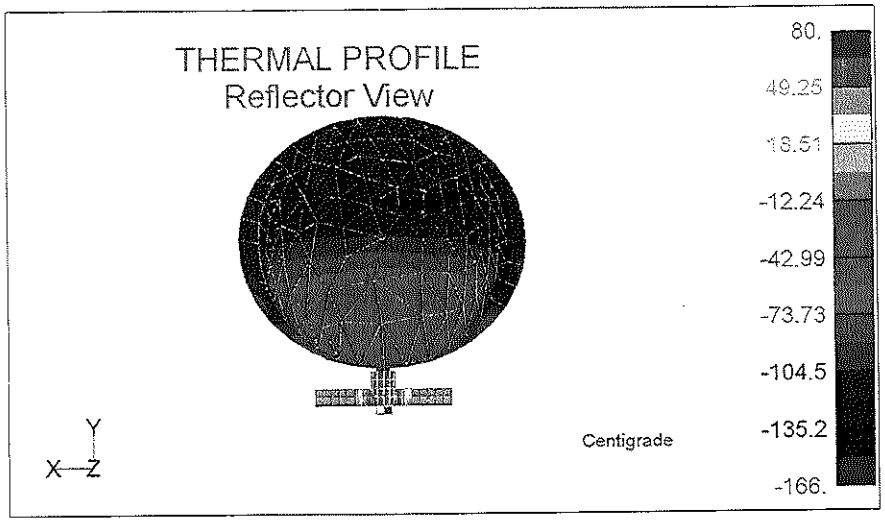

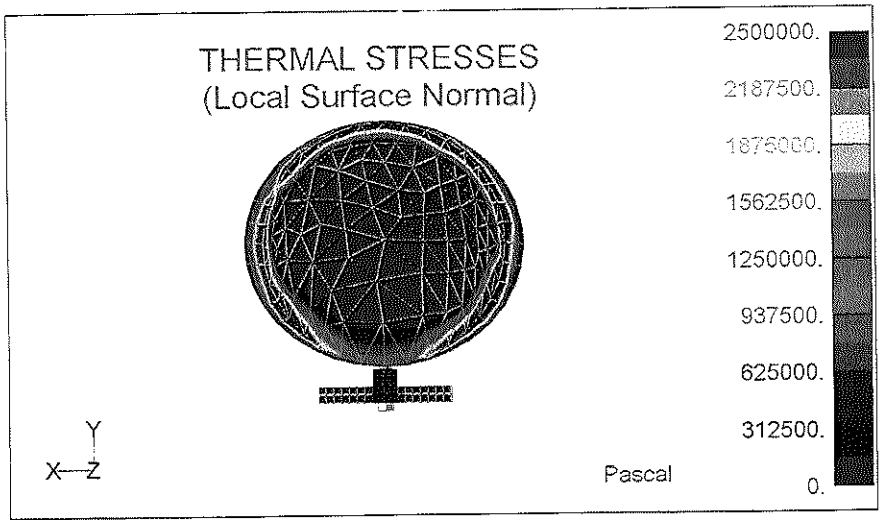

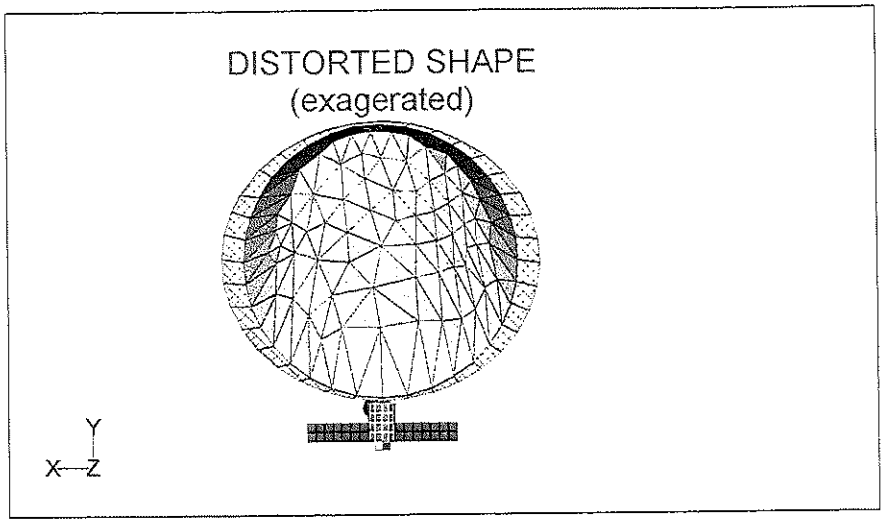

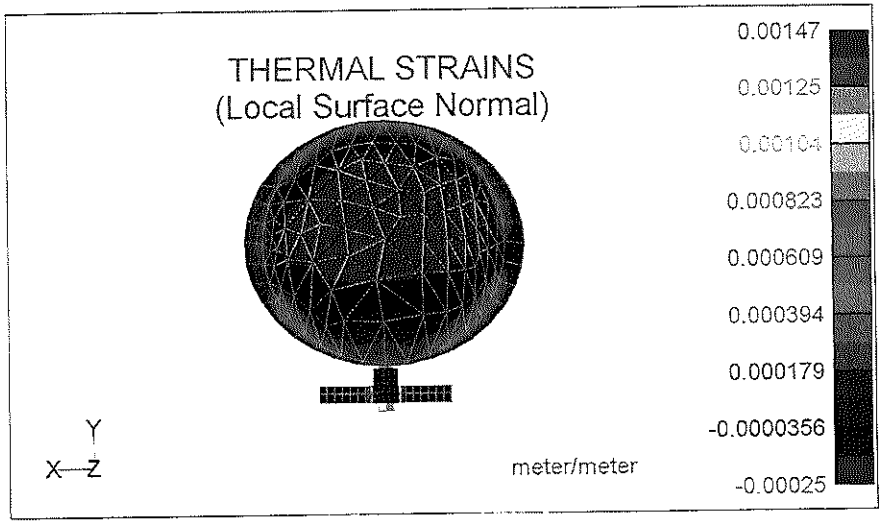

Sun Edge-On to Primary Reflector, Worst-Case Hot Orbit, Beta = 0 Deg.

ARISE Orbital Trajectory
(Thermal Analysis)

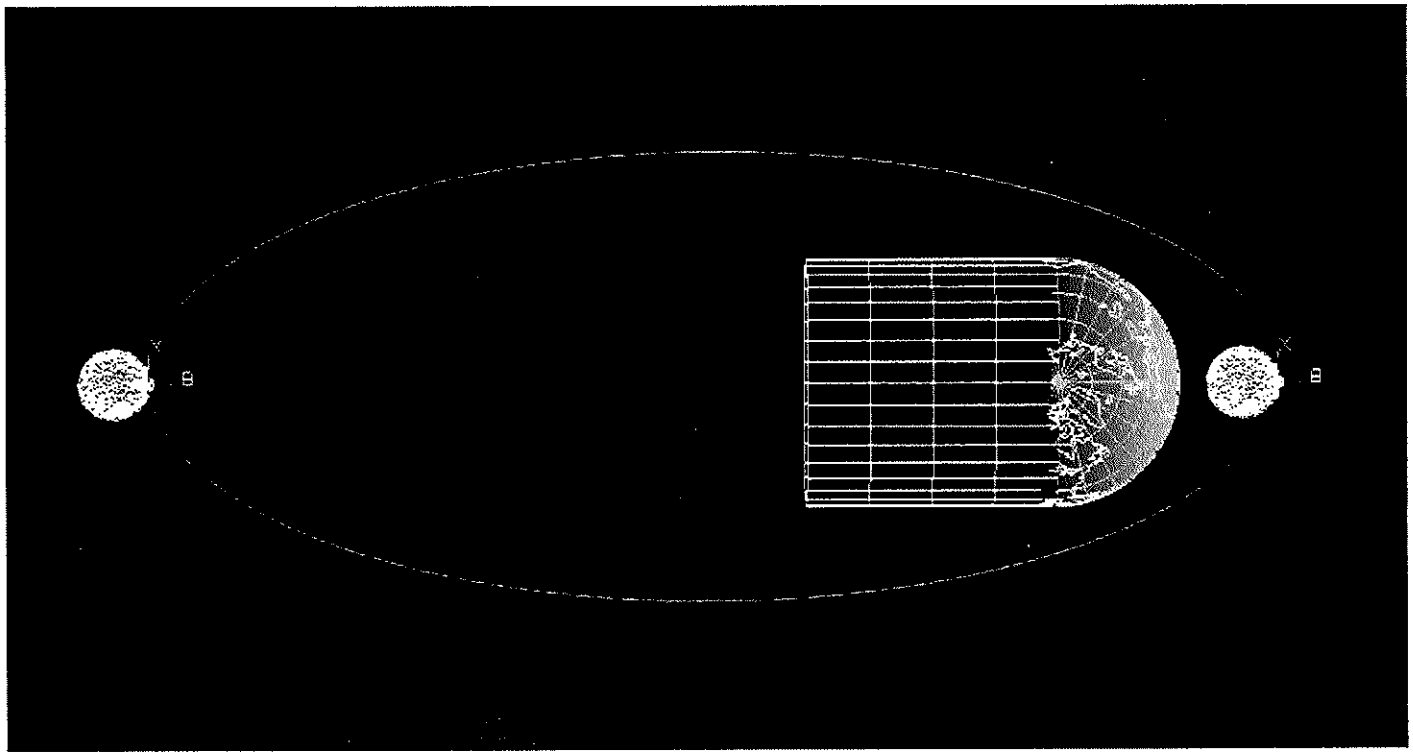

5000 km x 40000 km elliptical orbit
6 0° inclination

Steady-State Sub-Solar Point Results

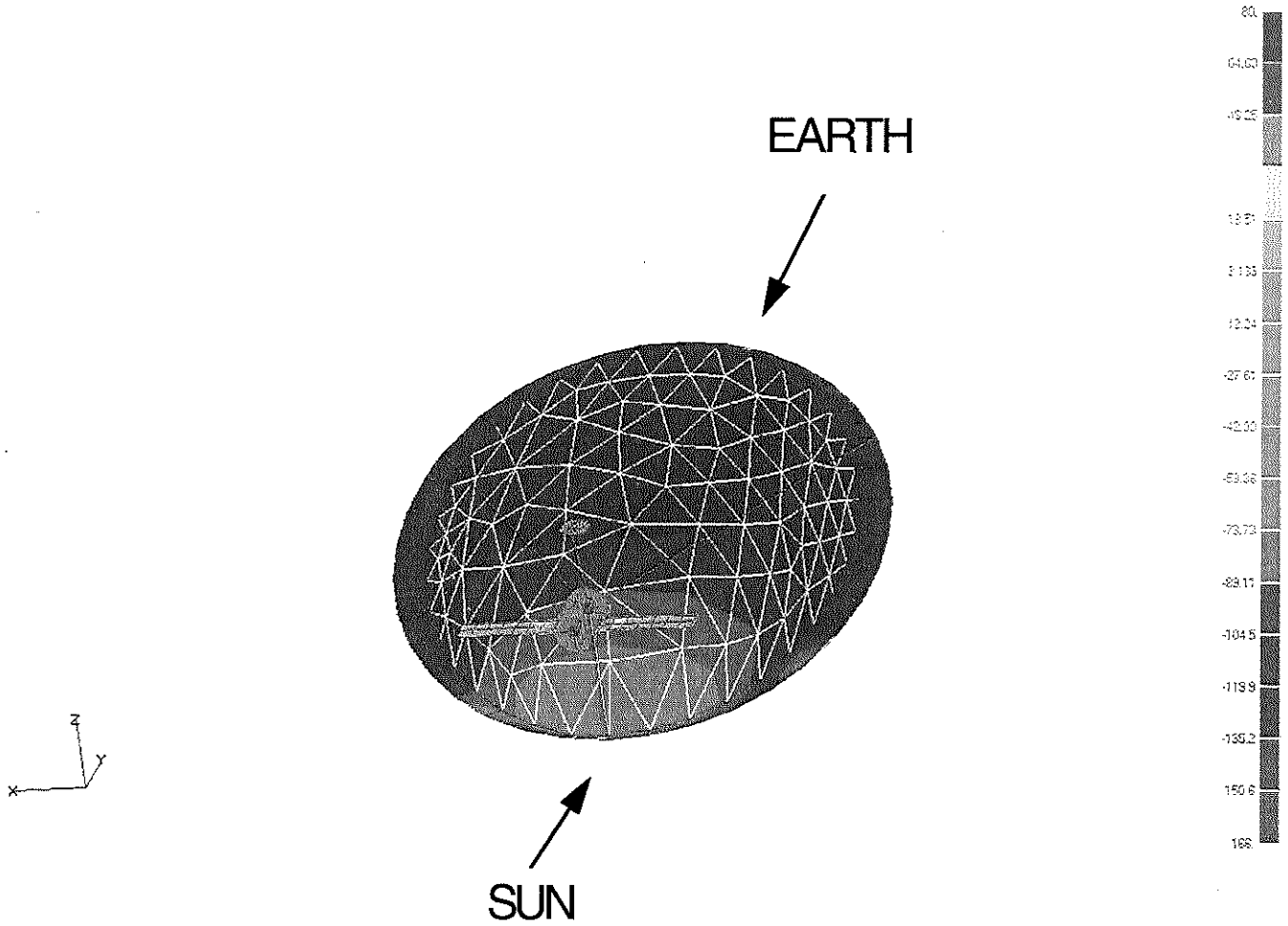

Acronyms

ADC	Analog to Digital Converter
ADCS	Attitude Determination and Control System
ADOTS	ARISE Data Oversight and Transfer System
AFOG	ARISE Flight Operations Group
AGN	Active Galactic Nuclei
AGOG	ARISE Ground Operations Group
AIPS	Astronomical Image Processing System
AMOH	ARISE Mission Operations Handbook
AO	Announcement of Opportunity
APT	Asia-Pacific Telescope
ARISE	Advanced Radio Interferometry between Earth and Space
ASOG	ARISE Science Operations Group
ASRC	ARISE Science Review Committee
BB	Base-band
BOL	Beginning of Life
BPF	Band Pass Filter
BWG	Beam Waveguide
C&DH	Command and Data Handling
CDMU	Central Data Management Unit
CEC	Constant Envelope Converter
CIS	Copper Indium Diselenide
COI	Composite Optics, Inc.
CSA	Canadian Space Agency
D/C	Down-converter
DAT	Digital Audio Tape; Data Acquisition Terminal
DFP	Deformable Flat Plate
DoD	Department of Defense
DOF	Degree of Freedom
DS-1	Deep-Space One
DSN	Deep Space Network
EIRP	Effective Isotropic Radiated Power
EOL	End of Life
ESD	Electrostatic Discharge
EVN	European VLBI Network
F-OPS	Flight Operations
FAIM	Finite-element Analysis for Inflatable Membranes
FCC	Federal Communications Commission
FDM	Frequency Division Multiplexed
FEEP	Field Emission Electric Propulsion
FWHM	Full Width at Half Maximum
G-OPS	Ground Operations
GBT	Green Bank Telescope
GCS	Ground Command Station
GEO	Geostationary Earth Orbit
GLAST	Gamma Ray Large Area Space Telescope
GO	Geometrical Optics
GPS	Global Positioning System
GRT	Ground Radio Telescope

GSTS	Global Space Radio Telescope Schedule
GTO	Geosynchronous Transfer Orbit
GTS	Ground Tracking Station
GVWG	Global VLBI Working Group
H&S	Health and Safety
HALCA	Highly Advanced Laboratory for Communications and Astronomy (VSOP)
HEMT	High Electron Mobility Transistors
HGA	High Gain Antenna
HST	Hubble Space Telescope
IAE	Inflatable Antenna Experiment
IF	Intermediate Frequency
IMOS	Integrated Modeling of Optical Systems
InP	Indium Phosphide
IOC	In Orbit Checkout
IR	Infra-red
IRU	Inertial reference Unit
ISAS	Institute for Space and Astronautical Science (Japan)
ISI	Intersymbol Interference
ITO	Indium Tin Oxide
ITSAT	Inflatable Torus Solar Array Technology
JIVE	Joint Institute for VLBI in Europe
LDD	L'Garde Deployment Devices
LEO	Low Earth Orbit
LNA	Low Noise Amplifiers
LO	Local oscillator
LPF	Low Pass Filter
$M_\odot$	Solar Mass
ME	Mission Elements
MLI	Multi Layer Insulation
MMA	(Atacama Large) Millimeter Array
MMIC	Monolithic Microwave Integrated Circuit
MMNAV	JPL Multi-Mission Navigation
MMSCH	DSN Multi-Mission Scheduling
NFRA	Netherlands Foundation for Research in Astronomy
NGST	New Generation Space Telescope
NRAO	National Radio Astronomy Observatory
NSTAR	NASA SEP Technology Application Readiness
NTO	Nitrogen Tetroxide
PA	Power Amplifier
PI	Principal Investigator
PMAD	Power Managment and Distribution Unit
PO	Physical Optics
QAM	Quadrature Amplitude Modulation
QPSK	Quadrature Phase Shift Keying
RF	Radio Frequency
RMS	Root Mean Square
ROM	Rough Order of Magnitude
RPM	Revolutions per Minute
SBIR	Small Business Innovation Research
SEFD	System Equivalent Flux Density
SEL	Single Event Latch-up
SEU	Single Event Upset
SMBH	Supermassive Black Hole
SNR	Signal-to-Noise Ratio

SOH	State Of Health
SRC	Science Review Committee
SRRC	Square-Root Raised Cosine
SRS	Space VLBI Radio Telescope Schedule
SRT	Space Radio Telescope
SSPA	Solid-state Power Amplifiers
TCF	Time Corrections File
TCS	Thermal Control System
TDRSS	Tracking and Data Relay Satellite System
TID	Total Ionizing Dose
TT&C	Telemetry, Tracking, and Control
TWTA	Traveling Wave Tube Amplifier
U/C	Up-converter
USO	Ultra-stable Oscillator
UTC	Universal Time (Coordinated)
VIA	VLBI Recorder Interface Adapter
VLA	Very Large Array
VLBA	Very Long Baseline Array
VLBI	Very Long Baseline Interferometry
VSOP	VLBI Space Observatory Program

References

[1.1] ARISE Science Goals, April 1999, NASA/JPL, NRAO. Editor: J. S. Ulvestad.

[3.1] J. S. Ulvestad, "86-GHz Blazar Imaging on ARISE-VLBA Baselines", VLBA Scientific Memo No. 19, January 29, 1999.

[4.1] D. Duan, Y. Rahmat-Samii, IAAA Transactions on Antennas and Propagation, January 1995.

[4.2] S. Weinreb, R. Lai, N. Erickson, T. Gaier, and J. Wielgus,"W-Band InP Wideband MMIC LNA with 30K Noise Temperature"; IEEE-MTT-S, International Microwave Symposium, Anaheim, CA, June 1999.

[4.3] Glaister, D.S., Donabedian, M., Curran, D.G.T., Davis, T., "An Overview of the Performance and Maturity of Long Life Cryocoolers for Space Applications," Cryocoolers 10, Ed. Ross, R., Plenum Press (1999).

[4.4] Ross, R.,"JPL Cryocooler Development and Test Program: A 10-year Overview" Proc. IEEE Aerospace Conference (March 1999).

[5.1] H. Hirabayashi, et al., "Overview and Initial Results of the Very Long Baseline Interferometry Space Observatory Programme", Science, Vol. 281, 18 September, 1998.

[5.2] ARISE Telecommunication Design Study, Tsun-Yee Yan, Section 33, NASA/JPL.

[6.1] Radiation Environmental Comparison of Four Potential ARISE Orbits, Interoffice Memorandum 5052-98-024, February 3, 1998.

[7.1] J. Mueller, "Thruster Options for Microspacecraft: A Review and Evaluation of Existing Hardware and Emerging Technologies", 33rd AIAA Joint Propulsion Conference, July 1997.

[9.1] A.B. Chmielewski, "ARISE Antenna", Ultra Large Optics Challenge Workshop, February 1999.